Doctoral Dissertation

Study on Optimization Method of Architectural Design Process based on Environmental Performance Indicators and Implementation of Generative Algorithm

September

2022

Rendy Perdana Khidmat

Fukuda Laboratory
Architecture Course
Graduate School of Environmental Engineering
The University of Kitakyushu
Japan

Preface

In a world where temperatures are continuing to rise and there is a crisis in the energy sector, building performance simulation and powerful computational approaches in the early stages of architectural design help us set goals for future building performance and look into possible ways to make buildings less harmful to the environment. Due to the complexity of physical reality, simulation may not provide a concrete solution, but it does improve understanding of the interrelationships between design parameters and its performance. Through eight computational experiments investigating design parameters and design performance goals, this thesis reveals a potential in performance optimization and efficiency related to environmental and structural considerations during the early phase of the architectural design process. By putting this research into perspective in complementing recent research on similar topics, a lot of work should be done in the future to tackle the issues. This research is expected to enrich the field of design and benefit stakeholders in terms of architectural design decision-making.

Dedication

I dedicate a tiny contribution of this thesis to the field of knowledge, especially in computational design field, to teachers, my parents, my family, my alma mater, and my institutions.

Acknowledgement

First and foremost, I want to thank my advisor, Professor Hiroatsu Fukuda, for his important guidance and assistance throughout my doctoral program. His insights, ideas, and guidance on research and academic life have been extremely important and invaluable to me.

In addition, I would like to express my gratitude to Professor Bart Dewancker, Professor Weijun Gao, and Professor Takashima for serving on the jury committee for the evaluation of my thesis. Their comments and suggestions have helped me a lot throughout the whole process of making my thesis better.

The academic staff in at The University of Kitakyushu, Nomura-san, Itahashi-san, Maki-san, Matsumoto-san, and Murakami-san, for assisting with so many minor and major things, as well as administrative issues.

I would like to thank my institution, Institut Teknologi Sumatera (ITERA), as my home base for the support and the responsibility that they have given to me for study assignments.

Fukuda Laboratory members: Wang Lu, Leng Yi, Jiang Yijun, He Chengchen, Liu Zhaoowen, Zhu Yuewei, Borys Iryna, and my seniors Zhang Tao, Pak Alex, Pak Sugi, Pak Agus, Ma Qingsong, Bu Beta – thank you supporting my student life as well as every discussion, brainstorming, encouragements, and advice.

Importantly, I would like to thank my parents and siblings most of all for everything. Their unwavering affection, support, and encouragement shaped who I am today. To my wife, Kustiani, and my three adorable girls, Nisrina, Qinania, and Asyana, thank you for always being there to provide me with energy, motivation, and support. I am fortunate to have you all accompanying me on this adventure.

I could not have done this without support of my friends. My colleagues in Department of Architecture, Institut Teknologi Sumatera for all your support and motivation. To my Indonesian friends whom I struggle with in Coventry and have become a support system during my doctor course. Bridging 2018 alumni: Pak Andi, Pak Syafiq, Mba Ratna, Mba Fina, Astri, Nia, Mba Padma, Kak Ainul, and Kak Ida – thank you for the support you all have given me and for our constant discussion in academic and life.

Lastly, I would like to say thank you to the Ministry of Education, Culture, Sports, Science and Technology of Japan (MEXT) for the scholarship. With the fund and support, this thesis and my doctoral is successfully established. Also, LPPM Institut Teknologi Sumatera (ITERA), LPPM Universitas Pendidikan Indonesia (UPI) for the support during the experiments.

Abstract

Design decision-making process can be complicated and immense. Considering the high level of uncertainty during early phase architectural design process, designer often neglect design parameter that could mitigate future building performance and environmental impact. Utilizing generative design algorithm and genetic optimization for the management of contemporary data-driven and performance-oriented architectural design is prevalent. Due to their computationally intensive nature, it can be challenging to use them to optimize environmental potential and structural considerations that are affected by the geometry and the material employed. This thesis focuses on the deployment of parametric approaches and generative exploration and optimization processes to optimize design objectives related to environmental performance indicators. Exploration mechanism should be considered as an option for identifying and finding design solutions with better performance efficiently and effectively. In this thesis, we propose techniques for achieving the best design solutions during early-phase architectural design process, investigating the objectives of environmental indicators together with the study of design parameter's role.

The thesis consists of four main bodies. In Chapter 4, the experiments were meant to develop a methodology for investigating daylight performance and its relationship with glazing ratio, overhangs, louver shading, and room orientation. The chapter offers a novelty in iterating a common feature such as overhangs, louvers, glazing, and orientation to optimize daylight performance in specific regional contexts such as Sydney; Australia, Jakarta; Indonesia, and Birmingham; U.K., into three experiments. First experiment implemented design exploration experiment for Jakarta showed improvement in the useful daylight illuminance (UDI) by about 13.1% compared to the benchmark model. In the second experiment, a computationally developed benchmark model increase UDI by about 2.58% to about 6.17% depending on which type we prefer. In the best winter performance, the heating energy was improved by 3.36%. In the third experiment, study for Birmingham showed UDI improvement by about 80% and energy consumption by 28%. Study for Jakarta show UDI improvement by 146.26% and energy consumption by 3.26%. The Sydney case study, UDI improved by 79.48% and energy consumption by 2.99%. Parameter Spacing and Blade size were found to be the most influential parameters driving design objectives in almost all the sensitivity analysis studies.

In Chapter 5, the experimentations characterized an approach for improving the configuration of a material with a long-standing and well-known reputation, the expanded metal sheet that was designed as a shading device, to demonstrate that the utilization of this material can improve daylight provision and serve as an alternative material for shading devices. The study provides an innovative way of investigating a well-known, inexpensive, and long-standing reputable material, expanded metal sheet, as a solar shading device with its daylight performance. Given the context of Japan's sky conditions, the best expanded metal configuration and daylight performance were successfully identified and proven to merit the daylight

requirements of LEED v4 Daylight credits. The experiment on the expanded metal reveals that in Japanese Industrial Standard (JIS) G3351 grating type, the XG13 and XG14 are the most preferable types for UDI, while the XG24 is the best type for daylight glare probability (DGP) and from the fitness function calculation. XS91 is the best for the view objective. Aperture was negatively correlated with UDI. Furthermore, undergoing a comprehensive investigation of daylight from 3176 generated design solutions, the best design solution was solution number 1728, reducing annual sunlight exposure (ASE) by up to 100% and improving UDI by up to 50%. Focusing on daylight glare probability (DGP), the optimization achieved a reduction in DGP by 38%. In this chapter, Strand and Height are found to be the most influential parameters driving the objectives.

In Chapter 6, we developed a parametric and optimization platform to observe the building geometry-affected potential for optimizing outdoor thermal comfort and reduce energy consumption. The purpose of this chapter was to examine how the geometry of a two-story wooden house with a novel geometry that uses the *Reuleaux* triangle as its base profile affects the universal thermal climate index (UTCI) situated in the Orio District, Kitakyushu, Japan. The study provides significance in finding the best twisted *Reuleaux* triangle cylinder geometry to respond to the climate of Kitakyushu, Japan. The results revealed insignificant improvement in one-day based simulation with 0.07°C improvement in UTCI, 0.02 kWh/m^2 in surface radiation, and 0.01 kWh/m^2 in the site radiation. However, in this chapter, a contradiction emerges where the analysis toward the annual cost showed that the improvement was not guarantee the energy consumption efficiency.

In Chapter 7, the experiment investigated the relationship between the design parameters of a novel *Hyperboloid* wooden structure to the structural and daylight objectives. The study provided a novelty in the structural investigation and cost efficiency of a unique *Hyperboloid* wooden structure made of 105 mm x 105 mm x 4000 mm Japanese cedar, together with the identification of the best glazing size and position that performed the best daylight situation. The optimization and exploration yielded 10,098 solutions in structural analysis and 406 solutions in daylight exploration and successfully dragged the pareto front and the fitness function calculation individuals to the searching area in the population fields. Applying fitness function calculations, the nine best solutions were ranked and the tendency between parameters and objectives was revealed. Besides, design exploration in the daylight simulation has been successfully observed the ten best solutions performing optimum UDI in the summer and winter period.

The research contributes to the field of computational architecture design by providing insight into how form finding leads to design goal optimization and a method for examining the link between design parameters and design objectives at various scales of the design project. By understanding the relationship and trend between parameters and design objectives in the context of early-phase architectural design, design goals can be quantitatively justified, and the optimal solution can be attained. For instance, the information of a particular louver, expanded metal configuration, or building geometry can be beneficial for designers, manufacturers, users, and regulators in recommending the proper configuration

based on the regional context to achieve future energy efficiency and optimize daylight and energy consumption, which can have a long-term positive effect on human health, the economy, and the natural environment.

Keywords: Parametric, Generative Algorithm, Multi-objective optimization, Daylight, Energy consumption, *Hyperboloid* structure, *Releaux* triangle, Design exploration.

Table of contents

List Of Figures

List of Tables

Nomenclature

ASE	:	Annual Sunlight Exposure
ASE_i	:	Each value in optimal ASE outcome
ASE_{max}	:	Minimum value of ASE optimization set
ASE_{min}	:	Maximum value of ASE optimization set
ASF	:	Adaptive Solar Façade
AUDI	:	Adjusted Daylight Illuminance
BM	:	Benchmark Model
BPS	:	Building Performance Simulation
BV	:	Building Volume
CABE	:	Climate Adaptive Building Envelopes
CAD	:	Computer Aided Design
CAM	:	Computer Aided Manufacture
CDA	:	Contonous Daylight Autonomy
Cfa	:	Koppen climate classification for humid subtropical climates
CFS	:	Complex Fenestration System
CIE	:	Commission Internationale de l'Éclairage
COP26	:	The 2021 United Nations Climate Change Conference
CORE	:	The processor's core
CPU	:	Central Processing Unit
DA	:	Daylight Autonomy
DAYSIM	:	Daylighting analysis software
DF	:	Daylight Factor
DGI	:	Discomfort Glare Index
DGP	:	Daylight Glare Probability
DH	:	Overheating degree Hour
DIVA	:	Daylighting and energy modelling plug-in for Rhinoceros
DUH	:	Daylight Unsatisfied Hours
EC	:	Energy Consumption
EMMA	:	Expanded Metal Manufacturers Association
EPW	:	*EnergyPlus* weather data
EQ	:	Indoor Environmental Quality credit in LEED
EUI	:	Energy Use Intensity
EVF	:	External View Factor
EXP	:	Expanded Metal
FF	:	Fitness Function

FF_i	:	Fitness function equation
FY	:	Yield stress
G3351	:	Standard code for expanded metal in JIS
GA	:	Generative Algorithm / Genetic Algorithm
GB	:	Giga byte
GDP	:	Gross Domestic Product
GH	:	Grasshopper
GPU	:	Graphic Processing Unit
H_0	:	Null hyphothesis
HDI	:	Hourly Daylight Illuminance
HEC	:	Hourly Energy Consumption
HL	:	Horizontal Louver
HSI	:	Hourly Sunlight Illuminance
HypE	:	An algorithm for fast Hypervolume-Based Many-Objective Optimization
IDA-ICE	:	Indoor climate and energy simulation software
IEA	:	International Energy Agency
IES	:	Illuminating Engineering Society
IES LM-83-12	:	IES Lighting Measurements (LM) 83-12, Approved Method: IES Spatial Daylight Autonomy (sDA) and Annual Sunlight Exposure (ASE)
IESNA	:	Illuminating Engineering Society of North America
jEPlus+EA	:	Tools used for optimisation process
JIS	:	Japanese Industrial Standard
JMP	:	Statistic software
JST	:	Japan Standard Time
KUKA-KR9-900	:	Robot arm type
LCC	:	Life Cycle Cost
LEED	:	Leadership in Energy and Environmental Design
LEED v4.1	:	Standard for green building design, construction, operations, and performance
LM	:	Lighting Measurement
LV	:	Louver shading
LW	:	Expanded metal height
MAS	:	Multi-agent system in architectural design
MEPS	:	Minimum Energy Performance Standard
MODEII	:	Optimization toolbox
MOO	:	Multi-Objective Optimization
NAAMM	:	National Association of Architectural Metal Manufacturers

NFA	:	Normal Force Average
NSGA	:	Optimization techniques
NURBS	:	Nonuniform rational B-splines
NVIDIA	:	Technology company
OTTV	:	Overall thermal transfer value
PBM	:	Parametric Behaviour Maps
PC	:	Personal Computer
PM	:	Perforated metal
PPD	:	Precentage of Dissatisfied
PPOF	:	Passive Performance Optimization Frame- work
PRC	:	KUKA Robot arm plugin software
PTP	:	Point to point
Puv	:	Protection from UV rays
PV	:	Photovoltaic
PVSD	:	Photovoltaic integrated shading device
QC	:	Quebec, Canada
QV	:	Quality of View
RAD	:	RADIANCE software engine
RAM	:	Random Acces Memory
RAMDAC	:	Random-access memory digital-to-analog converter
RGB	:	Red, Green, Blue
RTB	:	Rural Tourism Building
RTX	:	Ray Tracing Texel eXtreme
SANAA	:	Japanese Architectural firm
SAP2000	:	Structural software
SDA	:	Spatial Daylight Autonomy
sDA_i	:	Each value in optimal sDA outcome
sDA_{max}	:	Minimum value of sDA optimization set
sDA_{min}	:	Maximum value of sDA optimization set
SFR	:	Skylight to Floor Ratio
SHGC	:	Solar Heat Gain Coeficient
SNI	:	Indonesian National Standard
SPEA	:	Strength Pareto Evolutionary Algorithm
SRC	:	Standardised Regression Coefficient
SRF	:	Shape and Opening Ratio
SW	:	Expanded metal component
SW	:	Distance between centers in direction of short mesh
TDH	:	Thermal Discomfort Hour
TE	:	Total Energy

TED	:	Influential videos from expert speakers
THERM	:	Software in heat transfer
TR	:	UV recorder type
TRNSYS	:	Transient System Simulation Tool
TT	:	Thornton Thomasetti
UAE	:	United Arab Emirates
UDI	:	Useful Daylight Illuminance
UDI_i	:	Each value in optimal UDI outcome
UDI_{max}	:	Minimum value of UDI optimization set
UDI_{min}	:	Maximum value of UDI optimization set
UHI	:	Urban Heat Island
UK	:	United Kingdom
USGBC	:	The U.S. Green Building Council
UTCI	:	Universal Thermal Climate Index
UV	:	Ultraviolet
$View_i$	:	Each value in optimal View outcome
$View_{max}$	:	Minimum value of View optimization set
$View_{min}$	:	Maximum value of View optimization set
VL	:	Vertical Louver
VT	:	Visual transmittance
W	:	Step width
WWR	:	Window to Wall Ratio
ϱ	:	Surface reflectance
ϱB	:	Surface reflectance Blue
ϱG	:	Surface reflectance Green
ϱR	:	Surface reflectance Red

Chapter 1. Introduction

1.1. General background

1.1.1. Building, energy, and human comfort

In recent years, climate change has grown to be a serious issue that demands attention from people in many different fields. Technology improvements that implicate many sectors have potentially increased the generation of CO_2, which is the only thing that may create the phenomenon of global warming. A massive human activity that involves cars or the burning of fossil fuels can directly increase the amount of CO_2 in the atmosphere. The greenhouse effect or, more broadly, global warming are terms used to describe this phenomenon. Every year, the environment receives about 3,3 billion tons of carbon dioxide. This process weakens the ozone layer and raises the earth's surface temperature progressively.

Global warming has raised global energy concerns in recent decades and has become a major study topic among researchers and practitioners. One of the causes of the crisis is the building sector, which generates 20%–40% of the discharge of carbon emissions. The recent COP26 meeting in Glasgow, Scotland, reminded us of a serious situation regarding global temperature rise, and the goal of achieving a zero-carbon society by 2050 was highlighted. 40% of overall energy use and 36% of total emissions of greenhouse gases in the European Union are attributable to buildings [1], whereas cities account for about 75% of global energy consumption [2]. More specifically, the thermal and visual performance of a proposed construction project is frequently linked to a variety of outcomes, including people's health [3] and the occurrence of the Urban Heat Island (UHI) phenomenon [4]. By 2050, it is predicted that cities will consume 75% of all energy, with energy use during the occupation period making up the majority of this. Additionally, it is predicted that world temperatures will rise by 1.5% and that construction needs will climb by 32%. The warming alarm and this circumstance would later cause the heat island effect, which would be harmful to human health and regional stability in general.

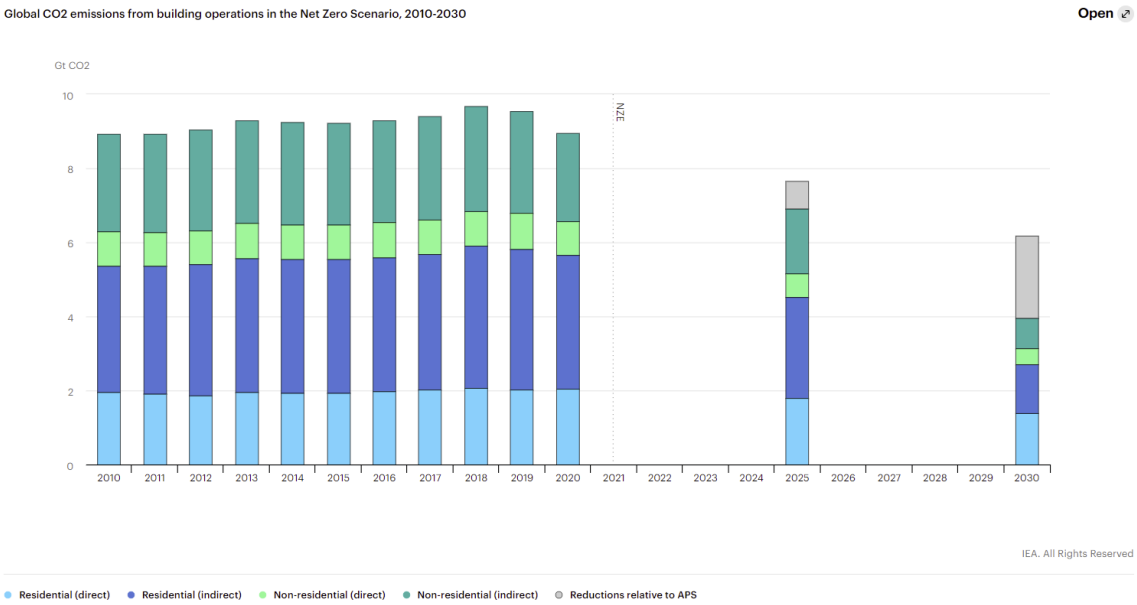

Figure 1.1 Global CO_2 emissions from building operations in the Net Zero Scenario, 2010-2030 [5]

However, according to the data from the International Energy Agency's (IEA) global energy assessment, the vision of growing carbon emissions from the building industry has improved in target proportion. Despite rising at a rate of 1% per year in 2010, a 9-billion-ton (Gt) decline is expected in 2020 [5]. This achievement shows that the building sector will achieve carbon neutrality by 2050. According to Figure 1.1, the residential sector was the largest source of carbon emissions each year, followed by the non-residential sector.

According to the bar chart, the peak was recorded in 2018 to reach almost 10 Gt CO_2. The trend was steadily goes down in two consecutive years of 2019 and 2020. The visualization indicates the expected situation after Net Zero Scenario is implemented. It is observed that the residential sector, both direct and non-direct are expected to have a significant reduction in carbon emission in 2025 and 2030. Overall, message from the measurement shows a tendency in improvement of CO_2 carbon emission before the Net Zero scenario before 2021, and after the implementation in residential sector presented by International Energy Agency (IEA).

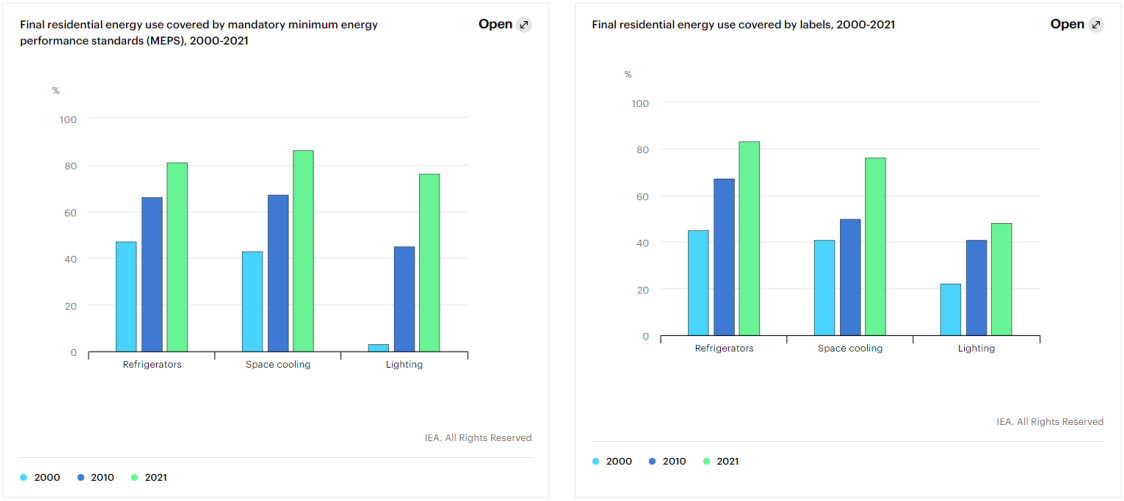

Figure 1.2. Report on final residential energy: (left) Final residential energy use covered by mandatory minimum energy performance standards (MEPS), 2000-2021, (right) Final residential energy use covered by labels, 2000-2021. [6]

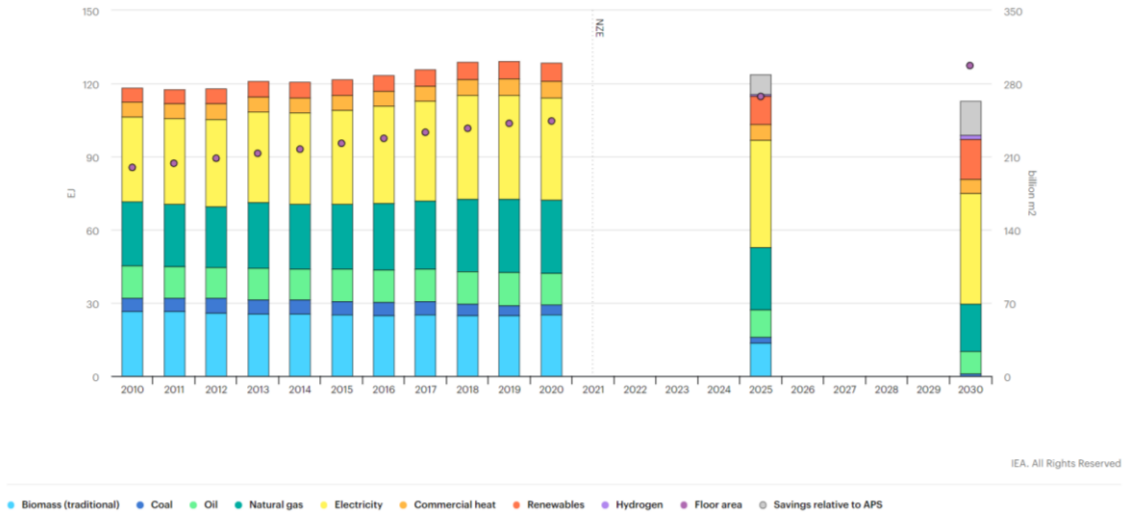

Figure 1.3. Global building energy use and floor area growth in the Net Zero Scenario, 2010-2030. [7]

Regardless the policy of mandatory in the application of minimum energy performance standard (MEPS), Figure 1.2 shows that the energy used in three labels named refrigeration's, space cooling, and lighting has been increasing in 20 years. Figure 1.3 shows that electricity accounts for the majority of global energy use, with natural gas

coming in second and biomass coming in third. By the end of the scenario, in 2030, the usage of coal and biomass was supposed to be reduced to a bare minimum, while renewable energy was supposed to be encouraged.

Because of its rapid transformation, the global climate is in a precarious state. Since 2010, improvements in energy efficiency and decarbonization have lagged behind the increase in demand for energy services in buildings, especially electricity to power cooling systems, appliances, and connected devices. The percentage of households with access to space cooling climbed from 27% in 2010 to 35% in 2020. Record-breaking high temperatures and prolonged heatwaves have increased demand for air conditioning in a number of nations. In actuality, 2020 tied with 2016 as the hottest year on record, and nine of the ten warmest Augusts (the month with the largest cooling demand worldwide) have occurred since 2009. During the summer of 2021, the average temperature in Asia was greater than 1.5°C above the pre-industrial norm, and a number of locations, such as Mexico (50.4°C on August 3, 2021) broke new records [5].

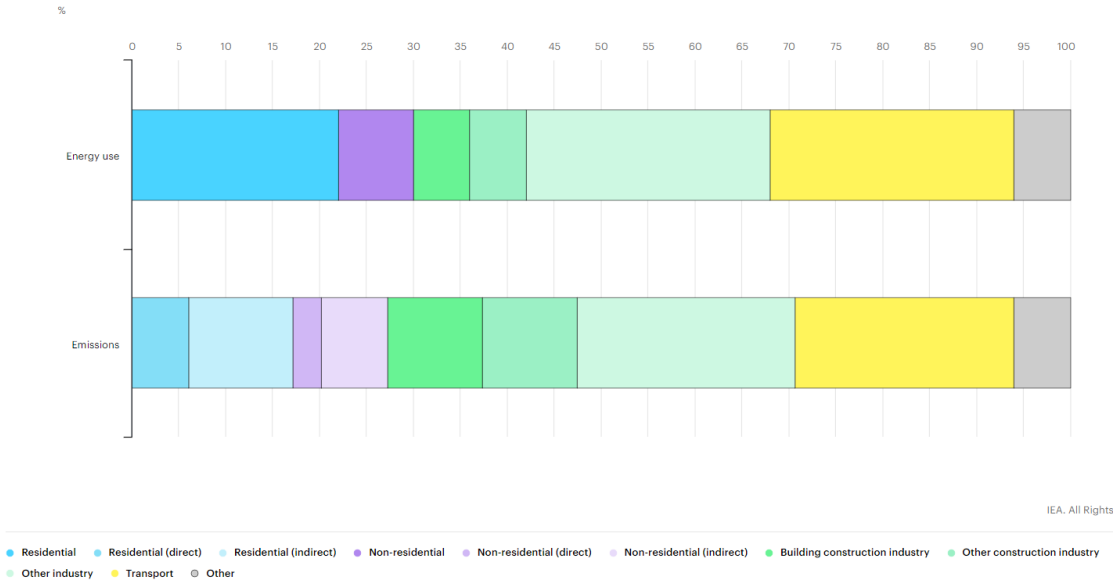

Figure 1.4. Global energy use and energy-related CO_2 emissions by sector, 2020. [8]

Figure 1.4 compares global energy use and carbon emissions categorized by sector in 2020. Building sector occupied about 25% in terms of energy used in line with emissions that recorded of about 24%. Almost all sectors have a similar percentage comparing energy use and emission except building construction sector.

Another argument is that, because of the impact of buildings on human health, the coming pandemic in late 2019 will have a detrimental impact on various areas, including economy, education, and human health [9]. Considering the pandemic situation, the design and construction industries ought to contribute to the improvement of the built environment. Architects, designers, researchers, and construction workers are primary stakeholders in determining the physical and psychological success of the built environment through strategic design and construction. Concerning the pandemic condition, both the physical environment and the psychological sensations of the residents' discomfort should be addressed. The policy protects human health by preserving the physical quality of the indoor and outdoor environments. Thermal and visual comfort, for instance, can be improved to assist people's daily tasks, such as by ensuring adequate airflow, the ideal temperature, and optimal light intensity. Moreover, enhancing daylight and ventilation through passive design is intended to be one of the primary design aims for preventing outbreaks and reducing the spread of microorganisms, germs, and viruses [10].

As a result, it is important to investigate how to avoid buildings from having a harmful influence on the environment and human health. To reduce harmful environmental impact, a so-called "passive design strategy" should be considered. When it comes to a consideration of passive design concepts, shading and building geometry in architecture are critical [11]. Engineers must think imaginatively to address climate change and challenges such as the pandemic, in addition to the issues outlined above and the carbon produced by companies. Toward the betterment of environmental aspect, low impact building design and construction have become a need in architecture. The passive technique can reach a high degree of energy consumption and human comfort and well-being efficiency, highlighting the significance of construction and operational cost reductions as well as health care expenditures.

1.1.2. Daylight, façade, and passive design strategy in early design phase

The universe of architecture and the built environment is being extended by daylight. When it comes to visual comfort, natural light and ventilation become critical. It's important to incorporate ideas for choosing the correct shading devices and orientation for the building to get the most out of natural light and heat. Natural light's value in creating a healthy indoor atmosphere cannot be overstated. The supply of daylight affects a number of things, including the occupant's health [3], visual comfort, and energy efficiency potential. In tandem with ecologically sustainable architecture design, the research of daylighting strategies becomes crucial. Given that people spent the majority of their time indoors [12,13], The supply of daylighting in relation to window shading and building orientation is necessary to enable passive design strategies. In this sense, a thorough analysis of the factors that favor passive design strategy is required. Despite scant and well-documented evidence of the connection to human health [14,15], daylight is an essential aspect that can favorably influence human health [16] providing evidence of improving work and lifestyle conditions [17]. Moreover, the correct daylighting technique can cut energy use [18].

Passive design strategy heavily depends on daylighting and natural ventilation. Shading devices' utilization is one of the approaches to achieving environmentally friendly design vision, particularly in achieving visual comfort. Numerous methods have been implemented to regulate daylight. Nonetheless, exterior and interior shading systems continue to be viewed as a key element in adapting to the continuously changing sky conditions [19,20]. Shading fenestration acts as a filter to limit daylight and solar radiation before it strikes the glazing surface and enters the interior of the structure. Thus, by implementing a shade strategy, only the intended and appropriate illuminance intensity and targeted solar radiation can reach working and living areas. These include aesthetics, cost-effectiveness, sustainability, energy efficiency, productivity and well-being, functional and operational efficiency, a comfortable working environment, and safety. External and interior shading systems have become the primary means of managing lighting and adapting to changing sky conditions. The shade fenestration acts as a solar

control device, eliminating unwanted sun illuminance while allowing only useful daylight illuminance to enter the working environment.

Incorporating shading devices serves a variety of purposes, including aesthetics, comfort, and security. External shade devices have been investigated and implemented in a variety of configurations, including vertical and horizontal louvers, perforated metal, shading inspired by folding and origami, venetian blinds, and expanded metal. Include the procedures for setting the building's shading devices and orientation to maximize daylight and natural heat. In addition, to produce an adequate amount of daylight illumination, it is necessary to consider exterior views and the physiological connection between the neighbourhood and the vegetation through shading devices [21]. It is expected that a suitable approach to daylight methods will promote visual and thermal comfort, allowing for the maintenance of the immune system through mental and physical experiences, as well as the eradication of undesired infectious organisms within buildings [10]. To prevent glare and filter only useful daylight that enters a room, louver shading has been widely implemented and developed worldwide. It is utilized primarily for aesthetic comfort, energy efficiency, and to enhance passive design, typically as a design element to reduce direct solar radiation before it strikes the window surfaces. With their regional and cultural approach, which encompasses various design patterns and a broad variety of materials, shading devices can be utilized for wide range purposes such as solar protection, structural support, and aesthetics.

Using computer simulation, the inquiry to optimize the design can be undertaken early on in the design process. The evolution of computational architecture enables the designer to intricate design-related computations. The computational procedure employs rigorous mathematical calculation, which may result in design optimization. The daylight forecast enables the architect and designer to optimize numerous aspects of design for comfort and efficiency. It is thought that shade is one of the most effective techniques to use passive design strategy [22]. The shading system can be the frontliner components in controlling solar to bring the useful intensity and reject glare and excessive radiation and heat during the summer period and at the same time ensuring heat to penetrates the room in the winter.

1.1.3. Advancement in computational architecture

The development of architectural computation has had a significant impact on contemporary architecture. The computer can perform and handle complex mathematical calculations that could lead to the production of extra ordinary design outcome. Thus, the outcomes produced by the iterative mechanism may exceed beyond the designer's imagination. So-called parametric design [23], considered as defining design with parameters, integrating how informatics solves the mathematical problem with an algorithm enables the architectural design process to be associated with design solutions of a high level of complexity and dependability via form-finding or solution generation.

The distinctions between traditional design process and parametric design depend on how the design phase is conducted. While the classical design tends to evaluate the design performance once the first alternative has been completed, the parametric design process is in opposite targeting the intended design performance at the early phase of design and creating the parametric system that driven by a set of parameters as a formulation to produced multiple individuals in which embed performance objectives. One of the benefits of its use is minimizing the negative impact on the environment where the building is constructed, such as reducing carbon from the energy consumption associated to the cooling and heating load, comfort sensation that impacts the health of people [3] and urban heat island phenomena [4]. For instance, the parametrical plus environmental study or platform can be utilized for the intention of increasing daylight performance or improving energy efficiency.

Moreover, this capability frequently coincides with the measurable design objectives to observed and find the desired building performance; hence, the quality of the design output could be empirically assessed and validated. In the 21st century, technology plays a crucial role in the design and building industries. As a result of its capacity to handle complicated design formulations, computational architecture is gaining popularity for boosting architectural practice. In terms of the design process and how people interpret contemporary architecture, this has a profound effect. The use of computational methodologies enables the optimization and iteration of previously inconceivable design choices based on desired performance through the automation process. The innovation challenges

design's data rather than its form. Consequently, the design must meet four requirements, including being complex, understandable, unpredictable, and appealing [24]. The primary distinction between traditional and computational or parametric design is the manner in which the design process is carried out. In contrast to the standard or traditional design process, which evaluates the design after it has been completed, the parametric process requires the targeted performance goals or value to be established early on in the design phase and the creation of source code as a generator for the iterative process or bottom-up approach. Advanced computational approaches were revolutionized and implemented in several design and planning activities, ranging from the purpose of predicting future performance of the building during the early design stage through simulation [25,26] to the post-occupancy evaluation. This advancement holds promise for improving design quality, particularly in terms of its impact on the environment.

The impact of digitalization on contemporary architecture has been enormous. Simultaneously, architecture evolves and demands complexity at every stage of its operations. "digitalization" or "computerization" is utilized not only for presentations and other visual purposes, but also for complex problem solving, analysis, and simulation. In certain ways, human sense is possible to be replaced by artificial intelligence or a machine in contemporary design. So-called parametric and generative algorithm, the design process that transforms and modifies the conventional design process from human, classical form-making to the possibility of automation, iteration, and form-finding [27]. From "simple to complex" and from "form to code" are two phrases that can be used to describe how architecture is developed in the contemporary world. From anticipating future building performance purposes to post-occupancy evaluation, these methods are utilized across the spectrum of study. Its utility is contingent on its capacity to manage complex formulations relating to design concerns. This innovation has transformed the static graphic primitive workflow into one that is highly controlled. To meet the stringent requirements of what a design is supposed to be and to address concerns of performance and efficiency, one of the correct steps to do is to utilize the powerful potential that is inherent in digital systems. The development of numerically controlled machining spurred the development of computer-aided design (CAD) systems, and the adaptation of sensor-enabled robotic

systems necessitates a rethinking of design processes and geometric representations in order to establish a stronger link between the computational model and the physical world [28].

A digital movement in design has been shifting the way designers and architects think. Through digitalization, the complex mathematical calculations required by the design criteria can be solved. Automatic design exploration has nowadays become possible by deploying the ability to read and process large amounts of data in a relatively short time, automatic design exploration nowadays become possible. Despite its association with extraordinary and ambitious geometry, this digital approach has the potential to generate and explore design variations that can further assist non-experts in collecting sufficient information-related design [29]. When the iteration and automation are conducted to gather information about the building's performance, a huge amount of design feedback concerning its performance can be obtained to observe the design that is possibly unexpected. Besides, multi-objective optimization (MOO) has recently become an approach in the built environment [30,31] to see the genetical trade-off between design objectives. Using such a technique, the environmental awareness design optimization process will be more robust, opening the possibility for a discovery in design efficiency. Multi-objective optimization (MOO) is a technique that uses genetic algorithms (GA) to generate the optimal design options empirically. The integration of MOO and building performance simulation (BPS) was used to demonstrate the possibility of achieving design objectives [32–35]. It is used to conduct an extensive investigation of design alternatives in order to identify high-performance solutions based on the intended design objectives. It is not only about appearance and output, but also about optimization and effectiveness. Along with the rise of low energy consumption in building performance challenges, the design process requires a heightened focus on efficiency at each step and in the establishment of specific objectives. The parametric design process lets you run the optimization scenario in the early stages of the design.

In structural analysis, parametric design evolved as the shift from manual and traditional design to parameter definition [36,37]. In addition to being able to generate

several designs based on the rules specified, parametric design can also tackle time-consuming and intractable design issues. Michael Hansmeyer's "Columns" project, for instance, provides an overview of the possibility of computer use in the construction of a fascinating column. Even though the computer cannot be parallelized with human capability, the experiment demonstrated that time taken is incredibly effective. In a 2012 TED talk, he reveals, for instance, that roughly 16 million facets may be completed in 35 seconds, whereas physically arranging them requires 200 hours. The phenomenon of computerization's progress has also contributed to the evolution of manufacturing, known as CAM (computer aided manufacture). This is a great improvement in production techniques, with an emphasis on closing the architectural detail gap. This enhancement makes it easier to control and alter the interaction between the virtual process and manufacturing. A data set generated during the virtual design phase can be sent straight to the manufacturing process as the primary data input.

1.1.4. Building performance simulation

A lot of work is needed in the first design phase due to the unexpected outcome and uncertainty about how the building will perform, especially in terms of daylight and how much energy it will use [38]. This investigation is needed so that an approximate solution can be found for approaching a realistic model complexity in the real world. Up to this point, it enables higher possibilities to come up with a solution that performs closer to the targeted design performance. In the early phase of designing, where the uncertainty of the design aspects is happening, the building performance prediction through simulation was conducted to support the decision-making process [2]. Building performance simulation, or better known as BPS, has two approaches to contributing to the architectural design phase. Firstly, it provides better design support if compared to the design that does not involve the BPS, and secondly, it supports information for further building operation and management. However, it does not only provide fix solution and that very often difficult to justified and ensure the solution because the term BPS is a complex task. Simulation of building performance has advanced the field of the built environment.

It connects the interest between a building's design phase and its operational phase. In addition, it can aid in predicting or calculating the environmental performance of a structure or site during the early design phase, when ambiguity regarding design produces almost exact findings. Consequently, with this advancement, the negative impact of the intended project could be investigated and reduced as early as the design process started.

1.1.5. Materials consideration (wood and expanded metal)

In addition to physical and energy-related performance, materials play a crucial part in determining an architectural object's carbon footprint. Compared to other building materials, wood is regarded as an environmentally friendly building material with a distinguishing characteristic. First, wood grows everywhere and is generally accessible in every region of the world. This availability decreases dependency on production and distribution systems and their ecological footprint. Second, the relatively rapid increase in regenerative availability offers greater accessibility compared to other materials, such as brick or concrete, that require more processing before they can be utilized. Thirdly, the material's light weight and modular shape make it more practical and relatively simple to process, whether in the factory or on-site [39]. This technique has been carried down for generations especially in Japan, which has a long history of employing wood as a key building material.

Japan is well-known for using wood as the main building material and the tradition has been inherited over generations. Besides, in architecture, wood is considered an environmentally friendly and sustainable building material due to its availability in all areas of this country. When compared with concrete or steel, wood is considered a more sustainable material because of its regenerative ability, which is much faster than the aforementioned two. What is more, the production of wood can be controlled by humans and the preparation tends to be cleaner and more practical [39]. One of the motivations promoting wood is that in collaboration with Meldia Research for Advanced Wood, the University of Kitakyushu has established a laboratory that has a specialty in wooden advanced research and construction. To fulfil one of the research agendas, the laboratory tends to design and build a two-story wooden house made entirely of wood that

furthermore become one of the subjects of this study. Wood has always been a valuable resource as an easily sculptable yet long-lasting material [28]. In addition, wood is a common building material. Wood has played a significant part in the history of the built environment since long before people began constructing structures. Wood is one of the oldest building materials on record. In addition to its traditional uses for aesthetics and durability, this material can also be employed to influence human psychology [40], give a relaxing sensation, and help to maintain an optimum living environment [41].

Japan has a long tradition of wood construction. In Japan, wood is more than just a building resource; it is also a cultural element. In this country, the usage of wood signifies respect for life and nature. The fact that wood grows organically sets it apart from nearly all other building materials. Wood possesses both physical and aesthetic properties. It is both an antique and modern material. Wood is a fragile and very sensitive material that necessitates extreme care in its handling and imparts a warm and important ambiance to a building as a result of its presence. The usage of wood also offers numerous benefits. It is simple to distribute and effective in assembly [42]. In addition, wood is a material that is available in both global and local markets [43]. Compared to other building materials, wood has a special character in terms of design uniqueness, as it is naturally grown, fully recyclable and an extremely energy efficient building material [44,45]. Considering the aforementioned features, the design of wood will continue to be a challenge for architects who wish to include wood into their designs.

Utilizing wood in building can minimize CO_2 in the environment [46]. It can also serve as a catalyst for an increase in environmentally conscious design and building practices. According to the nature-society interaction, wood is the only significant building material that is grown [43]. The original wood installed on the construction component will never have the same appearance or qualities as the other used wood components, otherwise it is industrialized and fabricated. Recently, the benefit of utilizing wood has also been linked to its possible earthquake resistance. In tandem with the development of Japanese wooden construction, Japan has endeavored to expand the use of wood in architectural practice. Japan possesses numerous varieties of wood that are primarily employed in building. The application of various types of wood is always determined by

the function of the component. Both structural and non-structural components have a specific and distinct function that required design considerations.

Among the numerous types of wood accessible in the country, one of the chapters of this thesis focuses on the usage of Japanese cedar wood, also known as Cryptomeria Japonica. In its native habitat, Cryptomeria Japonica is a fast-growing tree that can reach 55 m in height and 3.7 m in diameter. The trees are native to Japan, the highlands of southern China, and certain regions with considerable annual precipitation. Due to its rapid growth, Japanese cedar can attain a height of 7.6 meters in ten years. Along with the development of industries and wooden construction, Japan has pushed the use of wood as a key building material. The benefit of selecting Japanese cedar is that it grows rapidly, thus the price is reasonable. It is readily available because its habitat, lumber companies, workshops, and retailers are abundant in the majority of Japan's regions. Moreover, compared to other types of wood, such as Japanese cypress, this wood is lighter for use in building construction.

Discussing material consideration more in this thesis, among the systems and materials typically used for window shading, another chapter of this thesis focuses on expanded metal sheet, which has gained a great image as a modular material due to its adaptability and accessibility. A lengthy period of standardization, for example from the Expanded Metal Manufacturers Association (EMMA) as a National Association of Architectural Metal Manufacturers, follows the material's longstanding reputation (NAAMM). Due to its features, the expanded metal is unique. The material is regarded as highly effective and efficient in terms of its production process. Due to the material's industrialized market and production, it offers a great deal of versatility in terms of color, patterns, functions, materials, and types. Besides, it is durable [47] material that is recyclable and reusable. In addition, expanded metal has satisfied at least three critical aspects of the USGBC LEED Green Building rating system's key areas performance, such as "Energy and Atmosphere" where window shading protects the interior from direct sun, "Indoor Environmental Quality" where it provides a connection between the outdoor and indoor, and "Material and Resources" where it contributes to the material waste management system and availability on the local market.

1.2. Problem statement and research question

Even though the graph in Sub-chapter 1.1.1 shows improvement in global mission on the environmental considerations related to energy consumption improvement, the needs for the betterment of the building sector still have to be taken into account. Triggering the phenomena of global raising temperature, the building sector contributes to the 30% to 40% of total energy consumption. Engineers and designers are responsible for coming up with a recommendation and a way to design according to the vision of minimizing the detrimental impact on the environment during the design process of a building. Considering the high level of uncertainty during early phase architectural design process, designer often neglect design parameter that could mitigate future building performance and environmental impact thus design often subjectively implied with human ability that could not probably handle. Even though the application of parametric and multi-objective optimization strategies to environmentally friendly design vision has been the subject of extensive research and practice in the field of study, however, a comprehensive optimization approach from conception to the design solution ranking process has been described infrequently, and design parameters are often neglected during the early design phase.

The utilization of computation capability in exploring architectural design potential is still limited and challenging. Considering that in the early phase of designing, identifying design variables could lead to optimization and alternative observations to observe the potential for finding the best solution related to design. Although aspects like façade and geometry can still be computationally exploited, they are not considered globally. In the early 21st century computational advancements in architecture, engineering, and design have provided new insights into defining appropriate action into the design decision-making processes. Researchers and engineers work tirelessly to determine the potential of conducting computation approaches, and events have demonstrated that a quantitative approach that approaches the subjectivity of design improves building performance while limiting its environmental impact. In terms of regional context, this research raised the environmental setting in several sky and weather

data conditions of different cities, such as: Kitakyushu City, Japan; Jakarta, Indonesia; and Sydney, Australia, and Birmingham, U.K.

The computational technique has been shown to increase building performance and reduce the negative environmental effect of buildings. Several previously mentioned design-related aspects have been investigated using a parametric, automated design exploration, and building performance simulation strategy. In general, besides of the intention to confirm the ability of computational approach in optimizing design objective, the purpose of the method also is to reduce energy usage by maximizing daylighting and see the optimization of geometry material performance. In addition, structural and material stability and durability were crucial factors that needed to be addressed. While parametric and computer simulations have been used in the field of architecture, few studies have looked at the effect of design variables, such as façade design components, a specific material configuration, and irregular geometry, in achieving the desired design performance goals. The study about façade has been conducted using a parametric approach [23] and multi-objective optimization [48,49] as well as relate the skylight to energy consumption [50,51], geometry and urban form [2] related has inspired this main research intention. However, focusing on material and structure characteristics [52] as well as adopting a form-finding principal in giving design solutions connected to façade and geometry during the early design phase is still considered insufficient. Furthermore, because environmental performance simulation is context-dependent, this study attempts to introduce and propose a design technique for use in each region, as detailed in dedicated chapter.

To find a thing means to observe from numbers instead of a single option or choices. Therefore, to deal with a number of data is appropriate. The methodology proposed in this research is a development of a set of computational simulation incorporating parametric design approach in virtual environment as a hypothetical model which the design defined by parameter arrangement targeting optimize design objective that set from the early design stage such as human comfort, energy consumption, and structural consideration responding to a specific environment and material context, together with the introduction of a multiple analysis from autonomous design exploration and

optimization followed by statistical analysis. To give broader insight and enough range of design scale, several cases has been chosen from small scale of shading component to a role of geometry in driving thermal comfort and structural objective.

This study's research questions include, considering human comfort, energy consumption, and structural objectives, whether or not a parametric and generative algorithm platform proposed in this study can optimize building performance during the early stages of design, identifying tendency between parameters and objectives as well as finding the most influential parameters, and whether it can assist a designer or engineer in making design decisions. Consequently, the hypothesis of this study is that the proposed platform can optimize building performance simulation and aid stakeholders in design decision making, while the null hypothesis is that the proposed parametric and optimization methodology has no effect on building performance and offers no advantage in design decision making.

1.3. Aims and objectives

Responding to the problem that has been described above, a multi-level design parameter analysis in the early phase of the architectural design process through the development of thinking and platform using parametric and generative design exploration and optimization approaches to optimize building performance and identify the role of design variables will be applied to a hypothetical model. In broader sense, the aim of this study is to explore the utilization of parametric and multi-objective optimization (MOO) platform to improve design target performance concerning environmental factors by iterating a set of design parameters as dynamic variables during early stage of architectural design processes. In addition, the proposed methodology is meant to be used to investigate the tendency between design components which are parameters and design objective as well as identify the role of design dynamic variable. Besides, the purpose of this study is to explore whether the proposed methodology can improve design performance related to environmental consideration based on a specific given context.

Specifically, latter in each sub-chapter, purpose and intention will be varied and narrowed according to each topic that raised. In chapter 4, several scenarios have been

applied by the purpose of seeking the best louver shading configuration and room orientation that come up with best daylight performance. In chapter 5, the purpose of the experiment is to investigate and prove that the expanded metal can improve daylight provision when it is act as a window shading. In chapter 6, The purpose of parametric and multi-objective optimization (MOO) is to investigate the implication of building geometry and see the potential to improve outdoor thermal comfort together with reducing energy consumption. In chapter 7, the purpose of the study is to optimize the structure and daylight of the *Hyperboloid* wooden structure that is intended to be a two-story house and find which parameter combination perform minimum structural force with minimum cost.

1.4. Novelty and contributions

In the field of study, even though researchers and practitioners have done a considerable number of works on the use of parametric and multi-objective optimization approaches the environmentally aspect in the design [2,49,53,54]. This approach offers the multi-level investigation combining the identification of tendency, role of design parameters, and the value range in the most influential parameters driving the design objective, besides only to find the best solution from the optimization or exploration process. However, a comprehensive optimization approach from scratch to the design solution ranking process has still been limitedly reported. This thesis focuses on the use of generative and parametric approach to observe the relation between design parameters and design goals to draw an environmental and structural phenomenon, as well as discovering the best design solution through form-finding process together with the tendency and the parameter roles. In the thesis, we propose a different design optimization target that implied to a range of design scale. Aside from the research's main novelty and contributions that is to provide a comprehensive optimization method, which propose a new way in which to conduct form-finding processes, specific significance has been stated in each research study case. To be exact, for each main experiment, the research contributes novelty to the fields of study that described in Table 1.4.1.

Table 1.4.1. Research novelty and contributions

Scope and section	Novelty	Contribution
Main	The bigger idea of combining a parametric and MOO using specific regional context and material used	We propose several platforms to investigate the relationship between design parameters and design objectives, while simultaneously optimizing the design objective (target building performance). This contrasts with the traditional design process, which is relatively ineffective at identifying problem-specific information.
Chapter 4. Exploration of window shades and room orientations	Design exploration and optimization of simple and ordinary material of overhangs and louver. Components specific: Overhangs, and louver shadings. Context specific for: Sydney, Australia; Jakarta, Indonesia; Birmingham, U K; and Kitakyushu, Japan	We propose parametric and multi-objective optimization techniques and a platform that enable problem-specific data on the relationship between overhangs and louver shading and daylight performance to be obtained in a relatively expedient manner. It contributes to the shading-daylight design factor in the specified context.
Chapter 5. Expanded metal shading in relation with daylight provision	Design exploration and optimization ordinary material while have	We propose parametric and multi-objective optimization techniques for investigating

	longstanding reputation that is expanded metal Material specific: Expanded metal sheet. Context specific for: Kitakyushu, Japan	daylight by iteratively varying the design parameters that determine the expanded metal configuration's performance in daylight. A comprehensive study on the effects of this material configuration on daylight has still limitedly reported. It contributes to the design and production of this type of metal sheet as well as its use in a particular region.
Chapter 6. A novel geometry and the outdoor thermal comfort	Design exploration and optimization of a unique two story twisted cylinder house implementing *Releaux* triangle as the base profile. Context specific for: Kitakyushu, Japan	We propose parametric and multi-objective optimization techniques for iterating and optimizing a novel geometry form that could be constructed from wooden panels, examining the effect of its geometry on UTCI and energy consumption. This research is expected to contribute to the field of design by studying the connection between building geometry and outdoor thermal comfort and energy efficiency.

Chapter 7. Structural, cost, and daylight related exploration and optimization	Design exploration and optimization of a unique two story twisted cylinder house implementing *Hyperbolid* structure. Material specific: Japanese cedar 105 mm x 105 mm x 4000 mm. Context specific for: Kitakyushu, Japan	We propose parametric and multi-objective optimization techniques for iteratively and optimally optimizing the novel geometry of a Japanese cedar *Hyperboloid* structure. The proposed methodology combines structural and cost-effective objectives. By examining the relationship between dynamic parameters and geometry components and the structural stability of *Hyperboloid*, this research is expected to contribute to the field of study while enhancing the richness of Japanese wooden culture in architecture.

1.5. Thesis structure

The thesis divided into three main parts. First is the introduction consisting of Chapters 1 and 2, methodology in Chapter 3, and body of the thesis that consists of Chapters 4, 5, 6, and 7, and lastly the discussion and conclusion that is in Chapter 8 and 9. More specifically, this thesis consists of 9 chapters presented in Table 1.5.1.

Table 1.5.1. Thesis structure

Chapter 1. Introduction	The chapter discusses the research context that was offered in the broader perspective. In addition, problem

	statement, research scope, and objectives, originality and contributions of this research also described.
Chapter 2. Literature review	This chapter gives a list and explanation of the literature that serves as the conceptual foundation for this research effort. This chapter presents the most recent and pertinent research on parametric multi-objective optimization and building performance simulation. This chapter also includes a summary of the methodologies applied for this thesis. This chapter addresses the overall workflow, parametric platform, environmental simulation, and optimization method. Each subchapter topic will be introduced and concluded with a thorough and contextual explanation of the methods utilized.
Chapter 3. Methodology	This chapter provides an overview of the methods utilized for this dissertation. This chapter discusses the general workflow, parametric platform, environmental simulation, and optimization procedure. The chapter will introduce and conclude with a detailed and contextual explanation of the methods employed in each subchapter topic.
Chapter 4. Design exploration and optimization of louver shading devices and room orientation toward preferable daylight performance	This chapter presents a methodology for investigating the relationship between canopy, glazing ratio, louver or slat shading devices and room orientation, as it pertains to daylight performance. This chapter consists of three topics or cases, each of which describes a distinct technique to observing the role of louvres in daylight provision utilizing parametric and multi-objective

	optimization. In the first scenario, in addition to an approach for determining the optimal solution for louver shadings, room orientation was also considered. In the second scenario, a design exploration platform and two-story home were created to serve as a benchmark model for overhang and building orientation as dynamic design variables. In the third scenario, daylight performance and energy consumption have been analyzed in various towns located south of the equator.
Chapter 5. A Comprehensive parametric daylight investigation of the expanded metal sheet as shading devices	This chapter introduces a method for improving the configuration of a material with a long-standing and well-known reputation, expanded metal, as a shading device, with the intent of demonstrating that the material can improve daylight provision and serve as an alternative material for shading devices. This chapter is comprised of three study cases and one review of its application in a recent architecture project. In the first case, the expanded metal in Japanese Industrial Standard Japanese Industrial Standard (JIS) G3351 was simulated to identify which sort of standard performed the best in daylight. In the second case, a comprehensive parametric and optimization analysis was undertaken in Japan to demonstrate that expanded metal can meet the daylight credit requirements. In the third case, increased metal shading was the subject of a simulation on the daylight glare probability (DGP).
Chapter 6. Design exploration and	In chapter 6, the parametric and optimization procedure was conducted to observe the potential optimization in

optimization of twisted *Releaux* triangle geometry toward outdoor thermal comfort and energy consumption	energy consumption affected by the building geometry. The chapter tried to see changing in outdoor thermal comfort implicated by the geometry of two-story wooden house that adopted *Releaux* triangle shape for its base profile.
Chapter 7. Design exploration and optimization of a *Hyperboloid* wooden structure concerning cost, structural, and daylight objective	This chapter investigates the link between parametric simulation in terms of structure optimization and cost, as well as the daylight. This chapter presents a parametric and multi-objective optimization (MOO) strategy for optimizing a two-story timber *Hyperboloid* construction with iterative window ratio and orientation.
Chapter 8. Discussion	This chapter provides an overview of the situations discussed in the preceding chapter. This chapter will describe the contributions and standing of each case's research in the respective research domains. In addition, this research's limitations and recommendations will be discussed.
Chapter 9. Conclusion	This chapter presents a summary of the situations covered in the previous chapter. This chapter will describe the contributions and standing of each case's research in the respective research domains. In addition, this research's limitations and recommendations will be discussed. This chapter also summarizes the full parametric and multi-objective optimization platform that was applied to a specific instance based on the

	explanation provided previously, as well as each conclusion and analysis.

Figure 1.5 illustrates the logic behind this thesis. The main idea is to implement a computational approach in the early stage of architectural design to answer the research question of whether the approach will lead to the potential of optimization and efficiency. The computational approach will be conducted to four different cases targeting the objective of visual comfort, thermal comfort, energy consumption, and the structural objectives. The chapter conclusion will be answering the questions and revealing a deeper investigation such as the tendency among parameters and objectives, as well as the most influential parameters driving the design objectives in each case for instance in the context of daylight, energy consumption, and structure.

The final conclusion will answer, from all experiments, either or not the proposed methodology can come up with optimization and identify the tendency and role of dynamic variables or design parameters. In addition, seeking the reliability of the proposed approach, the final conclusion furthermore will be confronted with the research questions and hypothesis.

Figure 1.6 illustrates the structure of this research including the sib-chapter explaining a more specific study considering design target and cases. The diagram shows the sequence of the chapter where the logic of this research is implemented. The four experiment was conducted mostly following the proposed methodology explained in Chapter 3 that has been inspired by the recent research in the research field implementing parametric and generative algorithm to investigate and optimized environmental indicators as well as the structural consideration, responding to the research problems and questions that has been discussed in Chapter 1. The position of this research will be explained by comparing the findings and the existing research in the field. Lastly, based on the research findings, several factor and limitation will be described and followed by the recommendation for further research concerning the use of computational design and its factors that drive to the conclusion of the simulation aspects.

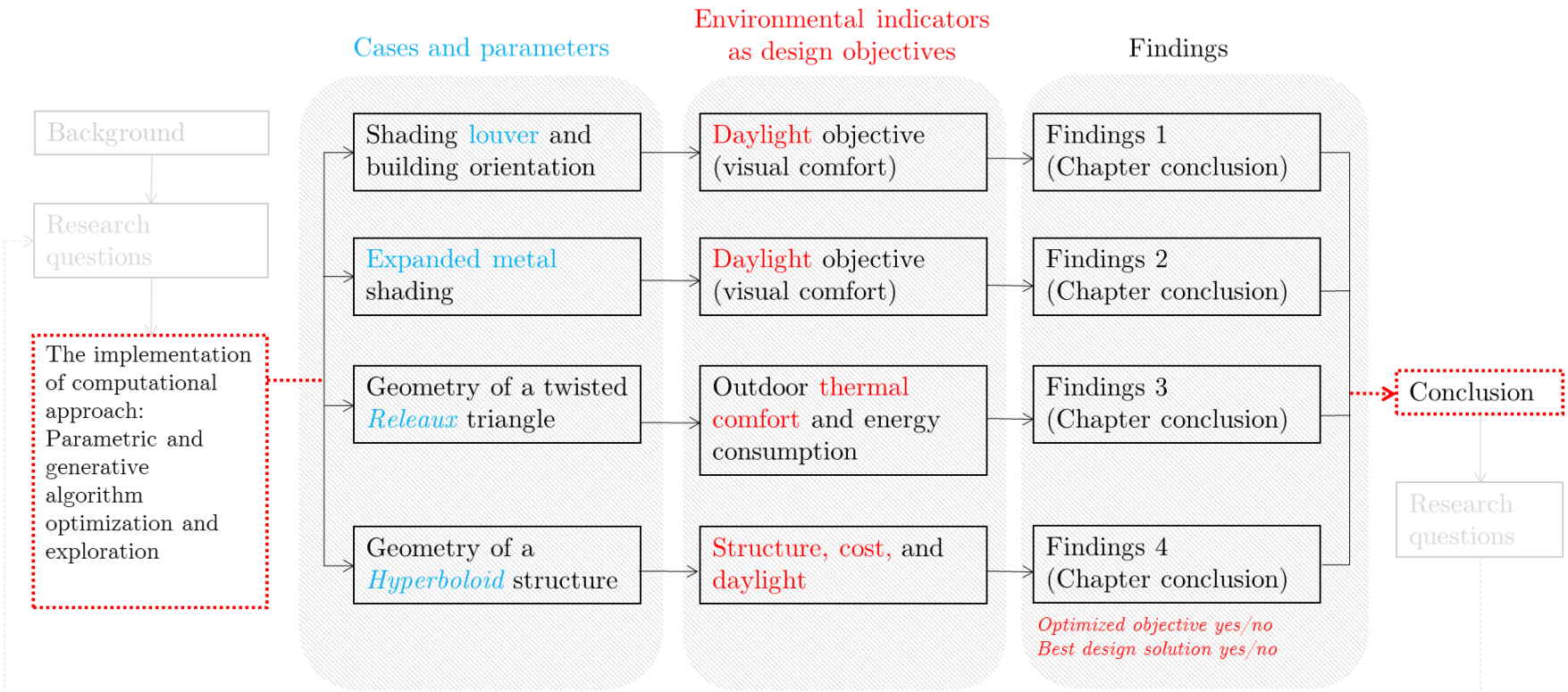

Figure 1.5. The scheme and the logic behind the thesis

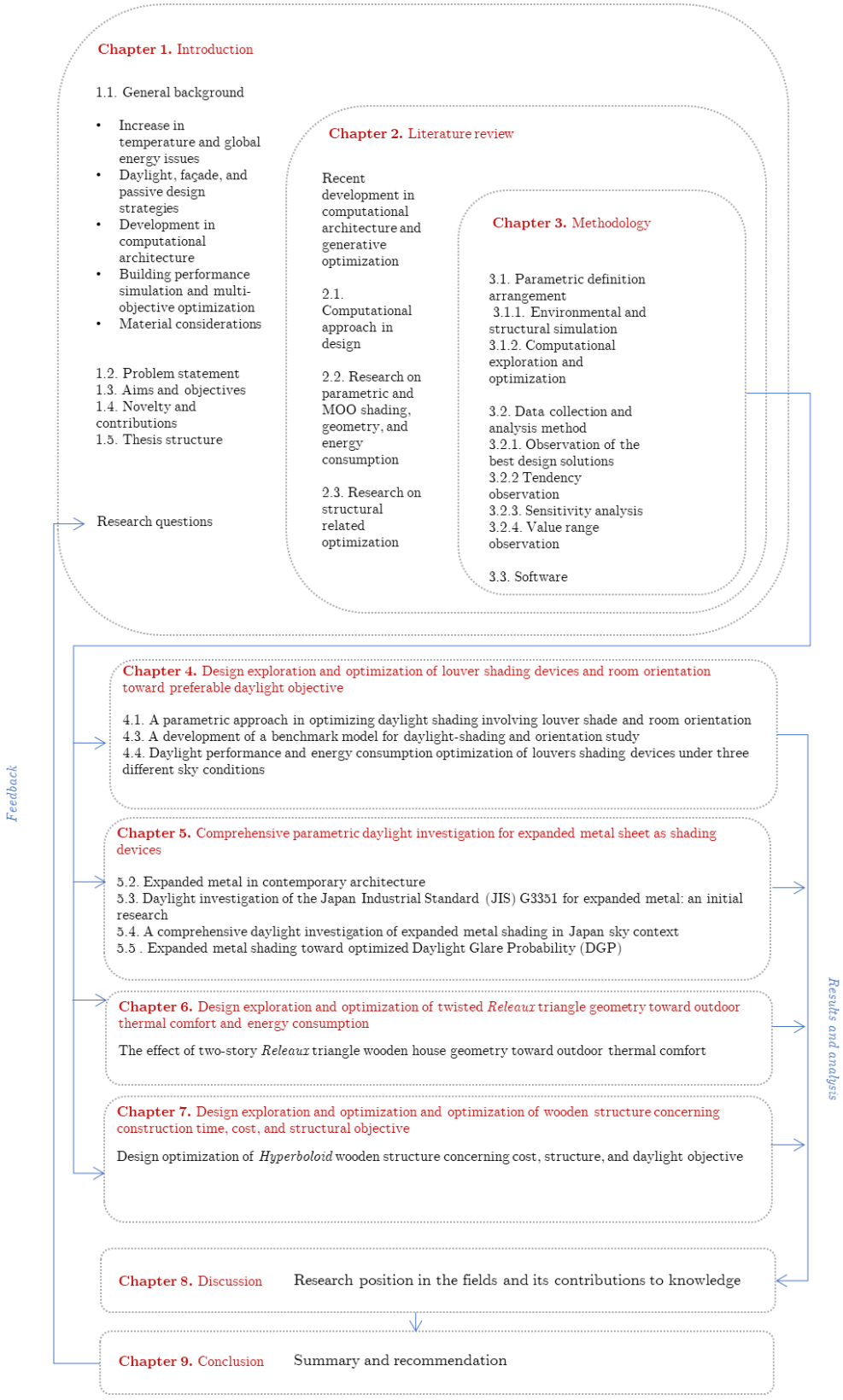

Figure 1.6. Research structure

Chapter 2. Literature review

2.1. Computational approach in design

2.1.1. Generative and Parametric Architecture

Technology plays a major part in the design and built sectors. Simultaneously, architecture evolves, and each stage of its operations requires complexity. Recently, the growth of computers, often known as "digitization" or "computerization," has had a profound effect on the world of design. Techniques are essential, not just for the presentation and other visual purposes, but also to illustrate the complexity of issue solving, analysis, and simulation.

CAD (Computer Aided Design) was introduced to architecture in the early 1970s. "From Simple to Complex" and "From Form to Code" are two phrases that can be used to characterize the evolution of architecture in the contemporary world. The growth of computers in architecture leads to a paradigm shift from classical to parametric design. This new improvement has transformed the workflow for static graphic primitives into one that is heavily controlled. To have such a suitable approach to design in the digital era, it is crucial to apply a standard. In order to reach the high standards of what a design should be and to address concerns of performance and aspects of efficiency, one of the proper things to do is to utilize the great potential inherent in digital systems.

Coined as “parametricism” by Patrik Schumacher, partner in Zaha Hadid, the style in architecture rebel old fashion in design process and it centers on free-form architectural concept. "Parametric problems can only be resolved with advanced parametric technology" [55]. The parametric method [56–59] gives a multitude of design alternatives that could not be developed using the traditional method. In addition to being able to create alternative designs based on the specified rules, the parametric is also capable of solving design challenges that would take an architect too long to tackle alone. The character comes from irregularity in shapes, curve, lines, and geometry. It is mostly defined in four distinct characteristic such as combining complexity and variety, thereby rejecting utilitarianism's uniformity, priorities involving urbanism, interior design, an architectural marvel, and even fashion that are shared, the principle that all design

elements are interdependent and malleable, and as a preference for algorithmic, computer-aided design [60].

Parametric design is a method of design in which building parts and technical components are created based on computational methods, as opposed to the conventional design process in which they are shaped physically. In this technique, the connection between design intent and design response is determined by criteria and regulations [61]. The term parametric refers to input variables or parameters that are fed into the algorithms. In article “Parametric Modelling as a Design Representation in Architecture: A process account” by Woodbury (2006), Propagation-based system, in which algorithms result in unknown final shapes based on prior parametric inputs, through a dataflow model and constrain scheme, in which final constraints are decided and algorithms are utilized to define foundations (structures, material use, etc.) that satisfy these constraints. The process eventually led to the terminology of "form-finding," where the process is performed within a propagation-based system. The design object is "found" based on these constraints [62]. The majority of parametric designs shown in 3D interactive views graph and nodes are represented by presenting the instance of the nodes associated with the current configuration of the graph's independent variables. The display algorithm is dictated by the node type: point nodes are displayed as points, line nodes as lines, etc [63].

CAM, or computer-aided manufacturing, has also emerged as a result of the occurrences of computerization's progress (Computer-Aided Manufacturing). This is a great improvement in production techniques, with the emphasis on closing the architectural detail gap. This enhancement makes it easier to control and alter the interaction between the virtual process and the manufacturing. A data set generated during the virtual design phase can serve as the principal data input for the manufacturing process. In other words, the management of global integrated processes in architecture is tight and even specific.

Parametric design leads to the paradigm of form finding rather than form making. However, Aish stated that not only bring the advantages in enhancing the way the architecture has been designing, but the process also has shortcomings such as the need

of in-depth knowledge related to informatics and requires more focus due to the ability in producing a bunch of design solutions [63]. The paradigm switched from manual design cycles to parametric design, which gives the designer access to a substantial amount of control and automatically generates variant design solutions and design goals [64]. It is currently accountable for mass customization among architects and construction industry professionals. As a result of recent advancements, it is thought that automatization, the replacement of human labor with computation, will increase efficiency in several areas, such as economics and energy usage [65].

Complex computations can be handled with a high degree of flexibility thanks to the control provided by parameters, which may result in an unexpected or unpredictable outcome. Furthermore, it has the potential to change the circumstances that lead to the greatness of freedom shape generation [66] open the possibility to come up with a high number of design production. The difference between classical design and generative algorithm design relies on its sequences during the initial phase of designing. Figure 2.1 compares the classical design process with that of parametric or generative algorithm design processes. Classical design tends to have a fixed design variable, despite the fact that it can be manually explored while remaining in the designer's visual imagination. The procedure began with the conception and was examined along the way to improve efficiency. When the results of the initial review do not fulfill the intended design goals, additional evaluations are done. When the second design fails to match the desired criteria, the design process is repeated. This procedure continues until the objective is attained and the desired performance is obtained. In contrast, generative algorithm procedures employ top-down methodologies. In contrast to traditional design, which places the goals at the conclusion of the process, the generative algorithm places the goals at the beginning of the process. Following the formulation of targeted objectives, the following stage is to establish the design parameters as dynamic design variables. The complete system is comparable to a collection of calculators containing a variety of functions or source code. The source code is utilized to determine the design variables leading to the optimal design solution.

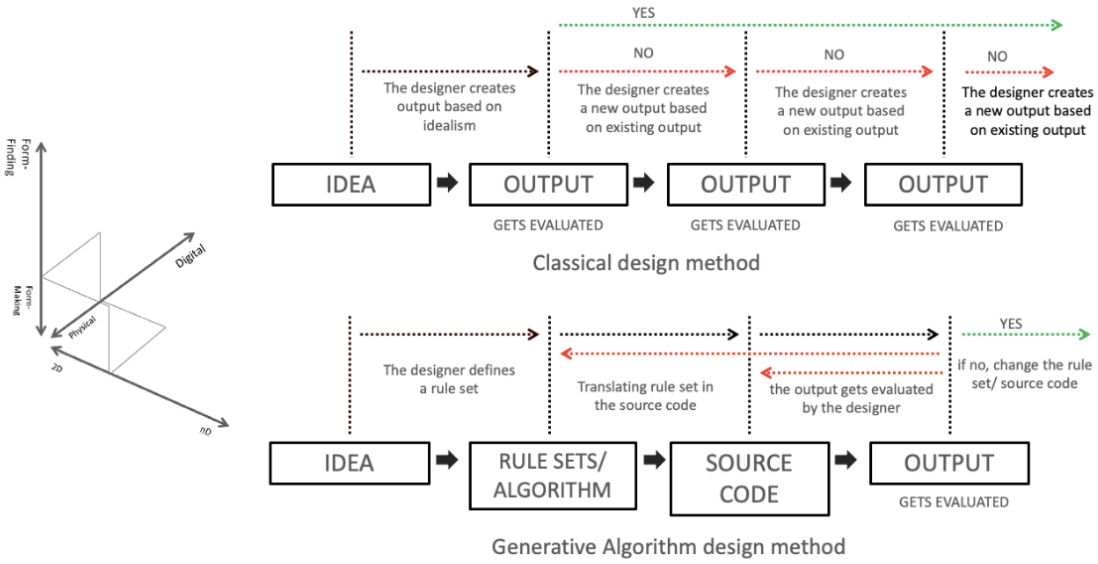

Figure 2.1. Classical design and Genetic Algorithm design processes

2.1.2. Evolutionary computation and Multi-Objective Optimization (MOO)

The evolutionary design method and evolutionary optimization are both motivated by the work of nature, by natural processes and by the creativity of nature in biological artifacts as the results of the most creative way called evolution. In terms of computation, the processes mimic this evolutionary process to make use of the creative process integrated in design thinking and computation in creative and innovative new design ways. Evolutionary computation is the mixture of evolutionary biology and computer science [67]. In this genetical system, survival of the fittest will reproduce itself and grow to the next generation. Thus, it reproduces genetic information. For example, in our body, this gene chromosome encoded in our gene structure that was survived a very long time ago and which was changed and manipulated, but this is basic information of life, and it tries to reproduce this in an algorithm. This kind of search process needs to formulate what the intention is or what we are looking for, and the algorithm tries to help to find the optimal design.

At the other side, what is called multi-objective optimization occur as the searching process deploying multiple phenotypes or parameters and multiple genomes or objectives. This framework consists of parametric model-based form generation, numerical assessment and simulation-based performance evaluation, and multi-objective optimization (MOO). These three elements are iterated to generate and evaluate a large number of design options. Several designers and researchers employ comparable methods to support integrated design [68]. In such a process, parametric modelling enables the association of building elements and the generation of multiple design options while maintaining predefined geometric relationships. Simulations allow for the evaluation of various design alternatives' facets. Among the design alternatives included in the process of optimization, those with superior performance can be identified based on specific evaluation criteria related to the design specifications [69].

Optimization processes and its systems used in this research applies Pareto front principal. The Pareto front, which is commonly accepted [70] and also known as Pareto frontier or Pareto set, is a set of all Pareto that have been considered efficient produced from generation processes in multi-objective optimization and enables observer to focus on the set of efficient options and make compromises within this set, as opposed to examining the whole range of every parameter.

2.2. Research on parametric and MOO shading, geometry, and energy consumption

Numerous researchers have been integrating shading and glazing strategy and employing parametric computational approach and Genetic Algorithm (GA) optimization to address the possibility of efficiency and optimization regarding daylight and visual comfort, and some of them have related this research to the efficiency of energy consumption. Bakmohammadi et al. [71] introduces parametric and optimization platform to see the best layout and glazing strategy of a classroom in responding climate condition in Tehran, Iran. The research uses Grasshopper as a main parametric platform to model the

classroom and ladybug and honeybee as environmental analysis engine to conduct the daylight and energy simulation. The simulation iterates glazing window to wall ratio, glazing number, wall angle and building rotation of the dynamic parameters. The study successfully reveals the best layout solution for the classroom at the same time open the possibility of 47.92 kWh/m^2 reduction of the energy consumption. Cachat et al. [19,72,73] in a range of research coupled the computational simulation, optimization, and field measurement through the model of PV integrated shadings devices to see the insight of the proposed computational system towards its implication in daylighting and energy strategies dedicated to the Nordic climate of Norway. The research reveals the smaller shading performs better in the given condition and the possibility of lower energy consumption up to 47.92 kWh/m^2. Elbeltagi et al. [74] conducting parametric approach to visualize and predict energy consumption of a simulated residential in Cairo, Egypt. The research resulted that the visualization could considerably benefiting designer in analyzing data related energy consumption. Besides the proposed system claimed to address energy prediction more accurately. Eltaweel et al. [23,53,75] in a range of research experimenting parametrically advanced louver slats and venetian blinds to predict the distribution of incident natural daylight intensity in 21st of selected moths in one simulated office room situated in Cairo and New Cairo, Egypt, targeting the steady distribution of daylight illuminance ranged 300 lux - 500 lux of 90%. The research concluded that the proposed parametric control system of the advanced slat louver and venetian blinds is promising to exploit the optimum targeted daylight performance. Fang et al. [76] Coupling a parametric framework to assess the daylight and energy performance of a simulated office space in Miami, Atlanta, and Chicago. By iterating dynamic characteristics such as building depth, roof ridge position, skylight width, skylight length, skylight location, south window width, louver length, north window width, and skylight orientation, UDI and EUI become the optimization objectives. The results indicate that the width and length of the skylight are the two most significant characteristics among those listed. Besides, the optimization has successfully increased the UDI value and on the other hand decrease the EUI. Gerber et al. [77] introduces multi-agent system in architectural design (MAS) to assist the designer to explore larger sets of informed

solutions parametrically combining generative algorithm and user light preferences. The finding of this research conclude that the proposed MAS can generate unique design configuration that perform environmentally better than the normative façade shading. Grobman et al. [78] Comparing static and kinetic toward the daylight performance targeting adjusted useful daylight illuminate (AUDI) oriented the 8 major orientation in Mediterranean climate. The result of this research shows that the dynamic strategies perform outweighs the seasonally adjusted shading by increasing the AUDI value of 51%. The results found out the specific value of each parameter that bring the optimum amount of daylight valuing 250 lux. Kim and Clayton [48,54] introduces parametric behavior maps (PBMs) to evaluate energy performance of climate-adaptive building envelopes (CABEs) to enables designers in conducting building energy and daylight-related simulation and analysis. The origami-like shading was applied in the small office situated in Houston, Texas as a controllable dynamic shading operation. The finding indicate that proposed method can be applied to simulate CABE and Both dynamic and static contribute to the optimum CABE performance. The use of the proposed system clamed to support architect and designer ultimately the decision-making process through well informed dynamic scenarios. Table 2.2.1 wrap up and remarks research investigating daylight through shading using parametric platform.

Table 2.2.1. Research utilizing parametric investigating daylight performance

Source/author/year	Parameters	Tools	Simulation type / Metric	Context and analysis period	Sky and room type	Objective	remarks
[79] Ayoub et al. (2018)	Elementary cellular automata	Rhino, Grasshopper, DIVA, Archsim	Daylight and energy consumption HDI, HEC, HSI	Hot-dessert climate of Alexandria, Egypt One year 08:00 am - 06:00 pm	Office	To assess the performance of the Elementary Cellular Automata patterns that will be utilized for dynamic shadings.	The adjustable façade outperformed the static shading solutions, allowing for sufficient natural daylighting while minimizing the negative effects of excessive solar penetration and minimizing

							energy requirements.
[71] Bakmohammadi et al. (2020)	WWR, Orientation, Glazing num, wall angle	Rhino, Grasshopper, Ladybug, Honeybee, Octopus	UDI, DA, ASE, DGP	Tehran, Iran, 21st March 2018 to 20th March 2019; 8 AM to 8 PM. 21st Dec (DGP)	School	To design a classroom arrangement in Tehran, Iran that maximizes the aesthetic comfort and energy efficiency of its occupants.	Enhancements in occupant visual comfort and reductions in energy usage for 47.92 kWh/m^2.
[72] Cachat et al. (2020)	Tilt angle of Louver integrated PV	Rhino, Grasshopper, Ladybug, Honeybee, Octopus	Thermal and Raytracing DA, sDA	Trondheim, Norway, June 2019 to August 2019		The purpose of the validation study was to predict the temperature and illuminance level of an 11 m2 room.	The model accurately reproduced the various illuminance dynamics, albeit not as precisely as a thermal simulation.
[73] Cachat et al. (2017)	Fix Louver-blade system integrated PV	Rhino, Grasshopper, DIVA	Daylight and energy DA, cDA, UDI	Trondheim, Norway One year		To determine the effect of the geometry considering solar altitude angles and solar irradiance of 48 m^2.	The blade angle affecting sensitively heating and cooling demand. Besides, the angle was improved cDA value.
[19] Cachat et al. (2019)	Angle of louver blades, Z coordinate of the center point of each blade	Rhino, Grasshopper, Ladybug, Honeybee, Octopus	Thermal, electric, and lighting cDA, DA	Oslo, Norway One year		To design and assess the performance different optimized configuration of a fixed exterior louver PVSDs.	The optimization process reveals that smaller louver were preferable and increased the PVSD performance.
[74] Elbeltagi et al. (2017)	Building length, Width, Height, Orientation, WWR	Rhino, Grasshopper, DIVA, Viper, TT Toolbox	Energy consumption, U-Value, SHGC, VT	Cairo, Egypt One year	Residential	Using parametric approach to provide new strategy in visualising and predicting energy consumption,	Parametric energy analysis has improved the accuracy of energy analysis and provides designer friendly data visualization.
[53] Eltaweel et al. (2020)	Azimuth, altitude, solar intensity, sky conditions,	Rhino, Grasshopper, Ladybug, Honeybee,	Daylight simulation UDI	Cairo, Egypt 21st of March, 21st of June, 21st of September and 21st of December	Office (Clear, Intermediate, overcast)	To offer three sophisticated daylighting designs based on parametric control of louvers with reflecting slats that can reach a daylight coverage of 90%.	The proposed louver design can provide generally consistent and distributed daylight coverage with a 90% range of 300 lux-500 lux.

[75] Eltaweel et al. (2017)	Conventional, parametric normal, parametric reversed, automated reversed, glazing materials, flat and chamfered ceiling	Rhino, Grasshopper, Ladybug, Honeybee,	Daylight simulation UDI	New Cairo, Egypt, 21st of March, 21st of June, 21st of September and 21st of December	Office	Propose a sophisticated integrated lighting system that combines many architectural aspects and can be parametrically regulated.	The use of integrated system can achieve satisfactory distributed daylight coverage with range 300 lux-500 lux of 90%.
[23] Eltaweel et al. (2017)	Venetian blind	Rhino, Grasshopper, Ladybug, Honeybee,	Daylight simulation UDI	New Cairo, Egypt, 21st of March, 21st of June, 21st of September and 21st of December	Office	To propose a control system of a venetian blinds to reflect the incident sunlight into the ceiling and respond to the sun altitude parametrically.	The study exploits the optimal use of natural daylight and provide shades simultaneously.
[76] Fang et al. (2019)	Consider skylight width, skylight length, skylight orientation, south window width, louver length, north window width, and skylight orientation.	Rhino, Grasshopper, Ladybug, Honeybee, TT Toolbox	Daylight and energy simulation UDI, EUI	Miami, Atlanta and Chicago, The U. S One year	Office	To propose a parametric optimization process to help designer evaluate the daylight and energy performance and generate optimized design.	When compared to the typical performance value, the UDI increases and the EUI decreases after the optimization process. The most essential elements are the width and length of the skylight.
[77] Gerber et al. (2017)	Number of windows, Glazing ratio, Number of panels, Percentage of panel types, panel length, panel extrusion, extrusion type, generation angle.	Rhino, Grasshopper, Ladybug, Honeybee,	Daylight simulation DLA, CDA, UDI	Los Angeles, California, The U. S One-year, extreme day 9.00 a.m.– 6.00 p.m.	Office	To create and evaluate a design process that allows designers to experiment with a wider number of solutions by combining generative design tools.	The MAS design system can develop unique design configurations that outperform the normative in terms of environmental performance.
[78] Grobman et al. (2020)	Orientation, shading depth, type (horizontal, vertical, and diagonal)	Rhino, Grasshopper, DIVA	Daylight simulation AUDI	Mediterranean, 21st of March, June, September December at working hours 8.00 a.m. 6. 00 p.m.	Office	To present an assessment and comparison between static and kinetic shading toward daylight performance using parametric approach.	The dynamic shading performs better that the seasonally adjusted one. The proposed design increased the AUDI by 51%.

[22] Hariyadi et al. (2017)	Sudare	Rhino, Grasshopper, Ladybug, Honeybee,	Daylight and energy simulation, OTTV, UDI, DGP, Watt/m2, kWh	Jakarta, Indonesia One year	Office	Identifying an additional style of facade arrangement employing external horizontal blinds based on the Sudare shape in order to achieve the minimal requirement of Indonesian National Standard (SNI).	The best form of the Sudare blind, with a diameter of 10.01 mm and spacers of 5 mm, lowered OTTV by 5% and thermal energy consumption by 6% relative to the benchmark building.
[54] Kim et al. (2020)	Degree of CABE openness	Rhino, Grasshopper, Ladybug, Honeybee, Octopus	Solar radiation simulation W/m^2	Houston, Texas, The U. S Yearly, Seasonal, Monthly, Daily, Hourly	Office	To Introduce parametric behaviour maps (PBMs)	The proposed system enables designer to integrate the energy performance of CABE that leads to design process improvement.
[48] Kim et al. (2020)	Degree of CABE openness	Rhino, Grasshopper, Ladybug, Honeybee, Octopus	Daylight and energy simulation sDA	Houston, Texas, The U. S Hourly, Daily, monthly, weekly	Office	To achieve energy saving and high-comfort daylighting conditions with the use of CABE and PBM	Both dynamic and static factors contribute to the optimal performance of the CABE. The use of the suggested technology is claimed to support the decision-making process of the architect and designer through well-informed dynamic scenarios.
[80] Konis et al. (2016)	WWR, Building footprint and massing, windows, and exterior shading.	Rhino, Grasshopper, Ladybug, Honeybee, Octopus	Daylight and energy simulation sDA, EUI, sUDI, kWh/m^2	Helsinki, New York, Mexico City, Los Angeles September 21 from 9 AM to 5 PM	Office	To show how the Passive Performance Optimization Framework (PPoF) can be used to optimize daylighting, sun management, and ventilation.	The result shows that PPOF can reduce Energy Use Intensity between 4% and 17% while simultaneously improving daylighting performance between 27% and 65%.
[81] Ma et al. (2016)	Glazing area/ window size	Rhino, Grasshopper, Ladybug,	Daylight and energy simulation UDI,	Beijing, China		To find the window area on each wall to maximize the	South and Noth direction ware the best for minimizing

		Honeybee, Galapagos	Lux, J			UDI, and minimizing energy consumption	energy consumption, in terms of daylight, vertical, square, and horizontal is by order performed the best.
[82] Mahmoud et al. (2016)	Rotation of a hexagonal kinetic façade, WWR	Rhino, Grasshopper, DIVA	Daylight simulation, Lux	Cairo, Egypt March 21, June 21, September 21, and December 21 at 9:00 am, 12:00 pm, and 3:00 pm.	Office, Clear sky conditions	Through the lens of morphology, this study investigates the kinetic composition possibilities afforded by moving facades.	Results demonstrate the analysis of rotational and translational kinetic motions at an early stage of design, as opposed to a conventional window (base case)
[83] Mahdavinejad et al. (2017)	Room dimension and fillet angle	Rhino, Grasshopper, Ladybug, Honeybee, Galapagos	Daylight and energy simulation, UDI, kWh	Tehran, Iran One year	Office, Overcast sky	To determine the optimal fillet angle of the curved office building facade in order to increase UDI and reduce energy consumption.	The best fillet angle 177.66° is the best in maximizing UDI, while 110° is the best for minimizing thermal energy consumption.
[20] Mangkuto et al. (2019)	Blind's type, slat angle, blind material secularity	Rhino, Grasshopper, DIVA	Daylight simulation sDA, ASE, DGP	Bandung, Indonesia March 24, 2018, at 10.30-12.30	Office (Overcast sky with 64% cloud cover)	To illustrate the application of computational daylight modelling to optimize interior shading device based on many daylight parameters.	The results shows that metrics used in this research are all can satisfy the design criteria.
[20] Marzouk et al. (2020)	Skylight shape, Shape and Opening Ratio (SRF)	Rhino, Grasshopper, DIVA, Octopus	Daylight and energy simulation sDA, ASE, UDI, kWh/m2	Cairo, Egypt One year	Museum	To suggest energy and daylight enhancements using various skylight layouts and applicable technology.	Reduced cooling load by an average of 6.5% and increased UDI by an average of 133%.
[84] Moghadam et al. (2020)	The depth, angle, and quantity of interior light shelf shelves	Rhino, Grasshopper, Ladybug, Honeybee	Energy simulation PPD, TE (kWh/m^2)	Mashhad city, Iran One year	Residential	Examining the influence of all light shelf design parameters and employing MOO to determine the optimal light shelf design for achieving optimal thermal	Reduce the overall energy consumption for heating, cooling, and electricity by 25,819 kWh/m2, 49,176 kWh/m2, and 34,853 kWh/m2.

						comfort and energy consumption.	
[50] Motamedi et al. (2017)	SFR of skylight	Rhino, Grasshopper, Ladybug, Honeybee	Daylight and energy simulation sDA, UDI	San Francisco, The U. S One year	Office	To propose algorithm to find optimize skylight design to save energy consumption.	The recommended ratio of skylight to floor is 5,5 to 6 percent, reducing energy demand by 19%. Certain percentage with energy efficiency which ranged 3-14%. 5-10% SFR provide adequate daylight and avoid glare.
[85] Naderi et al. (2020)	Shading location, dimensions, angle, and material	Energy plus, jEPlus þ EA through NSGA-II	Energy and visual simulation TE, PPD, DGI	6 Iranian cities One year	Office	This research aims to demonstrate how a multi-objective simulation-based optimization of architectural requirements and control parameters of a smart shading blind can be carried out.	Compared to the benchmark design, the proposed optimization technique reduces annual total building energy consumption by between 2.8 and 47.8%, DGI and PPD indices by between 15.5 and 69.9%, and DGI and PPD indices by between 8.5 and 56.3%.
[86] Naji et al. (2021)	Wall, roof, glazing's component, window size, glazing factor	TRNSYS, jEPlus +EA	Daylight and energy simulation TDH, DUH, LCC	8 Australian cities One year	Residential	To develop multi-objective optimization framework that to minimise TDH, LCC and DUH in 6 climate zones of Australian cities.	Reduction in TDH 6-55% and the reduction for LCC 27-31%.
[87] Pilechiha et al. (2020)	WWR, Window dimension, window location.	Rhino, Grasshopper, Ladybug, Honeybee, Octopus	Daylight and energy simulation ASE, sDA, QV, EUI	Tehran, Iran One year	Office	Develop a technique for optimizing office The objective of window design (position and area) is to reduce energy consumption while increasing daylight and visual performance.	The increase QV genome for 1%. EUI improvements 12%. The design system of windows should be modified to conform to the standards.

[88] Rabani et al. (2021)	Glazing and construction envelope ratio of window to floor area	IDA-ICE, GenOpt	Daylight and energy simulation DH, DF, PPD	Oslo, Norway One year	Office	To offer a system that automates the approach for determining the optimal combination for minimizing energy consumption while maximizing thermal and visual comfort.	The results demonstrated that the inclusive optimization technique might cut building energy consumption by up to 77% while simultaneously enhancing thermal and visual comfort.
[89] Rizi et al. (2021)	Rotation angle of slate's edge, occupants' position	Rhino, Grasshopper, Ladybug, Honeybee, Octopus	Daylight and energy simulation UDI, kWh/m^2	Tehran, Iran March 21st, June 21st, Dec 21st 10:00 PM. 13:00 PM, 16:00 PM	Office	The purpose of this study is to present a multi-criteria design strategy for shading devices that includes fading protection as an evaluation criterion regardless of geometrical complexity.	76% improvement in visual comfort, 60% improvement for the heat gain, and a 59% improvement achieved when compared to the benchmark model without shading.
[90] Rocha et al. (2020)	Depth of the fins, distance of the shading device from the façade, width of the fins, height of the fins	Domus, Daysim, sp-MODEII optimization toolbox	Daylight and energy simulation EnerSav, PUV, UDI300 2000, DA lux300, Uav	Rio de Janeiro, Brazil, Working hours	Office	To present a multi-criteria method for the design of shading devices, including fading protection as an evaluation criterion, regardless of geometry complexity.	The proposed method is an effective process for constructing optimal shading devices to reduce energy consumption, optimize daylight usage, and prevent fading.
[91] Samadi et al. (2020)	Louver slats 3D rotation and 2D movement	Rhino, Grasshopper, Ladybug, Honeybee, Galapagos	Daylight simulation UDI	Tehran, Iran December 21, June 21, September 21, and March 21.	Office	To construct a shader that allows the movement and rotation of deployable shading units to be controlled in order to maximize the amount of daylight entering a building.	Utilizing this proposed shading system under ideal conditions can considerably improve the effectiveness of indoor daylight.

[92] Samuelson et al. (2016)	Building shape, building rotation, WWR	BeOpt		Beijing, Shenzhen, New York		Using parametric whole-building energy simulation, propose a system for developing early-design recommendations to advise architects and policymakers.	When designing for several energy objectives, such as (a) reducing Energy Use Intensity, (b) minimizing peak-loads, and (c) boosting passive survival, synergies and trade-offs were discovered.
[93] Tabadkani et al. (2019)	Rotation motions, indoor view angles, time hours and transmittance properties	Rhino, Grasshopper, Ladybug, Honeybee, Galapagos	Daylight Simulation UDI, DGI, DGP	Tehran, Iran 21st of March, June, September, and December at 12 P.M.	Office	To examine the development process of ASF based on parametric design techniques, with a particular focus on its visual comfort indices via a configurable shading system.	The proposed technique considerably increases the shade system's adaptability for controlling visual comfort.
[94] Thanh et al. (2021)	South, North, East, West, South-East, North-East, South-West, and North-West or the cardinal directions.	Rhino, Grasshopper, DIVA	Daylight and energy simulation sDA, ASE	Ho Chi Minh City, Vietnam, One year	Office	Develop an innovative concept for an Origami-inspired shading device based on dynamic sunlight that can be used to improve the daylight performance of a target building while reducing its energy consumption.	The results demonstrate that the proposed kinetic device operates brilliantly, as it helps the building achieve 2.3 LEED v4 points in four unique directions: north, north-east, south, and north-west.
[95] Toutou et al. (2018)	WWR, Glass material Wall construction, Shading width, Shading count, Shading rotation	Rhino, Grasshopper, Ladybug, Honeybee, Octopus	Daylight and energy simulation UDI, SDA, EUI	Helwan, Egypt One year	Residential	To examine the potentials of parametric design optimization over the residential building to obtain a more sustainable design, as well as the computational design methodology in the design process, in order to activate the	SDA value was 84.11, an almost 110% improvement from the base case design, and EUI was 166.01 kWh/m2, a reduction of around 3.5%.

						computer's involvement in the design process.	
[96] Vera et al. (2017)	CFS rotation angle	mkSchedule, GenOpt	Daylight and energy simulation sDA, ASE, kWh/year	Santiago (Chile) Montreal (QC, Canada) Boulder, Colorado, Miami One year	Office	To optimize an office's fixed exterior CFS component	The key conclusions are that a CFS that is optimized purely for overall energy usage fails to achieve the visual comfort parameters.
[97] Wagdy et al. (2015)	WWR, number of louvers, louvers' tilt angle, screen depth ratio, and reflectivity of the screen	Rhino, Grasshopper, DIVA	Daylight simulation sDA300/50 %, ASE1000/250 h, DGP	Cairo, Egypt One year	Classroom	Examine the impact of a variety of solar screen configurations on daylighting performance.	The simulation results revealed a pattern of converging solutions beginning with a 1:1 depth ratio and sloping downwards.
[98] Wagdy et al. (2016)	Slats curve, venetian blinds	Rhino, Grasshopper, DIVA	Daylight simulation SDA, ASE, EVF	Cairo, Egypt One year	Hospital, Clear sky	Under a predominantly clear sky in Cairo, Egypt, deciding the shapes of horizontal blind slats that complement the style of a regular hospital patient room layout.	According to the sDA bed surface criterion, the variety of permitted slat shapes was greater than that of the room as a whole. The ASE performance of each studied slat shape was satisfactory.
[98] Wagdy et al. (2017)	Sun-breakers WWRs, the angle of tilt (h), and the angle of cut off (a).	Rhino, Grasshopper, DIVA	Daylight simulation SDA, ASE	Cairo, Egypt One year	Hospital, Clear sky	To identify the fundamental properties of sun-blocking materials that could be utilized to regulate solar access into hospital patient rooms under clear-sky conditions.	All evaluated WWRs for the two patient room layouts with cutoff angles ranging from 50° to 54° with the wall provided efficient daylighting performance.
[99] Yun Kyu Yi et al. (2018)	Kirigami	Rhino, Grasshopper, DIVA	Daylight simulation	Champaign, IL, US January		Building energy simulations are used to demonstrate a strategy for capturing the complexity of physical characteristics in novel materials.	

[66] Zani et al. (2017)	Incision depth, d/D factor; Upper and lower angle rotation (from 0° to 25°)	Rhino, Grasshopper, Ladybug, Honeybee, Octopus	Daylight and energy simulation DA, sDA, UDI, kWh/m^2	Milan, Italy 25 Feb 12:00, 21 Mar 12:00, 1 April 12:00, 15 April 12:00, 21 May 13:00, 21 Jun 13:00	Office	To build a high-performance concrete static shading system based on numerous criteria such as radiation control, outside view and daylight indexes, and energy performance, employing a computational design method and genetic algorithms for optimization.	The findings show that by employing this method, it is possible to build an efficient shading system that can manage radiation throughout the year while still ensuring a high level of outdoor perception and visual comfort.
[25] Zhang et al. (2019)	WWR, building materials, shading devices, etc.	Rhino, Grasshopper, Ladybug, Honeybee	Energy simulation W/m^2	Beijing, China Nov. 15 to Mar. 15 Jun. 1 to Aug. 31	Residential	On the basis of a case study of a Beijing residential construction project, demonstrate an optimization workflow and its effects.	The investigation found that optimizing the spatial form and building envelope parametrically during the design phase is a promising strategy for reducing residential building energy consumption.
[100] Zhang et al. (2017)	Considerations include orientation, room and corridor depths, window-to-wall ratios at various interfaces, glass materials, and shading types.	Rhino, Grasshopper, Ladybug, Honeybee, Octopus	Daylight and energy simulation DA, cDA, UDI, ASE, DAmax	Tianjin, China 1st of November to the 30th of April	School	To show the application of simulation–optimization tools in determining the optimal trade-off between decreasing summer discomfort time and maximizing Useful Daylight Illuminance while minimizing heating and lighting energy use.	The energy consumption for heating and lighting can be lowered by 24–28% and summer thermal discomfort by 9–23% while simultaneously increasing the UDIavg (100–2000 lx) by 15–63%.
[101] Zhao et al. (2020)	Building orientation, window and shading system configuration, including materials for each layer of a	DesignBuilder, NSGA-II	Energy simulation kWh, h	Hohhot, Tianjin, Shanghai, Guangzhou	Office	To present an easy-to-use, practical, and effective multi-objective optimization strategy for minimizing	Pareto optimum solutions can present designers with a variety of scheme options based on preferences,

	double-layer window, installation angle, and overhang depth					energy consumption in China's diverse climatic regions.	which is extremely useful for providing guidance and suggestions to designers throughout the early stages of building design.
[102] Zhu et al. (2020)	RTB shape (width, depth and height), and WWR	Rhino, Grasshopper, Ladybug, Honeybee, Octopus	Daylight and energy simulation UDI, sDA, PPD	Tianjin, China One year	Tourism	Propose a plan for better understanding the situation of RTBs in northern China and supporting scientific design for improved RTB performance in terms of energy conservation, indoor daylighting, and thermal comfort.	Overall, the method contributes to the scientific design of RTBs, and the data presented here can guide the development of RTBs in northern China and other similar regions.

2.3. Research on structural related optimization

Besides the intention in minimizing detrimental impact of the building to the surrounding environment, the use of MOO also give advantage in investigating structural-related performance. Yi K.Y. et al. [103], investigated skylight roof system for structural integrity, daylight, and cost of materials. Yi created a way for integrating a MOO system into a truss system, taking into account structure compression, tension, and displacement, as well as cost and daylight performance. The results demonstrated that MOO was able to identify a number of solutions that met the design objectives, with the post-MOO identifying solutions by rank. Pan et al. [69] proposed a design method that applied flexible parametric model, interdisciplinary assessment utilizing MOO to explore the roof of sports arenas. The system was arranged considering the basic spatial composition of arenas. The used criteria include view quality, acoustic, and structures. The outcomes of the case studies indicate the effectiveness of the method and the necessity of incorporating diverse structural solutions into the greater design area. Brown et al. [104], employed MOO investigating finite element structural modelling and building energy simulations

to optimized building geometry. The results showed how MOO can produce extraordinary architecture expression, high-performing designs, as well as provided a new insight into specific design response to the environmental condition. Yang et al. [105], proposed an innovative simulation-based multi-objective optimization method which constructed in an interactive optimization problem re-formulation, aimed at achieving a realistic MOO model. The outcomes demonstrated that the proposed strategy could produce quantitatively superior and qualitatively more diversified pareto solutions. Dzwierzynska [106] used the form-finding method in Rhinoceros, presented algorithmically-assisted curvilinear steel bar roof structures. Results indicated that the use of generative design might be enhanced to build structural shapes that are both strong and aesthetically pleasing. In another research, Dzwierzynska et al. [107] developed a unique, scientific, and practical way for creating roof shells composed of Catalan surface modules. Using Rhinoceros 3D, the study linked the roof's geometry to its structural analysis and optimization. The study concluded that the simulation allowed for the evaluation of different roof shell forms and the selection of the optimal option. Bande et al. [108] analyzed parametric design, construction, and energy impact of a villa in Al Ain, United Arab Emirates. Comparing the 2020 full-year electricity bill to the proposed methodology's structure, the results indicated a 10% reduction in energy use and an increase in the Universal Thermal Climate Index (UTCI) were seen. Chi et al. [109] used parametric tools to optimize adaptive shadings in an open public space in Mexico. The environmental simulation and optimization used to reduce the UTCI and resulted in an improvement of thermal comfort of 3.9, 7.4, and 3.1°C at 8, 12, and 16 h in the summer and 1.4, 3.5, and 2°C at 8, 12, and 16 h in the winter. Emami et al. [110] integrated structural and environmental performance assessment of perforated concrete shell construction in Boston, U.S. The approach was meant to solve the question of how design parameters influence performance and what the performance trade-off is. Results indicated that the perforation ratio was the most influential parameter on structural and environmental performance, and 10% to 20 % was recommended for shell structures when translucent glass is fitted without shades.

Danhaive et al. [111] used generative modelling and artificial intelligence, a design collaborator was created that enables designers to intuitively discover design possibilities without using automated processes. The findings demonstrated that the design subspace learning produced by the research provided a new paradigm for performance-informed design exploration and a navigable map for exploring the design options that can influence the designer's design decision-making process. Focusing in *Hyperboloid* structure, Dzwierzynska [52] incorporated Grasshopper and Karamba 3D, the Genetic Algorithm (GA) and MOO were used to optimize hyperbolic paraboloid roofs for the best structure in terms of division. The results demonstrated that MOO does not always provide an obvious optimal solution, especially when the expected requirements are incompatible. However, it is able to estimate potential solutions and choose the most advantageous ones. Khoraskani et al. [112] used Grasshopper, Karamba and SAP2000 to investigate the influence of form factors on the structural response of the structure to lateral loads, such as the ratio of width to height; the ratio of ground floor to roof diameters; the horizontal and vertical segmentation of the DiaGrid system, and others. He [113] proposed a computationally efficient global-local optimization platform for optimizing a truss layout of bridge structure using Peregrine in Rhino and Grasshopper environment. The results of He's research suggest that layout optimization is considerably efficient for identifying the structure with less material used. Besides, the proposed platform allows a rapid observation in the early phase of conceptual design process. Cascone [114] proposed a diagrid-inspired configuration for tall building structure. The results suggest that the parametric formulation helps to extend the proposed configuration to be applied easily to any building geometry and size. Besides, it was confirmed that the proposed procedures able to define the patterns that perform better performance compared to normal diagrid. Quaglia [115] presented a multi-objective shape optimization methodology to balance energy efficiency and structural performance to a military deployable shelter. The results suggest the finding where the methodology could come up with reasonable option of design that has minimum deflection and thermal energy load. Besides, according to the comparison with single objective optimization, the multi-objective one clearly indicated the compromise between two single objective individuals.

Chapter 3. Methodology

3.1. Parametric definition arrangement

This chapter explains the general overview of the methodology used in this thesis that furthermore will be implemented in more detail according to each given cases in the dedicated chapter. Based on the pragmatism research philosophy, where knowledge is constantly questioned and interpreted rather than being fixed, the process is classified as computer simulation research methodology, deductive or quantitative approach especially using parametric [63] and generative algorithm [56]. This is due to the fact that the experiment involves a large number of calculations and design configurations that are only possible in the virtual world rather than the real measurement due to cost and limited time consumed. In general, the experiments conducted to construct this research were conducted in 7 consecutive phases.

As it can be seen in the figure, the process begins with the ideation in which the scratch is intended to respond raised issues in certain background and answer research question. The first phase is ideation when the issue is formulated. In this phase the information and background behind each experiment is collected. The ideation phase meant to respond the research aim and answering the question in the first step of scenario. The ideation process will lead the process to the production of experiment scheme or experiment design. The ideation process concludes with the decision of what is simulation type to be arranged together with what is parameter and design goals to be used.

The ideation process followed by the categorization where, in this thesis, the intention is divided into three distinct research idea which are investigate shading-daylight related, investigating geometry-related outdoor thermal comfort, and structure-cost investigation and optimization. Next phase is the process in defining design parameters and performance objective of each research idea. Each process started by defining exactly what is the design parameters and the design goals, together with is metrics. After the parameters and the objective is decided, the process followed by the arrangement of making parametric geometry modelling. In this phase, fist arrangement and dynamic parameter in the parametric platform is built.

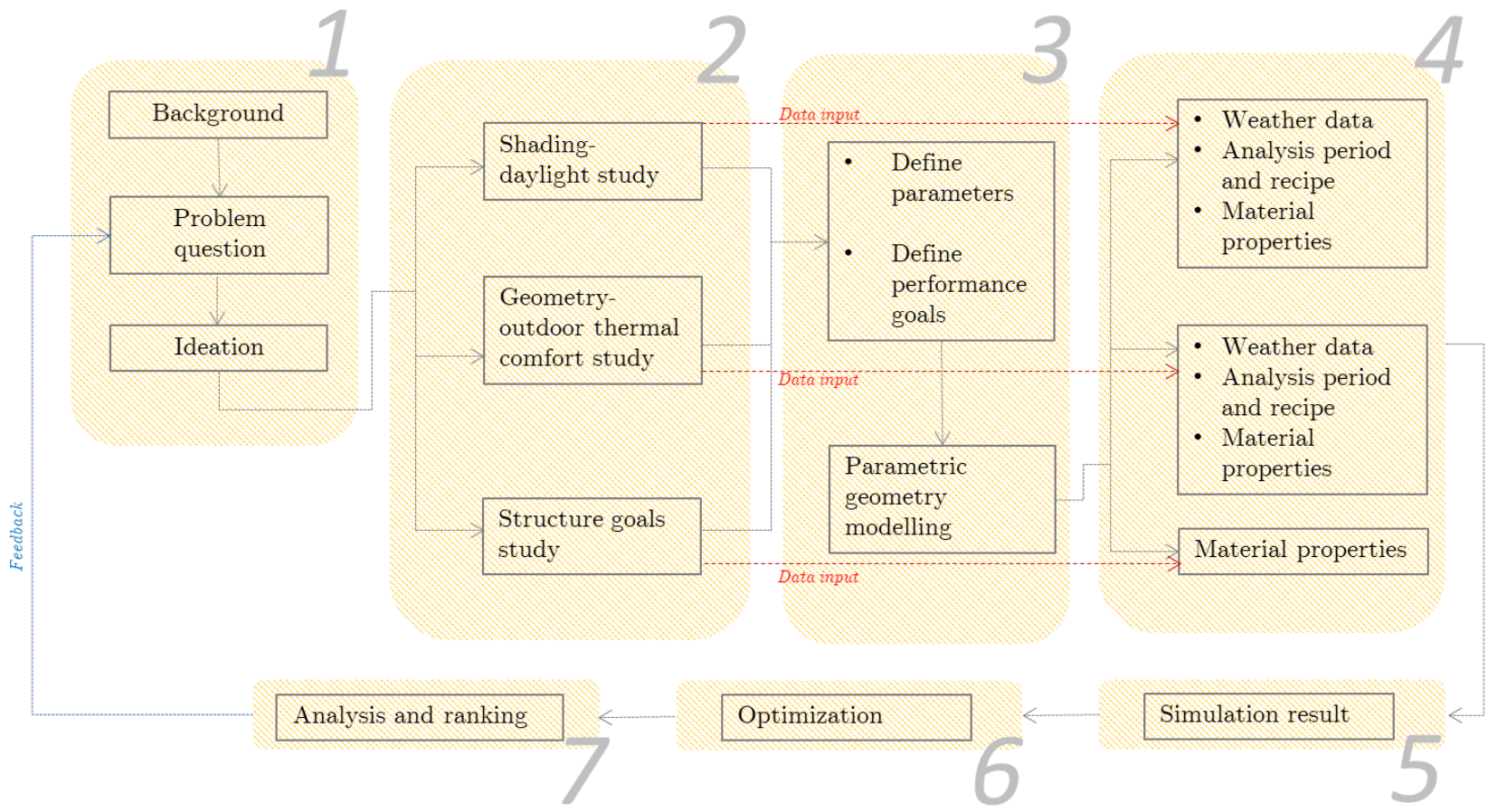

Figure 3.1. General workflow of this thesis

Each parameter is set to be a value range that have certain number of movements in which in the generation profess this value range become the trigger to move the iteration continuously. The design objective is a certain value from the simulation that produces based on the component functions provided in the software, for instance, environmental analysis function in Ladybug and Honeybee, and structural analysis in Karamba.

The further process is the making of environmental or structural-related parametric definition, where the weather data and material properties become a data input and then calculated and simulated. The simulation will produce single design solution according to the built parametric definition. This single results furthermore become the feed in the exploration and optimization processes. The last step in data analysis and visualization. The results based on analysis furthermore be confronted with research question and objectives.

In the first phase of ideation, this research raised the issues that have been discussed in the introduction chapter yet more to the utilization and deployment of computational architecture in responding to the environmentally friendly global design vision. The research aims, objectives, and questions are distributed into each sub-chapter. In the second phase, the idea was broken down into three main intentions that translated into four chapters. The idea of daylight-shading related experiments has various approaches distributed into different chapters. Chapter 4 studied the louver, window glazing ratio, and building or room orientation, while in Chapter 5, the dynamic parameter was proposed for expanded metal shading. The daylight metrics were different in each case. In Chapter 6, the idea of investigating outdoor thermal comfort was conducted by iterating the parameters of building geometry. In Chapter 7, the idea of optimization was translated into the investigation of structural strength and cost by iterating dynamic parameters, which were the *Hyperboloid*-driven components.

3.1.1. Environmental and structural simulations

Looking at Figure 3.1, in phase 4, environmental (daylight and energy) and structure-related simulation is conducted. Weather data used is EnergyPlus weather data (EPW) file that provided by EnergyPlus. In Chapter 4, the simulation uses weather data and

analysis period as an input for mimicking or representing sky condition and temperature. The weather data used in this chapter including the weather data for Jakarta, Indonesia. Besides, the other experiment also simulated sky and temperature for Sydney, Australia; Birmingham, U K; and Kitakyushu, Japan. In Chapter 4, 5, 6, and 7, EnergyPlus material library is applied to represent the properties of wall, ceiling, glass, and floor, while some of experiment using adiabatic material. Except in Chapter 7, the material properties are inputted manually to be a feed for Karamba.

In phase 3, the dynamic design and objective of each experiment are decided, and the geometry modelling process is conducted. In this phase, the parametric definition is intended to form movable and changeable geometry according to a set value range. The number of dynamic parameters varies depending on the object that will be made. In Chapter 4, a parametric system is conducted to generate and iterate parameters such as window to wall ratio (WWR), canopy length, louver rotation, louver division, louver size, and room orientation. In chapter 5, the components that shape expanded metal, such as bond, length, height, angle, and strand, were set to be dynamic parameters. In chapter six, the parameter is the component that constructs a *Releaux* triangle-based cylinder to shape a two-storey wooden house. The parameters used in Chapter 6 are radius 1, radius 2, twisting factor, roof slope, rotation (orientation), height, U-panel, and V-panel. In Chapter 7, the parameter used is the component that shapes a wooden structure, forming a *Hyperboloid* structure. The parameters are radius-bottom, radius-top, twisting level, roof slope, wooden bars number, offset distance, and height.

3.1.2. Computational exploration and optimization

Looking at Figure 3.1, in phase 5, the automation produces single design solutions for each parameter movement, together with embedded parameter combinations and design objective value. Each single value produced by each experiment in general becomes a data point or individual in the optimization process in phase 6. In phase 6, iteration adopted two different systems both exploration and genetic optimization. The first is the genetic algorithm for multi-objective optimization (MOO) using Octopus and the second is design exploration using Colibri.

Statistical analysis and manual observation are both conducted to identify the best among the best solutions from the filtering process in phases 6 and 7. The final results yielded from this last phase will be confronted with the research objective and research questions such as: the optimization of daylight in the experiments of Chapters 4, 5, and 7; the best UTCI and energy consumption in Chapter 6; and the most cost-effective and most stable *Hyperboloid* structure at the same time in Chapter 7.

3.2. Data collection and analysis method

3.2.1. Observation of the best design solutions

The parameter and other data input of the environmental and structural simulation are calculated in the parametric platform yielded a series of number as rough data. Each experiment results in a series of numbers. The generative process during the optimization and exploration are set to record the data of parameters and objective to an excel or comma-separated-values files. As the original visualization in the software used, the data formed in variety of plots. The original data from Octopus come in 3D to 5D population field while the data from exploration process may formed as parallel coordinate plot. The rough data in excel or comma-separated-values files furthermore being processed, visualized and analysed through both manual and statistical analysis to observed mainly the relationship between parameters and also the role of each parameter.

As one of the research's aims to discover the best design solution through iteration process, the observation process is conducted in multiple ways. The first mechanism is the manual observation for both optimization and exploration process such it is demonstrated in Sub-chapter 4.1., 5.1., and Chapter 6. In the results of multi-objective optimization, the observation uses reinstate solution function in Octopus while in the exploration process in Colibri, manual observation is conducted by highlighting the wires in the desired objective value.

The second approach finds the best solution by ranking the MOO's pareto front solution and the colibri exploration. The ranking process is conducted using the fitness function as it is adopted in [51,80,87,116] calculation in excel as it is implemented in

Chapters 4, 5, and 7. The formulation is applied to each case specifically according to its unique data findings, parameter conditions, and design objectives.

The difference between the manual observation and the fitness function calculation is the use of ranking, where the desired solutions tend to be objectively presented in series, while the manual one is limited to the human visual sense. Besides, the results from fitness function are quantitively produced. Means it can be observed objectively and justified by number or value.

3.2.2. Tendency observation

The tendency observation is conducted to see the relationship between design parameters and the design objectives as well as among the design objectives in the context of multi-objective optimization (MOO). The benefit of using this type of observation is that the relationship can help the designer in analyzing in which parameter range the generative process leads to the desired value of the objective range. The observation is conducted through the manual drag and drop function of the parallel coordinate plot that filled up with lines or wires connecting each individual's parameter and design objective combinations, as it is also used in [25,26,93,117].

The parallel coordinate plot is formed of the entire data yielded from optimization process that is plotted in Phyton based plotting software called Jupyter Lab launched in Anaconda. The data only distributed based on its maximum and minimum value range of each parameter and objective vertical axis that has been recorded during the genetical optimization process. The manual observation is directed to the density that shows the distributions of each solution's parameter and objective values. By dragging the control points in the observed vertical axes on the plots, the swarm or dense density of the wires and lines that connects the parameters and objectives value will show the distribution of value that only focus in that certain area, indicating the tendency could be analysed in this dense area.

3.2.3. Sensitivity analysis

To identify the most implicated parameter driving the design objectives, sensitivity analysis is conducted [25,34,118]. Knowing which parameter that have the most implication benefits the designer or operator to only focus of treat more these parameters to obtain more optimized design objective.

The sensitivity analysis was performed by implementing an SRC to measure the *t*-test to study the role of each parameter on the objective values and evaluate variable relevance. The SRC was conducted using the analysis software JMP, using the fit-model command to look for parameter estimates, with each standardised objective defined as a role variable and each standardised parameter set as a construct model effects.

The sensitivity analysis results will be presented in tornado plots that shows the value of SRC distributed along horizontal axis showing whether it is implicating positive or negative directions. Each bar of the tornado plots illustrates how much influencing is the intended parameter toward the objective as a role. In terms of parameter-objective correlation context, the process is applied to justified value besides the option, therefore the identification could be carried out more deeply.

3.2.4 Value range observation

After the most influential parameters are identified, each parameter will undergo closer observation to see in which value range influencing the desired objective value is concentrated. The value range observation is conducted using the statistical analysis software JMP utilizing analysis the function and will furthermore be illustrated using box plot. The value observation conducted in Sub-chapter 5.4.

The advantage of finding the value range from the most influential parameter is that where the design intention will be followed up more, for instance for future research or design intention, the designer can only focus on the specific range which have shorter value spectrum to be able to come up with more optimized results. The findings from this micro-observation can be applied to different context of relationship, not only see the specific range that lead to optimization, also to avoid range that seem not to have any implications in optimization procedures.

3.3. Software

Figure 3.2 illustrates the distribution of software used in this thesis. The main software for the modelling process is NURBS-based 3D modelling, called Rhinoceros, and a plugin called Grasshopper. In the environmental simulation phase, the system utilizes plugins called Ladybug and Honeybee. The two programs are included in the set of Ladybug tools, which were developed to simulate environmental considerations such as human comfort, wind, radiation study, etc. In order to simulate structural simulation, a plugin called Karamba was used.

The optimization and exploration process uses different scenarios and software. For single-objective optimization, a component in Grasshopper called Galapagos was used, while the multi-objective optimization process used Octopus as a genetic algorithm engine. In contrast to the previous two processes, the Colibri from Thorton Thomasetti plugin was used to generate all the possibilities that could be produced by parameter combination. The details of each software description will be discussed in each experiment in the dedicated sub-chapter. In phase 7, resulted data from optimization processes is analyzed and ranked. The software used in data analyses are statistical analysis software called JMP, Phython-based data visualization Jupyter Lab in Anaconda launcher, and Microsoft Excel.

In this thesis, the combination of software was used according to the needs of the experiments as well as based on the intention of what kind of data to be presented. For examples, the multi objective optimization used where the number of design solution is expected to be significant. It is due to the fact that in MOO, not all parameters value will be iterated. The iteration runs according to the Pareto principals or genetical calculation that will lead to only best solutions among the individuals. In opposites, design exploration in Colibri was conducted where the expected solutions are not too many. It is possible to be conducted because design exploration process tends to iterate all possible solutions and equipped with no capability of searching best solution genetically. At the end, a set of software is used based on the constrains that was implied for each experiment.

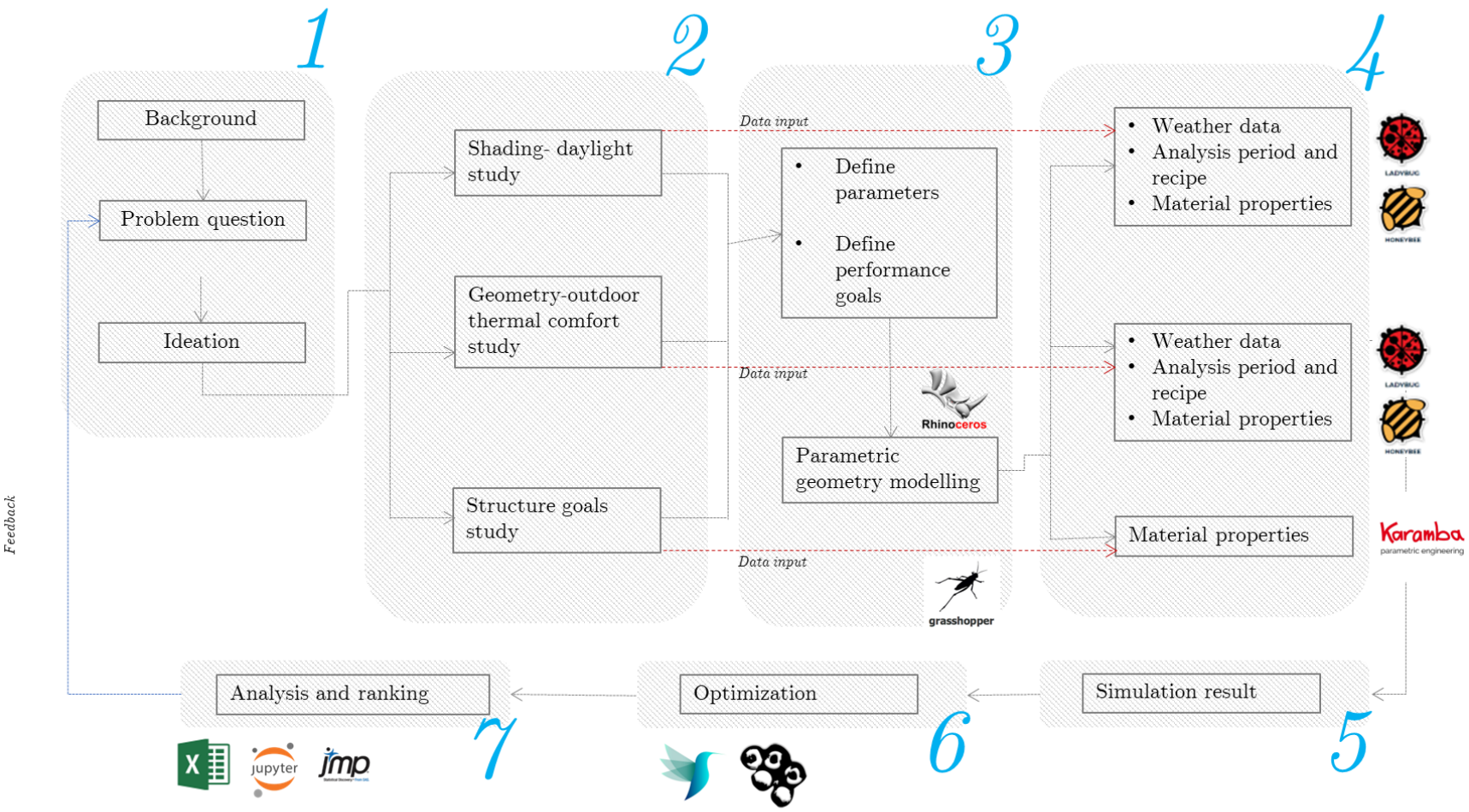

Figure 3.2. Tools used in this thesis

Chapter 4. Design exploration and optimization of louver shading devices and room orientation toward preferable daylight performance

4.1. A parametric approach in optimizing daylight shading involving louver shading device

4.1.1. Introduction

This sub-chapter focuses on computationally determining the optimal daylight performance with respect to the application of louver shading in Jakarta, Indonesia. This study seeks to identify the probably best louver design element with optimal targeted useful daylight illuminance (UDI) distribution within a simulated environment.

The goals are to organize the parametric definition for the overall simulation and design exploration processes and to map and analyze the design solution generated by the iterative process. The results are expected to provide an understanding of how the arrangement of louver shading would affect the daylight distribution within a space given a certain context and analysis time, as well as a recommendation as to which arrangement is optimal for the specific circumstance.

The research in this sub-chapter will undergo environmental analysis to investigate parameter-objective relationship utilizing louver shading to respond sky condition of tropical hot humid area using design exploration in Colibri and analyze the best design solution showing the configuration of louver shading in responding given sky context.

4.1.2. Methodology

4.1.2.1. General overview

This part of experiment incorporates a parametric-based computational design method [75] to calculate and explore daylight performance design ideas measured in useful daylight illuminance (UDI) metrics. The initial step began with the generation of ideas and was followed by the specification of the dynamic parameters as a design variable. Parametric definition creation employs EnergyPlus historical data known to as the EPW file of Jakarta, Indonesia in order to calculate and evaluate daylight performance [119]. Figure 4.1. Research workflow illustrates the workflow used in this sub-chapter.

4.1.2.2. Geometry modelling

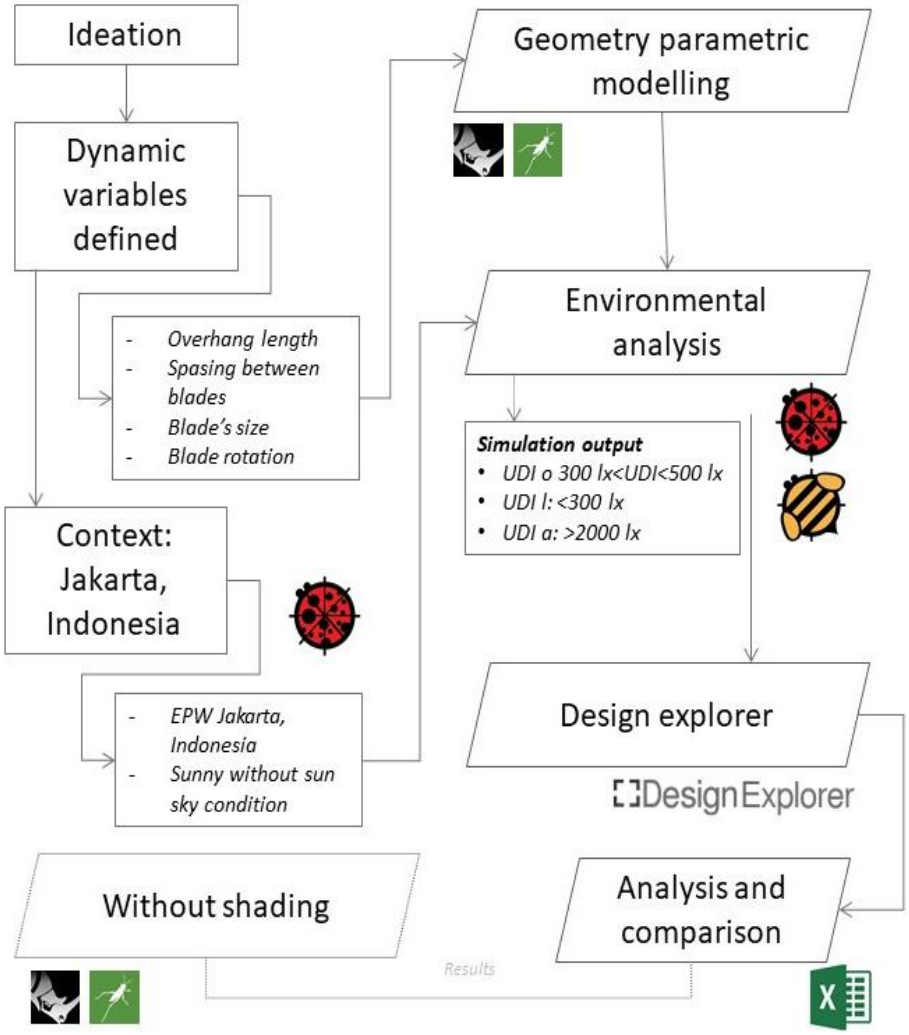

Figure 4.1. Research workflow

The virtual space was designed to resemble an Indonesian modular school or office. The room is 8 m x 12 m x 3.5 m. The opening was constructed with approximately 40% of the glazing ratio. Several dynamic parameters, represented by the number of slider components, were used to configure the shading. The primary design variable is the overhang or eaves. The second component is the distance between the blades. The third parameter is the size or width of the blade, and the final dynamic parameter is the

rotation of the blade. Model and analysis are shown in Figure 4.2, while the range of dynamic parameters that can be used as a design variable is shown in Table 4.1.1.

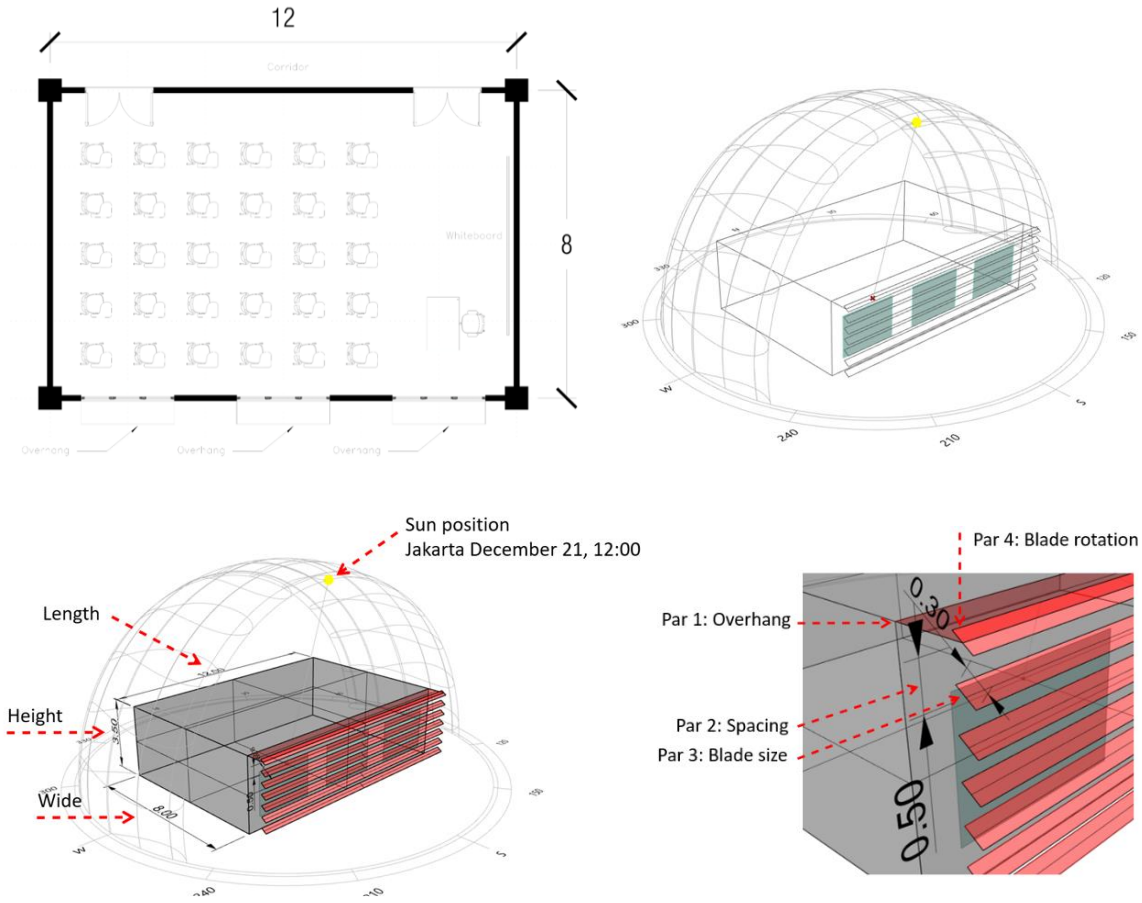

Figure 4.2. Simulated room and design variables: (upper-left) classroom plan, (upper right) the simulated room before simulated room, (bottom-left) room dimensions, (bottom-right) dynamic parameters

Figure 4.2 demonstrates the virtual shading devices and their components as design parameters (independent design variables) which furthermore serve as a context surface in the daylight simulation process. This model does not employ any specific materials to determine the simulation's overall effects also the thickness of each component is disregarded. However, the average RGB Rad material level for the glazing was set to 0.5. Figure 4.3 demonstrates one of the visualization outcomes and the significance of the

grid-based analysis for each test point for more daylight analysis. Left picture shows the simulated model with distributed UDI value in the test mesh while right picture shows a value of each grid test point.

Table 4.1.1. Dynamic parameters as design variables

Parameters	Division	Step	Range	Total
Overhang	1-3	30 (cm)	30-90 (cm)	3
Spacing	2-10	5 (cm)	5-50 (cm)	9
Blade size	2-9	5 (cm)	10-45 (cm)	8
Blade rotation	0-9	5°	0-45 (°)	10
Total iteration				2160

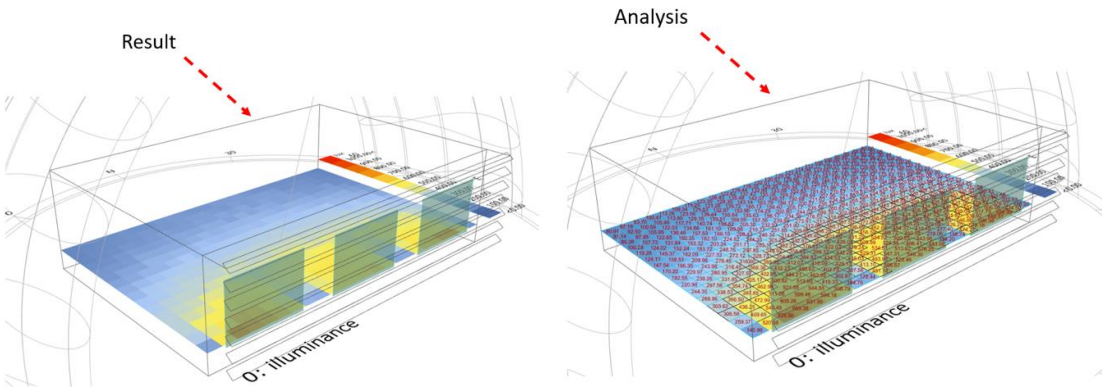

Figure 4.3. Results and analysis visualization showing the illuminance distribution of legend coloring (left), and illuminance value in lux (right)

4.1.2.3. Context and analysis period

As environmental data supplied to the environmental analysis engine, this study utilizes EnergyPlus's EPW file for Jakarta. Jakarta's coordinates are 6.2088° South, 106.8456° East. The simulation uses the sun's position on December 21, at noon. The sun is about positioned at a height of 73°, facing 180° to the south.

4.1.2.4. Computational tools

The entire parametric system is arranged in the modelling software called Rhinoceros [120] and the conceptual parametric-based plugin called Grasshopper [121]. For environmental analysis purposes, Ladybug and Honeybee [122] were incorporated.

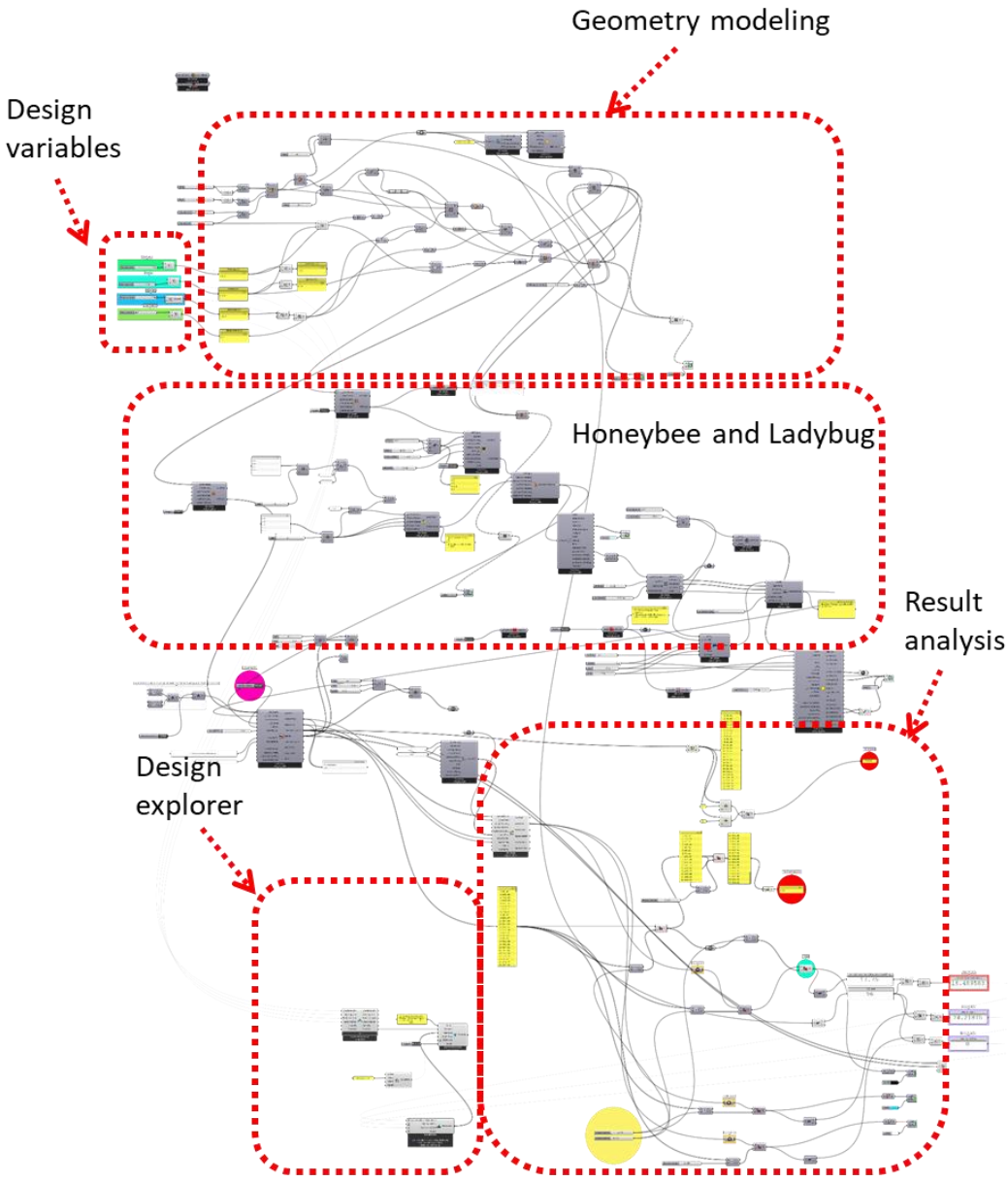

Figure 4.4. Grasshopper definition clustering

The plugin allows the import of EnergyPlus Weather Data EPW for the purposes of data analysis. In addition, it was designed to let engineers and designers do environmental study in a relatively shorter amount of time. Honeybee and Ladybug are integrating well-known and proven simulation engines like as EnergyPlus, THERM, Radiance, and OpenStudio during the design phase in order to simulate and calculate environmental phenomena based on the provided meteorological data. Figure 4.4 illustrates the parametric definition of the entire modelling and simulation system in Grasshopper.

4.1.2.5. Design exploration

The design exploration process was generated by the plugin software TTtoolbox with the components called Colibri. Colibri was developed by Thornton Tomasetti [123] and it allows the generation of an interactive parallel coordinate plot for each step of iteration for the designer's exploration and visualization purposes [124].

As it has been described in methodology chapter, in contrast to the multi-objective optimization or MOO process, in which the targeted solution tends to be genetically generated based on the desired targeted value, the Colibri iterates all the total possibilities that are precisely produced by multiplication each step in parameter from the input sliders (genotype) and calculates the entire targeted value (phenotype) in this manner.

4.1.2.6. Measurement metrics

The grid-based daylight simulation and exploration aims to maximize the amount of useful daylight illumination (UDI). UDI defines "illuminance" as the incidence of annual illuminance within the range deemed useful by occupants. Typically, the UDI varies from 100 lux to 2000 lux. However, Nabil [125] classified the UDI range into groups that are insufficient with less than 100 lx of illuminance, effective with 100 lux to 500 lux, desired with 500 lux to 2000 lux, and exceeding with more than 2000 lux of illuminance. [125,126]. This research only focuses on and calculates the range between UDI_0 300 lux and 500 lux [75]. Another UDI investigated in this research is the UDI_l with an illuminance value of below 300 lux and the UDI_a with an illuminance value of above 2000 lux. [75]. This

research also examines the UDI_l with an illuminance value of less than 300 lux and the UDI_a with an illuminance value of more than 2,000 lux.

4.1.3. Results

This section will give a detail explanation of the simulation outcomes generated by design exploration procedures. The system iterates parameters and comes up with 2,160 design solutions where each solution informed with parameter values and UDI values. The findings and discussion are separated into three sub-sections: first the comparison model, which is the simulation room without shading, the recommended UDI_0 results, the undesirable UDI_0 results, the trend, and the explanation. Second, the value distribution map, also known as a parallel coordinate plot, is created so that the relationship between the dynamic factors and the desired outcomes can be observed. And lastly, the analysis process where the results and design option are manually observed within the parallel coordinate plot.

Figure 4.5 demonstrates the Design Explorer TTtoolbox interface's parallel coordinate plot. It consists of 2,160 wire connections, with each wire representing a design solution with embedded variable values. The first four axes are the design variables: overhang, spacing, blade size, and blade rotation, with correspondingly divided value ranges. The red-dotted bubble indicates the search region for the specified value. The searching region corresponds to the portion of the UDI_0 axis containing the highest percentage value.

Figure 4.6 demonstrates numerous samples of the design explorer's output. It depicts the randomly selected design options that were most likely generated during design exploration. Each solution contains information regarding the arrangement of louver component characteristics (independent variables) and daylight objectives (dependent variable). In terms of design or data visualization, during the early stages of design, this sort of visualization conveys the daylight distributions and design geometrical feedback directly to the designer and stakeholders.

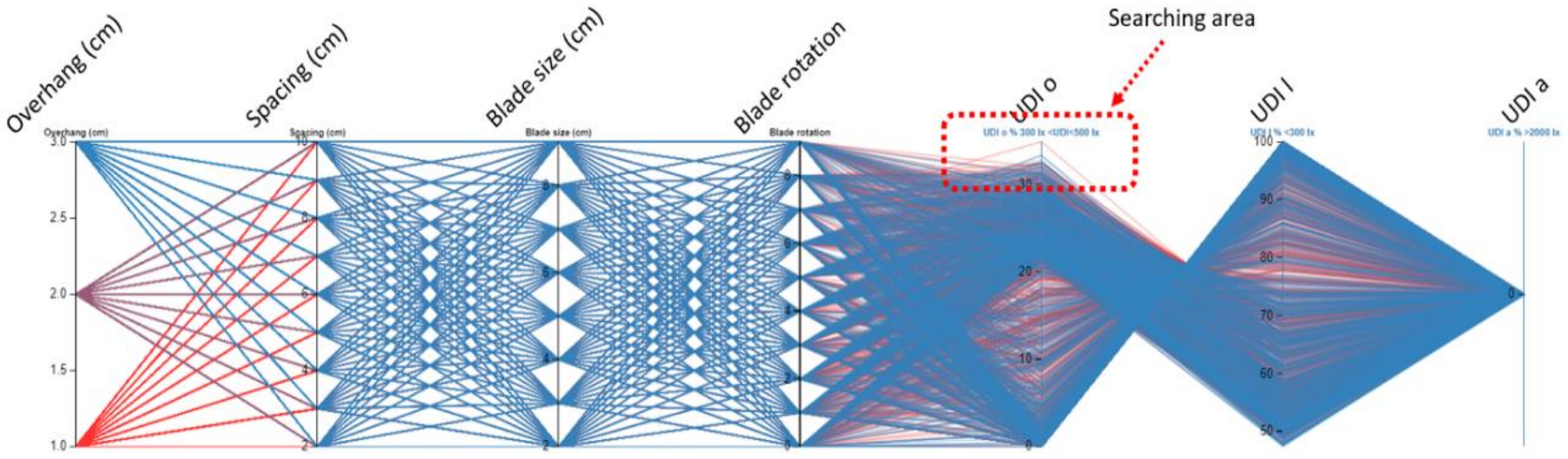

Figure 4.5. Parallel coordinate plot of the exploration results showing the wires connecting each individual's parameter and daylight objectives (highlighted in dotted line)

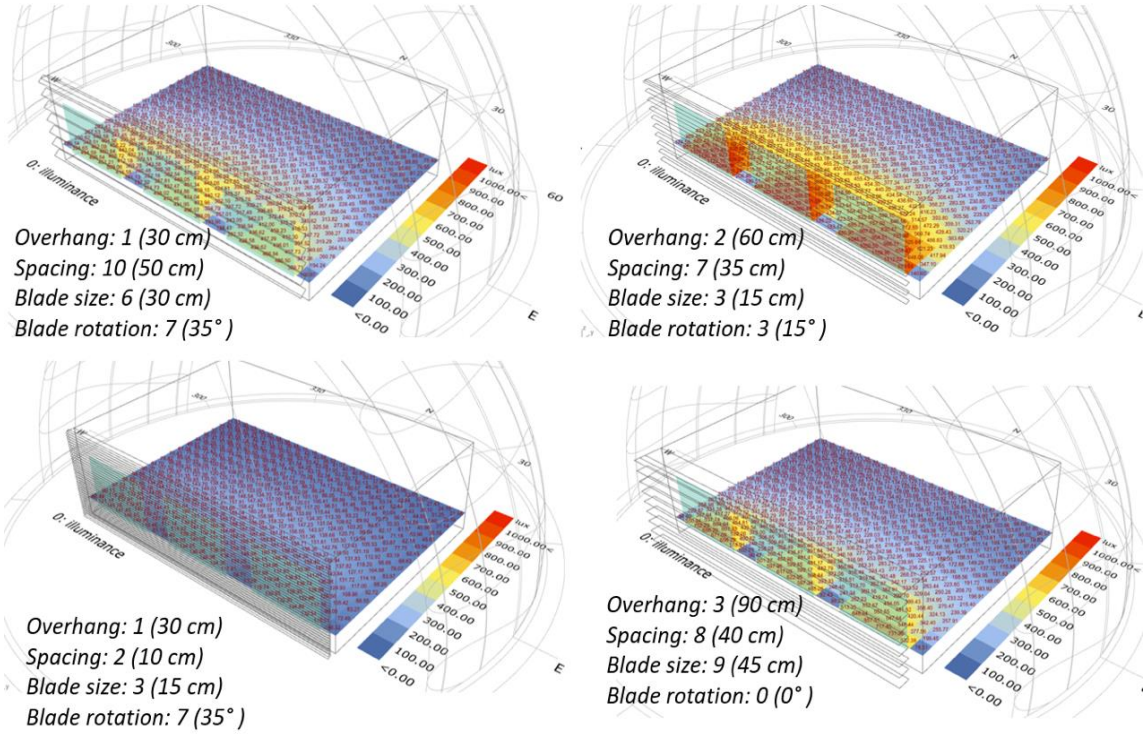

Figure 4.6. The sample of the results with its variables

4.1.3.1. Comparison model

The comparison model was constructed for benchmarking purposes. This model is a simulation of a room that equipped with no shading devices. The sky condition that directly strikes the glazing surface is meant to reveal how UDI is distributed within the simulated space when no filter stops direct sunlight from entering. Figure 4.7 shows the visualization result of the comparison model. The picture shows that the area indicated in red, which valuing illuminance value of more than 900 lux, is distributed about under the openings. The comparison model performs UDI_0 at 21.87%, UDI_l at 44.27%, and UDI_a at 1.87%.

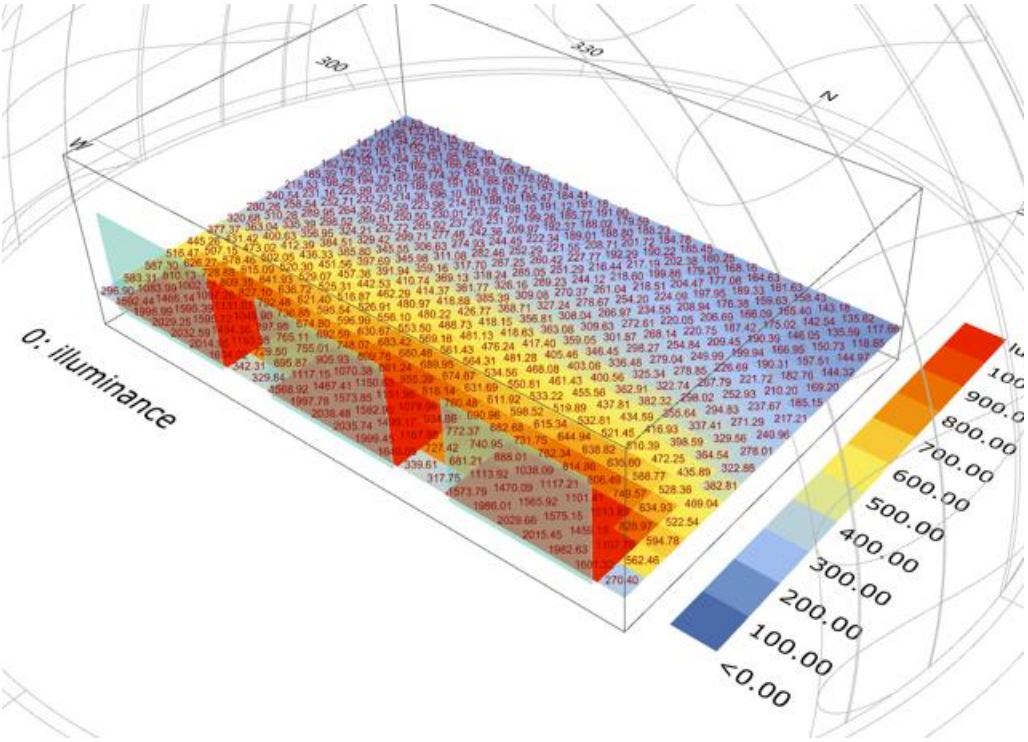

Figure 4.7. Results and visualization of the benchmarking model, the simulated model without louver shading

4.1.3.2. Preferred UDI_0 results

As a result of the exploration procedure, the model with the chosen UDI_0 is the one that achieves the greatest possible UDI_0 with an illumination between 300 lux and 500 lux. The targeted area percentage is calculated by dividing the grid mesh with UDI_0 by the total grid mesh area. Figure 4.10. Parallel coordinate plot of the highest UDI0 shows the parallel coordinate plot of the highest UDI_0. The highlighted blue wire represents the combination of design variables that resulted in the highest UDI_0 among 2,160 simulations. The solutions had a single value for the first variable, the overhang, indicating that its length is 30 cm. Variable 2's spacing value of 10 indicates that the distance between each blade is 50 cm. The value 6 for the third variable, the blade size, indicates that each blade has a width of 30 cm. The last variable, the blade orientation, 7 means that each blade has a 35° rotation. The combination produced a UDI_0 of 34.97%, a UDI_l of 64.84%, and a UDI_a of 0%. The result shows that the individual solution founded by the iteration process has more areas of UDI_0 by 13.1% compared to the

comparison model. Besides, based on the simulation results, the louver removes 1.8% of the glaring possibility from the comparison model, resulting in a 0% UDI above 2000 lux.

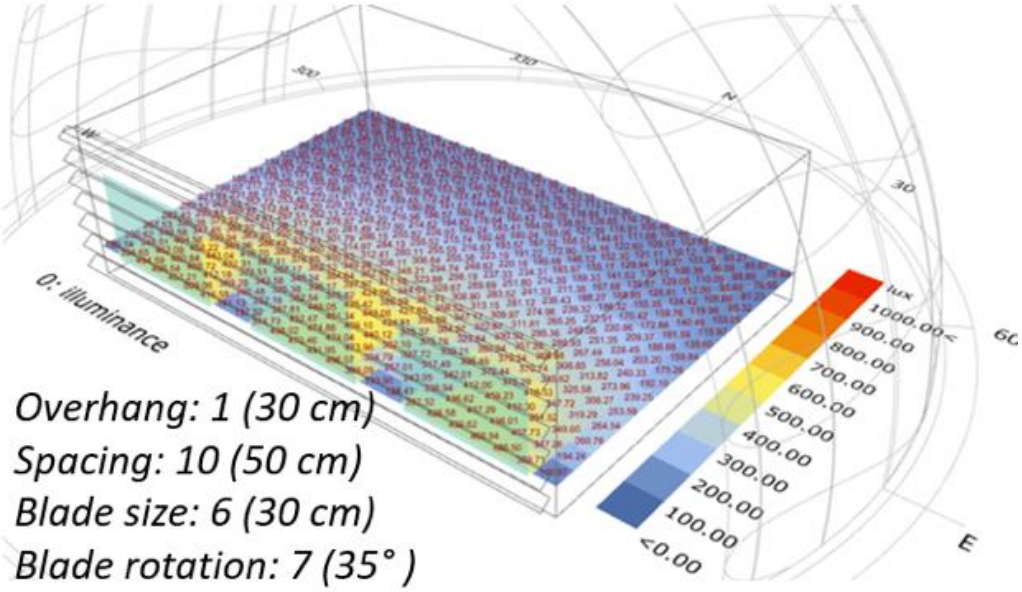

Figure 4.8. Louver configuration of highest UDI_0

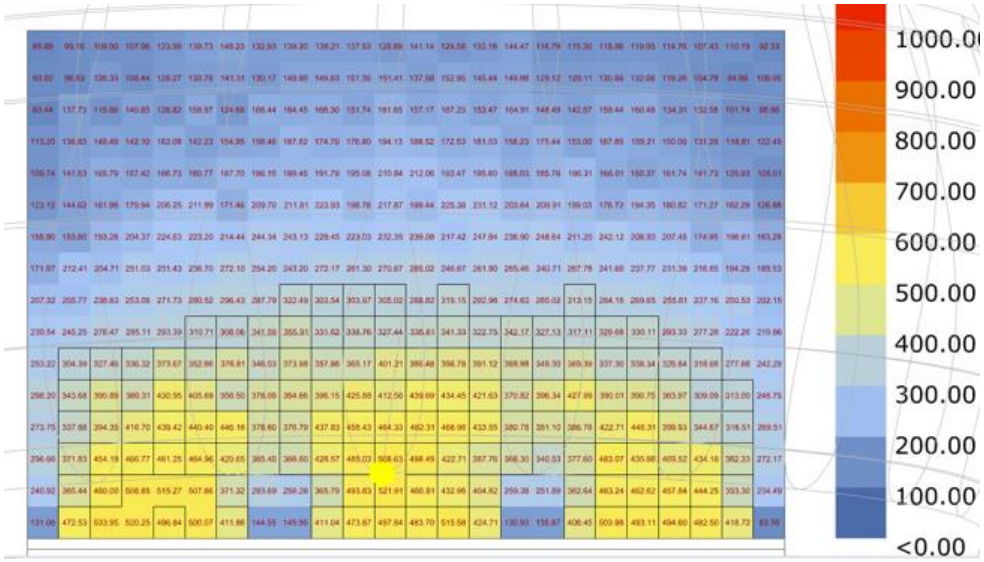

Figure 4.9. Results and visualization of the solution with the highest UDI_0

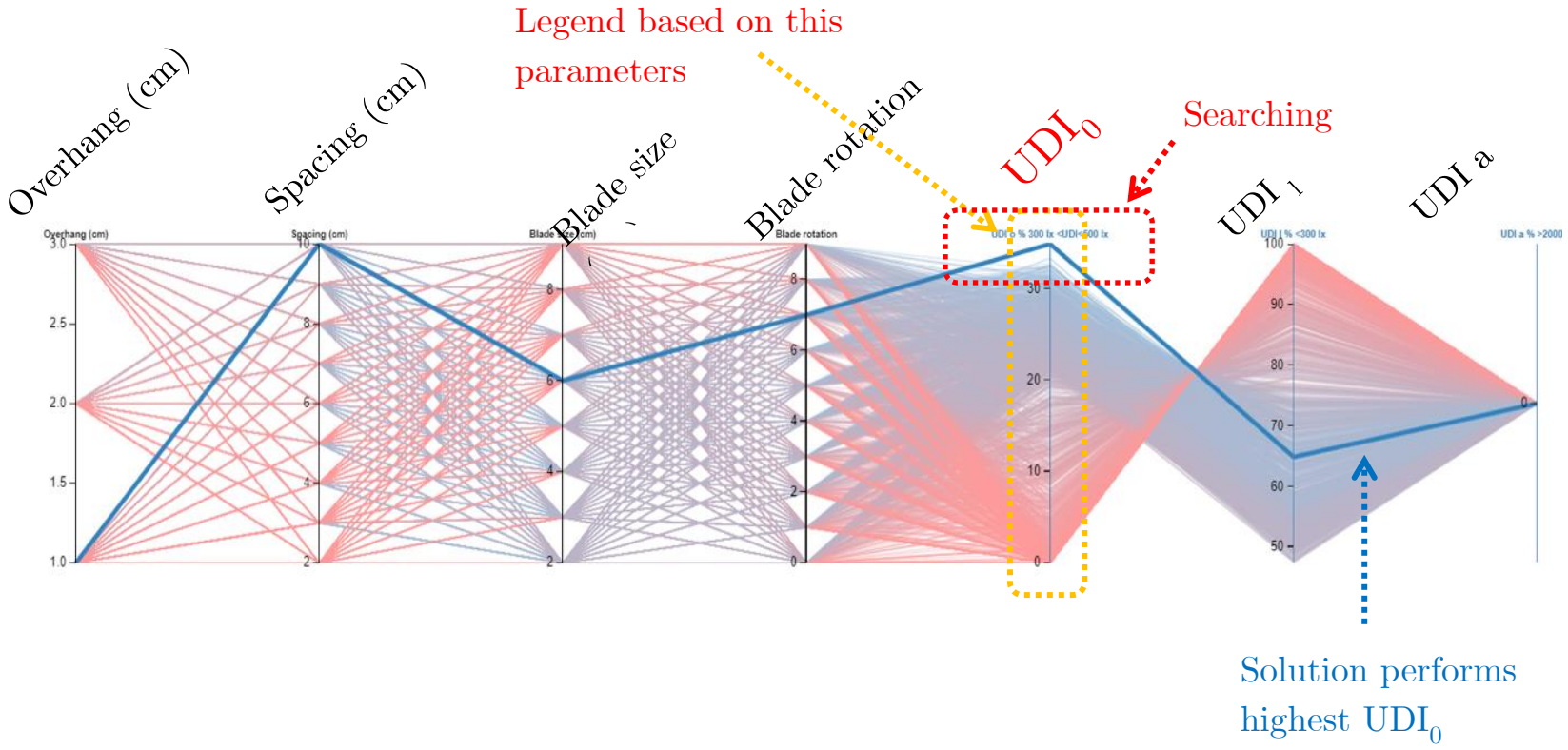

Figure 4.10. Parallel coordinate plot of the highest UDI_0

Figure 4.9 demonstrates the answer with the highest UDI_0 value. The luminance is between 300 lux and 500 lux, represented by a bluish-to-yellow color gradient. It can be seen that a significant portion of the value is dispersed from the areas under the windows to the area around the room's center. Nonetheless, the number of UDI_0 reverses the number of UDI_l to divide the entire tested area. The image demonstrates that above 300 lux illumination permeated the passageway and all areas beneath the windows. In addition, UDI below 100 lux of illumination is presented in the aforementioned sections.

4.1.3.3. Unreferred UDI_0 results

The unpreferred solution that performs the lowest value of UDI_0 is not produced in a single solution. Figure 4.11 displays the plot of parallel coordinates for the lowest UDI_0. In the UDI_0 axis, the wire displays several connections, each of which corresponds to the UDI_0 value 0. The highlighted numerous selections in this scatterplot represent the multiple solutions with a unique mix of dynamic design variables that resulted in 0% UDI_0. This issue is significantly attributable to the dense louver design that obscures the skylight. The blocking could be created by the blade's dense spacing, its broad size, and the angle at which it turns.

4.1.3.4. The tendency

In contrast to the conventional design technique, which assesses multiple completed design ideas to determine the trend, design explorer adopts a bottom-up strategy to identify the targeted solution based on the target goals stated during the ideation phase. It is difficult to discern the general trend from a large number of individual results generated by numerous combinations of design variables. On the design explorer platform, however, the trend can be identified by sliding the area along the axis, which will highlight the wires that correlate to the value within the plotted area.

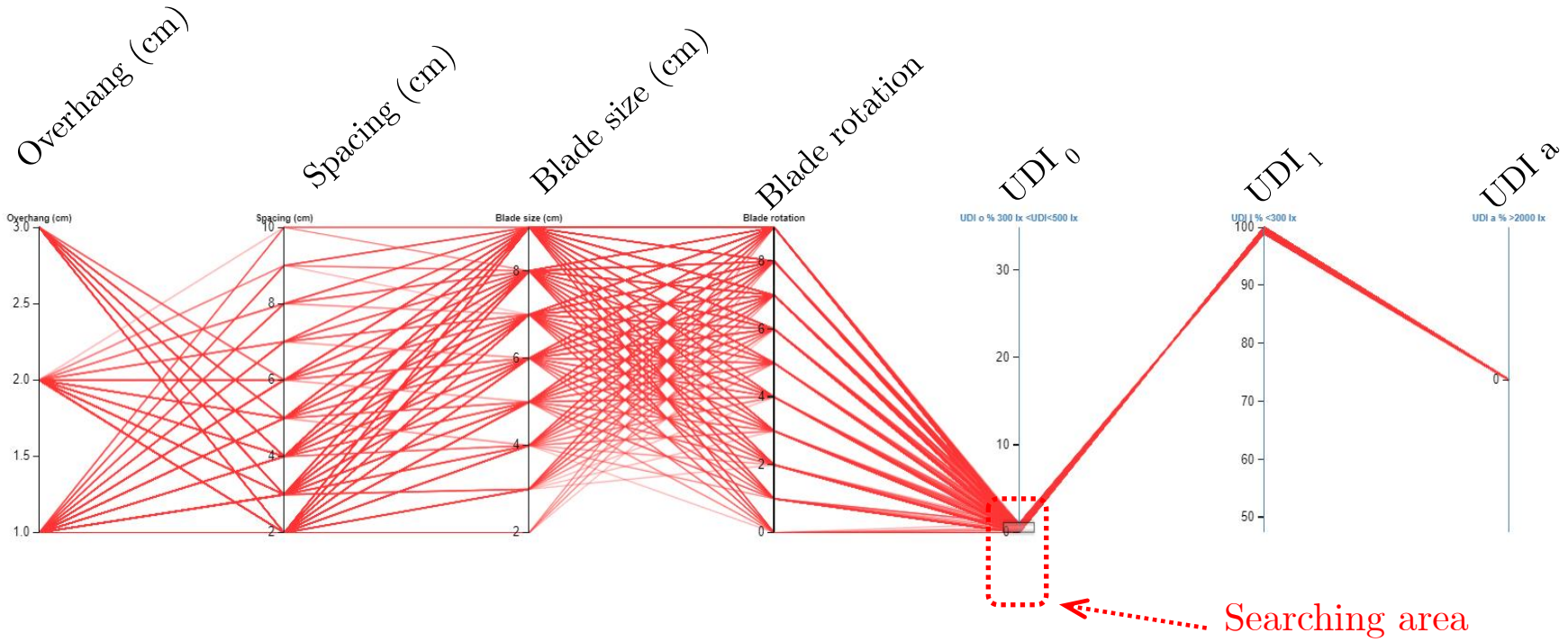

Figure 4.11. Parallel coordinate plot of the lowest UDI_0 (red)

Two tendencies for the highest and the lowest UDI_0 have been shown in Figure 4.12 and Figure 4.13. Highlighted by dragging the search region along the UDI_0 axis, the blue wires representing solutions with maximum values of UDI_0 reveal that the maximum UDI_0 corresponded to rotation angles more than 4 (20°), spacing greater than 2 (10 cm), and blade size less than 7 (35 cm). The contribution of the first variable, overhang, is practically same. The red wire representing the lowest UDI_0 solutions indicates that the low proportion of UDI_0 results from a balanced mix of variables. No combination of blade size 2 (10 cm) and blade rotation 0 (0°) results in 0% UDI_0.

Given the setting of Jakarta, Indonesia, the research addresses the methodological gap in configuring louver shading devices for design. Different combinations of louvers directly affect the distribution of natural light within the replicated space. In the MOO procedures, the design variables comprised louver components (i.e., overhang, spacing, blade size, and rotation) to yield the daylight metrics of useful daylight intensity (UDI) by parametric daylight modelling and optimization utilizing weather data from Jakarta. The results demonstrate that a certain configuration of louver shading generated by the MOO achieves the optimal optimization value objective for the given situation. In addition, the statistics illustrate the correlation between design factors and daylight objectives.

On the basis of the findings, it is evident that the proposed methodology may be utilized to optimize the link between shade and daylight performance. The significance of this study is the construction of a design exploration platform to analyze and identify the optimal solution for an Indonesia-specific shading device. Having been informed of a variety of design solutions and the tendency between parameters and daylight objectives, designers and stakeholders, such as those from a manufacturing company, can benefit in terms of decision-making processes by considering the design aspect of louver shading devices in a specific context to bring the intention of environmental architectural consciousness that has been proven to contribute positively to the operational occupied working hours. Consideration should be given to parametric design while designing louver shading devices and evaluating daylight performance.

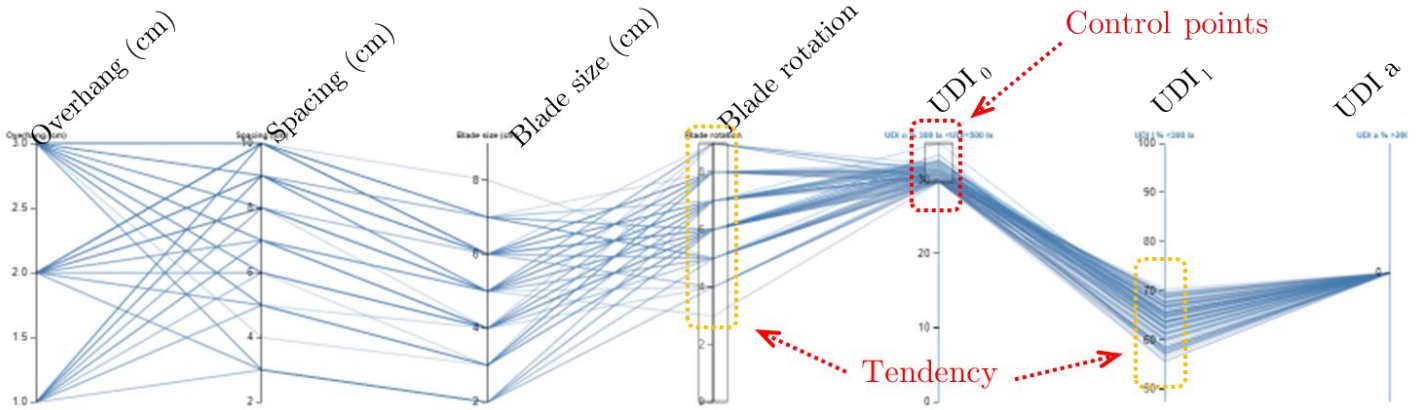

Figure 4.12. The tendency of the solutions with the highest UDI_0 (blue)

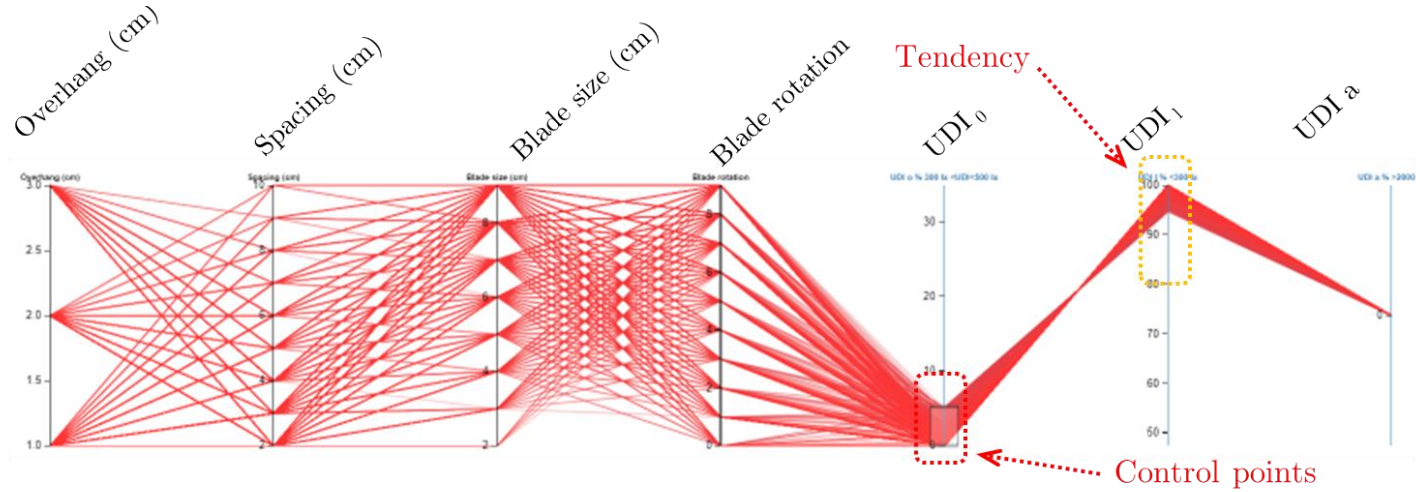

Figure 4.13. The tendency of the solutions with the lowest UDI_0 (red)

This subchapter focuses on the analysis of the louver shading geometry in relation to the distribution of beneficial daylight lighting (UDI). It omits the definition of specific materials and employs the material of the Grasshopper component, with the exception that the glazing is specified to have a transmittance of 0.5. The simulation does not incorporate direct sunshine. The metrics utilize only a single time simulation, unlike annual sunlight exposure (ASE) or daylight autonomy (DA). Also absent from the simulation is the building's orientation. In consideration of the hardware's constraints, the simulation uses a huge grid test point. A more accurate estimate would likely result from a smaller grid size. Thermal comfort and energy usage do not fall within the scope of this investigation.

4.2. A development of a benchmark model for daylight-shading and orientation study

4.2.1. Introduction

In the second case, with regard to the collaboration with Meldia research for advanced wood, the architecture department at the University of Kitakyushu has acquired experience in planning and experimenting with Japanese cedar for primary building construction. In the Orio District of Kitakyushu City, one of the continuing design projects is to create a two-story wooden house built of Japanese cedar. Environmental and structural study will be conducted using parametric design for the desired project. Therefore, the base case is required for comparison purposes before to and after attempting to identify the potential for efficiency. Thus, this study is the first step in the design of a two-story wooden house in the Kitakyushu District in Fukuoka, Japan. This sub-chapter aims to develop a benchmark model as a base case for further comparison needs regarding microclimate [127] and environmental aspects such as daylight and sun exposure, view outside, and energy consumption. The complete system was executed on a parametric and generative algorithm platform, with the Shimonoseki EPW file providing the metrological data input for the Kitakyushu city site. In addition, the objectives of this research are to develop a benchmark model for future comparison

through a parametric and MOO platform aiming for investigates the solution in which performing low energy consumption and maximum value of view and sun exposure, and to analyze the correlation between the dynamic design parameters and the winter and summertime objectives.

4.2.2. Methodology

4.2.2.1. Overview

The research utilizes a set of parametric and generative algorithms [27] calculators for calculating and simulating the design object based on the intended design objective in order to study the desired performance and the resultant design qualities. This section recommends methodology to find the desired solution in a very significant amount of data generated via iteration. The approach may generate a performance design solution that is generatively calculated and exceeds the designer's expectations. The study was carried out in a series of sequential stages, beginning with ideation, followed by the process of environmental simulation, design exploration and data collection, concluded with data analysis.

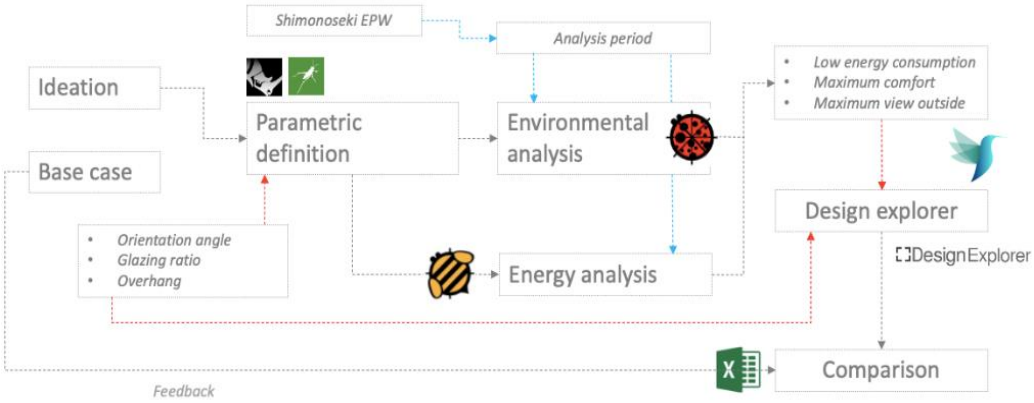

Figure 4.14. Research workflow

Figure 4.14 illustrates the entire system used in this research. The procedure began with the ideation phase, during which the parameters and potential outcomes were determined. In this stage, the dimensions of the standard regular box have been determined and it

has been assigned design variables based on the design dynamics parameters. In addition, the concept was implemented by constructing a parametric defining system for both the building and the environment. In this step, the design characteristics that serve as dynamic design parameters are selected and implemented. The next step, following the completion of the building and the site, is environmental analysis of the Ladybug and Honeybee. In this stage, the weather data input and analysis period were inserted. After the environmental analysis has been completed, the Honeybee will undergo an energy analysis. In this phase, a simple heating and cooling calculation has been established. After obtaining findings from a single simulation for both environmental and energy analyses, design exploration was conducted using Colibri, and a manual comparison between the found solution and the base case was performed in Excel. The tools used to simulate daylight objective was similar with what have had discussed in Sub-chapter 4.1.2.

Figure 4.15. Parametric definition arranged for the benchmark model and simulation illustrates the whole parametric definition utilized in this study. The dot bubble denotes the cluster in which the function was applied based on the specific requirement. The first cluster indicates the dynamic settings, which primarily consist of sliders. In this cluster, the parameter, in this case the logic of louver, is translated into number sliders. The second highlighted component is the Shimonoseki EPW file that was downloaded utilizing the Ladybug download EPW file component.

The third group consists of components of ladybugs for environmental analysis. Fourth is the cluster of energy plus analysis from Honeybee, and above this cluster is the cluster that is used to calculate the view and sun hours analysis. In this cluster, environmental simulation is conducted. The final cluster visible in the arrangement is the design explorer cluster containing Colibri's components. The design explorer cluster consists of Colibri components where the single value of parameter and single value of UDI results are collected and recorded. Specific in this sub-chapter, the parallel coordinate plots visualized from the platform, not from the raw Excel data. The observation conducted manually by clicking and dragging the wires on the plot along with the desired observation axes.

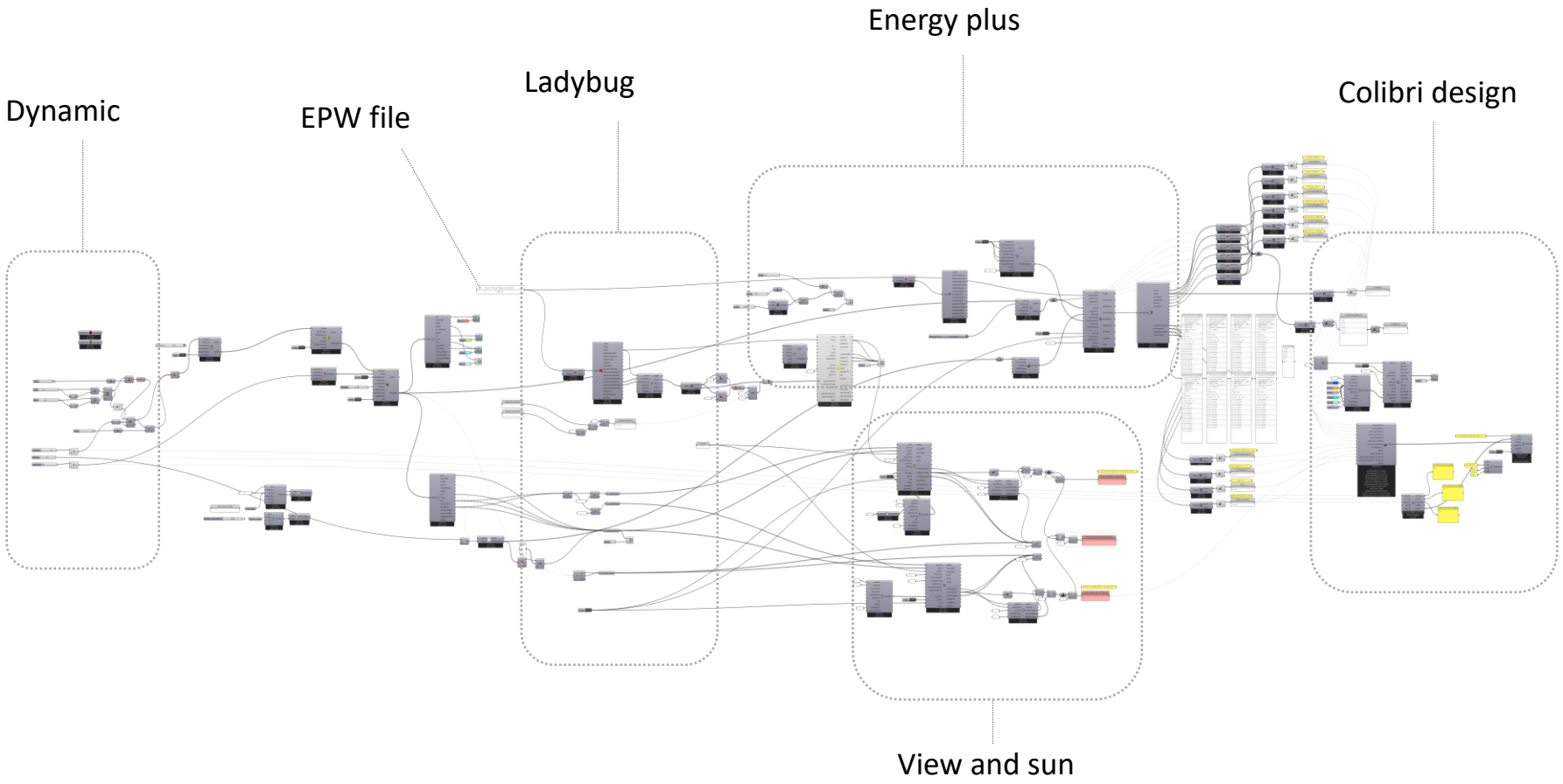

Figure 4.15. Parametric definition arranged for the benchmark model and simulation

4.2.2.2. Geometry parametric modelling and targeted goals

The design object's geometry is a simple cube symbolizing a two-story house with dimensions of 6 meters in length, 4 meters in width, and 6 meters in height, and it faces south. Several dynamic characteristics, including glazing ratio, overhang, and orientation, were modelled into the geometry using Grasshopper. A glazing ratio is a measurement of the proportion of glazing to the surface area of a window. In centimetres, the overhang is the length of the window's eaves. The final component of design is the orientation, which is the rotation angle shifted from the XY or North-South axis (from the top) in a clockwise or counterclockwise direction as measured by the radiant degree.

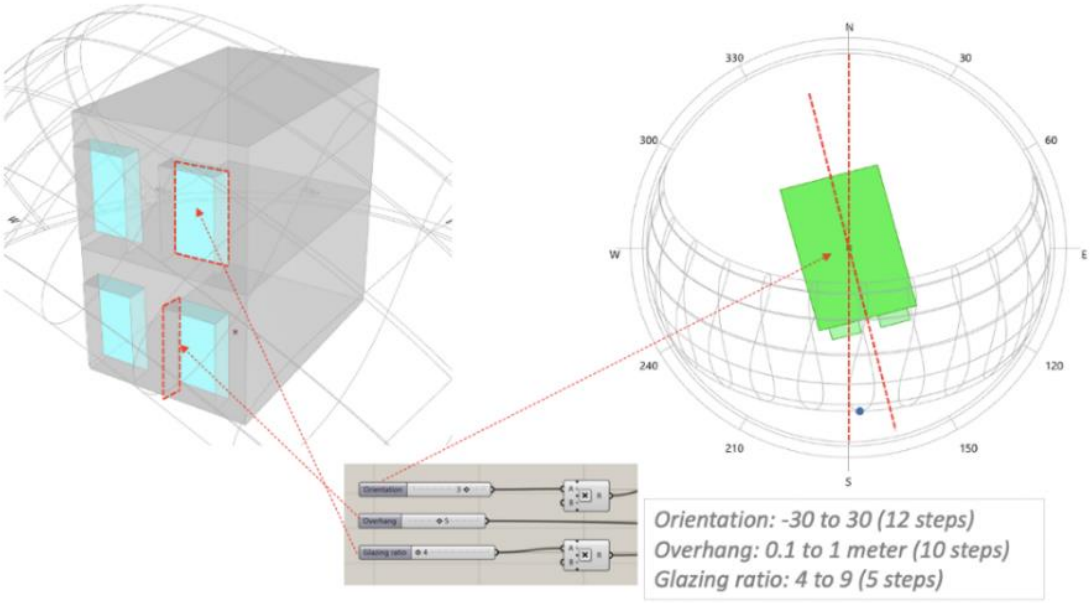

Figure 4.16. Geometry modelling and dynamic parameters

Figure 4.16 shows the position of each design variable in the geometry. For iteration purposes, each dynamic parameter has been set to undergo several movements. Glazing ratios were set to be on the south surface of the box with the portion ranging from 40% to 90% with 10% for each step, meaning that this design variable has five steps movements. The overhang is driven by a number slider with a value ranging from 10 cm to 1 m (100 cm) with 10 cm for each step, meaning that this dynamic parameter has ten steps

of movements. The last, orientation, has 12 steps ranging from -30° to 30°, with 5 degrees for each step. Overall, this system could iterate 600 iterations based on the multiplication of each parameter's movements.

The desired design solution is the minimal energy consumption influenced by the driven parameters over the winter and summer months, as determined by the energy plus calculation in Honeybee. The environmental study in Ladybug determined the lowest sun hours in the winter, the maximum sun hours in the summer, and the maximum view % from the eye view cone.

4.2.2.3. Site and analysis period

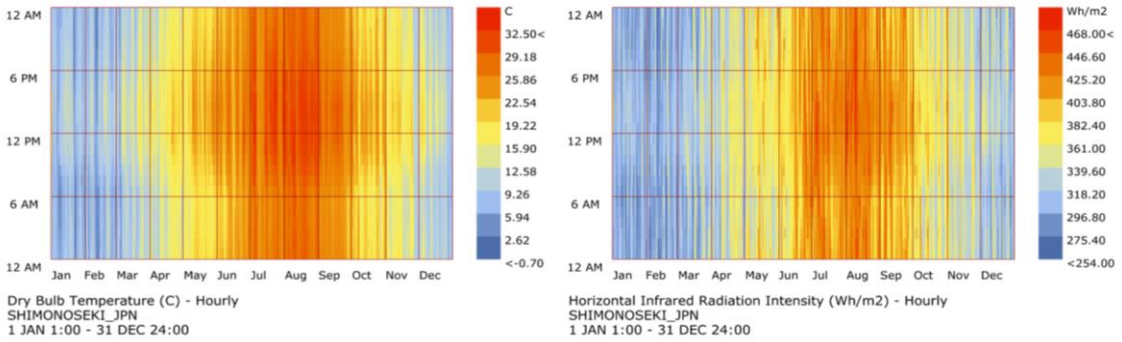

Figure 4.17. Dry bulb temperature and horizontal infrared radiation in Shimonoseki

The weather data used in this research is the EPW file of Shimonoseki, which is the nearest database available surrounding Kitakyushu city. The time taken for the analysis period is yearly, from January 1st to December 31st. Figure 4.17 illustrates the dry-bulb temperature and horizontal infrared radiation accumulated per month within one year generated by Ladybug. The chart displays that August is the hottest period, with an average temperature of 27.43°C and radiation of 414 kWh/m^2. The coldest period started from the end of December to the end of February with an average temperature of 7.9 °C and 299.48 kWh/m^2. Based on the graph, the hottest period begins in July and lasts until the end of September.

4.2.3. Results

This section will describe the results and conclusions from the experiment. The resulted findings are the overall conclusions based on the exploration, the base case, and the recommended design option for winter and summer energy usage, view, and sun hours. In this section, the relationship between the parameters and the outcomes, as well as the platform's effectiveness, will be described.

4.2.3.1. General findings

The overall conclusion of this sub-chapter is that the simulation process outcome is given apart from the system. For visualization purposes, value distribution maps are shown for each target objective. However, for iteration processes, the results are given in a parallel coordinate plot, illustrating the relationship or connection between the driven parameter and the desired result. Similar to the data visualization in Sub-chapter 4.1, where the plots are resulted from the design exploration platform.

Figure 4.18 (top) is the parallel coordinate plot resulting from the global parameter movements and the dynamics parameters or design variables are given along the first three axes in black type. The remaining portion of the blue-highlighted axis displays the analysis's output. The circle with dots represents the search region for the targeted solution. The blue dotted circle denotes the winter performance search area. Orange symbolizes the search region for both summer and winter performances.

The system iterates 760 iterations, resulting in the spread of value on the 2D visualization graph. Figure 4.18 (bottom) is the specific design objective retrieved from the general simulation objective aims. The search for the desired design solution, based on the parallel coordinate plot, occurs at the minimum value of the cooling and heating axis and the maximum view presented in percentage. The winter search region is in the axis of maximum sun hours, whereas the summer search area is in the axis of minimum sun hours. The observation will focus in the area where the perpendicular between lines and axis value is swarmed or dense. The density in each vertical axis indicates the distribution values that tend to have high value concentrations where the tendency or target value are possible to be found.

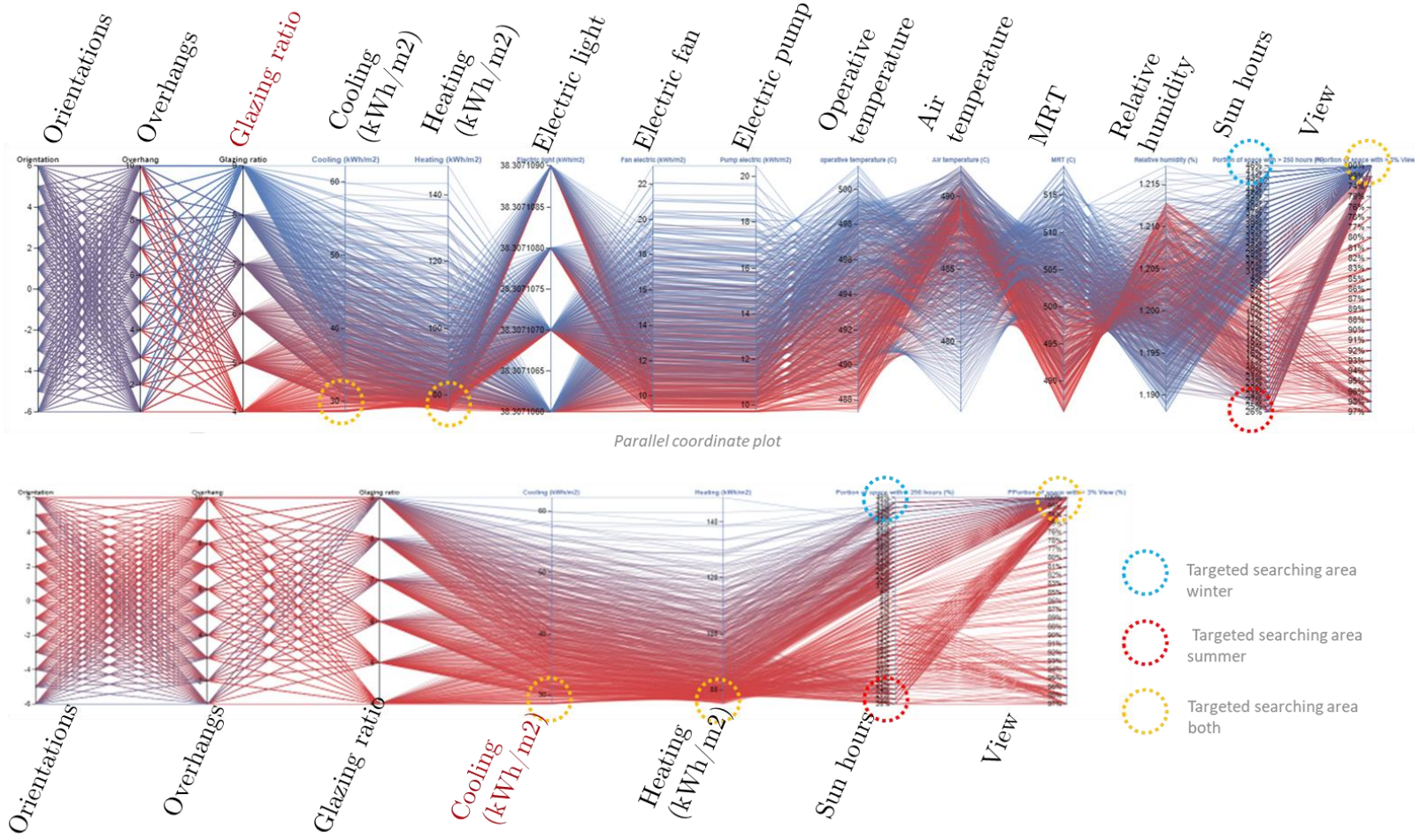

Figure 4.18. parallel coordinate plot of the iteration's results: (top) results of the overall parameters, (bottom) results of specific design target

4.2.3.2. Base case results

To find the optimization the development of base case model is needed. Figure 4.19 focuses on providing the results of the simulation procedure that took place in the base case model. The base case is the model with no treatment, and the setting for the feature is based on a common assumption. The parameters of the base case are not the outcome of a form-finding procedure, but rather are chosen by intention.

In terms of parameter, this base case model was attributed with a 40 cm overhang and a 50% glazing ratio with a 0-degree angle from the North-South axis. The design attributes and the results are highlighted in the parallel coordinate plot, which shows the relationship between the design parameters and the results. The chart has resulted in several targeted goals, such as cooling at 34.67 kWh/m^2 and energy for heating at 78.15 kWh/m^2. Another targeted design goal stated that 24% of the space has more than 250 hours of sun exposure and 99% of the area has more than 3% quality view of the outdoors.

According to the heat map-based legend in floor plan, the majority of the area is exposed to the sun for less than 250 hours. A small number of regions are covered by the value of more than 25 hours dispersed closer to the windows. The highlighted red border denotes the area with a yearly sun exposure of more than 250 hours. From the study of the cone of vision, it can be observed that the bold-highlighted area shows the area where the view quality to the exterior is greater than 3%, and the targeted area nearly encompasses the entire area. In the image adjacent to the horizontal cone of vision analysis, the glazing ratio and overhangs of the base case model are depicted. The results of the base case furthermore become a standard line to be compared to other exploration solutions.

Based on the data distribution along cooling and heating energy consumption, the base case model tends to perform low energy consumption in terms of cooling and heating. This can be observed where the highlighted lined positioned in the low area of density. Another tendency is this model has large area of sun hours and large area of view to the outside. Out of the context of exploration, the performance of the model still considerable to be a fit selection when referring to overall design target objective.

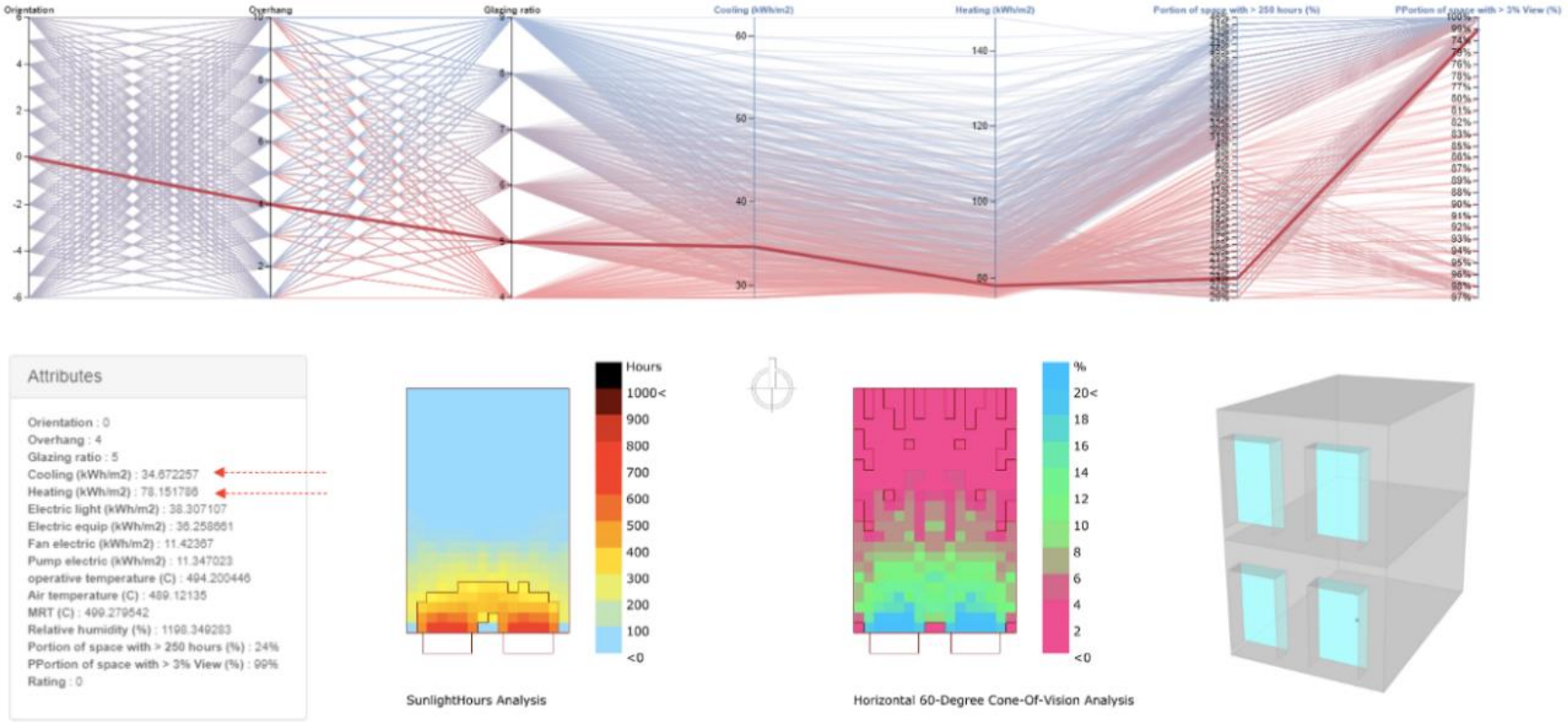

Figure 4.19. Base case performance

4.2.3.3. Model with minimum heating (winter)

Figure 4.20 shows the individual with minimum energy for heating. The minimum heating goals mean that the design attributes can be proposed for minimizing energy consumption in the winter period. For targeted design solutions with minimum heating, the simulation process produces a design with an orientation of 5^{o} towards south-east direction or anti-clockwise, overhangs of 4, and a glazing ratio of 40%. The design performs energy demand for heating at 74.79 kWh/m^2 and for cooling at 22.09 kWh/m^2. The relationship between parameters and the results is presented in the parallel coordinate plot, highlighted by the bold red line.

The sun hours analysis distribution map shows a small part of the space exposed to more than 900 hours. The minimal heating model for the winter season has more areas covered by the sun for more than 700 hours per year than the basic scenario. The analysis compares the horizontal cone of vision to the base scenario. More regions have a cone view of 3% or more, which is greater than 20%. However, the entire computation reveals that the number is less than the 91% base case since the glazing ratio decreases relative to the base case. Similar phenomena occur during the hours of solar exposure. The statement indicated a value of 18% area covered for solar hours greater than 250 hours, a 6% reduction from the benchmark situation.

Based on the plots, the winter target model performs relatively lower cooling and heating when look at the wire's density along these two axes. Align with this, the winter model also performs relative lower energy for electric fan and electric pump. Compared to the base case model, winter model recommends same size overhangs but with smaller windows. According to the heat map, the results shows that the winter target model has more areas of sun hours more than 900 hours that can be interpreted that the simulation come up with the introduction of more sun hours helping to reduce the energy for heating loads. Besides, the model also has more area for vision outside more that 18% compared to the base case.

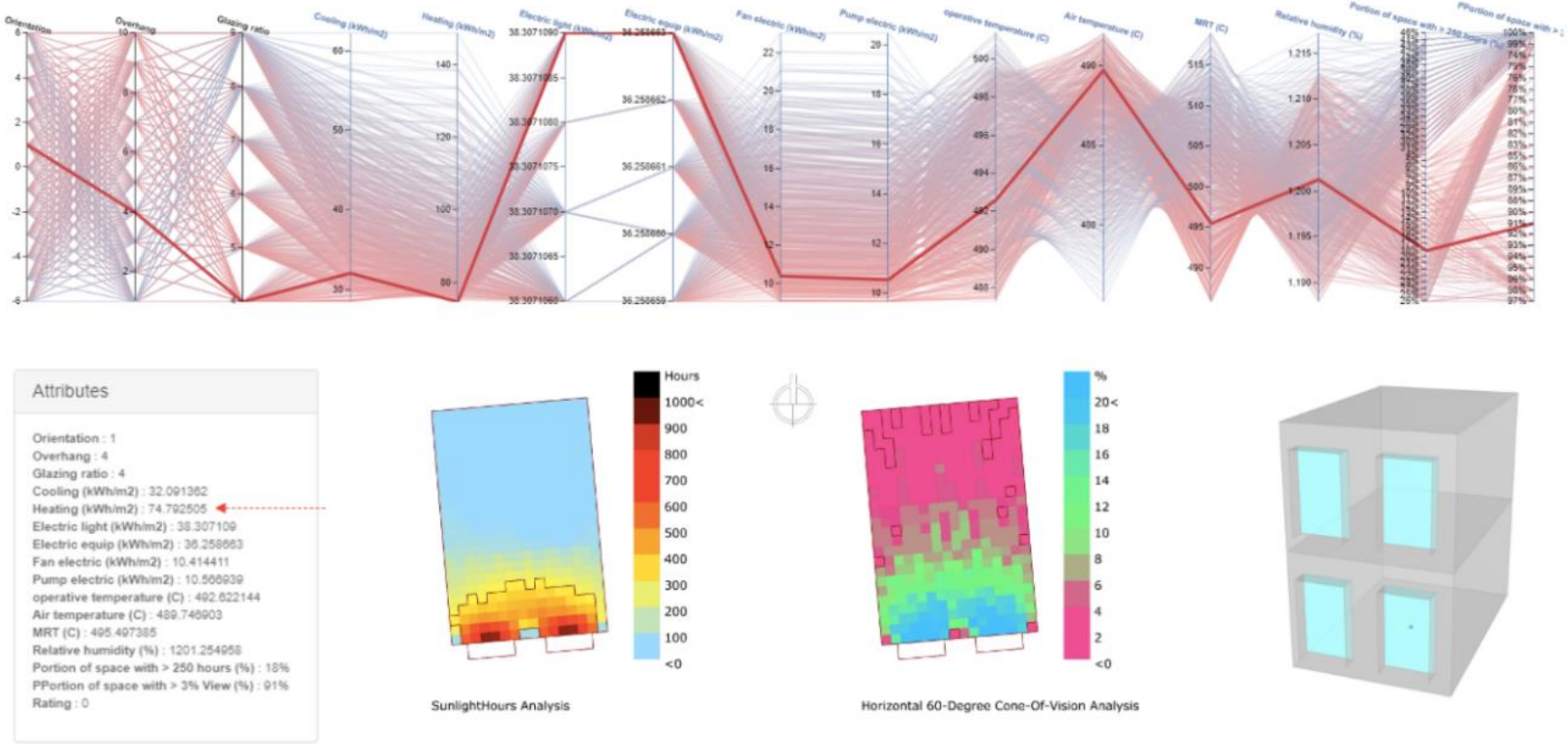

Figure 4.20. Targeted design solution with minimum heating

4.2.3.4. Model with minimum cooling (summer)

The minimum cooling goals mean that the design attributes can be proposed to minimize energy consumption in the summer period. Figure 4.21 presents the design solution results with the minimum energy consumed for cooling in the summer. The iteration comes up with the design attributed with 5 ^{o} orientation toward the east direction, 1 m overhang, and 40% glazing ratio. Moreover, the performance related to energy consumption resulted in 28.50 kWh/m^2 for cooling needs and 78.77 kWh/m^2 for heating needs. The portion of space with more than 250 hours of sun exposure stated a value of 5%. The portion of space with more than a 3% view toward the outside stated a value of 78%. Compared to the base case, this model has fewer parts of the area exposed by the sun with a value of more than 500 hours. Similarly, the view towards the outside that has a value of more than 3% is smaller. More extended overhangs cause this implication.

4.2.3.5. Tolerable design solution (MOO)

Figure 4.22 demonstrates the solution with acceptable daylighting and energy performance as determined via design investigation. The tolerable design solution enables the projected low performance to be utilized in both summer and winter. The value is not less than the other solutions obtained, but it illustrates the trade-offs between the parameters and the outcomes. The design comes up with the following attributes: 15^{o} orientation, 1 m overhang, and 40% glazing ratio. The cooling and heating energy consumption are 28.62 kWh/m^2 and 78.24 kWh/m2, while the portion of space with more than 250 hours of sun exposure states a value of 5%. The portion of space with more than a 3% view toward the outside stated a value of 76%. The connection between parameters and the results can be seen in the highlighted line on the parallel coordinate plot. From the distribution map, it shows that the sun hours that expose more than 800 hours is the minimum. Similarly, it is happening for the view to the outside 3% to more than 20%, considering the length of the overhangs.

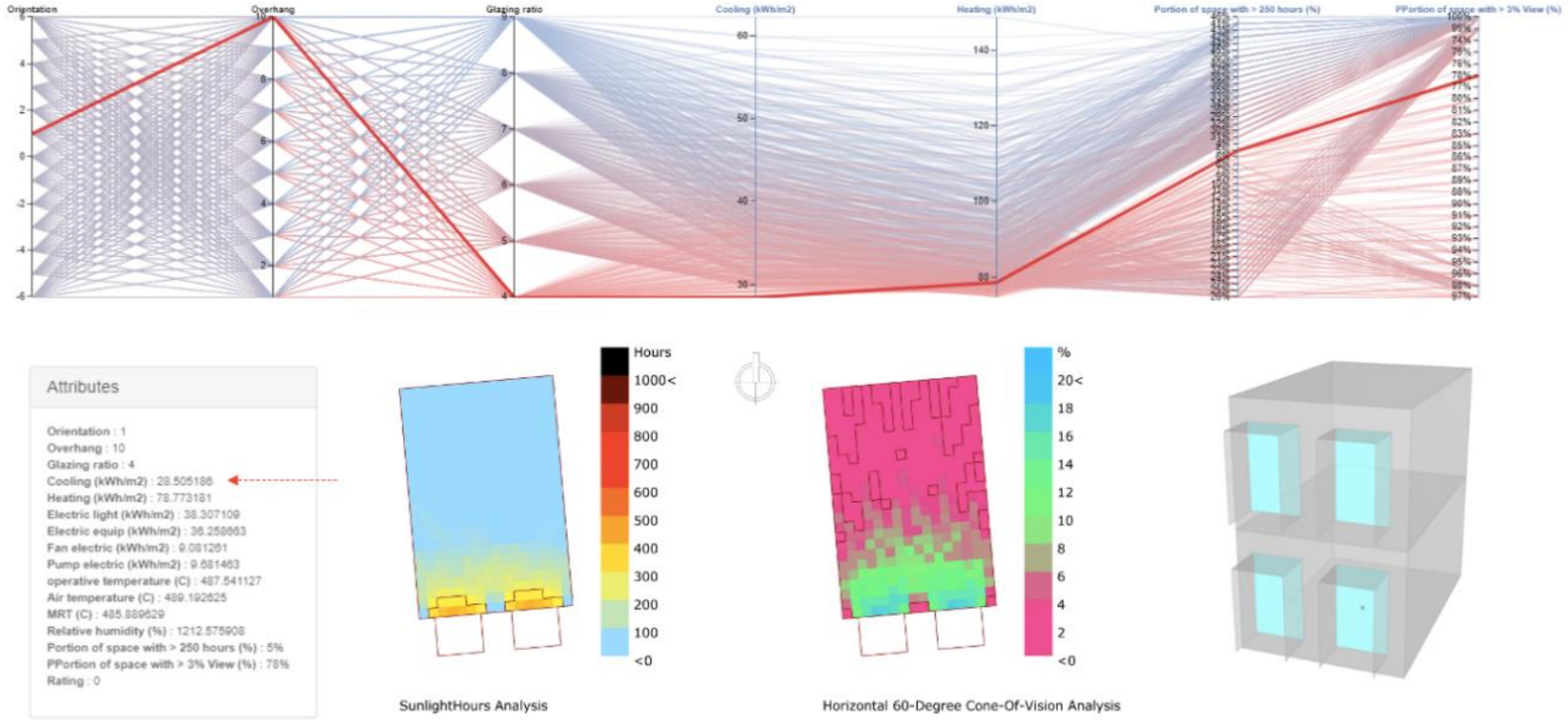

Figure 4.21. Targeted design solution with minimum cooling

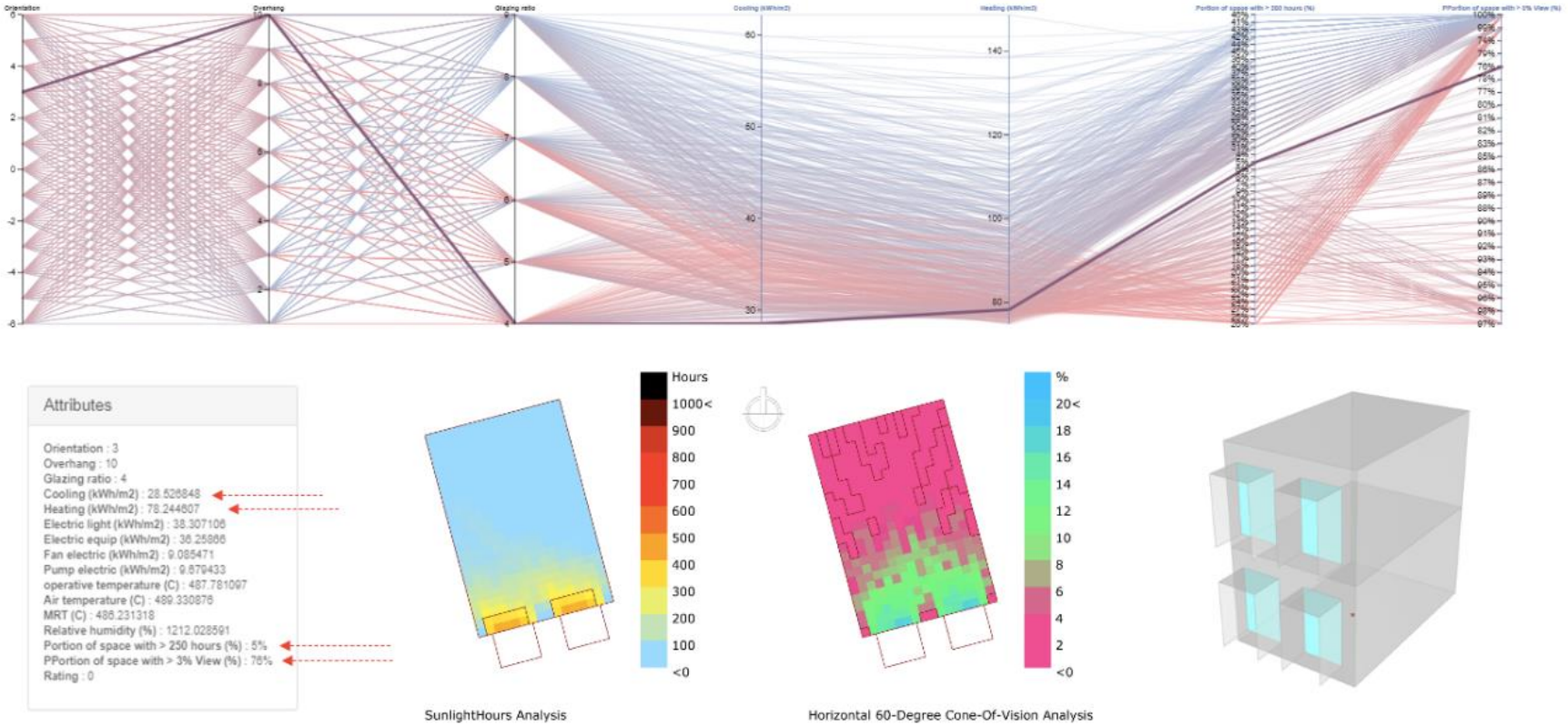

Figure 4.22. Tolerable design solution

4.2.3.6. Maximum view and minimum sun hours

Sun exposure analysis and an exterior view are two additional objectives unrelated to energy consumption reduction. Figure 4.23 (top) shows the solution with the highest value in sun exposure and view analysis. The model with the highest percentage of view, more than 3% to the outside, is attributed to design variable orientation 30^{o} towards the East direction, which reached 100%, overhangs of 10 cm and a 90% glazing ratio. This model performs 57.81 kWh/m^2 of cooling and 127.96 kWh/m^2 of heating. Figure 4.23 (bottom) shows the design solution with minimum sun hours that are attributed to -10^{o} towards the West direction, 1 m overhangs and a 40% glazing ratio. This model performs at 28.55 kWh/m^2 for cooling and 79.21 kWh/m^2 for heating. For both provided models, the highlighted wire on the parallel coordinate diagram depicts the relationship between parameters and outcomes.

4.2.3.7. Parameter tendencies

In the Design Explorer user interface, the designer is able to view the condition of each step of each relevant axis, and the wires at the chosen location are illuminated when the mouse or pointer is placed over them. The ranging value can be selected by clicking or dragging to reveal its relationship (multiple selections).

Figure 4.24 demonstrates the propensity of three design factors to accomplish the desired results, namely energy consumed for cooling and heating. The red-circled dots represent the desired position within the parameters, while the blue-dotted bubble represents the search area for least cooling and heating energy consumption. It can be seen from the aspect of building orientation, when the searching area pointed to the minimum values in heating and cooling, the wires in the orientation axis move to the step 0 to 2, It means that minimum values in cooling and heating were driven when building facing 0° to 10° to the East direction. In overhang parameters, the search for the minimum value in energy consumption directs the wires to the length of the overhang for four means that the minimum value is found in 40 cm of overhang. In terms of glazing ratio, the minimum value leads to the glazing ratio of 4. This means that the minimum energy consumption is mostly found in the glazing ratio of 40%.

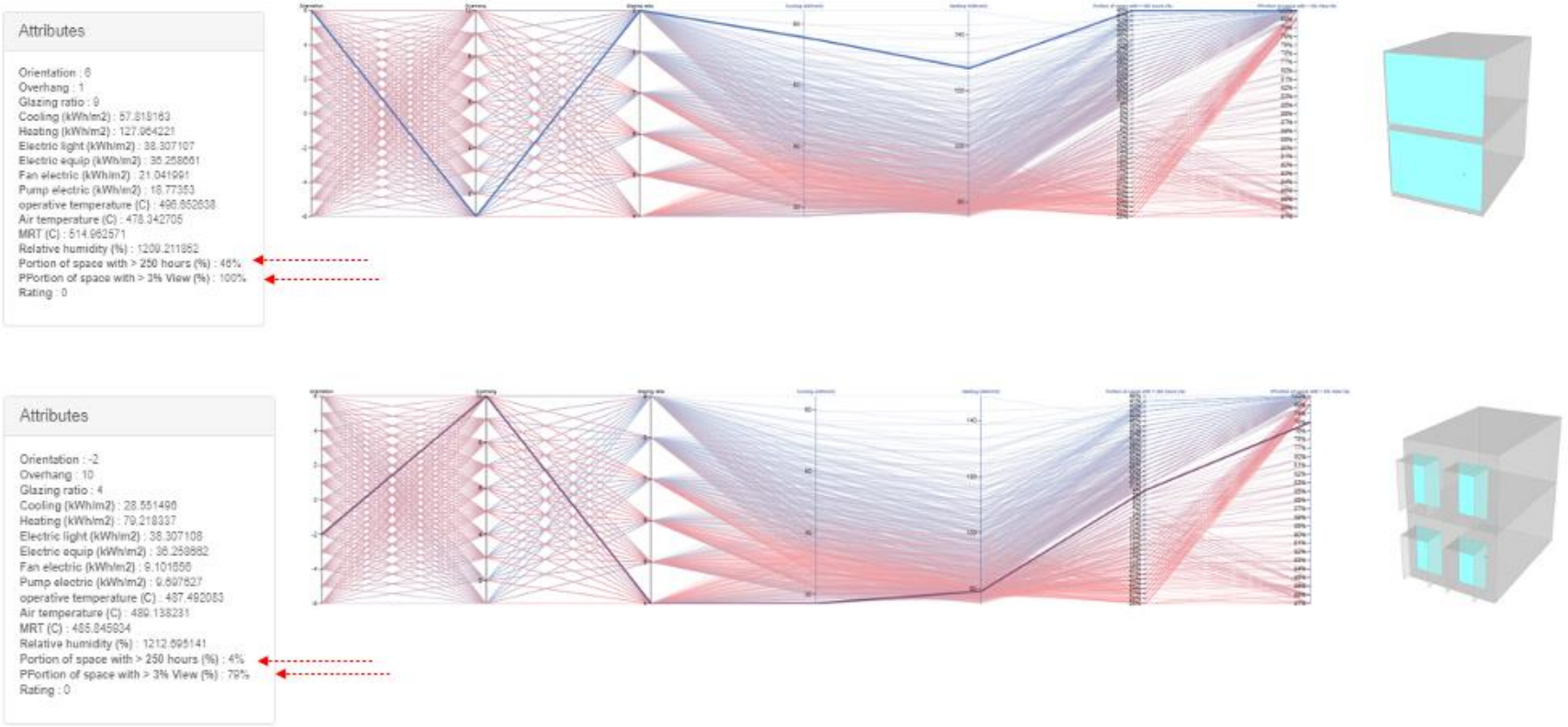

Figure 4.23. Targeted design solution in view analysis and sun exposure

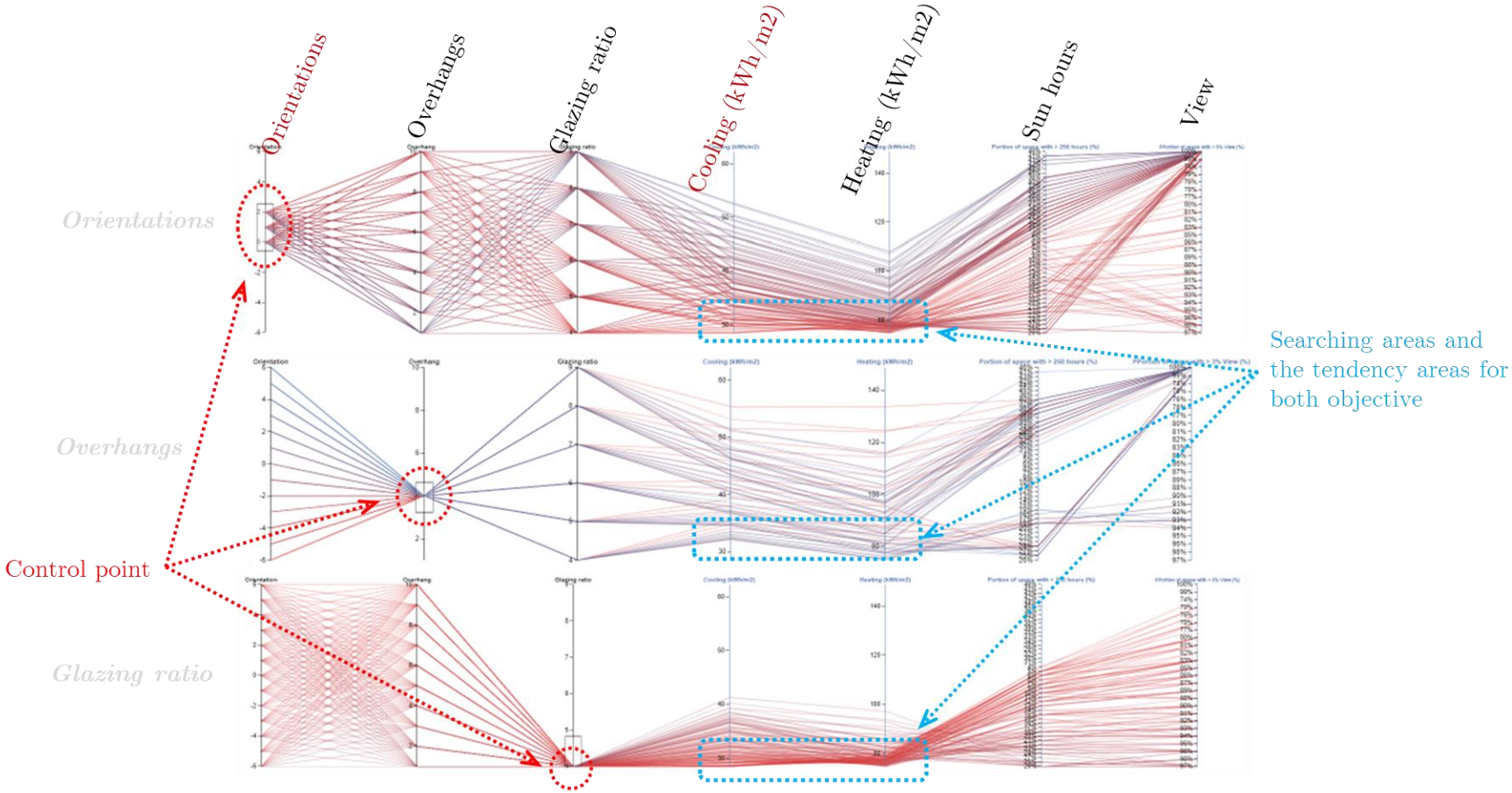

Figure 4.24. Tendency between parameters

4.2.3.8. Potential efficiency compared to the base case

Based on the aforementioned results and the correlation between parameters, there is a potential for efficiency by applying this method to study many performances when creating the benchmark model of a two-story wooden house in Kitakyushu, Japan. The efficiency will be evaluated by comparing the performance of the base case to the solutions generated through iterative methods. Figure 4.25 is dedicated to presenting the energy performance disparity from the comparative phase. The red bars reflect energy use for heating, while the blue bars show energy consumption for cooling. The yellow bars represent the difference in performance between the base case and the other models.

From the bar chart, the efficiency calculated for a whole year period stated by the winter best performance model reached 2.58 kWh/m^2 in cooling and 3.36 kWh/m^2 in heating. Summer's best performance model stated an efficiency of 6.17 kWh/m^2 for cooling but slightly exceeded it in terms of energy for heating compared to the base case. For the tolerable model, it was only the cooling that had that stated efficiency of 6.15 kWh/m^2. The best sun hours in the summer model stated efficiency of 6.12 kWh/m^2 in terms of cooling but slightly exceeded the performance for heating. For the best sun hours in the winter model, both cooling and heating energy consumption indicated a considerable value of about 20 kWh/m^2 for cooling and about 14% kWh/m^2 for heating.

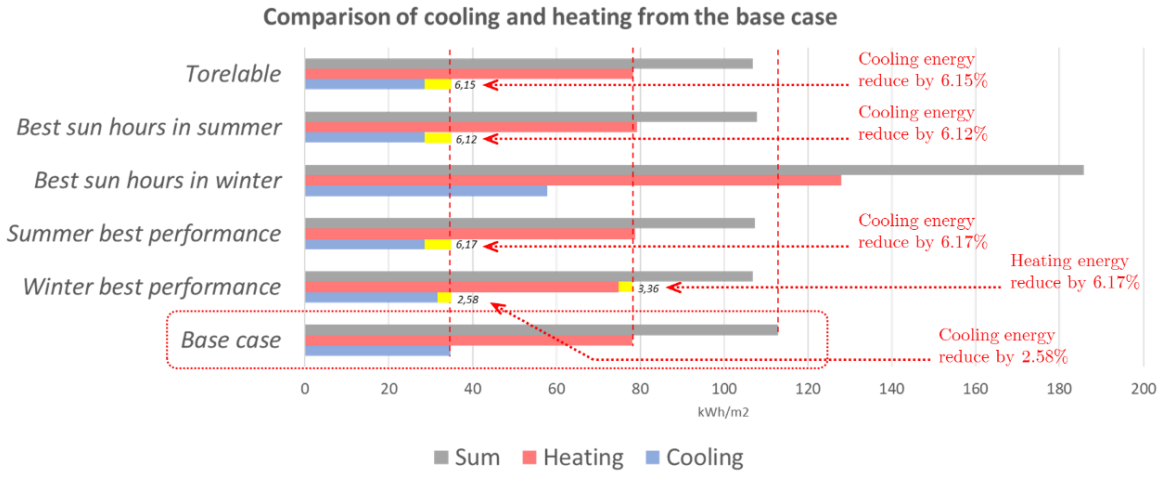

Figure 4.25. Comparison and potential efficiency

4.3. Daylight performance and energy consumption optimization of louvers shading devices under three different sky conditions

4.3.1. Introduction

While a development in computational tools offers the potential for approaching environmental performance through building performance simulation, and much research incorporates it in conducting shading-related daylight and energy simulations, a generative optimization intention while investigating and comparing different sky conditions and analysis periods is still limited. Thus, this sub-chapter presents a generative approach to investigating daylight and energy efficiency and seeing the possibility of optimization during the early design stage of a virtually designated office through the parametric process and multi-objective optimization, simulated in three different sky conditions and analysis periods, which are Birmingham, UK, Jakarta, Indonesia, and Sydney, Australia, aiming to answer the questions of whether the proposed approach can produce optimization and what the best design solution and its parameters can balance the daylight, view to the outside, and energy consumption objectives.

4.3.2. Methodology

4.3.2.1. Overview

The study was entirely conducted using virtual models and platforms using a parametric approach [95,128]. Figure 4.26 presents the workflow of the conducted research. The initial phase started by defining the metrics for the objectives. Geometry preparation, environmental and energy simulation were established by arranging the definition of the office model, dynamic louver configuration, daylight simulation definition set, and energy simulation definition set.

In the environmental simulation definition, the weather data of the targeted city was applied. The single results will be trained during the genetical MOO process to filter and produce pareto front individual solutions. The Pareto front solutions that were found will be ranked using a fitness function and compared to the benchmark model (BM) that

equipped with no shading. Rhinoceros and Grasshopper are the main platforms in the modelling, simulation, and optimization phases. Ladybug and Honeybee are the plugin bridging the well-known simulation engine such as THERM, Radiance, EnergyPlus, OpenStudio, and Daysim. While for the optimization, the plugin called Octopus has been used. However, for the data collection and design iterator, Colibri from TTtoolbox was incorporated. In the end, the statistical software JMP and Microsoft Excel were also used to look at the data from the MOO.

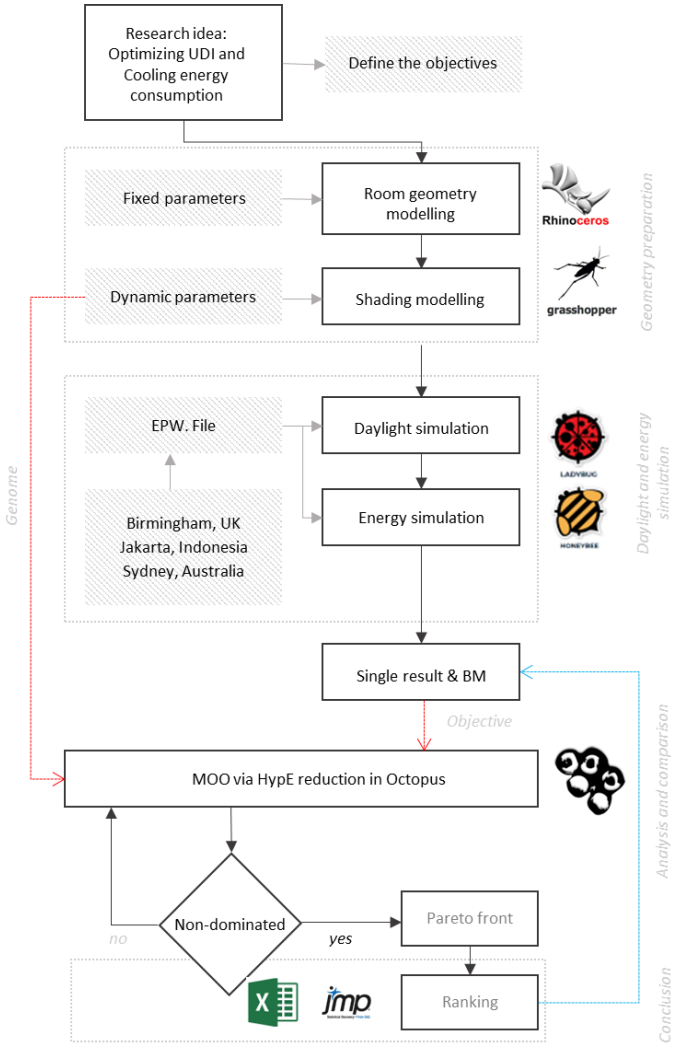

Figure 4.26. Research workflow

4.3.2.2. Geometry modelling

In terms of geometry modelling, as for UDI and cooling energy consumption data collection, a 12 m x 8 m x 3.5 m hypothetical office room has been virtually developed. The shading as a main feature has four dynamic parameters, namely overhang, spacing, blade size, blade rotation, and the additional parameters of rotation angle and room orientation, illustrated in Figure 4.27. Each parameter was set to have a variation between its minimum and maximum value. The parameters such as blade rotation and orientation were divided and multiplied by a multifaction or division factor to avoid uncontrolled and clashing iterations during the iteration processes. Besides, the strategy to divide the value was to limit the number of possible design solutions, saving time on optimization. The detailed dynamic parameters are presented in Figure 4.27.

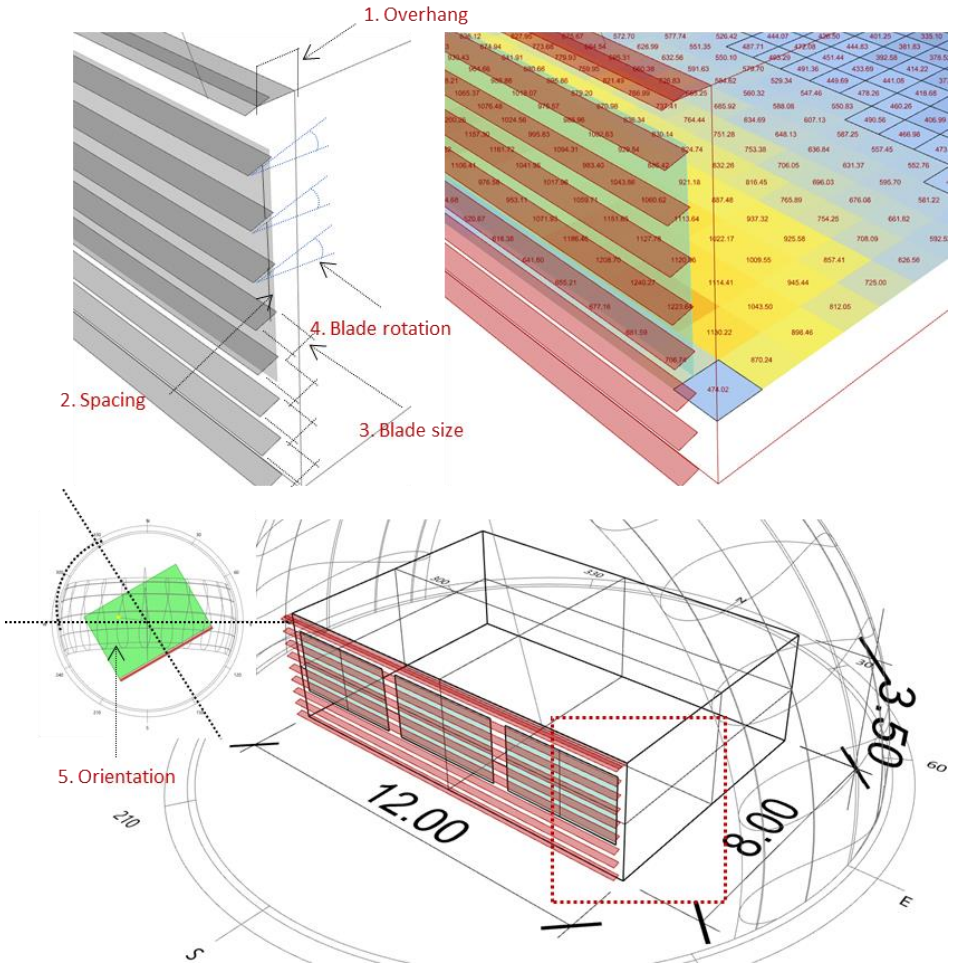

Figure 4.27. Dynamic parameters of the louver shading and the room orientation

Table 4.3.1. Dynamic parameter setting

Parameter	Lower limit	Upper limit	Multiplication factor	Units	Iteration
Overhang	1	3	30	cm	4
Spacing	2	10	5	cm	9
Blade size	2	9	5	cm	8
Blade rotation	0	9	5	°	10
Building orientation	-30	30	1	°	60

4.3.2.3. Context and simulation period

To undergo daylight and energy simulation, regardless the optimization process, environmental weather data is needed as data feedback supplying information of specific weather data based on specific regional context. The weather data for each city is supplied by using the EnergyPlus Weather File, or EPW File. Regarding the combination objective of energy (cooling energy consumption) and daylight (UDI), the analysis period taken was decided to be the hottest area based on the weather forecast engine online following the extreme hot week that was taken for the analysis period in the energy simulation.

The designated date and the sun position are illustrated in Figure 4.28 to generate sky conditions, the component "Honeybee Generate standard CIE sky" with the input of sunny without sun has been used to match the analysis period that designated day in Figure 4.28. As for the energy simulation, the extreme hot week from each city has been extracted from the EPW "statFile". The following period includes Birmingham, which was set to be August 8 to August 23, Jakarta, April 23 to April 29, and Sydney, February 2 to February 18. The periodical range of the simulated period are retrieved from the historical data of each city from the EPW file in Ladybug components.

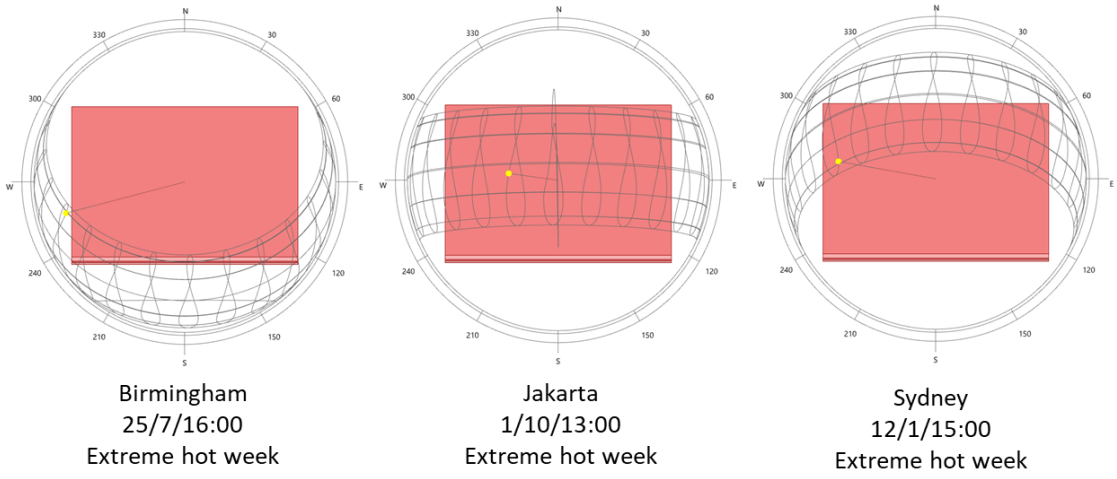

Figure 4.28. Sun position and the analysis period of each city

4.3.2.4. Daylight and energy simulation

As previously adopted, this part of research considered useful daylight illuminance (UDI) as a daylight metric (lux), the first performance objective. Nabil (2005) first introduced UDI as a new paradigm in assessing daylight in buildings. The UDI can be considered an annual occurrence of illuminance within the range of "useful" as considered by occupants. The daylight illuminance of less than 100 lx is generally considered insufficient, 100 lux to 500 lux is considered effective, 500 lux to 2000 lux is considered desirable or tolerable, and a range of more than 2000 lux is considered exceeding that can lead to visual discomfort [125]. This research only focuses on and calculates the range between 300 lux to 500 lux. The total cooling energy consumption (kWh) was the second performance objective. The third objective was a geometry objective in which the shading surface area was assumed to drive the ratio of the view to the outside. For material used in this hypothetical model of the simulated room, the properties of EnergyPlus (EP) construction and Radiance (RAD) material are presented in Table 4.3.2.

Table 4.3.2. EnergyPlus construction and Radiance material

Materials	Uvalue(W/m²-K)	Rvalue(W/m²-K)	ρR	ρG	ρB	Roughness	Specularity
Interior wall	2.58	0.39	0.75	0.75	0.75	0	0
Exterior wall	0.46	2.18	0.75	0.75	0.75	0	0
Interior floor	1.45	0.69	0.21	0.2	0.22	0	0
Interior ceiling	1.45	0.69	0.8	0.8	0.8	0	0
Windows	0.5	SHGC: 0.25, VT: 0.10	τR: 0.817	τG: 0.817	τB: 0.817		
Shading	56600	0.000018	0.8	0.8	0.8	0.2	1

4.3.2.5. Multi-objective optimization (MOO)

When the design targets only a single performance objective, the calculation of optimization will be straightforward. When more than one objective set to be the objectives, the conflicting trade-offs are undeniable. This research uses Octopus, deploying an algorithm for fast hypervolume-based many-objective optimization, HypE reduction [129], to undergo the multi-objective optimization (MOO) processes. The search was intended to combine multiple targets to minimize cooling energy consumption and shade surface area while maximizing UDI of 300 lux to 500 lux. The setting of the octopus is presented in Table 4.3.3.

Table 4.3.3. The Octopus optimization setting

Parameter	Setting
Elitism	0.5
Mutation probability	0.2
Mutation rate	0.9
Crossover rate	0.8
Population size	100
Maximum generations	25
Record interval	1
Non-dominate ranking method	HypE Reduction
Mutation strategies	HypE Reduction

4.3.3. Results

4.3.3.1. Benchmark model and the fitness function solutions

A total of 8509 automated simulations have been run for the purpose of this research. The MOO yielded 2594 possible solutions for Birmingham, 2597 possible solutions for Jakarta, and 2598 possible solutions for Sydney. As previously mentioned, a benchmark model has been developed for the needs of comparison and observation in efficiency. This model is the same model as the simulated one but without shading. The benchmark model situated in each case study facing the south direction, means that it has a zero-degree angle of rotation. The simulations that were carried out for these models took place in the same environmental setting. To visualize,

Figure 4.29 illustrates the different conditions of the benchmark model and the model obtained from the optimization and fitness function calculation process [80]. It can be observed in the figure that the presence of shade and the orientation had an impact on the distribution of the points. Furthermore, the fitness function calculation was applied to the pareto frontier individual yielded from MOO. Table 4.3.4 shows the characteristics and aims of various solutions, as well as their relative importance. In the general comparison chapter, each of the results will be discussed in further depth.

Table 4.3.4. The attributes for the best solution based on fitness function calculation

	Birmingham								
	Solution No.	Overhang (cm)	Spacing (cm)	Blade size (cm)	Blade rotation (°)	Building orientation (°)	Shading surface area (m^2)	UDI 300 lx-500 lx (%)	Cooling energy consumption (kWh)
BM	0	0	0	0	0	0	0	36.458333	87.427792
FF	2060	1 (30)	3 (15)	4 (20)	0 (0)	-26	55.2	65.625	62.833461
	Jakarta								

	Solution	Overhang (cm)	Spacing (cm)	Blade size (cm)	Blade rotation (°)	Building orientation (°)	Shading surface area (m^2)	UDI 300 lx-500 lx (%)	Cooling energy consumption (kWh)
BM	0	0	0	0	0	0	0	30.989583	616.868
FF	2509	1 (30)	6 (30)	8 (40)	1 (5)	-29	57.6	76.302083	596.714245

Sydney

	Solution	Overhang (cm)	Spacing (cm)	Blade size (cm)	Blade rotation (°)	Building orientation (°)	Shading surface area (m^2)	UDI 300 lx-500 lx (%)	Cooling energy consumption (kWh)
BM	0	0	0	0	0	0	0	36.71875	323.71875
FF	2276	1 (30)	6 (30)	7 (35)	2 (10)	-29	50.4	65.885418	314.020488

Figure 4.30 shows the four axes of the population field, which have the axis of the objective cooling energy consumption, UDI 300 lux to 500 lux, and the shading surface area represent the view to the outside, populated by the individuals during MOO training. The dots represent the cases of Birmingham, Jakarta, and Sydney. The closest individual to the coordinates 0, 0, 0, as the default setting in Octopus, is the targeted searching area. Table 4.3.4 depicts the qualities and goals of different solutions, as well as their relative relevance in the context of the overall problem. Each of the findings will be addressed in further detail in the general comparison chapter. Considering the configuration and pattern of individual distribution, Jakarta and Sydney perform similar pattern, it was possibly because the sun position between the two cities is almost the same in different sets of analysis periods (Figure 4.28 and Figure 4.29).

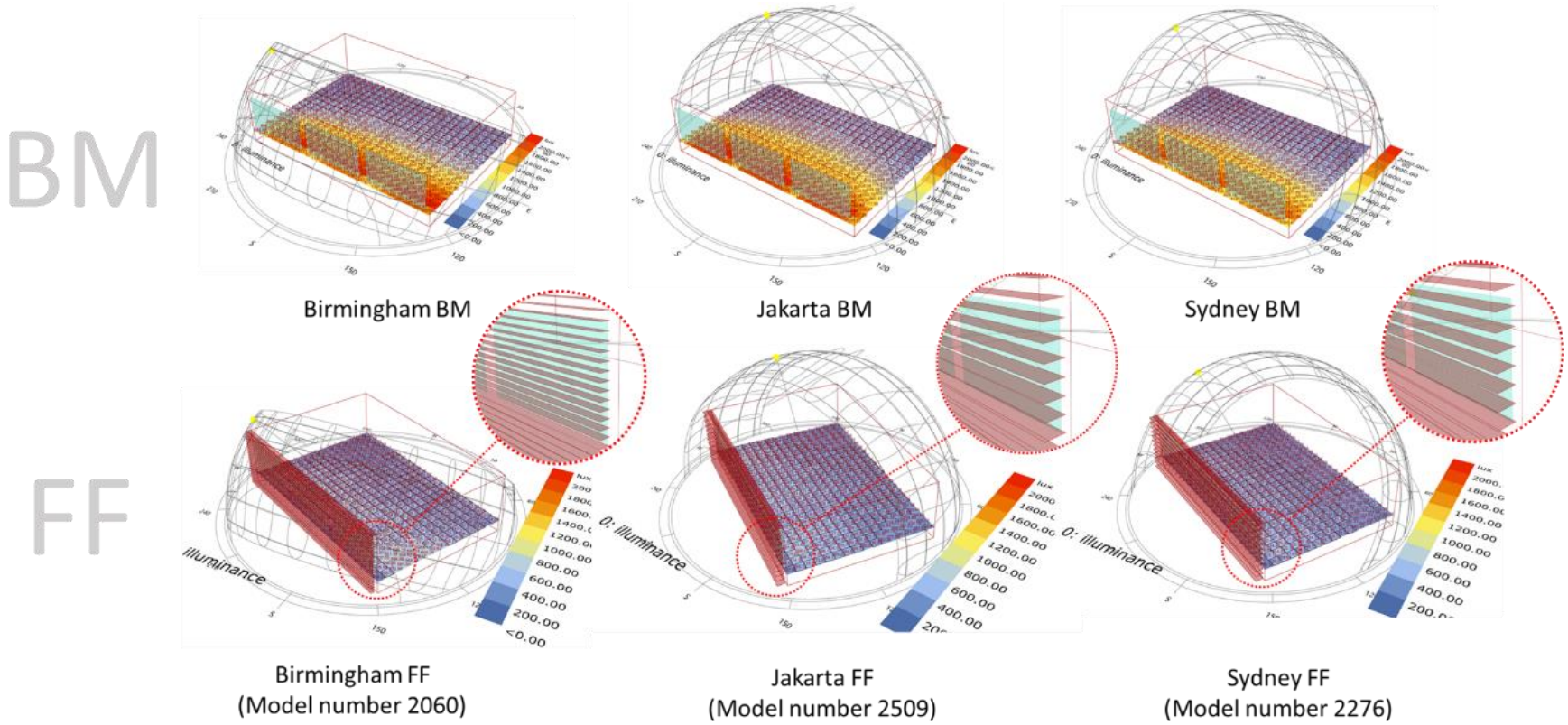

Figure 4.29. Benchmark model and the solution from fitness function calculation

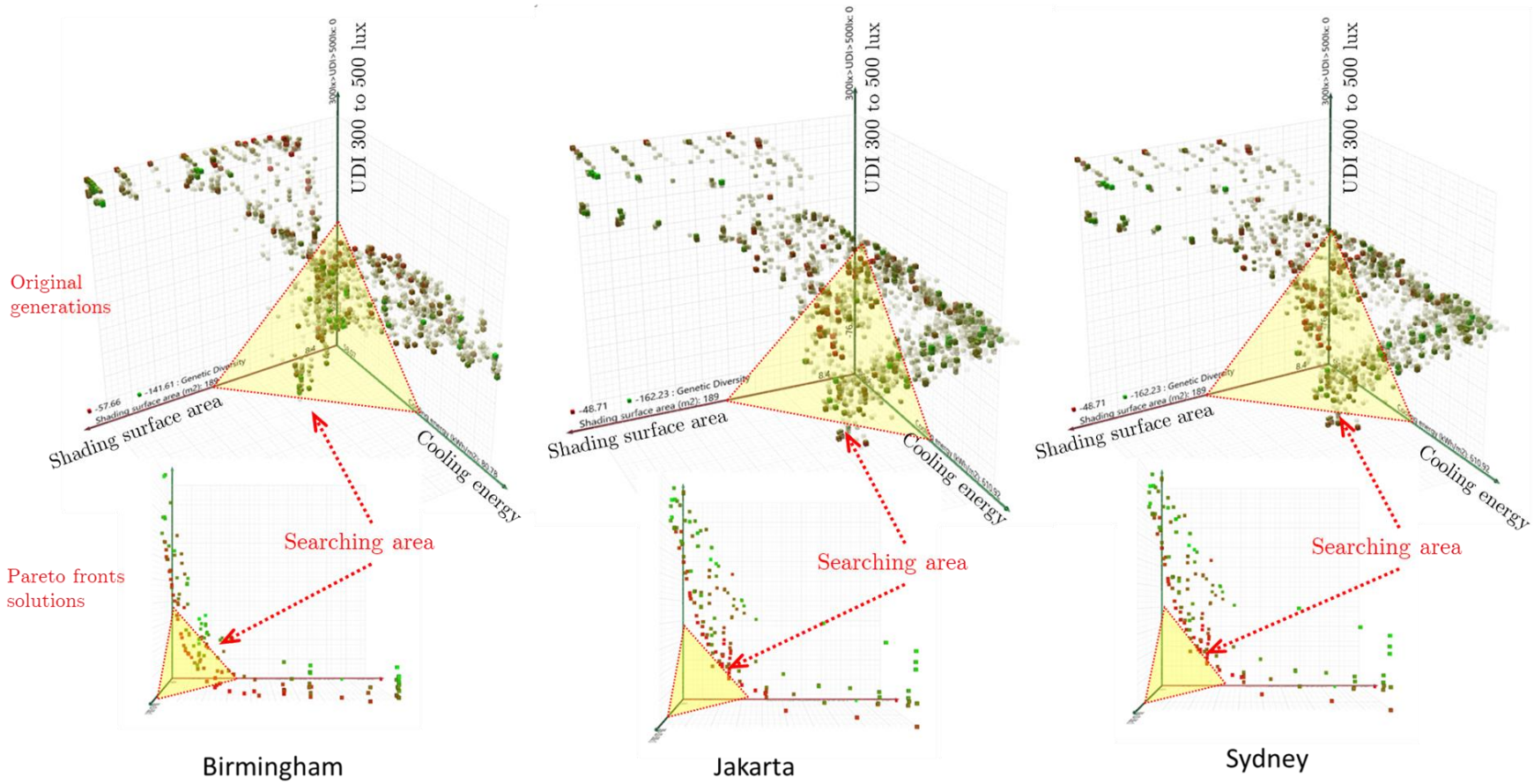

Figure 4.30. Original population field of the optimization results

4.3.3.2. Objective correlations

This part will describe the correlation among objectives. The total data was obtained as a result of the optimization procedures (Figure 4.30 to Figure 4.33). This indicates that throughout the training and weighting processes in MOO, they are influenced by the tendency of their goal target's genetical mating during the training and weighing procedures. As a result, the data utilized in this study may exhibit different trends than data from a study in which all the parameters are iterated. It has been decided to use a scatter plot in order to examine the distribution between two design objectives.

Figure 4.31 depicts the correlation analysis and the distribution of individuals in Birmingham. From the scatterplot, it can be seen that there is an insignificant correlation between shading surface area, UDI 300 lux to 500 lux, and cooling energy consumption. The distribution of pareto front solutions showed a concentration of smaller shading surfaces associated with UDI that ranged between 20% to 50%, while the largest UDI percentage was associated with a surface area between 55 m^2 to 75 m^2. The relationship between UDI and cooling energy shows that only the range of UDI maximum of 50% to less than 70% was associated with minimum cooling energy consumption. Moreover, related to surface area, lower surface area was correlated with the highest cooling energy consumption.

Figure 4.32 illustrates the scatterplot of objective distributions in Jakarta. In the case of Jakarta, cooling energy consumption has a quite significant correlation with shading surface area. The highest UDI percentage was at around 50% of the shading surface area. A density of individuals was concentrated on a shading surface of less than 50 m^2 with UDI of around 20% to around 55%. The lowest cooling energy consumption can be found in surface areas ranging from 125 m^2 to 175 m^2. Thus, the smaller surface area, is possibly positively corelated with higher cooling energy demand in the extreme hot week period. Even though the pareto fronts were distributed oddly toward these three presentations, however, the pareto front and FF individuals were inclined to swarm in the right direction. The FF has been successfully located in the axis of maximum UDI, but there are trade-offs in shading surface area and cooling energy consumption.

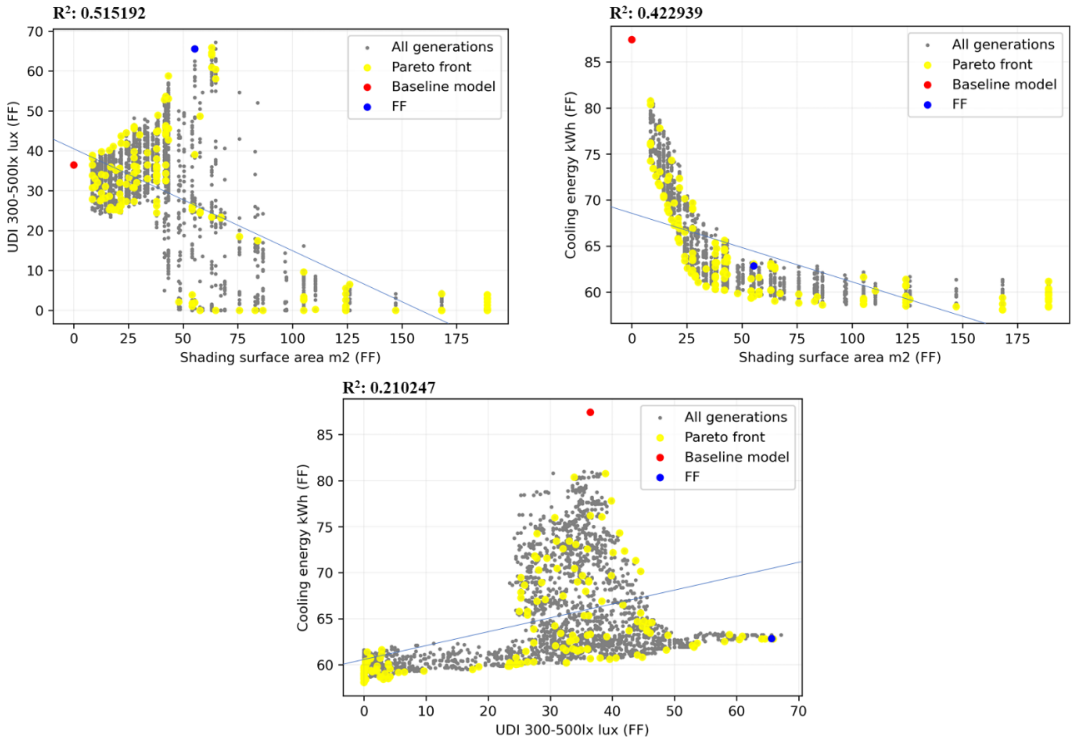

Figure 4.31. Scatterplot presenting correlation between two objectives of Birmingham

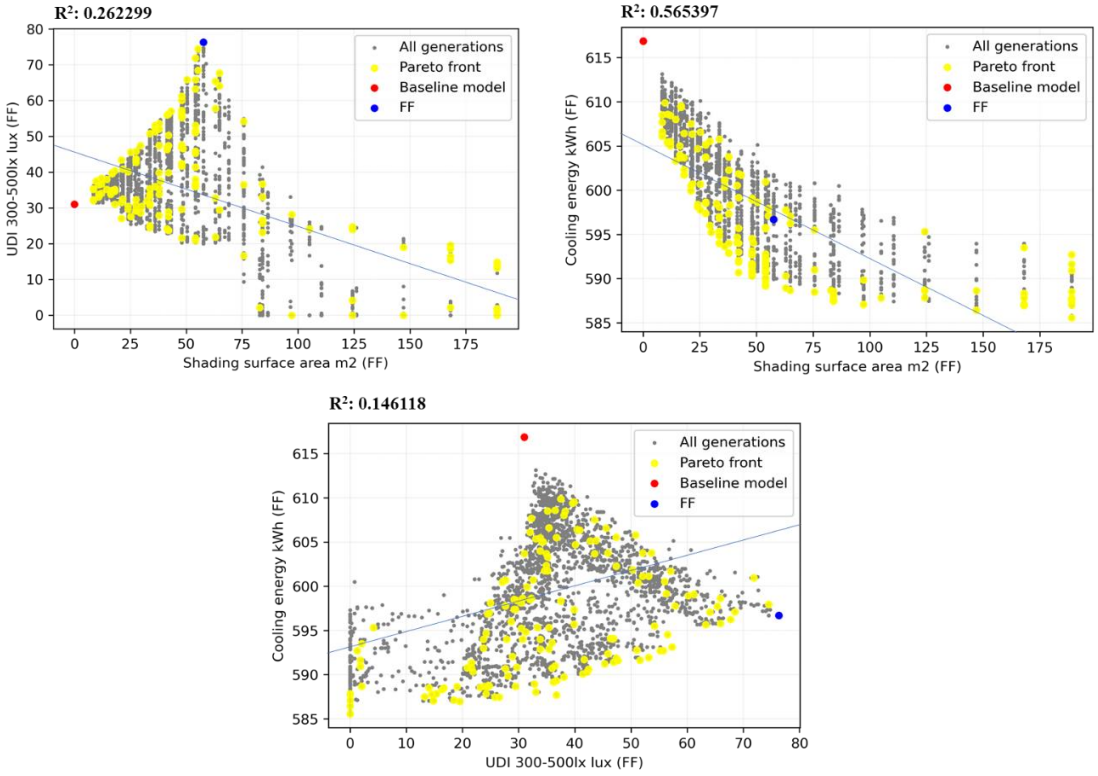

Figure 4.32. Scatterplot presenting correlation between two objectives of Jakarta

The distributions of Jakarta and Sydney show a high similarity in population field appearance except in their objective values and correlation. According to the Fit Y by X function in JMP fit line calculation, shading surface area has a strong negative correlation with both cooling energy consumption and UDI, while the correlation between energy consumption and daylight objective is only 0.468305.

When viewed from the position of the FF solution, both Jakarta and Sydney have located the solution with the largest percentage of UDI in the middle of each objective's range value. In general, the MOO results in Jakarta and Syndey showed similar tendencies but in shading to the UDI 300 lux to 500 lux correlation. Based on the findings, the share similarity between Jakarta and Sydney can be affected by the location that tend to be closer each other compared to Birmingham geographically. The tendency indicate that the system is reliable to be used as it supports common sense with showing similarity of the two regions.

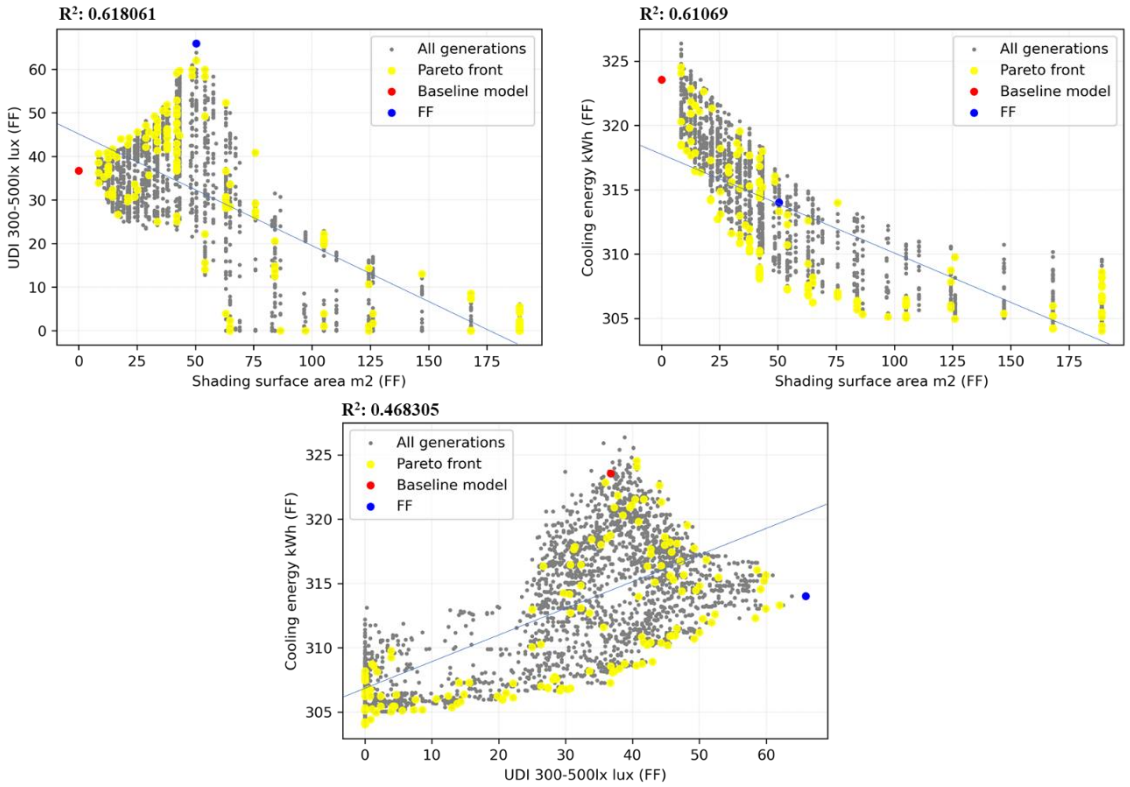

Figure 4.33. Scatterplot presenting correlation between two objectives of Sydney

4.3.3.3. Parameter to objective tendencies

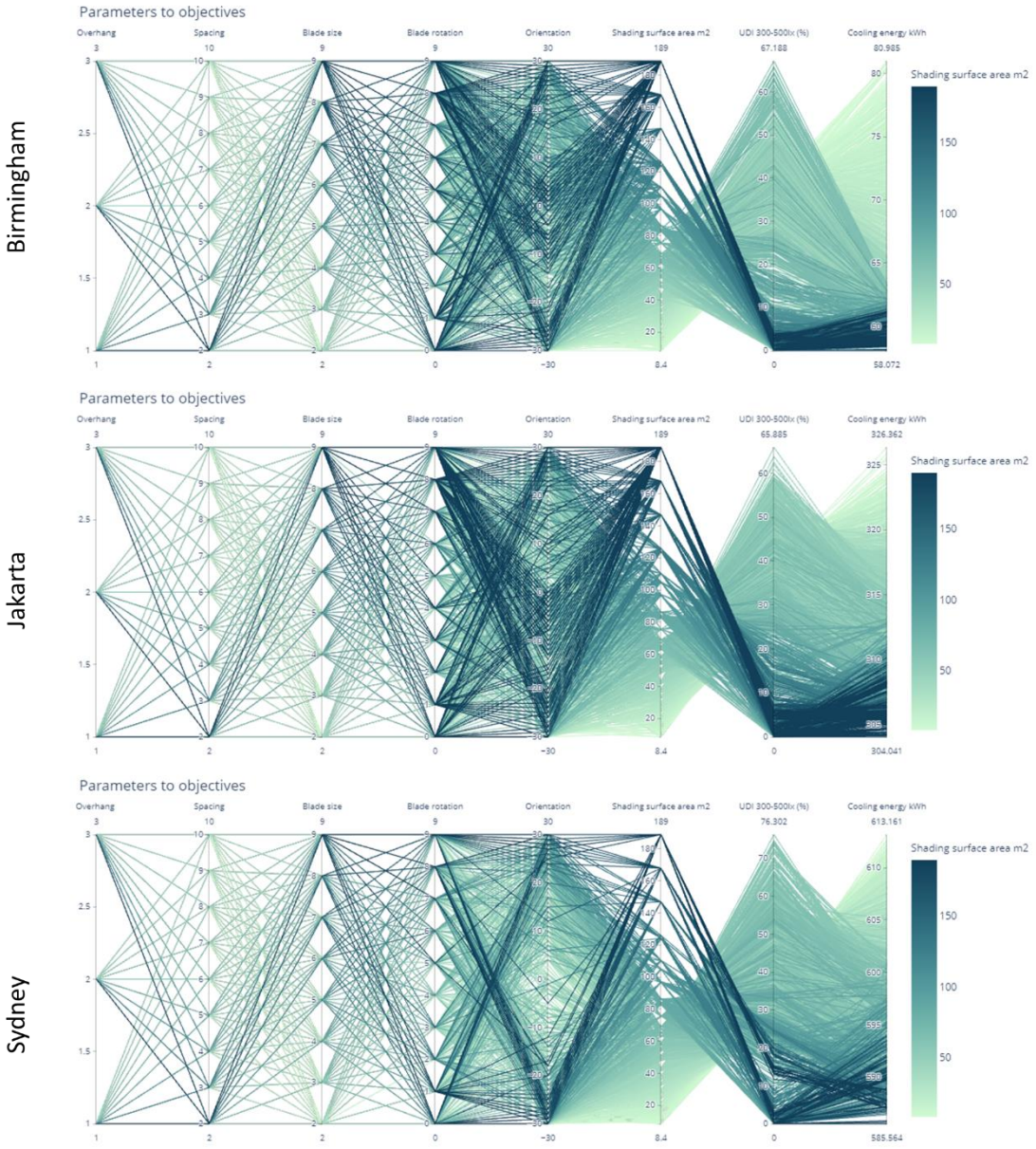

Figure 4.34. Parallel coordinate plot showing the connection between parameters and objectives for all three cases

It has been decided to add a parallel coordinate plot to demonstrate the relationship between the parameters and the optimization targets. The distribution of wires connecting each individual's parameters and the resulting performance in each of the circumstances are presented in Figure 4.34. The parameters genome is represented by the first five vertical axes, and the goals are represented by the next three vertical axes. While color gradation employs the shading surface area for its scale.

There is a similarity between the three different locations. Firstly, a larger shading surface area is associated with the lowest UDI and energy consumption. The desirable UDI value is associated with a shading surface area ranging from 40 m^2 to 80 m^2. By seeing the parallel plot, it is difficult to see the distribution tendency of overhang, blade rotation, and orientation since it shows an even distribution. Minimum energy simulation can be achieved from the combination of minimum spacing and larger blade size. However, this inclination leads to minimum UDI and vice versa. As a matter of common sense, maximum in spacing and minimum in blade size drive minimum shading surface area and directly implicate the possible middle value of UDI (between 25% and 40%) and the highest amount of energy consumption for cooling needs.

4.3.3.4. Results from sensitivity analysis

A sensitivity analysis was performed to determine which parameter has the greatest influence on shaping the performance objectives (Figure 4.35). The analysis was conducted by utilizing the Fit Model function in JMP statistical analysis software, picking the standardized targeted objective as Y or role variable, and putting all standardized parameters in the construct model effects column. The analysis was run by using Standard Least Square for Personality and emphasizing Effect Leverage. The analysis showed that spacing and blade size are the most influential parameters for almost all cases except for Jakarta cases related to UDI 300 lux to 500 lux. The difference in Jakarta cases might be caused by the inclination during the MOO process, considering that the MOO would rather direct the search according to its training process instead of iterating all the parameters. Overhang and orientation are the least influential parameters

recorded in this research. The finding of influential parameters can be a main consideration in further design processes.

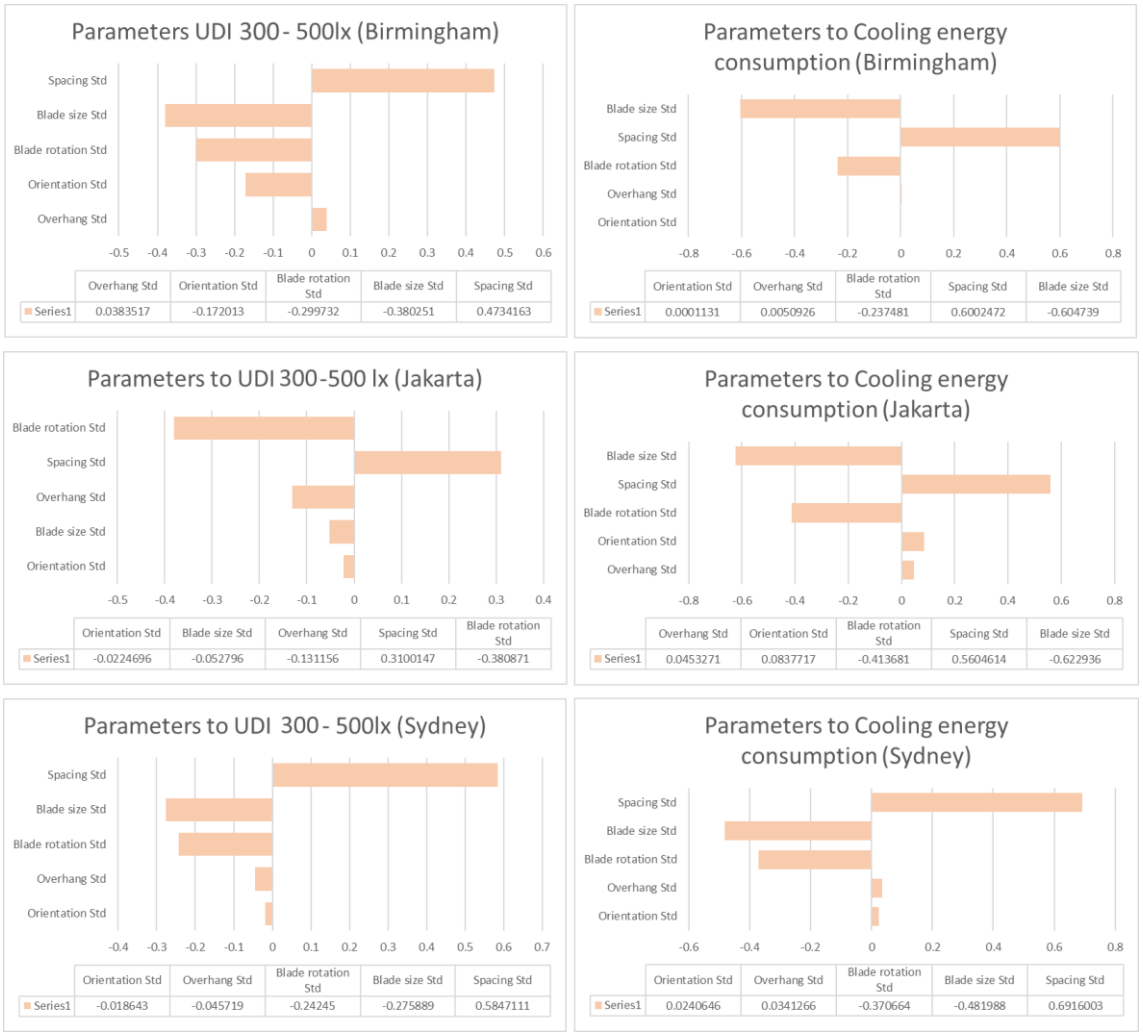

Figure 4.35. Tornado plot showing the results of sensitivity analysis

4.3.3.5. General comparison

The research's ultimate goal of this sub-chapter is to optimize and maximize the efficiency of the proposed approach. By weighing targets in evolutionary algorithm optimization, the efficiency goal is to maximize UDI while minimizing cooling energy use. The efficiency is determined by comparing the benchmark model to one that has been subjected to double filtering during the optimization process and the calculation of the fitness function.

Figure 4.36 illustrates the comparison between the benchmark model with the fitness function and the other observed solutions. In Birmingham, UDI 300 lux to 500 lux has about 80% improvement. In terms of cooling energy consumption, the best solution performed at 25 kWh, or 28% lower than the benchmark model. The solution finding processes have found the highest UDI and cooling energy, and the lowest solution consumed the least cooling energy consumption. In general, the shading strategy in the Birmingham context provided a design solution in terms of daylight and energy consumption. In the case of Jakarta, UDI improved by 146.26 % to reach a level of 76.6%. The energy consumption was optimized for about 20.2 kWh, or 3.26%. In Sydney, the UDI percentage increased by 79.48% and the energy consumption for cooling decreased by about 9.7 kWh, or 2.99%, from the benchmark model performance.

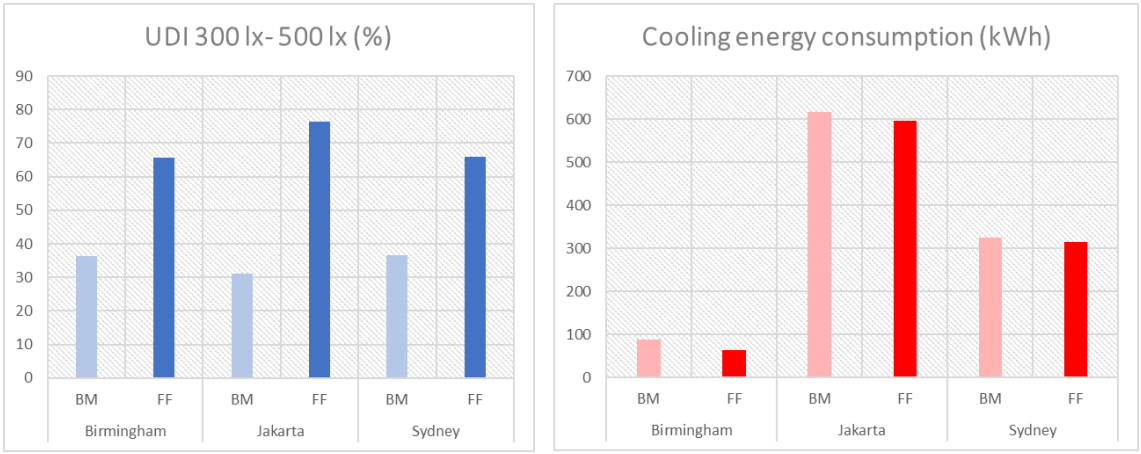

Figure 4.36. General performance comparison between benchmark model and the solution found

This research presented a MOO framework to investigate daylight and cooling energy consumption in Birmingham, Jakarta, and Sydney. The parameters to be used in MOO include the component that shapes the louver shading system. The objective performance was the maximization of UDI 300 lux to 500 lux and the minimization of cooling energy consumption. The simulation was conducted during the extreme hot week for each city,

for energy simulation, and on the hottest day based on weather data for the daylight simulation.

The main finding of this research is that the proposed top-down approaches were proven to be able to find the optimized solution and its parameters that balance multiple design goals. This research also observes the tendency of the parameter distribution toward the objectives. Besides, the spacing of the louver and the blade size are found to be the most influential parameters driving the objective performance. The finding of the research, beside its contribution to the capability of offering efficiency, is also expected to become a design consideration, helping designers or stakeholders to have a better understanding of and immediate performance and visual feedback to support the design decision-making process during the early phase of the design process.

4.4. Chapter conclusion

The chapter discusses three different investigations on approaching interconnection between louver shading and window parameters toward daylight objectives. The first case undergo simulation by iterating louver shading in the context of Jakarta Indonesia. The second case is the development of a benchmark model for two-storey wooden house. And the third case is the investigation of daylight concerning three different sky condition testing the louver shading device component with additional parameter of the room orientation.

Trough the simulation, we found that the best UDI solutions have 30 cm overhangs, 50 cm blades spacing, 30 cm blade size, and 35° blade rotation. The parameter combination produced a UDI_0 of 34.97%, a UDI_l of 64.84%, and a UDI_a of 0%. The best solutions improve UDI_0 by 13.1% compared to the comparison model. Besides, based on the simulation results, the louver removes 1.8% of the glaring possibility from the comparison model, resulting in a 0% UDI above 2000 lux.

Furthermore, the parametric and generative algorithm platform to develop a two-story wooden house benchmark model has been presented. The parametric system was

used to investigate the ordinary box, which represented a typical house with several design attributes such as building orientation, glazing ratio, and window overhang, situated in Kitakyushu city, Fukuoka, Japan. The iteration process produced the geometry with the preferred performance for some of the targeted periods. The design solution shows potential efficiency in terms of energy consumption for both winter and summer. Based on the results, the winter best performance model calculated an annual efficiency of 2.58 kWh/m^2 for cooling and 3.36 kWh/m^2 for heating. Summer's best performance model indicated an efficiency of 6.17 kWh/m^2 for cooling, but significantly exceeded it in terms of energy for heating when compared to the benchmark scenario. Only the cooling system for the acceptable model achieved the stated efficiency of 6.15 kWh/m^2 during the summer's peak solar hours, the model predicted a cooling efficiency of 6.12 kWh/m^2, but a slightly higher heating performance. During the winter model's best solar hours, both cooling and heating energy usage indicated significant values of approximately 20 kWh/m^2 for cooling and 14 percent kWh/m^2 for heating.

Implementing room orientation toward the simulated room with louver in three different areas, in Birmingham, UDI 300 lux to 500 lux has roughly 80% improvement. The optimal solution had a cooling energy usage of 25 kWh, or 28% less than the benchmark model. The solution finding processes identified the highest UDI and cooling energy, with the lowest solution consuming the least amount of cooling energy. Within the context of Birmingham, the shading approach gave a design answer in terms of daylight and energy consumption. In the instance of Jakarta, the UDI increased by 146.26% to reach 76.6%. The energy consumption was optimized by 3.26 percent, or approximately 20,2 kWh. The UDI percentage in Sydney increased by 79.48%, while the cooling energy consumption reduced by 9.7 kWh, or 2.99%, compared to the benchmark model performance. In addition, the spacing of the louvers and the size of the blades have been identified as the most influential criteria affecting the objective performance.

Due to the limited involvement of the material properties, several additional aspects must be considered. The research focuses solely on the relationship between geometry and orientation in terms of energy usage and comfort studies from multiple perspectives. In addition, more effort is encouraged to include more design variables and material properties as opposed to the default material. Even with a limited number of design variables, the results indicate that efficiency can be improved by working parametrically and examining design options for louver, glazing, orientation, and overhangs.

Chapter 5. A Comprehensive parametric daylight investigation of the expanded metal sheet as shading devices

5.1. Chapter introduction

Chapter 4 explains the potential of expanded metal sheet as shading devices. Design exploration and optimization utilizing generative algorithm and multi-objective optimization has been used to investigate daylight in the initial phase of design incorporating virtual simulated room. The detail of experiment setting, and measurement will be described in the dedicated sub-chapter along with the historical existence insight of the expanded metal. The chapter intends to give an insight in the uniqueness of the well-known and locally available material as a solar control in order to support passive design strategy at the same time increasing creativity and design flexibility using this metal material. The chapter divided into four main sections: first; an insight and the profile of expanded metal, second; the expanded metal grating type JIS G3351 daylight study, third; comprehensive daylight investigation of this metal sheet, and forth; is expanded metal study on DGP.

5.2. Expanded metal in contemporary architecture

5.2.1. The expanded metal

The fields of architecture and construction will not be separated from the range of materials used. There are now so many types of building materials that can be used for so many different things, thanks to technology. This gives the designer and other people who work on the project more control and creativity in how their projects are built. The core building materials such as brick, glass, metal, wood, and composites have both advantages and disadvantages regarding their applications. The application does not limit itself to building features. The use of these materials in contemporary architecture ranges from the macro to the micro-scale, including furniture, railings, and displays. However, metal has long been considered to have massive durability for its utilization. Metal can be explored as a building material, whether in solid form, pieces, or sheets. In sheet modulation, several well-known patterns are usually used for multiple purposes. For instance, perforated metal sheets and expanded metal sheets modular sheets of these two

metals can be found on the local market. They are often used for aesthetic and environmentally friendly design features.

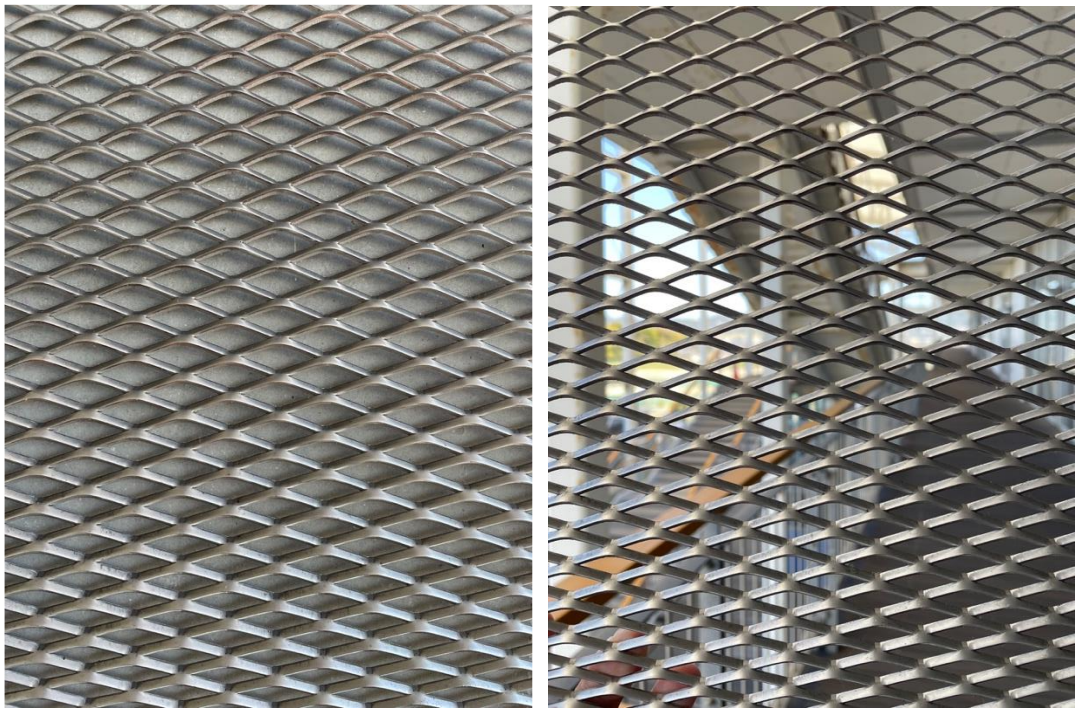

Figure 5.1. Expanded metal sheet. Photograph by the author.

Expanded metal has a long reputation as a building material due to its uniqueness and advantages compared to any other metal-sheet material. Patented in the 1880s, the expanded metal sheet has a long reputation and has become more popular as a building design feature. The flexibility of its applications and its broad availability are making this material one of the designers' favourite building materials. The material is globally promoted, considered, standardized, and industrialized due to it using benefits. One of the associations that authorizes this industry is Expanded Metal Manufacturers Association (EMMA) as a division of the National Association of Architectural Metal Manufacturers (NAAMM). Besides, its specific characteristics and flexibility functioning widely, from cladding to the stair handrail.

This sub-chapter describes and compiles the characteristics of expanded metal, and it is used in the recent contemporary architecture project. This sub-chapter aims to

understand why expanded metal is a preferable alternative material for aesthetic and environmental purposes when choosing building materials. Besides, the information gathered in this sub-chapter is expected to give an overview of how the use of this modular metal sheet successfully translates the designer's vision into a fascinating piece of art. Information in this sub-chapter is meant to show how expanded metal sheet's functional contributions have made a difference in the architectural field today.

Expanded metal has been utilized to enhance architectural and building components since its development in the 1880s. Expanded metal is a type of metal sheet that has been cut and stretched during the production process to generate a pattern of regular diamond-shaped holes and is typically employed in mesh modulation. Expanded metal is a unique substance. It has several distinguishing features:

- First, it is regarded as a very efficient material in terms of production. In contrast to perforated metal, which produces waste from its holes created by punching, expanded metal manufacturing uses a cutting and stretching mechanism, resulting in higher efficiency in production and processing expenses.
- Second, since expanded metal is industrialised and manufactured in mesh, it provides a wide flexibility. With various types, thicknesses, colors and patterns, this metal sheet may assist and elevate the designer’s concept to a new level of inventiveness.
- Third, it is a durable, reusable, and recyclable material.
- It is aesthetic, relatively cheap and sturdy.

With regard to sustainability, expanded metal satisfies at least three key aspects of the USGBC LEED Green Building Rating System’s key areas of performance:

- Energy and atmosphere: used for shade and protection from the sun on an exterior façade.
- Indoor environmental quality: used to support natural ventilation and connect occupants inside the building to outdoor spaces [130] since it functions as an opaque (perforated) shade.

- Materials and resources: contribute to material waste management because primary materials can be sourced from scrap, demolished metal or recycled content, which reduces the impact of extracting regional virgin materials where the industry and suppliers are locally available [131].

This metal mesh has five primary architectural applications: enclosure, protection, decoration, support, and filtration. In addition, it can be utilized in a variety of basic and sophisticated applications, including fences, partitions, and as a reinforcement mesh within structural concrete walls. It can also be utilized as a microscopic sound absorber [132]. Fixed expanded-metal shading devices, secondary skins, and building envelopes can also be employed to mitigate the issue produced by conventional curtain and blind systems. If the occupants opt to keep the curtains closed, for instance, the room does not fulfil the requirements for natural lighting and ventilation, which increases energy usage.

The expanded metal was manufactured and formed as an expanding press through the slits, cut, and pressed by the expanding machine. The machine has a special knife dedicated to the intended pattern from the metal sheet fed into it. The metal sheet usually fed into the machine is pulled out, then slit and pulled again (expanded) to form diamond-like openings of usually regular size in one process [131]. The knife, which some use as a laser cutter for metal [133], can be customized to follow the required or desired type of openings to provide a wide range of designs. The material used as the base of the metal sheet comes in a wide range of metal types and thicknesses, such as carbon steel, stainless steel, and aluminium. However, the material can be made of unique materials such as copper, alloys, titanium, and nickel. Combining the thickness, coatings, design opening, sheet modular, and material combination offered great versatility in terms of its utilization.

The expanded metal design parts usually consist of several parts named Strand, Height, Length, Bond, Angle. Furthermore, the design is developing, and each designer comes up with a new interpretation of the design parts, yet the principle is the same. What is more, through computational development, the design modules and openings are

widely explored, allowing great customization, versatility, and extraordinary and asymmetrical design. Even though this particular application cannot take into account the standard expanded metal sheet, yet it shows one standing point of the expanded metal deployment.

The application of expanded metal may vary, covering both exterior and interior needs. For exterior purposes, the expanded metal can act as a solar screening or solar control [134,135] to prevent direct sunlight and radiation from the sun. It allows airflow and still maintains the view outside. This function supported the outstanding of this material to the environmentally friendly design vision as an alternative to making a strategy alternating artificial light and energy consumption for cooling. Besides the solar screening, the sheet module allows this type of material to be applied as an exterior cladding. The durability of the metal and the creativity and versatility offered by its application can make a project that incorporates expanded metal appealing. Structurally, this material can be a support for plaster and stucco. What is more, it could potentially be used as an exterior balustrade, such as an exterior stairway, for ventilation or as an opaque wall. For instance, to cover parking garages or an outdoor pavilion for internal purposes, the expanded metal can be used for several functions, such as ceilings, wall partitions, and interior balustrades, for aesthetic and protection purposes.

5.2.2. Recent projects incorporating expanded metal

Three recent projects that incorporate expanded metal as its architectural element has been described. The explanation includes the project's profile, what the expression occurs when utilizing this material and in which function expanded metal is deployed. The first project is the New Art Museum. The project was established in 2007, covering an area of 58700 ft2. The architect was Kazuyo Sejima from SANAA, the architecture firm based in Tokyo. The project is located in New York, the United States functioning as an exhibition and museum building. This white box building brought the concept of clear and substantial impact. The expanded metal used in this project act as a façade cladding [136]. Besides this, the transparent cladding enhances the cladding while still keep the windows visible behind the mesh [137].

Figure 5.2. New Art Museum, by SANAA. Photo credit: Hiroatsu Fukuda

Second project is Messe Basel New Hall. This project is located in Mustermesse, Basel, Switzerland. The project covering an 83297 m^2 area and established in 2013. Well, known Architecture firm Herzog and de Meuron is the architect and designer behind this project. The building functioning as an exhibition hall. The façade was intended to eliminate the old previous hall façade that was constructed with monotonous brick. The new hall façade deploys the custom flowing expressed unique pattern of expanded metal. The different variation is reinforced, paradoxically, using homogeneous metal material to express the flowing of urban streets and responding people in the surroundings. Besides the aesthetic purposes, the pattern in the metal skin was to control and regulate the daylight to frame specific views from the people inside the building [138].

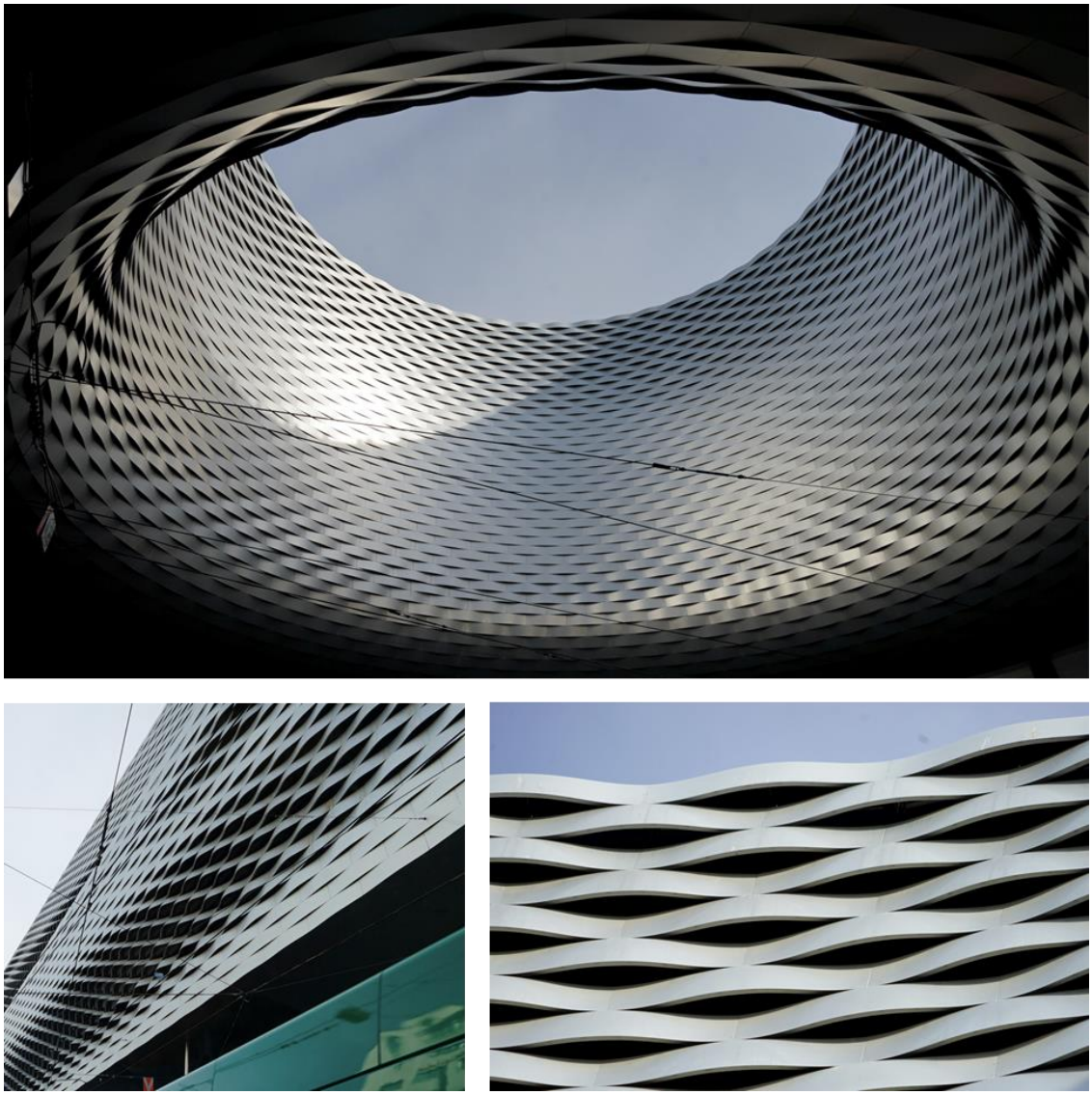

Figure 5.3. Messe Basel New Hall. Photo credit: Hiroatsu Fukuda

Third project is The University of Kitakyushu Institute of Environmental Science Laboratory. The building was designed in 2016, and the operation began in 2017. The university professor designed the project as a laboratory, facilitating research for the university researchers and professors. The project is located on the campus complex side by side with the old engineering laboratory. The laboratory orientating south-north following the sun conditions in Kitakyushu City. To improve the aesthetics and energy efficiency, the architect introduced the device shading using expanded metal. This material was used to get the effect of a falling shadow on the North facing building side while at the same time

preventing solar radiation during the summertime. This metal sheet has been carried out through environmental stimulation that stimulates several types of expanded metal patterns available in the market standardized by JIS G3351 [139].

Figure 5.4. The Laboratory's shading device. Photographed by the author.

5.3. Daylight investigation of the Japan Industrial Standard (JIS) G3351 for expanded metal.

5.3.1. Introduction

Based on the problem that the sub-chapter concerning the benefit of expanded metal shading toward daylight performance is still limited, while the mature industrialization of this material and the architectural field tends to make this material sheet become popular, this sub-chapter aims to examine the daylight performance of expanded metal shading based on the standardized expanded metal types JIS G3351. The objectives of the sub-chapter are to establish a parametric platform that undergoes daylight simulation given a geometrical input as a context. The intention is to answer the question of:

- What is the best type of performance for daylight objectives?
- What is the tendency among the parameters and the objectives?
- What is the tendency between the aperture and daylight objectives?

5.3.2. Methodology

5.3.2.1. Overview

This research undergoes a geometrical and daylight simulation analysis incorporating a parametric approach. The parametric approach means defining a design based on parameters. Consecutively, this research is divided into three major steps. Firstly, geometric modelling of the simulated model and expanded metal shading. Secondly, the definition of the establishment of daylight simulation. Lastly, result analysis and visualization. The sequence of the research is illustrated in Figure 5.5.

5.3.2.2. Geometry modelling

The modelling process includes the making of a parametric definition of the simulated model both for benchmark or benchmarking purposes (benchmark model) and for the expanded metal simulation. The simulated room and the expanded metal model use no dynamic parameters and only represent the features of the standardized market configuration. The simulated room is constructed at 4 m wide, 4 m high, and 8 m deep, representing a small workplace. The room aligns the North-South axis with the façade facing the south direction. The modelled room is equipped with a 70% glazing ratio that acts as a window.

The expanded metal shading was modelled according to the size of the standardized type of Japanese Industrial Standard (JIS) G3351. The components that shape the expanded metal that furthermore become design variables include height, length, strand, and bond. The angle is assumed to be fixed at 5°. Although JIS G3351 includes the other parameters of thickness and weight, however, in this sub-chapter, both parameters are excluded. Considering that the goal is to investigate the geometrical configuration toward

daylight performance, in Figure 5.6, the simulated room and the expanded metal model are presented. and the JIS G3351 standard dimension is presented in Table 5.3.1.

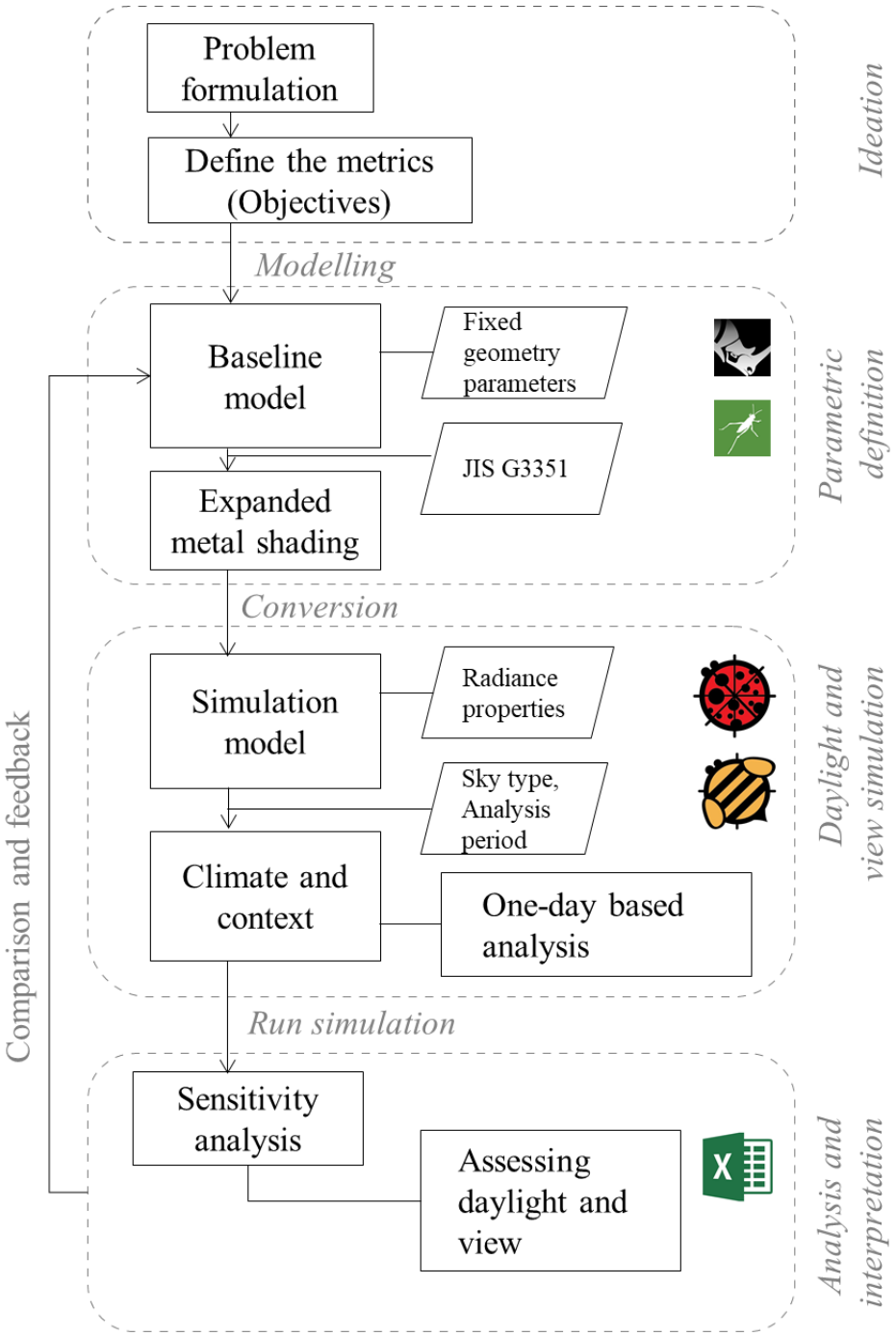

Figure 5.5. Research workflow

This sub-chapter deploys NURBS base 3D modeler Rhinoceros and the plugin Grasshopper to be a main parametric modelling platform. The daylight simulation uses environmental analysis simulation engine called Ladybug and Honeybee. The analysis was undergo using Microsoft Excel.

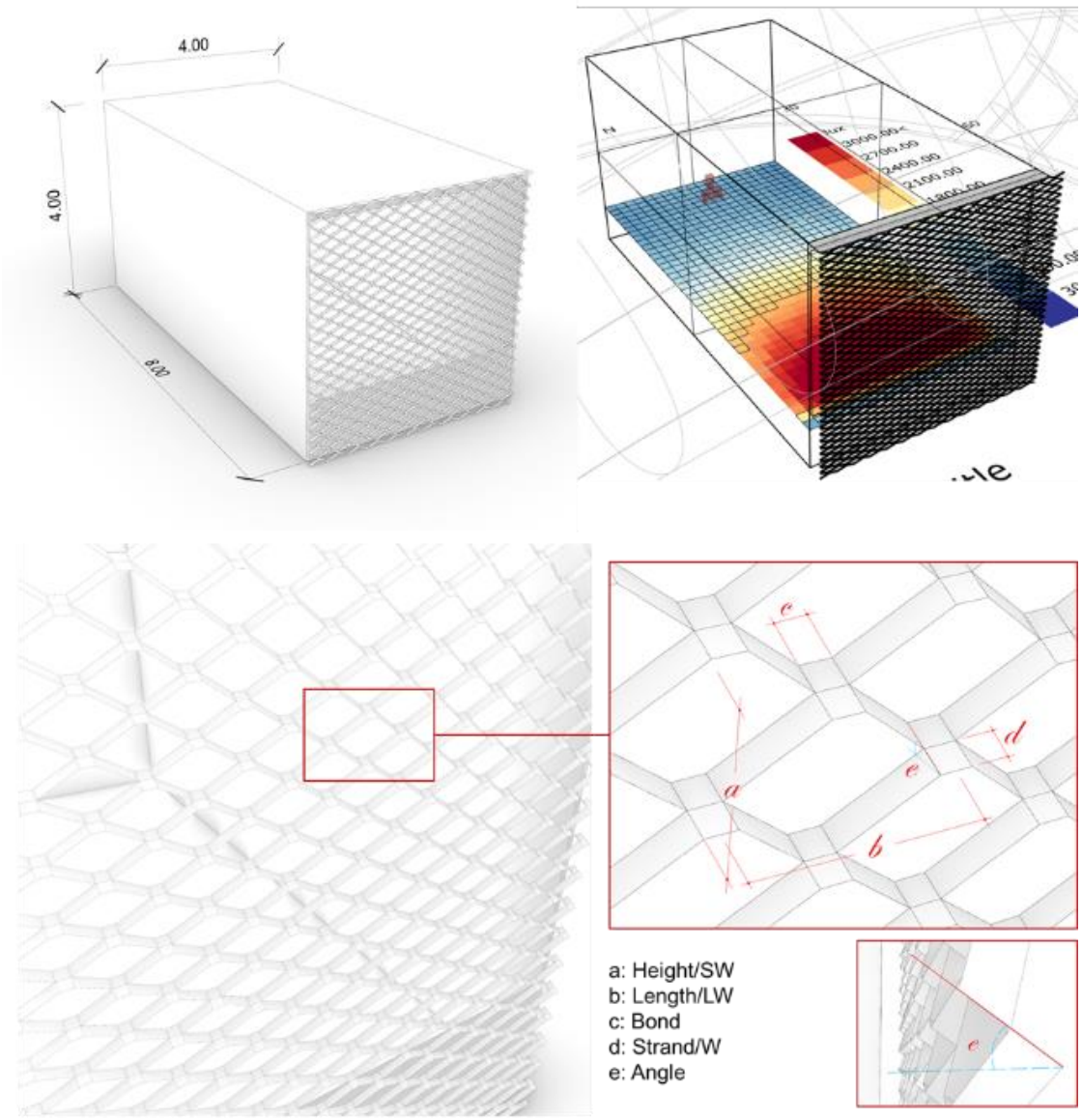

Figure 5.6. Simulated model and the design parameters

Table 5.3.1. JIS G3351 parameters value

JIS G3351 standard and grating types					
No	Type	SW (mm)	LW (mm)	W (mm)	Bond (mm)
1	XG11	34	135.4	7	30
2	XG13	34	135.4	9	30
3	XG14	34	135.4	9	30
4	XG21	36	101.6	7	10
5	XG23	36	101.6	9	10
6	XG24	36	101.6	9	10
7	XS31	12	30.5	1.5	10
8	XS32	12	30.5	2	10
9	XS33	12	30.5	3	10
10	XS41	22	50.8	2	10
11	XS42	22	50.8	2.5	10
12	XS43	22	50.8	3.5	10
13	XS51	25	61	2.5	10
14	XS52	25	61	3	10
15	XS53	25	61	4	10
16	XS61	34	76.2	3	10
17	XS62	34	76.2	4	10
18	XS63	34	76.2	5	10
19	XS71	50	152.4	3.5	10
20	XS72	50	152.4	4	10
21	XS73	50	152.4	5	10
22	XS81	75	203.2	4	10
23	XS82	75	203.2	5	10
24	XS83	75	203.2	6	10
25	XS91	115	304.8	5	10
26	XS92	115	304.8	6	10
27	XS93	115	304.8	7	10

5.3.2.3. Daylight simulation setting

Daylight simulations were conducted in Ladybug and Honeybee. The initial phase begins with the model conversion phase to the Honeybee surface and zones. Furthermore, the process was followed by the weather data input using the EnergyPlus weather data file (EPW) of Shimonoseki, as it was the nearest EPW file available around Kitakyushu city (about 6.47 km). The image-based simulation with the climate-based sky generator was used to simulate the daylight glare probability (DGP) test depicting the winter solstice sky condition on December 21 at 12:00 PM. For the useful daylight illuminance (UDI) test, we incorporated grid-based analysis using Generate Standard CIE sky in Ladybug, depicting the same period yet with a sunny without sun sky condition as the analysis recipe. The global horizontal illuminance in Shimonoseki is illustrated in Figure 5.7.

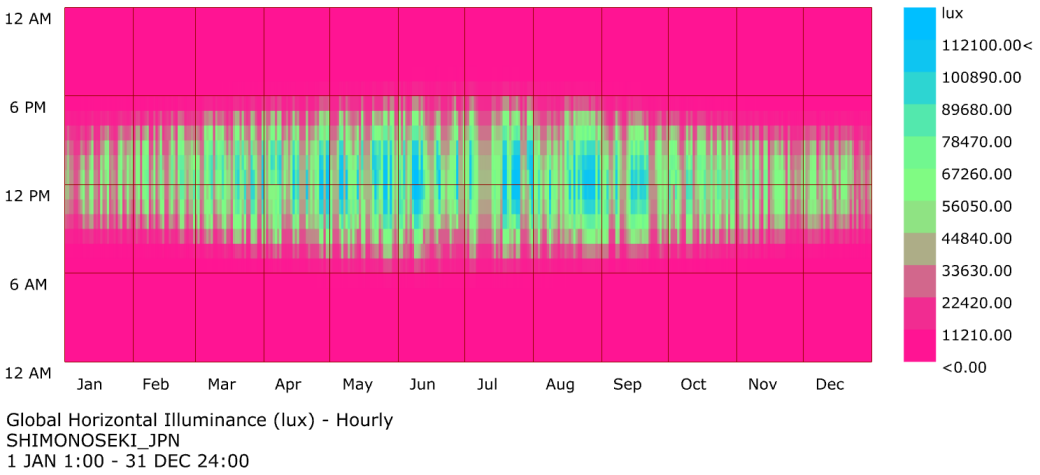

Figure 5.7. Global Horizontal Illuminance in Shimonoseki

5.3.3. Results and discussion

5.3.3.1. Benchmark model

The results of benchmark model are described. A maximum aperture yielded an Intolerable glare DGP (Figure 5.8) and in consequences a half of room distributes with UDI valuing between 100 lux to 3000 lux, presented in a highlighted mesh (grid). The results are presented in Figure 5.9. By seeing the heat map charts, without a shading, the over lit illuminance was occurred behind the glazing.

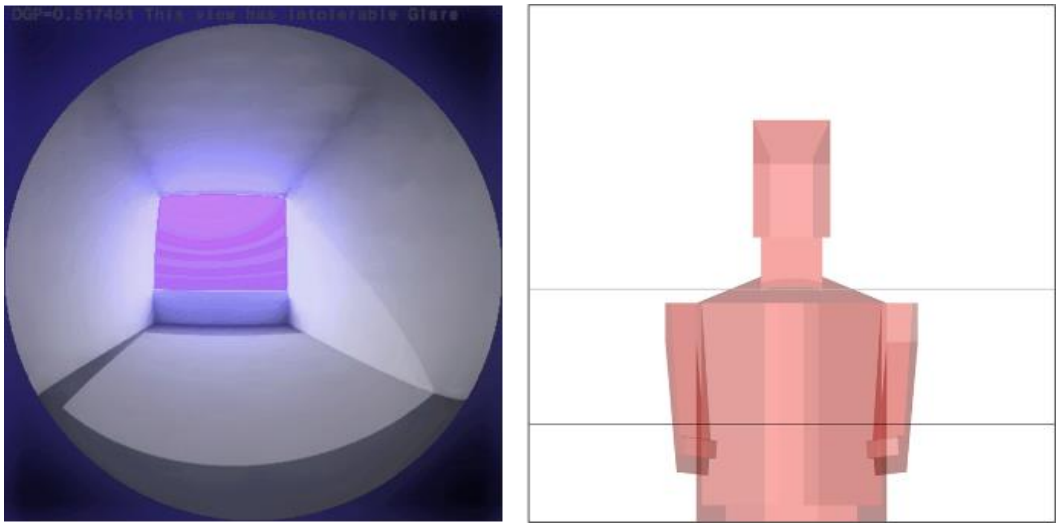

Figure 5.8. DGP and aperture of the benchmark model

The preferable UDI distribution is in approximately 2 m to 6 m ranging in the overall room's depth. In general, the room can be considered as comfortable considering that no test point performed UDI less than 100 lux (underlit) even though without a shading.

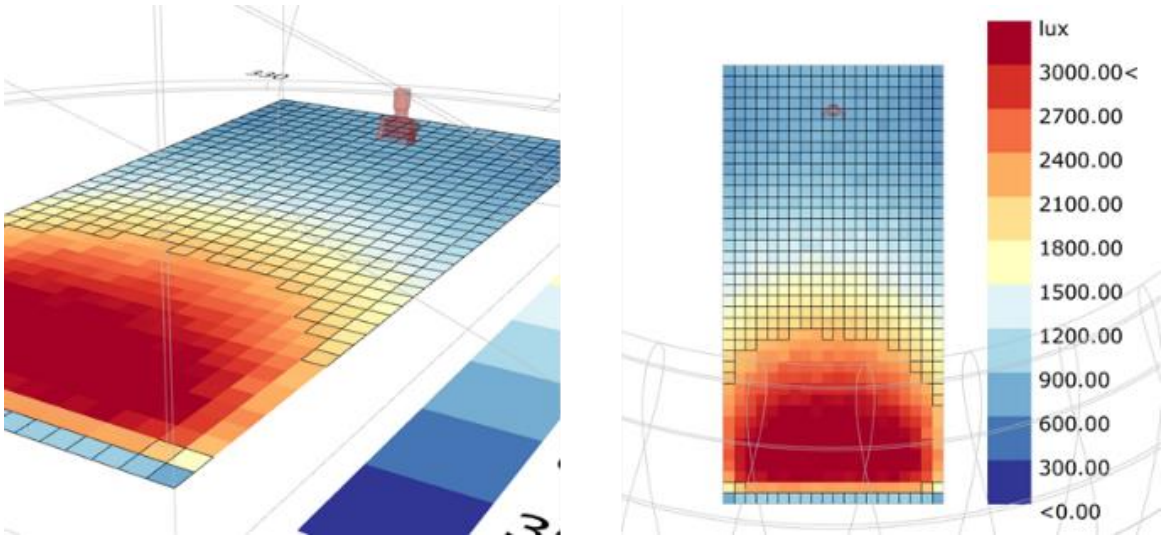

Figure 5.9. UDI performance of the benchmark model

5.3.3.2. JIS G3351 in Kitakyushu

The results of JIS G3351 will be described. The daylight simulation has been conducted on the 27 standard types of expanded metal, resulting in a list of daylight and aperture values. The result of the simulations is presented in Table 5.3.2. All 27 types performed an Intolerable glare of DGP. The range of UDI was greater than 70%. The preferable threshold of greater than 80% has been performed by several types, as recommended by [140].

Table 5.3.2. JIS G3351 results

JIS G3351 standard and grating types					
No	Type	UDI (%)	Aperture (%)	DGP	
	BM	67.63	100	0.517	IntG
1	XG11	81.5	83.13	0.481	IntG
2	XG13	87.25	75.71	0.464	IntG
3	XG14	87.25	75.71	0.465	IntG
4	XG21	80.38	84.52	0.487	IntG
5	XG23	85.38	77.48	0.466	IntG
6	XG24	85.75	77.48	0.463	IntG
7	XS31	75.25	92.32	0.503	IntG
8	XS32	78.37	87.91	0.492	IntG
9	XS33	86.63	77.85	0.469	IntG
10	XS41	74	95.37	0.508	IntG
11	XS42	74.62	93.39	0.504	IntG
12	XS43	78	88.75	0.49	IntG
13	XS51	74.38	94.59	0.507	IntG
14	XS52	75.5	92.79	0.503	IntG
15	XS53	77.88	88.65	0.493	IntG
16	XS61	73.75	95.54	0.509	IntG
17	XS62	74.75	92.97	0.505	IntG
18	XS63	77.62	89.98	0.498	IntG

19	XS71	71.38	96.83	0.512	IntG
20	XS72	73.13	96.14	0.51	IntG
21	XS73	74.5	94.44	0.506	IntG
22	XS81	70.5	97.94	0.512	IntG
23	XS82	71.25	97.09	0.511	IntG
24	XS83	72	96.18	0.51	IntG
25	XS91	70.5	98.39	0.513	IntG
26	XS92	70.75	97.89	0.512	IntG
27	XS93	71.13	97.32	0.512	IntG

5.3.3.3. UDI performance

Best UDI performance has been observed manually over the entire types of simulation results. It was found that the XG13 and XG14 demonstrated the best UDI performance. The aperture and the heat map visualization are visualized in Figure 5.10. The distribution almost showed a minimal area covered with UDI of more than 2700 lux. The most unpreferable types were XS81 and XS91, which are visualized in Figure 5.11. The illustration shows that the larger aperture may result in a more over lit distribution area. The UDI values ranging from 70.5% to the highest 87.25%, the aperture value ranging from 75.71% to 98.39%, and the DGP from 0.463 to 0.513. In contrast with Figure 5.9, the over lit area almost covers the 2 m perimeters.

From both figure the best and unpreferable UDI performance. It can be interpreted that smaller expanded metal configuration offers more UDI compared to the type with larger void. The different of illuminance situation is significant where larger expanded metal aperture performs more areas with UDI between 2000 lux to 3000 lux that considered can cause glare phenomena. The objective may vary where the intention of view outside is become a priority, the useful daylight illuminance can be sacrificed. In terms of visual comfort consideration, the manual observation in limited examples showing in this sub-chapter does not provide enough choices and alternatives of expanded metal designs.

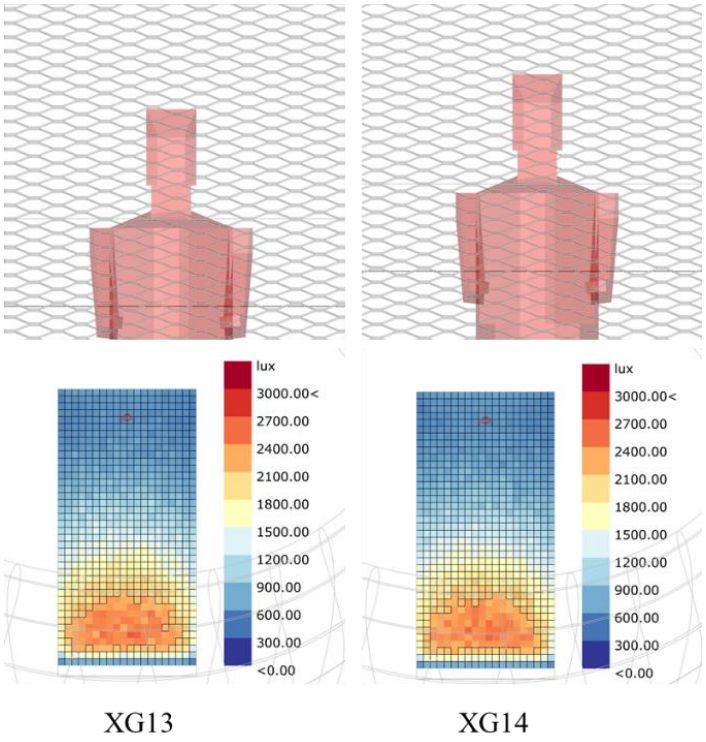

Figure 5.10. Most preferable UDI shading design

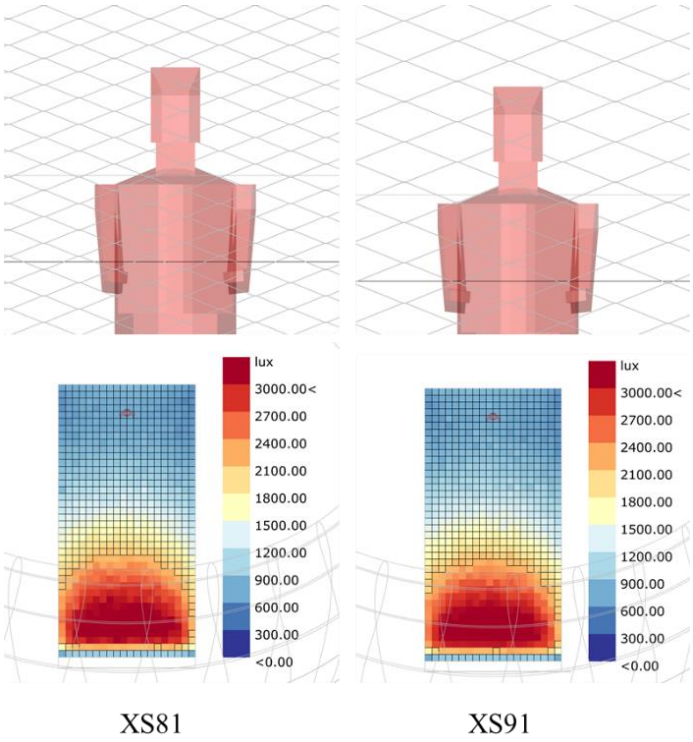

Figure 5.11. Most unpreferable UDI shading design

5.3.3.4. DGP performance

In terms of DGP objective, The XG24 was found to be the type that performed the preferable performance. The aperture and the DGP preview are presented in Figure 5.12. Compared to the most unpreferable DGP performed by XS91 (Figure 5.13), the implicit tendency that occurred showed that a smaller aperture demonstrates better DGP. However, none of the above-simulated types performed at least Perceptible glare. It was indicating several factors need to be modified.

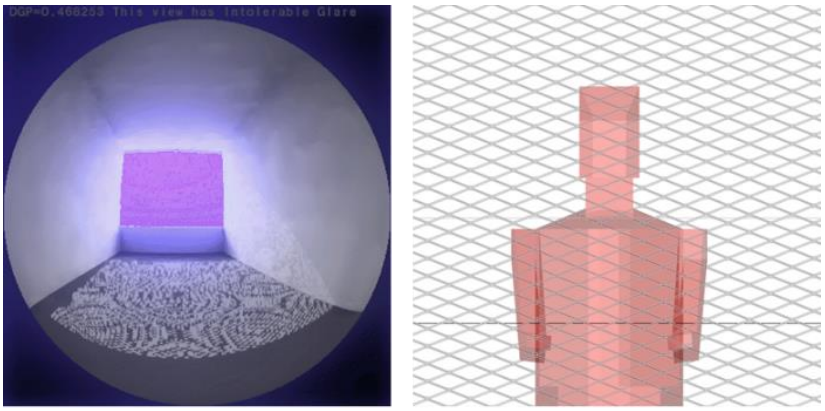

XG24

Figure 5.12. Most preferable DGP shading design

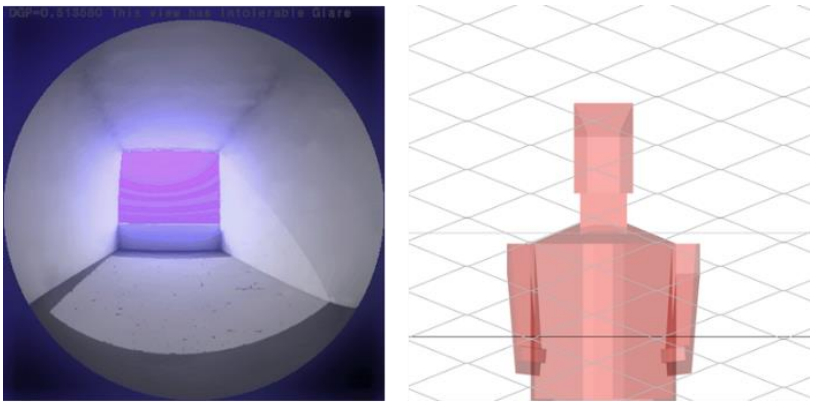

XS91

Figure 5.13. Most unpreferable DGP shading design

5.3.3.5. View performance

In terms of aperture objective, a large aperture is preferable to ensure a better view of the outside. The geometrical observation and visualization found that the XS91 had the largest aperture with a ratio of 98.39% compared to the benchmark model. However, because of the enormous amount of over lit area, the greater the aperture, the worse the UDI performance and the higher the DGP value. Figure 5.14 illustrates the DGP and the UDI distribution of XS91. Compared to the benchmark model, XS91 improved UDI by about 3% and DGP reduction by 0.004.

The UDI distribution map of the XS91 is illustrated in Figure 5.14. Looking at the figure, the type provided a tremendous area covered with over lit illuminance. The 2 m perimeter was dominated by illuminance that ranged from above 2500 lux to more than 3000 lux.

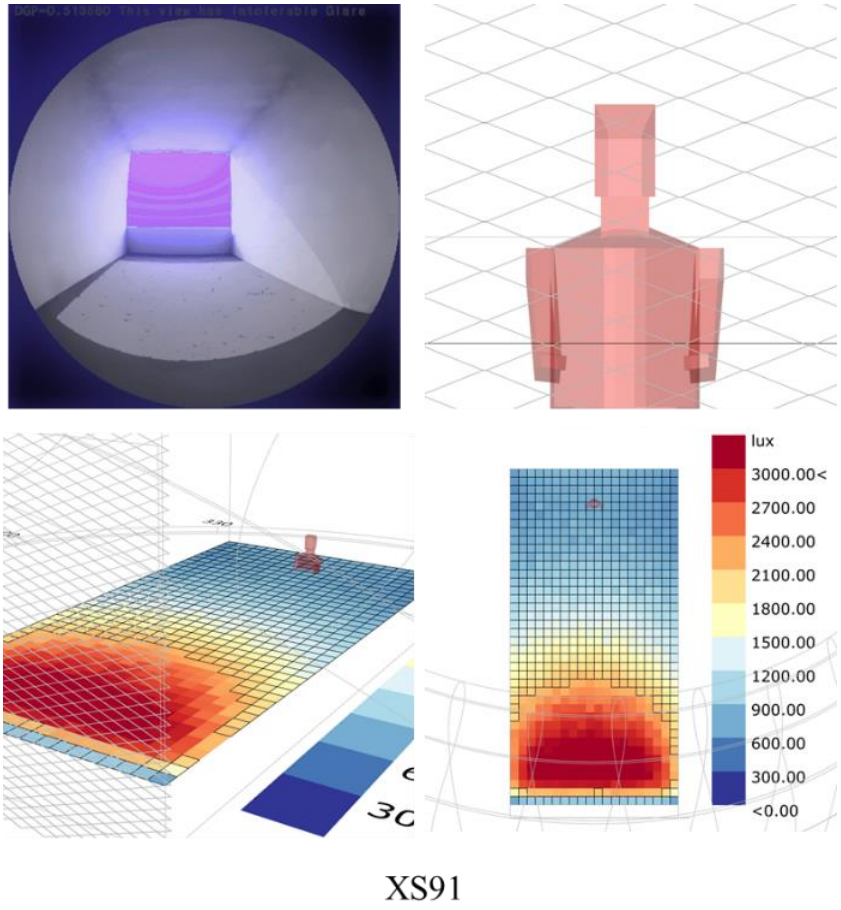

XS91

Figure 5.14. Most preferable design performing View

5.3.3.6. Fitness function calculation

Due to subjectivity and preferences in priority, the best type among the objectives cannot be determined. However, by applying fitness function calculation [80], by weighting each objective's desired performance, and maximizing the UDI and aperture while minimizing the DGP, XG24 was found as the best fit type. The appearance and the results of XG24 are presented in Figure 5.15.

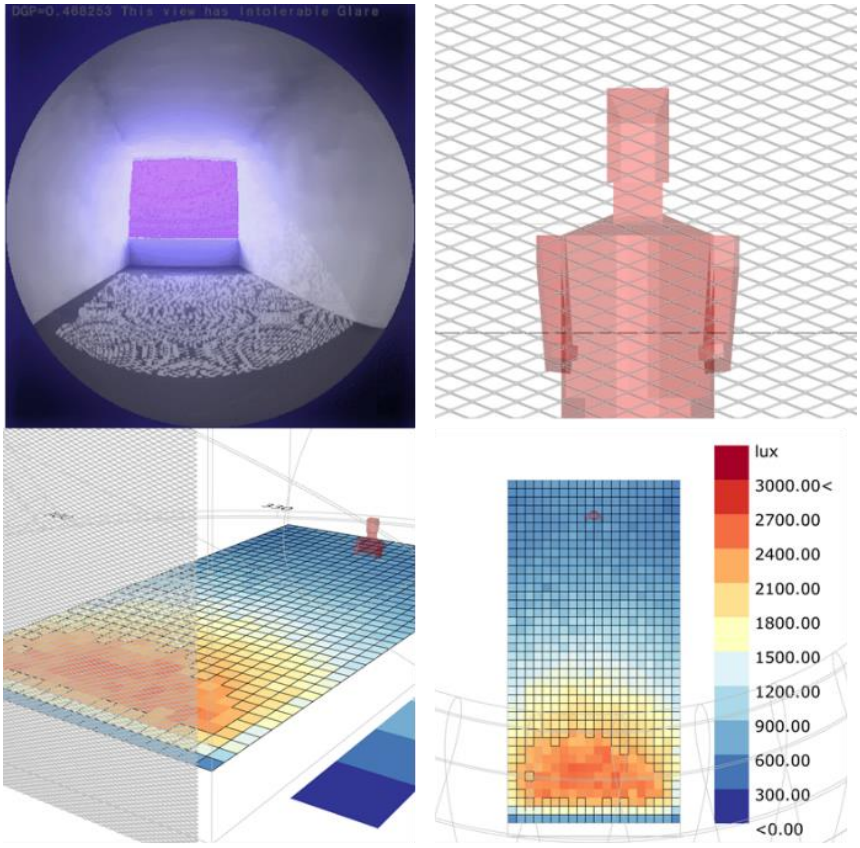

Figure 5.15. Best model from fitness function calculation

5.3.3.7. Results comparison

The result comparison of the objectives is presented in Figure 5.16 and Figure 5.17. The obvious phenomena can be seen from the chart is that the aperture was always have negative correlation with UDI and the DGP is positively correlated with the aperture.

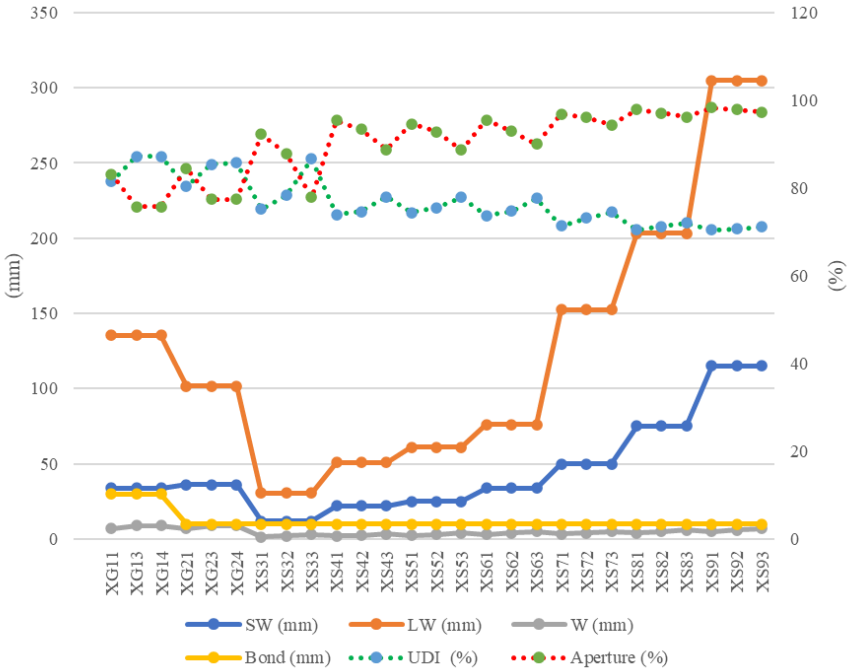

Figure 5.16. Objective and the parameters comparison

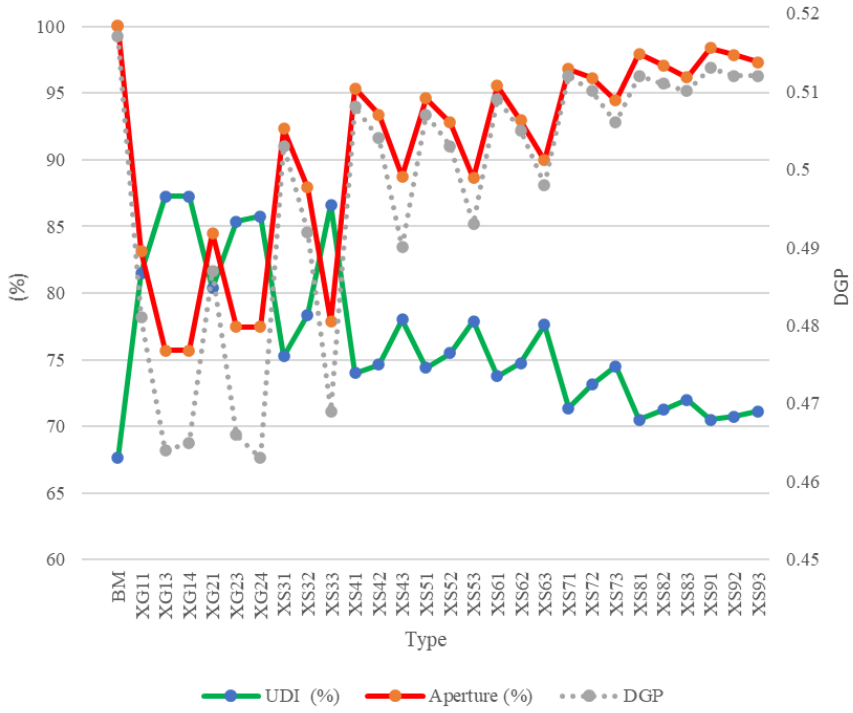

Figure 5.17. Objective comparison

The parameter value and the objectives are connected and presented using a parallel coordinate plot (Figure 5.18). From the plot, the phenomena discussed in Figure 5.17 are confirmed. The general tendency between parameters and objective is rather unclear due to the limited number of samples. However, the bottom plot shows the tendency among the maximum UDI performances, the SW and LW stated below 4 cm and 15 cm, respectively.

The tendency shows that DGP and aperture objective are negatively correlated with the UDI from the parallel coordinate plot. Besides, a higher DGP value implicated the Strand most by less than 7 cm that combined with considerable Length and Height. The tendency explained toward the DGP occurred in UDI. Two advantages of incorporating small height, length, and significant strands are getting the highest UDI and smallest DGP.

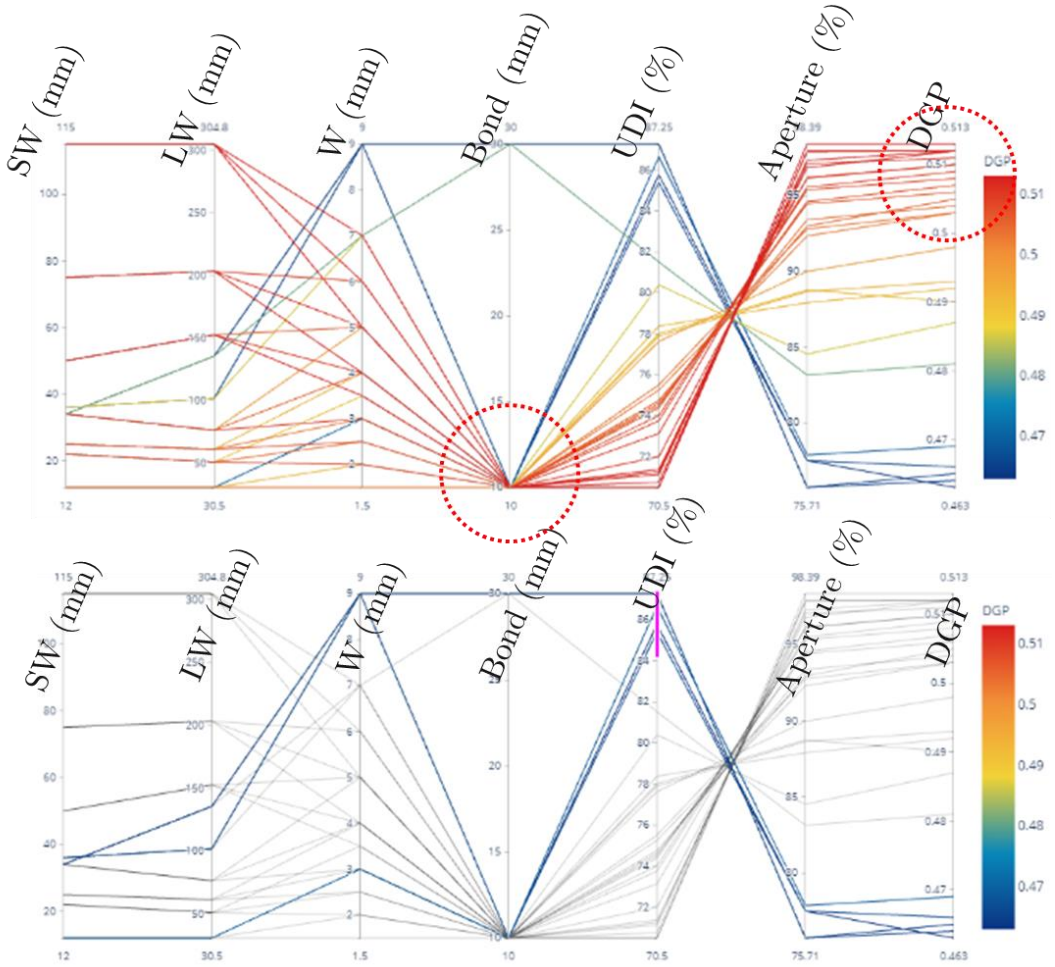

Figure 5.18. Parameter to objective observation

The sub-chapter examined the daylight performance of expanded metal shading based on the standardized type JIS G3351, given the sky conditions of Japan. By conducting parametric modelling, simulation, and observation, the best type of performance for desired daylight objectives was found. The result of this sub-chapter is expected to provide an overview and consideration factors to support the design decision-making process by designers and manufacturers during the early design stage following performance-based design.

5.4. A comprehensive daylight investigation of expanded metal shading in Japan sky context

5.4.1. Introduction

There have been numerous research evaluating the connection between shade devices and daylight performance. Even though the use of expanded-metal shading as an architectural component is prevalent among architects and designers, there have been few research on the effect of expanded-metal shading on building daylight performance utilizing a parametric design method and MOO, particularly in Japan. By examining its daylight performance, this subchapter aims to demonstrate and establish that expanded metal is an environmentally benign building material when used as a shading device. The research aims to establish a complete parametric framework for modelling expanded-metal shading and to conduct MOO in conjunction with daylight simulation. This research aims to answer the following questions:

- Given the sky condition of Japan, can a parametric study and MOO optimise daylight performance of expanded-metal shading?
- What is the relationship between daylight objectives in which expanded-metal shading is utilised?
- What is the relationship between the expanded-metal components as parameters affect the daylight objectives?
- What is the most influential expanded-metal shading parameter of the daylight performance objectives?

This sub-chapter proposes that the daylight performance of a building can be optimized if a parametric study and MOO are used to design expanded-metal shading while iterating the expanded-metal components as a design variable. The null hypothesis is that the proposed methodology has no effect on daylighting if a parametric study and MOO are used to design expanded-metal shading.

5.4.2. Methodology

5.4.2.1. General overview

The initial step of the study began with the formulation of the research problem and the decision on the daylight metrics used as the objectives. In the second phase, the modelling techniques, benchmark model, and expanded-metal parametric specification were established. In this phase, the overall function of the modelling components was tied to a single parametric-definition configuration. The third phase involved the production of natural light and the view simulation system. The model established in the preceding phase will be turned into simulated items and subjected to daylight simulation.

To this stage, the model's physical properties, climate, and urban setting have been added. The fourth phase was the optimisation procedure, during which the system created all conceivable design solutions and determined the most likely optimal solution based on the optimisation setting. The procedure multiplied the combination of each dynamic parameter movement that drove the expanded metal shading pattern configuration to increase the number of design possibilities. The method was completed by analyzing and interpreting the data obtained from the optimisation processes, which included close observation and sensitivity analysis to determine the significance of each parameter. The sequences of the five phases of this investigation are depicted in Figure 5.19.

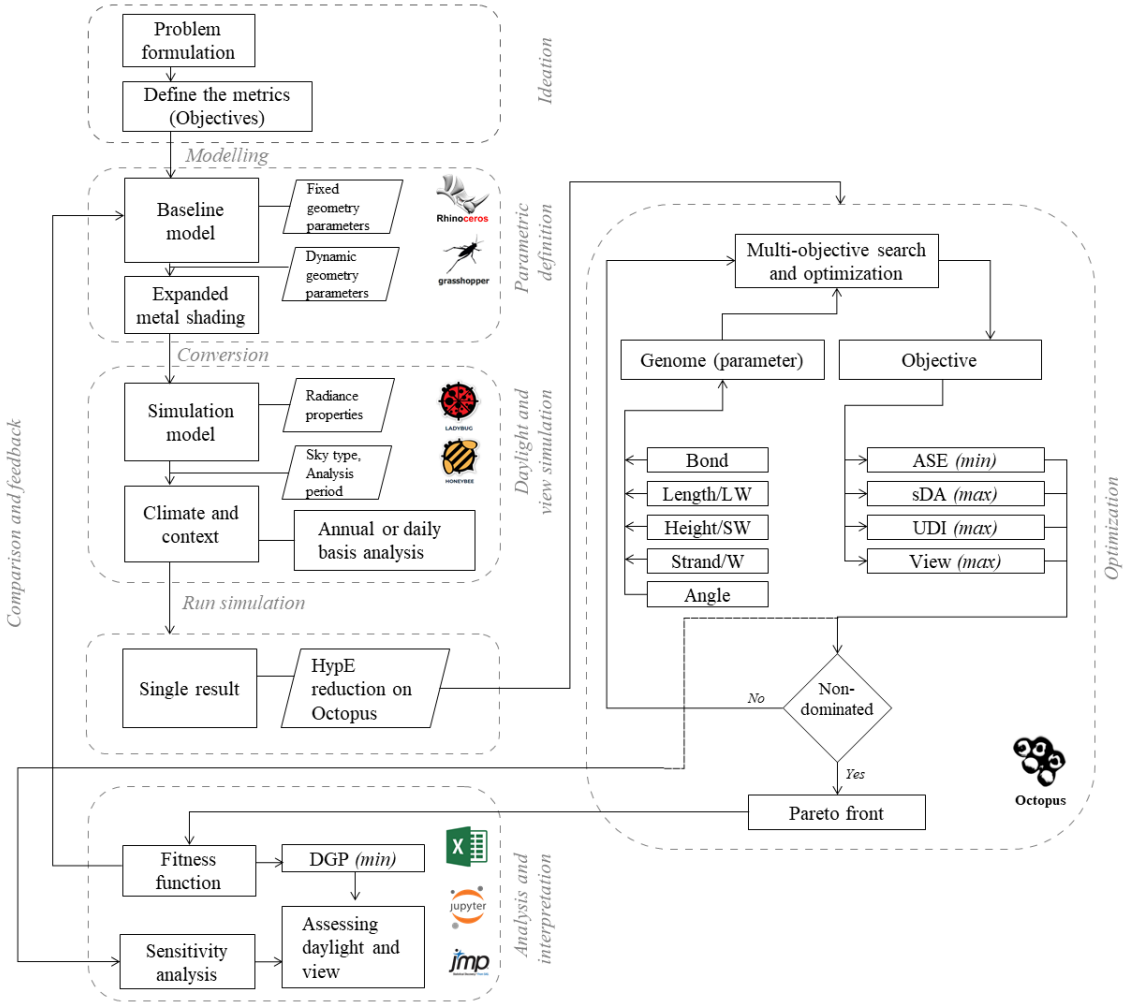

Figure 5.19. Research workflow

5.4.2.2. Defining daylight metrics and view (objectives)

The daylight metrics and criteria were selected based on the suggestions among daylight researchers and on recent advances in daylight measurement. Four daylight metrics and one self-developed design target were used to ensure that legitimate daylight values and assessments for occupant visual comfort were achieved. The first metric, as adopted in [51,97], ASE, is a term that refers to the amount of space that receives an excessive quantity of sunlight, which may cause visual discomfort to the occupants. Yearly, this daylight metric determines the percentage of the measured area with daylight illuminance

of 1,000 lux for at least 250 occupied hours ($ASE_{1000,250}$). This metric is regarded as the upper limit for daylight measurement. The following equation represents ASE, in which at_i is the occurrence count of exceeded ASE illuminance threshold at point i, and T_i denotes the annual absolute-hour threshold [87]:

$$ASE = \frac{\sum_{i=1}^{N} AT(i)}{N} \text{ with } AT(i) = \begin{cases} 1: at_i \geq T_i \\ 0: at_i \leq T_i \end{cases} \quad (1)$$

The development of daylight measurements suggests an additional metric to balance the concept known as sDA. The second metric was adopted in [141]; sDA determines whether a room receives sufficient sunshine to illuminate it during regular operating hours on a yearly basis. These metrics are typically measured and simulated using grids projected in horizontal work planes. The proportion of area that receives at least 300 lux for at least 50% of the time ($sDA_{300/50\%}$), often during occupied hours over one year, denotes sDA. The following equation can represent sDA, where st_i is the occurrence count of exceeded sDA illuminance threshold at point i, t_y is the annual timestamp count and τ denotes the temporal fraction threshold [87]:

$$sDA = \frac{\sum_{i=1}^{N} ST(i)}{N} \text{ with ST } (i) = \begin{cases} 1: st_i \geq \tau t_y \\ 0: st_i \leq \tau t_y \end{cases} \quad (2)$$

In addition to the two metrics used to assess a sufficient amount of daylight, another metric (third metric) called UDI was used. Introduced by Nabil and Mardaljevic [125,126], UDI defines useful illuminance as a range between 100 and 2,000 lux ($UDI_{100\text{-}2000lx}$), which was later expanded to 3,000 lux and classified into three classification metrics measured in percentages: below 100 lux, which is considered too dark, between 100 and 3,000 lux and illuminance valuing more than 3,000 lux, which is considered excessively bright [142]. The following equation can represent UDI:

$$UDI = \frac{\sum_i wf_i \cdot t_i}{\sum_i t_i} \in [0,1] \quad (3)$$

$$UDI_{\text{Useful}} \text{ with } wf_i = \begin{cases} 1 & \text{if } E_{\text{Lower limit}} \leq E_{\text{Daylight}} \leq E_{\text{Upper limit}} \\ 0 & \text{if } E_{\text{Daylight}} < E_{\text{Lower limit}} \vee E_{\text{Daylight}} > E_{\text{Upper limit}} \end{cases}$$

Additionally, the Illuminating Engineering Society of North America (IESNA) proposes another metric, Daylight Glare Probability (DGP), in IES LM-83-12. This was the fourth metric employed in this research, which incorporated a 1,000-lux illuminance to characterise the possibility of visual discomfort (glare) [143]. The authors devised and introduced the fifth objective to include the idea of providing a view as one of the optimisation objectives. So-called 'View' is defined as the expanded metal's square-meter (m^2) void projected in a planar vertical plane that is paralyzed by the glazing vector's normal orientation. This additional objective was not regarded as a daylight metric and, furthermore, was presented in percentage as a ratio of the overall façade surface area. The following equation represented DGP:

$$\text{DGP} = 5.87 \times 10^{-5} E_v + 0.0918 \log \left[1 + \sum_{i=1}^{n} \left(\frac{L_{s,i}^2 \omega_{s,i}}{E_v^{1.87} p_i^2} \right) \right] + 0.16 \quad (4)$$

5.4.2.3. Daylight standard and criteria

This research referred to the LEED v4.1 standard [144], as referred to in [94,97,145], as a daylight target-value objective of the year-based daylight simulation. In LEED v4.1 chapter EQ Credit, Daylight option 1, the $ASE_{1000,250}$ should be less than 10%, while the average value of $sDA_{300/50\%}$ for the regularly occupied floor area should be, preferably, at least 75% to achieve three credit points of standard assessment. For UDI, a higher value is desired [76]. However, the preferable minimum threshold of UDI is recommended as more than 80% [140]. To evaluate the approach to glare prediction, DGP was classified into four types. Imperceptible glare was comprised of DGP values less than 0.35. Perceptible glare was defined as a DGP value between 0.35 and 0.4. Disturbing glare consisted of DGP values between 0.4 and 0.45, while values greater than 0.45 were considered intolerable glare.

Computation of $ASE_{1000,250}$, $sDA_{300/50\%}$, $UDI_{100\text{-}2000lx}$ and DGP was performed in Ladybug and Honeybee using dedicated specialised components to calculate the daylight objective named *Run Daylight Simulation*, which resulted in illuminance values on the designated test points. The search for the openness objective was performed by conducting mathematical calculation in the Grasshopper origin functions, such as surface areas and vertical projection based on the resulting expanded-metal geometry.

5.4.2.4. Simulation tools

Based on the software employed, this sub-chapter is divided into two major sections: data collection and data analysis and visualization. The simulation and iteration procedures were organized in a single parametric system that was performed independently based on the simulation period in order to capture changing geometry data and design goals. The complete geometric modelling process was carried out via the Non-Uniform Rational Basis Spline (NURBS) 3D modeller in Rhinoceros and the parametric plug-in Grasshopper.

Environmental analysis plug-ins called Ladybug and Honeybee [122] integrated in order to undertake daylight analysis. Ladybug is a plug-in for the parametric platform Grasshopper that is used to analyze microclimate. It connects the early-phase design process with environmental analysis, allowing for a quicker and more efficient evaluation of the design process in relation to environmental concerns. EnergyPlus Weather (EPW) data can be imported using the add-on [119] adapted to the data analysis and visualization demands of the designer. In addition, Honeybee is supplementary to Ladybug's capabilities for developing computations linked to energy analysis. Honeybee incorporates well-known and tested simulation engines, including DAYSIM in Radiance, THERM, EnergyPlus, and OpenStudio, to produce energy-related analysis and visualization.

The MOO process was conducted using a plug-in called Octopus [146]. The tools used in this research were also used in similar studies, including [19,48,66,80,87,95,100,147,148]. After collecting data on the dynamic parameters and target value, the data was analyzed and visualised using Microsoft Excel, the statistical analysis software JMP and Jupiter Notebook, a Python-based platform operated in the Anaconda launcher. The daylight simulation and MOO of the two designated periods were run on a PC with Intel (R) Core (TM) i9-10980XE (36 CPUs) 3.00 GHz (36 CPUs) processors, 128 GB RAM and GPU NVIDIA GeForce RTX 3090 90 GB integrated RAMDAC, running in Windows 10 Pro 64-Bit platform.

5.4.2.5. Calibration process

To calibrate the daylight phenomena with the computer simulation, a mock-up model for the simulated room was developed, and one-day based (specific time) daylight measurement was conducted. Figure 5.20 shows the mock-up experimentation conducted to observe the implication of expanded-metal shading on the daylight situation inside the model. The measurement was collected using a 5 mm thick, 60 cm x 30 cm x 30 cm styrene board with paper. For the expanded-metal model, actual expanded-metal type XS33 from the standardised industrial type JIS G3351 [149] and 5.3 was incorporated. To measure the actual onsite illuminance, Illuminance UV Recorder TR-74Ui was used. The measurement was conducted under two different sky conditions: cloudy with sun and cloudy without sun. The result shows that the expanded-metal shading can significantly reduce indoor daylight illuminance in comparison with the model without the expanded-metal shading. A comparison of the setting and result measurements and simulations are shown in Table 5.4.1.

Comparing the measured and simulated data reveals that both daylight illuminance settings exhibit a similar pattern. Different material properties and censor sensitivity in computational calculation, different assumptions between sky-type datasets in the Generate Data CIE standard sky component in Ladybug and the actual sky condition, and different conditions between the weather database in the EPW file and the actual sky

condition may have contributed to the insignificant discrepancy. From the two measurements, the second (Table 5.4.1), when measured in an intermediate sky with sun, was nearly identical to the simulation using a sunny sky with sun. In this study's daylight simulation and MOO, however, the analysis period was based on an annual simulation.

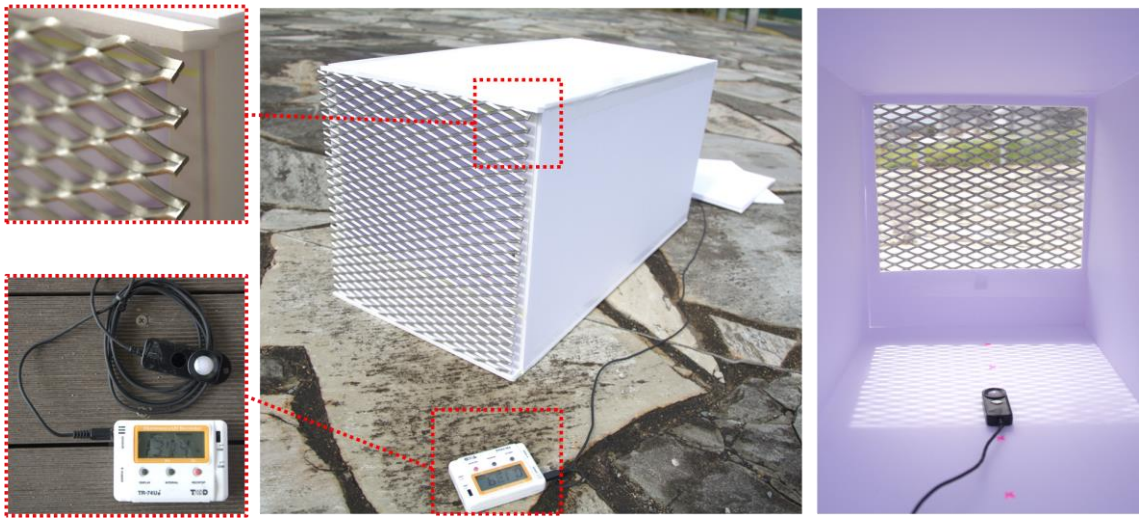

Figure 5.20. Mock-up room experimentation and onsite measurement

Table 5.4.1. Comparison of measurement and simulation results

Measured Model		Time	Sky condition/ Location	Outside (lx)	Inside BM (lx)	Inside Shaded (lx)
1	20/10/2021	11:00	Intermediate sun/ Wooden deck	7.570	4.527	1.982
2	20/10/2021	11:37	Intermediate with sun/Gravel area	60.350	30.140	7.554
Simulation Setting						
1	EPW Shimonoseki 20/10/	11:00	Intermediate without sun	12.039	2.988	1.739
2			Intermediate with sun	20.259	8328	2008
3			Sunny with sun	60.527	38.745	4.277

5.4.2.6. The benchmark model and fixed parameters

This model was created to highlight the significance of a benchmarking model with benchmark performance. This project created a four-meter-wide, eight-meter-deep, and four-meter-tall virtual simulation of a workplace. The façade of the replicated room faced south and was aligned along the north–south axis. As a window, the 70% glazed part on the south side of the model works as a window. The mock-up room is illustrated in Figure 5.20, and the difference between the benchmark model and the model with expanded-metal shading is illustrated in Figure 5.21. The benchmark model equipped with no shading systems to simulate daylight and permitted direct sunlight to reach the windows and interior surfaces. In this base model, no variables were specified to become dynamic parameters. The geometry-related fixed parameter was the model's dimensions, which comprise its height, width, and percentage of the window.

From the visualization between the benchmark model and the random shading system, quick insight shows significant reduction in glare phenomena indicated with red color heat map scaled near the windows. Up to this point, the simulation with shadings seems help to improve the situation of illuminance. However, to justified quantitatively the improvement, the parameter and simulation scenario also need to be justified. The justification will me described later in the dedicated section. In terms of material, the benchmark model and the room with expanded metal model provided with same material characteristics discussed in section 5.4.2.8.

In addition, the model with expanded-metal shading was selected as the primary model for global daylight simulation and MOO operations. Due to the expanded-metal shading's form-finding process, the expanded-metal model was expected to produce a variety of approximation data, whereas the benchmark model was projected to produce the benchmark daylight value. The objective of this approach was to get the total number of stated target performances as the benchmark and the value of each iteration for the upcoming comparison phase. The overall random-sample findings are depicted in Figure 5.22.

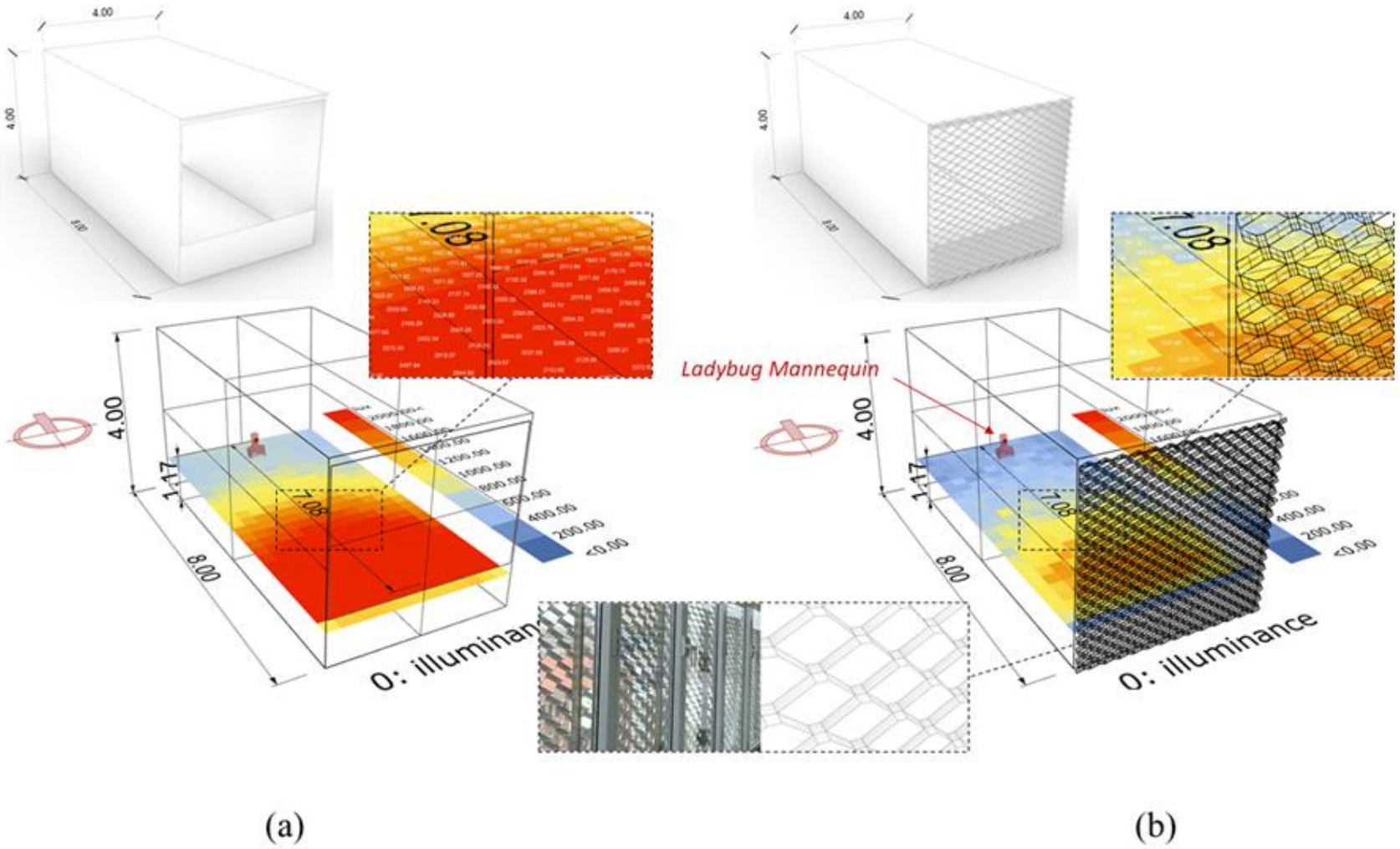

Figure 5.21. Simulated model: (a) Benchmark model, (b) simulated model with expanded-metal shading.

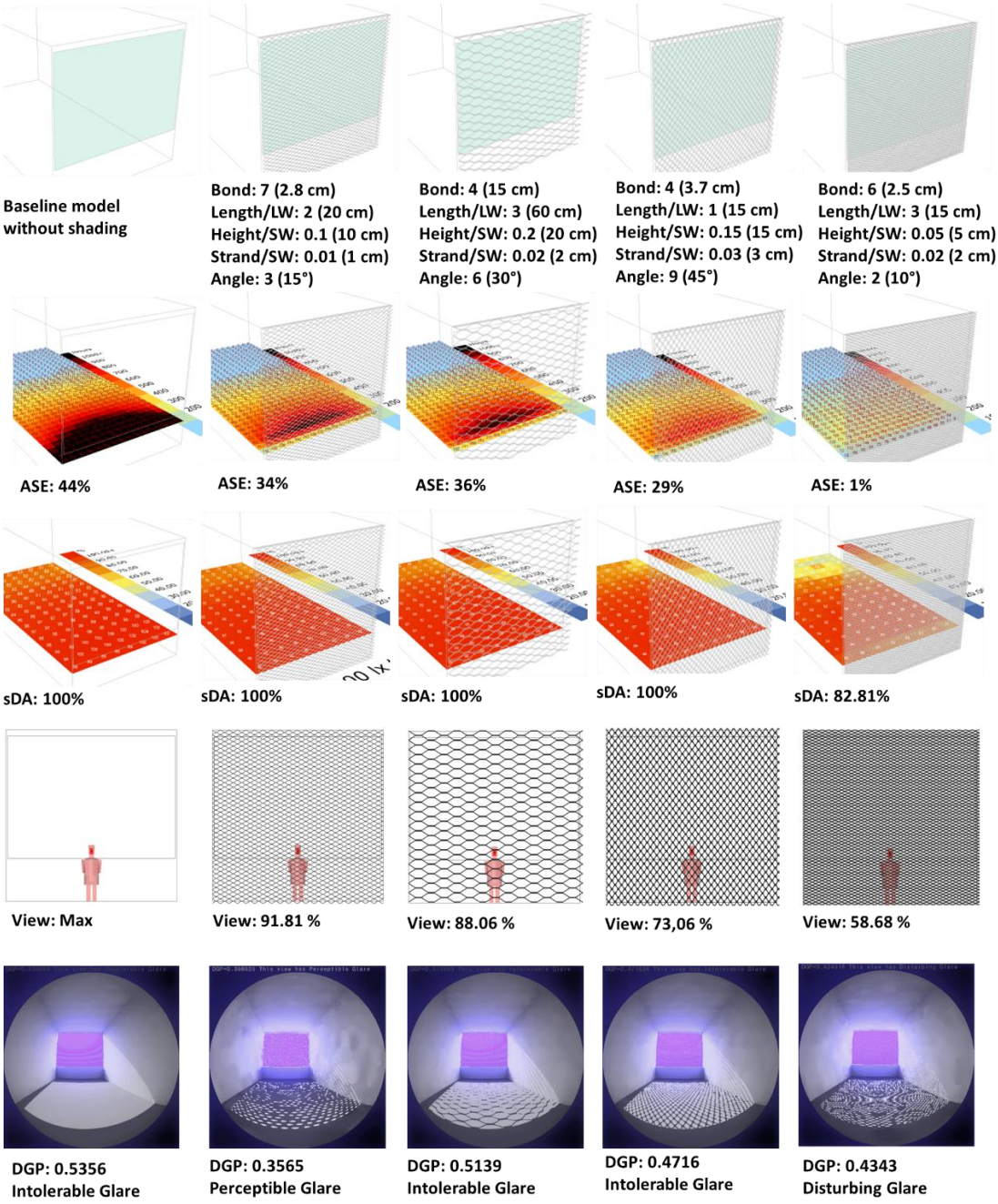

Figure 5.22. Result and visualisation of random parameter combination.

5.4.2.7. Expanded metal shading and parameters

The expanded-metal shading geometry modelling made use of the restriction mentioned in the introduction. In general, the shading was oriented to the south with a length and

height of 4 meters to match the maximum facade area of the space. The shade position contained a 10-cm overhang to prevent clashing geometry when the maximum slider setting resulted in overlap geometry. Using the capability to automatically optimise and iterate design solutions during the form-finding process, the parameter was set to be dynamic, which means it was generated as a range or domain as opposed to a single static integer. The variety of sliders allowed parameter combinations that guided the iterative process toward the intended design value. In addition, during the process of optimization, this parameter became the genome.

The model used in this sub-chapter is similar with the model discussed in Sub-chapter 5.3.2. referring to Figure 5.6. considering the complexity and flexibility inherent in expanded metal's actual physical form [134], the subchapter created the simplification of expanded metal to prevent additional calculations that simulation process tools could not manage. The expanded metal consisted of five major components: the 'Height' of the modular diamond or SW, the 'Length' of the diamond or LW, the 'Bond' representing the surface connecting each diamond vertically and horizontally, the 'Strand' representing the expanded metal's wide XY-plane, and the 'Angle' representing the angle between the strand and the horizontal plane.

Even if the number of features and dimensions that could be developed to simulate expanded metal are endless, the number of dimensions that can be represented in each part has been limited due to the simplicity of the geometry. The objective was to keep the pattern close to the standard, so avoiding uncontrolled movement or value changes that could cause an error during the simulation's calculating procedures. The authors estimated the Length/SW and bond based on the multiplication and division factors of the Height/LW in order to prevent unexpected competing calculations from affecting the proportion. The strand and angle were controlled independently using different sliders. Nonetheless, the optimisation mechanism repeated the fitness mating between the genomes in order to reach the target optimisation value. Table 5.4.2 lists the dynamic parameters' range values.

Table 5.4.2. Dynamic-parameter range value

Parameter	Min	Max	Unit	Driven factor	Movement
Height/LW	5	20	cm	-	15
Length/SW	1	5	cm	Height	5
Strand/W	1	10	cm	-	10
Bond	3	10	cm	Length	8
Angle	1	9	°	-	9
Total possible iteration					54.000

5.4.2.8. Material properties and building programme

To add to the daylight calculation in Ladybug tools, Radiance material was necessary. The Grasshopper geometry had to be converted to a Honeybee surface and zone. The surface model was modified using the Radiance Color Picker offered by Jaloxa [150] and adopted in [20]. Radiance Opaque Material and Radiance Glass Material were utilised to represent the geometric surface. The programme for the Honeybee zone was configured as an open office, as specified in the Honeybee List Zone Programme component. The reflectance and transmittance value employed in this sub-chapter is shown in Table 5.4.3.

Table 5.4.3. Interior surface reflection and transmission properties [20]

Surface	ρ	ρR	ρG	ρB	Specularity	Roughness
Ceiling	0.800	0.800	0.800	0.800	0.000	0.000
Interior wall	0.750	0.750	0.750	0.750	0.000	0.000
Floor	0.210	0.210	0.200	0.200	0.000	0.000
Glazing [a]	0.750	0.750	0.750	0.750	0.000	0.000

Shading	0.800	0.800	0.800	0.800	0.000	0.200

[a] For glazing, the value should be read as transmittance τ

5.4.2.9. Daylight simulation. Climate and context

Despite the fact that the proposed methodology can be employed whenever EPW data is available, the simulation model for this study was designed to be located in 33° 51' 6.52" north latitude and 130° 51' 1.22" east longitude in Kitakyushu, Fukuoka, Japan. The winter solstice happened on December 21, 2020, and the summer solstice occurred on June 21, 2020. The Koppen climate classification categorizes Kitakyushu's climate, which is located in southern Japan [151] as moderate, with no dry season and a hot summer (Cfa). However, due to lack of EPW file availability, the simulation used data from Shimonoseki, Yamaguchi, Japan, which is the closest available EPW file to Kitakyushu (about 6.47 km).

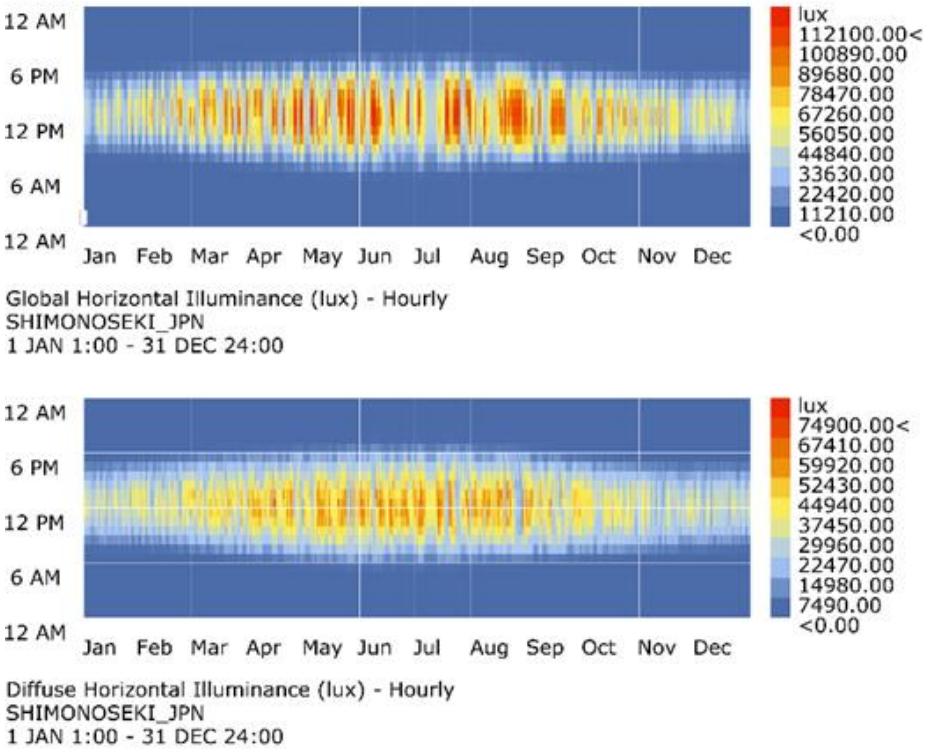

Figure 5.23. Annual sky-illuminance profile from the EPW file of Shimonoseki

The sky data was collected from historical data rather than field measurement to develop prediction modelling. The profile of sky illuminance for global horizontal, diffuse horizontal and direct normal illuminance in Shimonoseki, which represented Kitakyushu, is shown in Figure 5.23. From August to September, the plot chart tracks the cloud with the highest sky illuminance.

5.4.2.10. Sun Daylight Simulation

The Ladybug plug-in was used exclusively to simulate daylight. The simulation components "Run Daylight Simulation" and "Sunlight Hour Analysis" calculated the data input from the Shimonoseki EPW file, supplemented by several additional sets. The $ASE_{1000,250}$, $sDA_{300/50\%}$ and $UDI_{100\text{-}2000lx}$ simulations were used in grid-base analysis to spread the daylight value, while the objective View calculation only calculated the geometry's area. The DGP test used the View render-visualisation component to extract the illuminance data from "Run Daylight Simulation" that had analysis recipe input the average climate-based sky as a daylight source set for December 21 at 12.00 PM.

5.4.2.11. Optimization setting

In this sub-chapter, the Pareto front concept was included. Given the several objectives of this research, the pairing of the genomes was complex and involved a vast number of potential solutions. Thus, the idea was to simultaneously classify the presumed best solutions among the preferable and optimised generations in a local front for each field.

The usage of Octopus was outlined in the preceding section. Implementing various variables from forming expanded-metal shading and multiple objectives generated from daylight simulation and geometry's area calculation was expected to result in an optimized design solution. This proposal aimed to deliver rapid feedback to help the early design phase through Building Performance Simulation, utilizing the capacity to automate form-finding and develop the most optimal design solution [152]. The setting of the Octopus interface is presented in Table 5.4.4.

Table 5.4.4. The Octopus optimisation setting

Parameter	Setting
Elitism	0.500
Mutation probability	0.200
Mutation rate	0.900
Crossover rate	0.800
Population size	100
Maximum generations	200
Record interval	1
Non-dominate ranking method	HypE Reduction
Mutation strategies	HypE Reduction

5.4.2.12. Target value and fitness function

During the simultaneous discovery phase, the optimisation procedure iterated design variables (genome) and correlated all outputs with potential solutions. Then, the findings were filtered in line with Pareto front performance value targets. When aiming for the greatest axis, the input number should have been multiplied by -1. The genome and the optimisation approach used in this sub-chapter are presented in Figure 5.19. Research workflow. The objectives to be minimised were $ASE_{1000,250}$, whereas the objectives to be maximised were $sDA_{300/50\%}$, $UDI_{100\text{-}2000lx}$ and View.

The following equation [51,80,87,116] was used in the study to determine the fitness-function value for each individual in the Pareto front: The outcome of the fitness function indicated the individual who was most compatible with the intended objection value, which was a mix of criteria. In addition, the findings were personally observed by locating the Pareto-front individual on the graph and grouping the specified region along each axis.

$$FF_i = (sDA_i - sDA_{min})C_1 - (ASE_i - ASE_{min})C_2 + (UDI_i - UDI_{min}) C_3 + (View_i - View_{min})C_4 \quad (5)$$

$$C_1 = \frac{100}{sDA_{max} - sDA_{min}} \quad (6)$$

$$C_2 = \frac{100}{ASE_{max} - ASE_{min}} \quad (7)$$

$$C_3 = \frac{100}{UDI_{max} - UDI_{min}} \quad (8)$$

$$C_4 = \frac{100}{View_{max} - View_{min}} \quad (9)$$

5.4.2.13. Analysis and interpretation

To find the most influential variable, sensitivity analysis [153] was utilised. Several studies of the built environment have conducted sensitivity analysis on the role of the input parameters [25,91,92,154]. Sensitivity analysis can be described as the study of how the changes in output are assigned – either qualitatively or quantitatively [155]. As a result of the trade-off between objectives, MOO will not produce a unique solution. The trade-off could lead to the conclusion that one objective has a higher importance than the other. This step of decision-making frequently incorporates the subjectivity of the designer or the assessor for the purpose of design preference. Consequently, sensitivity analysis was considered in order to improve the feasibility and obtain an understanding of how each parameter affected the objectives. The parameters and objectives' data are displayed in parallel coordinate and tornado charts. Standardised Regression Coefficient (SRC) analysis was utilized to conduct the sensitivity analysis (SRC).

5.4.3. Results

5.4.3.1. Benchmark model simulation

The benchmark model was a simulated model of the room without shading devices. The results of the benchmark-model simulation are presented in Table 5.4.5 The benchmark model had similar radiance materials on its surfaces, yet the results were presented according to the simulation analysis period that was discussed in discussion of run daylight simulation. To determine the performance based on the simulation type, the objectives $ASE_{1000,250}$, $sDA_{300/50\%}$, $UDI_{100\text{-}2000lx}$ and DGP are visualised in Figure 5.22 and Figure 5.32.

Table 5.4.5. Objective results of the benchmark model

Benchmark model	Objectives				
Analysis period	$ASE_{1000,250}$ (%)	$sDA_{300/50\%}$ (%)	$UDI_{100\text{-}2000lx}$ (%)	View (%)	DGP
One year	44	100	61.65	100	0.517
21 Dec 12.00 PM			42.90		Intolerable glare

5.4.3.2. Optimization results

Daylight simulation and optimisation were conducted to measure, distribute and examine $ASE_{1000,250}$, $sDA_{300/50\%}$ and one-year $UDI_{100\text{-}2000lx}$. In addition, an extra geometric objective (View) was included in the MOO operations to assure visibility to the outside. The optimisation process was purposely halted after 30 generations, yielding 3,176 individuals, each embedded with the values of parameters and objectives.

Figure 5.24 (a) displays a four-axis 3D scatter plot filled with iteration outcomes depicting individuals developed in Octopus. Individuals were spread out as sequential points that embedded the parameters (genotype) and were positioned based on their objective value. The distribution shown in this graph depicts the tendency of optimal iteration movement, in which individuals swarmed towards the searching area of $UDI_{100\text{-}2000lx}$ and $sDA_{300/50\%}$ maximum and $ASE_{1000,250}$ minimum. However, the View objective, presented in the diverging-colored legend, did not indicate any movement in the targeted maximum value. Instead, the middle value of this objective was shown to be within the targeted searching area.

Figure 5.24 (b) depicts 155 Pareto front solutions yielded from the most recent generation of the optimisation processes. The global distribution was reduced to the minimum $sDA_{300/50\%}$ limit of 60% and the $UDI_{100\text{-}2000lx}$ of 70%. The Pareto-front solutions showed the swarm of $sDA_{300/50\%}$ maximum values along the vertical axis, valuing 100% of the objectives.

Similarly, $ASE_{1000,250}$ maximum solution was plotted along the horizontal axis, valuing 0% of the targeted objective. The distribution of $ASE_{1000,250}$ showed that the optimisation process pushed the two objectives into the targeted optimisation value. Up to this point, the phenomenon illustrated the success of the MOO process in simulating the assumed best-design solutions by weighing the desired value of every daylight objective.

As stated in the preceding section, the MOO method, unlike single-objective optimisation, could not generate a single final optimal solution because to the complex mathematical computations and the trade-off between the objectives. Despite the implicit pattern that emerged, the 3D perspective of this chart reveals that the relationship between objectives is rather ambiguous. Consequently, by grounding the optimization results, the supposed best solution and the correlation between objectives might be observed in analyses involving only two objectives. This concern is addressed in Table 5.4.6.

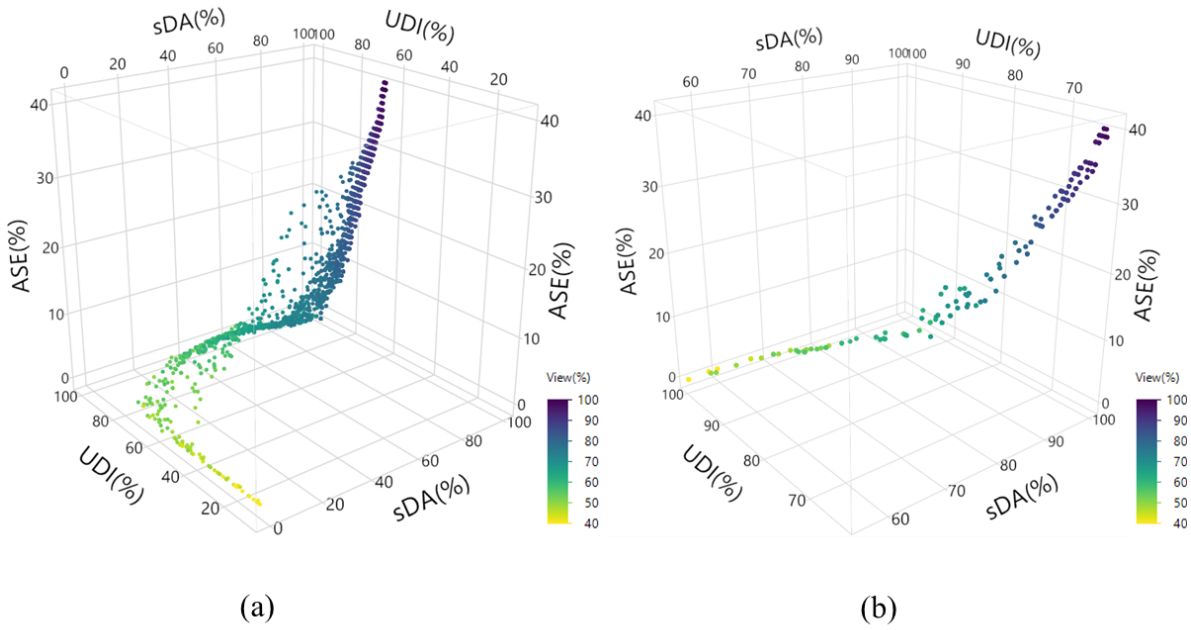

Figure 5.24. Results field: (a) 3D scatter plot based on the MOO results, (b) the Pareto frontiers

5.4.3.3. Optimal solutions

As one of the chapter aims, one or a range of the most fit solution tends to be observed. The 10 best solutions were discovered by applying the fitness function (Equation 5) to the Pareto-front individuals from the optimisation results. All ten best solutions perform ASE not more than 4%, SDA above 92.97%, UDI more than 89.93%, and View more than 62.13%. with fitness function value more than 197.89. Table 5.4.6 displays the top-10 attributes of the best solutions ranked based on fitness-function value.

As can be seen from the table, among the 10 best solutions, the maximum objective $ASE_{1000,250}$ performance shows only 4% in model number 1,169, the $sDA_{300/50\%}$ percentage ranges from 89.06% in model numbers 1,441 and 2,997 to 98.44% in model number 1,761, $UDI_{100\text{-}2000lx}$ percentage ranges from 89.14% in model number 1,169 to 93.73% in model number 2,997 and View percentage ranges from 60.56% in model number 1,708 to 67% in model number 1,169.

Table 5.4.6. The selected solutions based on fitness-function calculation

Solution rank	Objectives				Parameters					Model number	Fitness Function
	ASE (%)	sDA (%)	UDI (%)	View (%)	Bond (cm)	Length/LW (cm)	Height/SW (cm)	Strand/W (cm)	Angle (cm)		
1	0.00	96.09	89.93	66.75	0.04	0.12	0.12	0.04	5	1728	210.68
2	2.00	98.44	89.63	67	0.03	0.09	0.09	0.03	5	1761	210.48
3	0.00	92.97	92.75	63.44	0.047	0.14	0.14	0.05	5	1486	205.82
4	0.00	92.97	92.42	63.81	0.057	0.17	0.17	0.06	5	2269	205.56
5	3.00	95.31	91.26	65.56	0.04	0.12	0.12	0.04	10	1925	203.03
6	0.00	90.63	95.1	60.56	0.043	0.13	0.13	0.05	5	1708	202.15
7	4.00	96.88	89.14	67.25	0.012	0.06	0.06	0.02	5	1169	201.14
8	3.00	97.66	90.28	62.13	0.117	0.7	0.14	0.05	5	2805	199.92
9	0.00	89.06	93.76	62.38	0.027	0.08	0.08	0.03	5	2997	198.12
10	0.00	89.06	93.52	62.63	0.037	0.11	0.11	0.04	5	1441	197.89

In terms of parameter range value, the main independent parameter, Height, was found at a minimum of 6 cm and a maximum of 17 cm. Following the movement of Height, the Length division factor stated a minimum of 6 cm and a maximum of 70 cm. The division factor revealed only two movements from 1 to 2, which occurred only in model rank 8, indicating a minimal movement combination in the chosen solution. It can be interpreted that this number dominates the Length's role in the best solution or that the number that occurred was caused by the lack of movement in this parameter during the iteration. Similarly, the Bond stated only three division-factor movement combinations: 3, the dominant (eight times), 6 in model rank 8 and 5 in model rank 7. The Strand had a greater range of variance, with values ranging from 2 cm to 6 cm. The Angle parameter exhibited only two variable movements: 5 (multiplication factor 1), which dominated almost the entire selected solution, and 10 (multiplication factor 2), which occurred only in model rank 5. In general, model number 1,728, with a fitness-function value of 210.68, was the optimal and preferable option based on the fitness-function calculation.

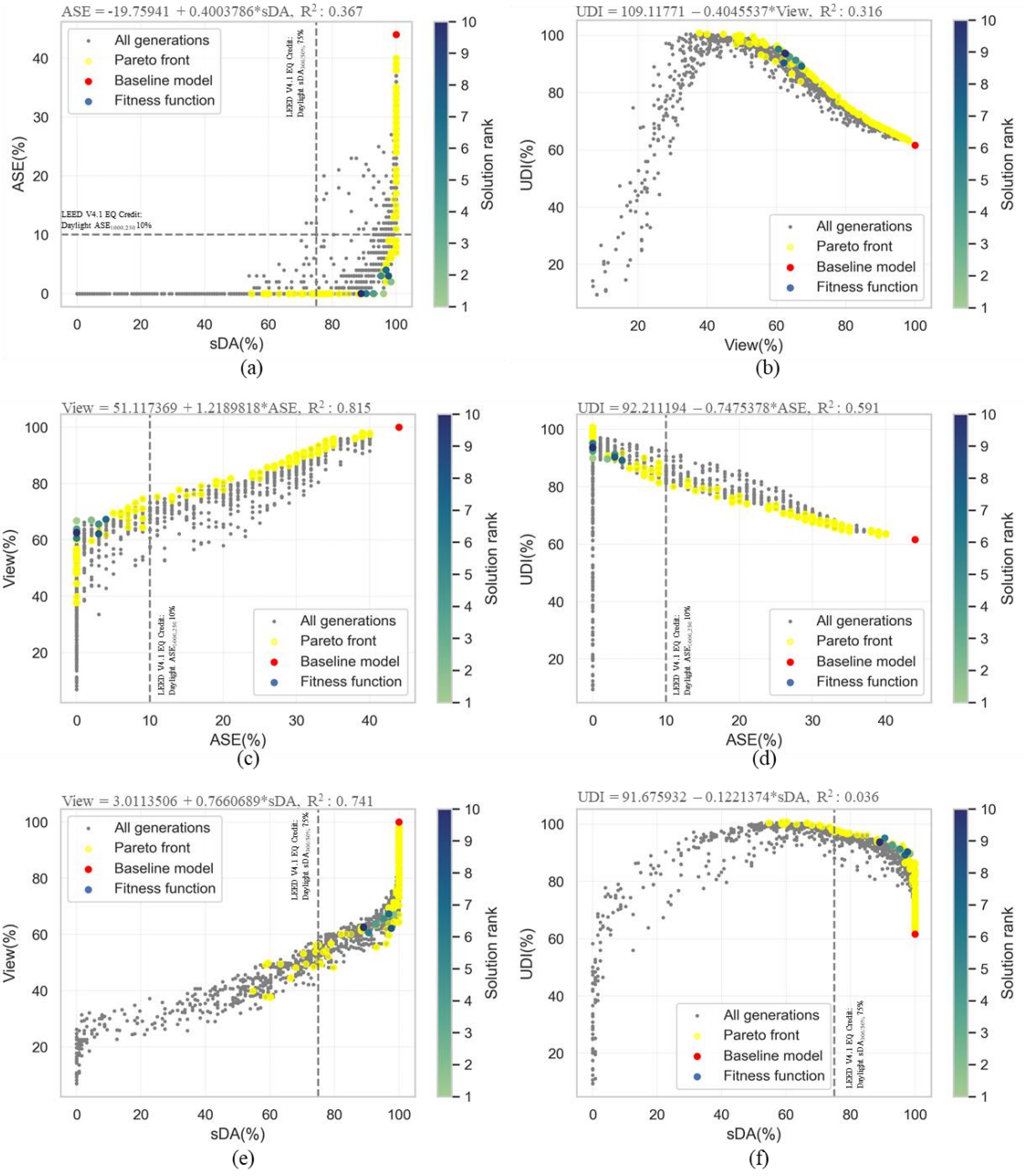

Figure 5.1. Scatter plot showing the relationships among the objectives

A 2D scatter plot was included to better view the Pareto front and the interaction between objectives. Figure 5.25 (a–f) shows scatter plots between two objectives. The vertical grey dashed line denotes the criteria borderline for $sDA_{300/50\%}$ minimum of 75%, fulfilling 3-point credits of EQ daylight credit in LEED v4.1. In comparison, the horizontal dashed line shows the maximum 10% limit of any frequently used places, with $ASE_{1000,250}$ in the same daylight standard. The optimisation procedure effectively discovered the appropriate solution within the specified daylight standard, as illustrated in Figure 5.25 (a). Similarly, the 10 best solutions from the fitness-function calculation have been placed in the targeted searching area.

The 155 Pareto-front solutions are distributed and presented in Figure 5.25 (a–f), highlighted as yellow individuals. As shown in the chart, the Pareto-front solution was distributed, along with the intended axis value designated in Figure 5.19, except in Figure 5.25 (d), where the Pareto -front UDI swarmed under majority solutions, instead of pushing into $UDI_{100\text{-}2000lux}$ maximum quadrant, and its distribution still performed a percentage of $ASE_{1000,250}$ outside the LEED v4.1 standard threshold. The $UDI_{100\text{-}2000lux}$ performs on the opposite side of the targeted value, indicating that during the searching process in MOO, consecutively, the solution was finding and configuring better performance configuration and fitness. However, the Pareto-front performance in $UDI_{100\text{-}2000lux}$ demonstrated a maximum value of 100% in the axis $ASE_{1000,250}$, valuing 0%.

5.4.3.4. Parameter to objectives (sensitivity analysis)

Aside from examining the daylight objectives, the variables that construct the parametric expanded-metal shading were investigated. The parallel co-ordinate plots depicting the link between parameters and objectives are presented in Figure 5.26 in order to understand how parameters were distributed when setting the value and percentage of $ASE_{1000,250}$, $sDA_{300/50\%}$, View and $UDI_{100\text{-}2000lux}$. The diverging-colored lines are based on the Height/SW parameter as the main independent variable. The lines represent the connection of all design solutions yielded in the MOO processes. The diverging-colored lines represent individuals based on specific highlighted criteria, in which the $ASE_{1000,250}$

objective is lower than 10%, and $sDA_{300/50\%}$ is higher than 75% (purple lines), while the grey lines are the unselected solutions.

Generally, in terms of parameters, it can be seen from the chart that the Bond value below 0.15, the Length/LW value below 0.6 and the Angle below 20° are dominantly shaping the overall outcomes, while the other two parameters, despite the uncertain precedent, are relatively evenly distributed. In terms of the objectives, the combination of the parameters shapes a density between 0% and 10% of $ASE_{1000,250}$ and greater than 60% of $sDA_{300/50\%}$, more than 30% of View and greater than 60% of $UDI_{100\text{-}2000lx}$. The selected criteria, which are fulfilling the criteria of LEED v4.1 EQ Credit Daylight – $sDA_{300/50\%}$ maximum 10%, and $sDA_{300/50\%}$ of at least 75% – are consequences implicated to the range of View of about 48%–75% and a UDI of about 81%–98% while sharing an even distribution in the parameters.

Figure 5.27 illustrates the sensitivity ranking of the design variables, indicating the importance of each parameter in relation to the linked objective. The positive sign (direct effect) denotes a positive relationship and an implication between the parameter and the targeted objective and vice versa. The charts show that the Strand/W parameter plays the most significant role in driving all four objective values by more than half of the SRC value. Generally, the $ASE_{1000,250}$ and View objectives were implicated the most by the sensitivity of the Strand/W with the SRC.

A value of almost one means that a minor movement in this parameter slider implicates a considerable variation in the value of the objective (confirmed in Figure 5.28). The second-most important parameter was Height/SW, with a significance ranging between 0.2 to 0.52 of SRC value. The third-most sensitive was Angle, with an SRC value ranging between 0.01 to 0.07. The last two parameters had the smallest SRC values, indicating that they have negligible impact on the target movements. When we look at the charts, Strand/W and Height/SW have opposite sensitivity directions in all the objective relationships.

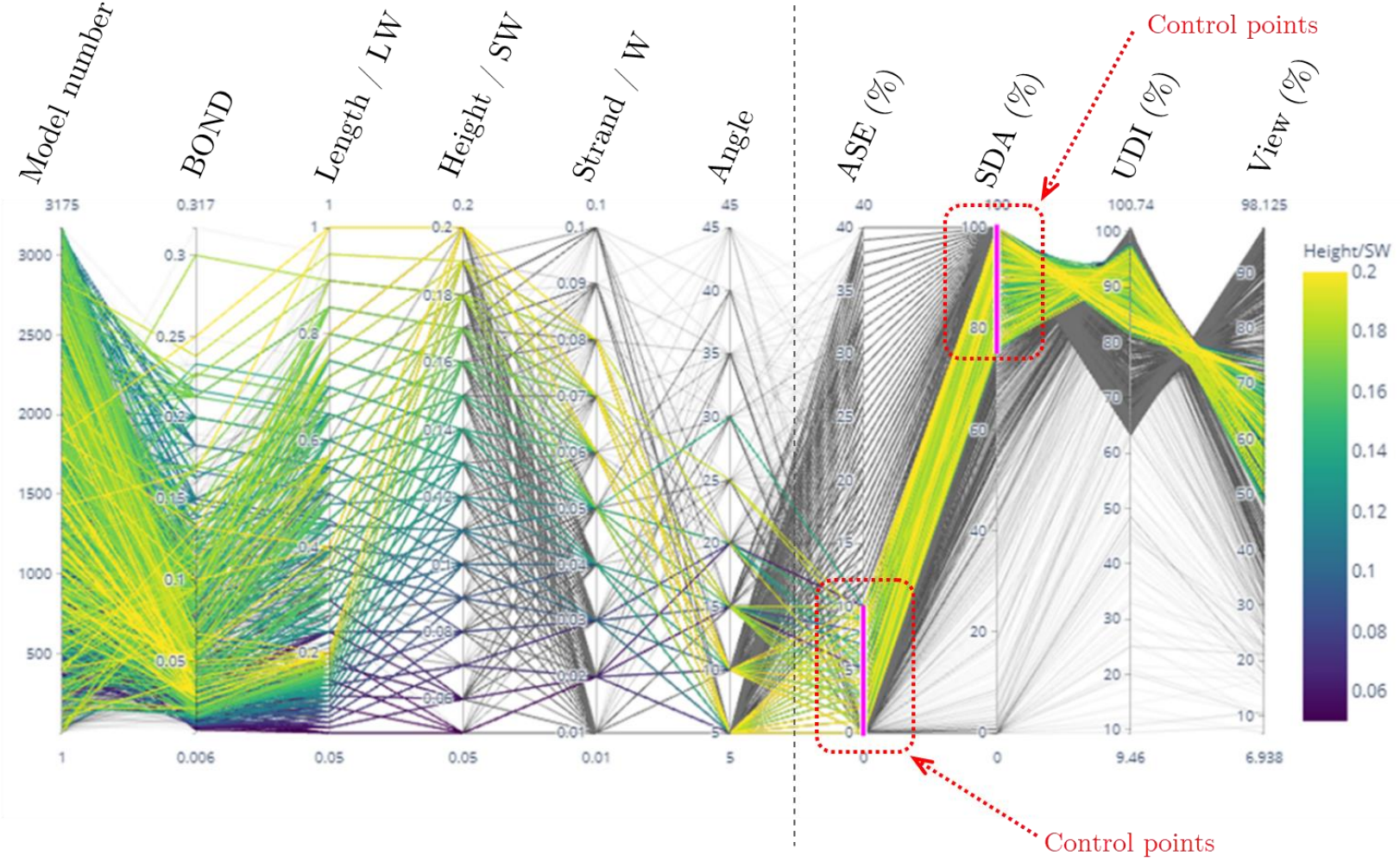

Figure 5.26. Parallel coordinate plot of the line of parameter values and objective values

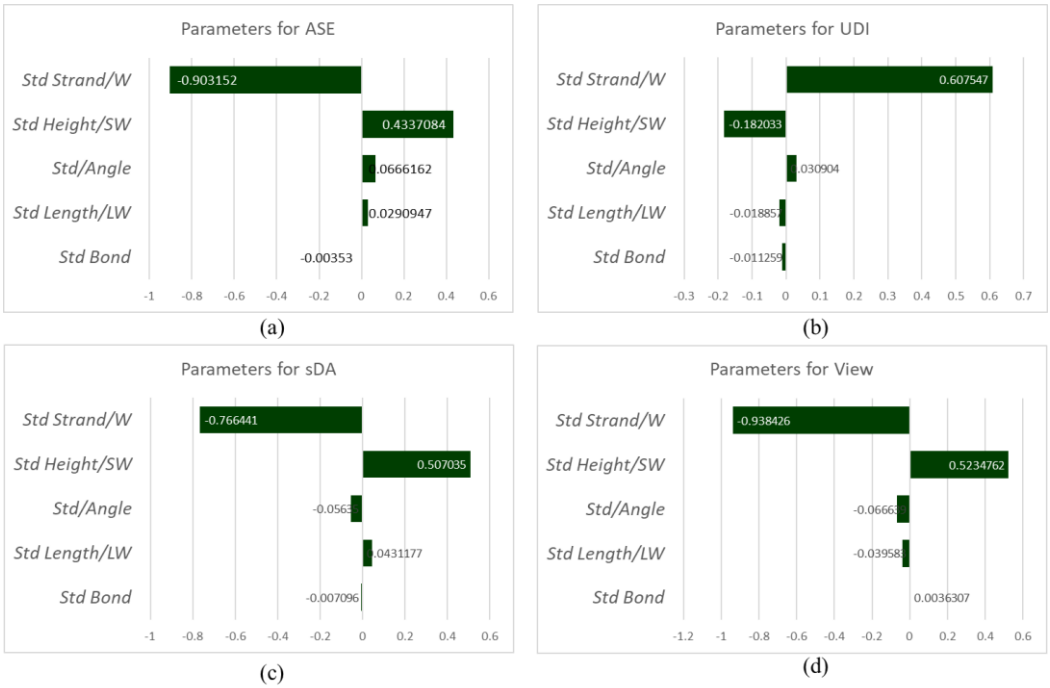

Figure 5.27. Sensitivity ranking of the design variables

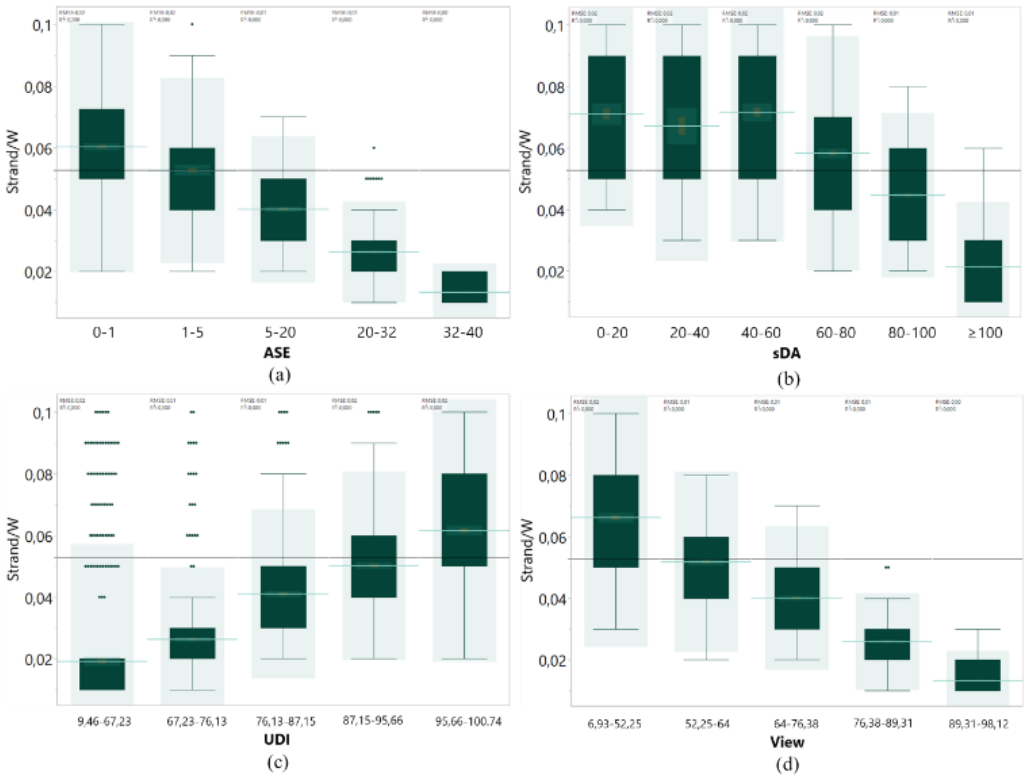

Figure 5.28. Box plot of the relationship between the Strand/W parameter and the objectives

Figure 5.28 portrays Strand/W as the most influential parameter of the expanded-metal shading in setting the percentage of $ASE_{1000,250}$, $sDA_{300/50\%}$, View and $UDI_{100\text{-}2000lx}$. In terms of $ASE_{1000,250}$, the Strand/W movement displayed high mean variability. The lowest (10%–20%) $ASE_{1000,250}$ percentage yielded by the Strand/W length was 2 cm to 10 cm concentrated in the range between 3 cm and 7 cm, while the smallest Strand/W length (below 2 cm) was responsible for the highest $ASE_{1000,250}$ percentage – 20%-40% concentrated in a range between 3 cm and 1 cm.

In relation to the $sDA_{300/50\%}$ objective, the wider Strand/W range was responsible for the low percentage of $sDA_{300/50\%}$. The variability of Strand/W was between 3 cm and 10 cm. The highest percentage of $sDA_{300/50\%}$ (80%–100%) yielded by the Strand ranged between 1 cm and 4 cm. Up to this point, the smaller Strand/W was preferable to procure a small value of $ASE_{1000,250}$ and a high value $sDA_{300/50\%}$.

In terms of $UDI_{100\text{-}2000lx}$, despite the occurrence of several outliers, the distribution of the Strand/W parameter almost yielded more than 60% of $UDI_{100\text{-}2000lx}$. The highest percentage of $UDI_{100\text{-}2000lx}$ distribution yielded varied relatively in samples and concentration. However, 95% $UDI_{100\text{-}2000lx}$ and above resulted from the middle to high parameter range, with the concentration between about 5 cm to 8 cm configurations of Strand/W.

The View objective representing the optical opening of the expanded metal projected in a vertical planar surface negatively correlated with Strand/W. It supported the common-sense concept that the higher the surface, the smaller the opening. Similar to $UDI_{100\text{-}2000lx}$, the variability of Strand/W length informing the pair objective varied. However, the highest percentage of View (forming more than 80%) yielded only a small concentration of Strand/W (between 1 cm and 2 cm), while the smallest percentage of View (forming less than 53%) yielded concentrated Strand between 5 cm and 8 cm.

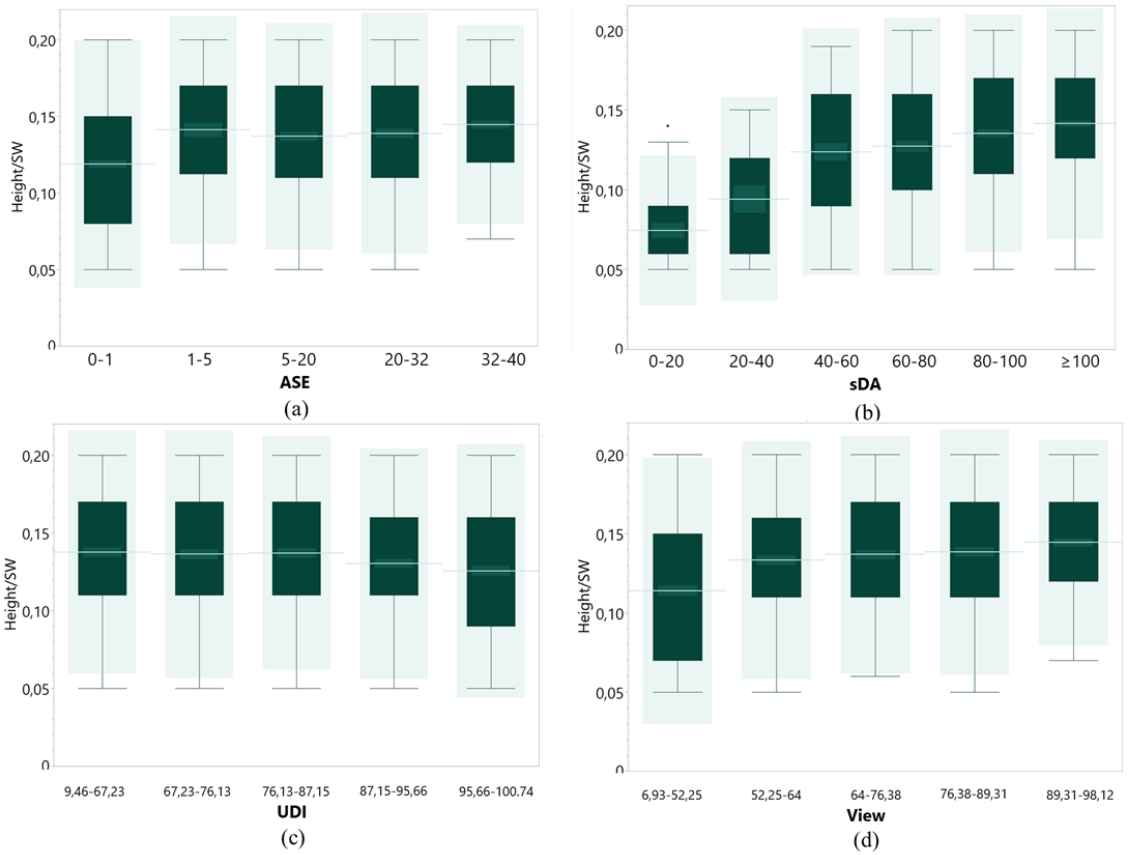

Figure 5.29. Box plot of the relationship between the Height/SW parameter and the objectives

The values of the second critical parameter in the SRC computation, Height/SW, are depicted in Figure 5.29. In terms of $ASE_{1000,250}$, the height of the diamond-shaped expanded-metal opening was distributed evenly to the percentage of $ASE_{1000,250}$. According to LEED v4.1 Daylight credit, it is not easy to investigate how height from the expanded metal is responsible for $ASE_{1000,250}$ below 10%. In relation to the $sDA_{300/50\%}$ objective, the diamond-shaped opening's height, which was greater than 10 cm, was responsible for the preferable $sDA_{300/50\%}$ with a percentage greater than 60%, particularly with concentrations between 10 cm and 15 cm. As Height/SW was distributed towards $ASE_{1000,250}$, the tendency was rather unclear due to the even parameter in the samples and concentration distributions. In general, despite the second-most pivotal variable shaping the value of four objectives according to the SRC calculation, the role of Height/SW per-value could not be clearly determined.

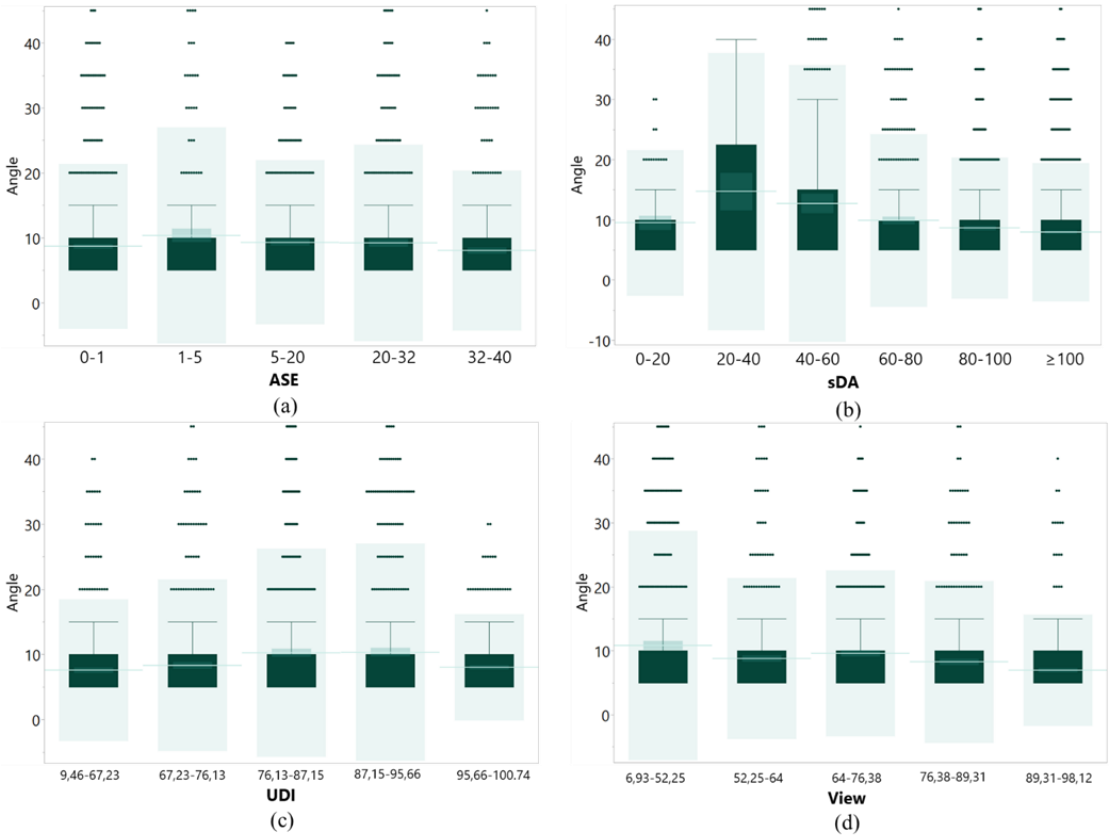

Figure 5.30. Box plot of the relationship between the Angle parameter and the objectives

Figure 5.30 shows the relationship between the range of Angle and the range of the objectives in a box plot. In general, the movement on the Angle towards $ASE_{1000,250}$, $sDA_{300/50\%}$, $UDI_{100\text{-}2000lx}$ and View showed monotonous variations that were the only samples from 5° to 15°, with concentrations limited between 5° and 10°. However, the relationship between Angle and $sDA_{300/50\%}$ showed more variety, with Angle yielding 20% to 60% of $sDA_{300/50\%}$ and the samples ranging from 5° to 40°, with the concentration of Angle ranging from 5° to 20°. The relation between Angle and the objectives shows a considerable number of outliers, which are considered individuals that could shift the correlation of the data. The occurrence of outliers indicates that only a portion of the samples is included in the calculation of the five-quartile outcome.

5.4.3.5. Result comparison

Figure 5.31 illustrates the comparison between daylight objective values of the 10 best solutions and the benchmark model. The fluctuation in the value of each solution reflects the trade-offs made during the optimisation process. Analyzing the chart, it is possible that the optimisation outlined in the research hypothesis improved some of the objectives, hence supporting the analysis in Figure 5.25. In terms of $ASE_{1000,250}$, the optimisation has been successfully solved, with a significant reduction compared to the benchmark model. For some design solutions, the $ASE_{1000,250}$ is stated as 0%, meaning that the reduction is 100%. Yet, for the rest of the objectives, for instance, the reduction in design solution number 7, the $ASE_{1000,250}$ decreases by 90%. Furthermore, the 10-best chosen solutions suggest that the percentage of $ASE_{1000,250}$ below 10% means that it fulfils the criteria required by LEED v4.1 EQ Credit Daylight. In other words, the $ASE_{1000,250}$ is being successfully optimised.

Analyzing the $sDA_{300/50\%}$ objective, all paired individuals perform a significant percentage. The benchmark model performs a maximum percentage of $sDA_{300/50\%}$, with 100%. In this scenario, the performance of the selected solutions typically degrades. The reduction is specified as being around 10%. However, the optimisation process maintains that most of the chosen solutions have $sDA_{300/50\%}$ greater than 90%, except for solution ranks 9 and 10. According to the results, the selected solution based on the optimisation processes and the benchmark model has fulfilled LEED v4.1 EQ Credit Daylight to achieve 3-point credit with more than 75% $sDA_{300/50\%}$ within a one-year period. Since the benchmark model performs the maximum possible percentage of $sDA_{300/50\%}$, it can be stated that the $sDA_{300/50\%}$ objective has not been optimised.

The finding from the results comparison shows that up to this point, firstly, the proposed methodology could observe the best expanded metal configuration performing optimized daylight goals. Secondly, the results suggest that indeed the expanded metal can have role in supporting environmentally friendly material when it is utilized as a shading in architectural or aesthetic purposes. Thirdly, it is also reducing glare probability, supporting the claim that it increases visual comfort.

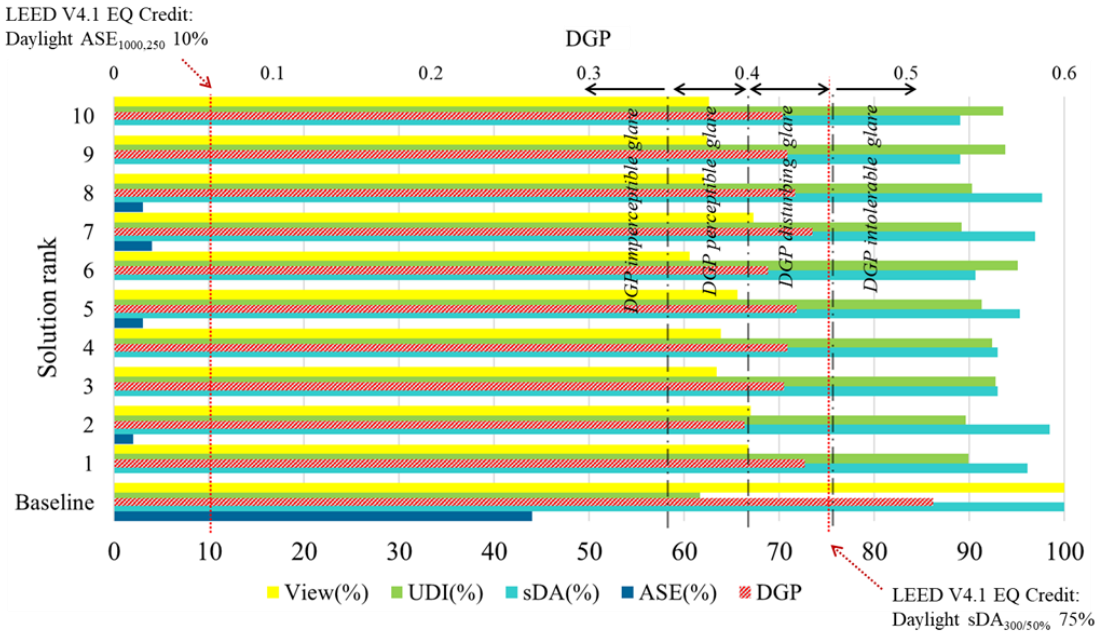

Figure 5.31. Comparison of daylight performance between benchmark model and the 10 best solutions from MOO

Similarly, the View objective was not optimised. The View objective was reduced to about 30% compared to the benchmark model. Even though the maximum target was set to optimisation input criteria, the overall opening without shading (benchmark model) performed a 100% opening. At the same time, the expanded-metal profile projection subtracted towards the assumed vertical planar surface. Thus, referring to the chart, the View comparison does not indicate any improvement, which means the outnumbered percentage was similar to the benchmark model. The desired objective percentage based on Figures 10 (b), (c), (e) and Figure 5.26 is presented closer in this chart (Figure 5.31).

The comparison demonstrated a significant improvement in the $UDI_{100\text{-}2000lx}$ objective. According to the chart, the $UDI_{100\text{-}2000lx}$ of the optimised solutions spans between about 90% and 100%, indicating that the optimisation successfully improved the annual $UDI_{100\text{-}2000lx}$ average by around 50%. Even though the $UDI_{100\text{-}2000lx}$ observation did not relate to any international standard requirement (the results based on the 10 ranked solutions' performance), the percentage of $UDI_{100\text{-}2000lx}$ was considered satisfying.

Solution rank	$ASE_{1000,250}$	$UDI_{100\text{-}2000lx}$	DGP	View	Remark
Baseline model	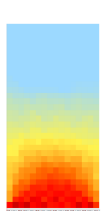		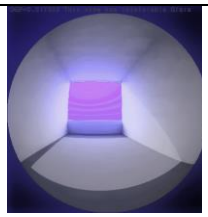		Bond: - Length/LW: Height/SW: Strand/SW: Angle: - DGP: 0.517 *Intolerable g* $sDA_{300/50\%}$:
1			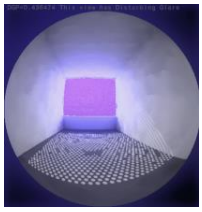		Bond: 0.04 Length/LW: Height/SW: Strand/SW: Angle: 5 DGP: 0.436 *Disturbing g* $sDA_{300/50\%}$:
2		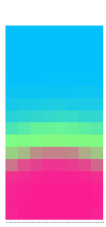	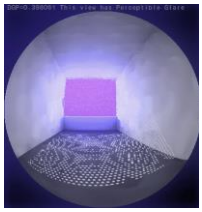	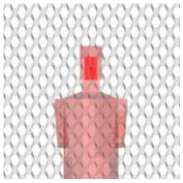	Bond: 0.03 Length/LW: Height/SW: Strand/SW: Angle: 5 DGP: 0.398 *Perceptible g* $sDA_{300/50\%}$:
3	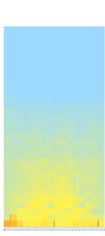	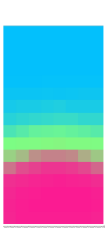	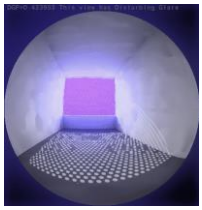	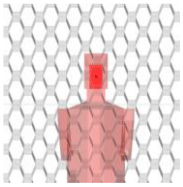	Bond: 0.047 Length/LW: Height/SW: Strand/SW: Angle: 5 DGP: 0.423 *Disturbing g* $sDA_{300/50\%}$:
4	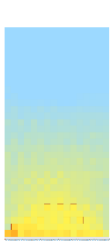		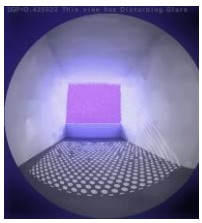	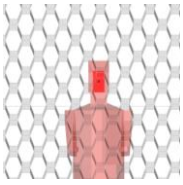	Bond: 0.057 Length/LW: Height/SW: Strand/SW: Angle: 5 DGP: 0.425 *Disturbing g* $sDA_{300/50\%}$:
5	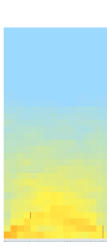	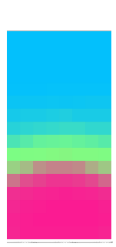	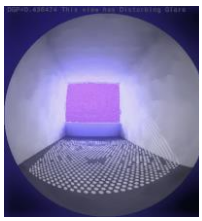	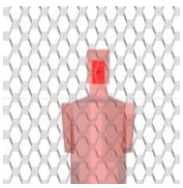	Bond: 0.04 Length/LW: Height/SW: Strand/SW: Angle: 10 DGP: 0.431 *Disturbing g* $sDA_{300/50\%}$:

Figure 5.32. The visualisation of the 10 best solutions based on fitness-function calculation and the benchmark model

The DGP gap was observed in this comparison. The investigation sought to determine whether the MOO findings performed a better DGP performance. Analyzing the findings revealed that the DGP level was lower than the benchmark model's performance. Regarding the DGP categories, whereas the benchmark model performed a DGP value of more than 0.45 (intolerable glare), most presented individuals exhibited a DGP value between 0.4–0.45 (disturbing glare). However, solution rank 2 was the only individual that performed perceptible glare among the presented individuals.

An evaluation of daylight performance utilizing a generative algorithm and MOO with input data from Japan's sky condition suggests that expanded-metal shading is a dependable material for enabling passive daylighting design strategies. By iterating the design parameters based on the expanded-metal components described in the early design stages, the designer is able to develop design solutions that go beyond what was envisioned before to the start of the design processes. The efficacy of the form-finding technique is evidenced by the fact that the optimisation procedure presented in this study created 3,176 design solutions using relatively brief simulations. Each design solution incorporated parameter values and four optimisation-specific values. This optimization technique can be repeated indefinitely, based on the parameters specified and the expected number of generations.

The fitness function was used to determine the 10 best daylight performances, where each design solution met the targeted performance criteria. These 10 design ideas demonstrated performance targets that meet the international daylight standard LEED v4.1 in two specified objectives, ASE and sDA. The finding demonstrates that the proposed methodology can be employed as an alternative strategy to meet the merit of daylight standards required for design objectives. These 10 individuals indicate optimisation of $ASE_{1000,250}$ and $UDI_{100\text{-}2000lx}$ objectives but not of $sDA_{300/50\%}$ and View because the benchmark model has a maximum value of 100% for these two objectives. Moreover, when the 10 best designs for these four daylight-optimisation objectives were subjected to a one-day DGP test, not all solutions produced perceptible glare. The majority of the solutions performed disturbing glare. These categories, however, alleviated the intolerable glare performed by the benchmark model. Additionally, while the

movement of the parameters suggests minor variance, the expanded-metal shape varied, as illustrated in Figure 5.32 shows the occurrence variation can also be considered an option as direct geometric and aesthetic feedback from the form-finding processes during the decision-making process. The proposed methodology successfully identified indicators that can be used to address the issues raised. From the resulting Pareto front (Figure 5.25), it was found that each objective had a relationship that was not always linear, with a high degree of correlation. Only the relationships between $ASE_{1000,250}$ and $UDI_{100\text{-}2000lx}$, View and $UDI_{100\text{-}2000lx}$ and View and $ASE_{1000,250}$ showed significant correlation. By analyzing the correlation results, the relationships between the objectives can be more easily predicted to determine their trade-offs. In contrast to the Pareto-front correlation analysis, where the correlation study was conducted across entire generations, only the relationships between View and $ASE_{1000,250}$ and View and $sDA_{300/50\%}$ were strongly correlated. The lack of correlation could be because the solution produced during the early phase of the optimisation process still performed a weak attachment to the optimisation target.

Regarding the relationship between expanded-metal components as design parameters and daylight objectives, this research succeeded in identifying the trend of shifting parameters towards the design target and the parameters that had the most influence on the daylight objectives. From the analysis, each parameter's tendencies towards the targeted objective value were identified. For example, regarding the fulfilment of the LEED v4.1, the distributions of Bond, Angle and Length/LW showed a more apparent trend than Height/SW and Strand/W. In addition, the density in the axis of the parallel co-ordinate plot indicates that the optimisation process succeeded in directing the design solution to the target optimisation value. The percentage of View was not always at the maximum when the objective values were in the LEED v4.1 requirement ranges. This tendency also showed that the fulfilment of this standard leads to the maximum $UDI_{100\text{-}2000lx}$ value, which was successfully added as an additional optimised objective. However, the trend of the minimal variation in the movement of this parameter indicated that the iteration process still lacked a generation number, like what was previously described, considering that the ratio between the total generations that

can be obtained (Table 5.4.2) and the number of individuals used as samples were still few and far between.

The most influential parameters on the objective movement were successfully identified by performing sensitivity analysis on all individuals produced by the MOO. Strand/W and Height/SW were the most influential parameters in this shading-to-daylight investigation. Knowing which parameter influenced which daylight objective, future research incorporating different variables and objectives can be carried out more thoroughly. In addition, the objective-value target can be obtained more optimally by anticipating the parameters that are considered to have the most effect. However, parameters considered less influential can be made simpler or even set aside (set to be fixed). The data used in this sensitivity analysis were based on the overall simulation generations. This means that, similar to the problem discussed earlier regarding the limitation in the number of generations, the small variation movement of one parameter can affect the overall sensitivity-analysis results.

The effect of each parameter's range value that had the most significant influence on the objective was successfully investigated. The box plot shows which parameter range most affected a particular targeted-objective value. Through this process, the minimum and maximum thresholds of the parameters could be explicitly set to the identified range with the most influence. However, in some plots, there were quite a significant number of outliers. The procedure could identify the parameter that could be optimised and then performed a deeper investigation to produce more optimal findings in the linked daylight study.

The system and objectives employed in this sub-chapter are in line with what was used in [25,50,54,71,87,93], but they differ in design parameters and energy calculations, which were outside the scope of this investigation. However, the research mentioned above shows optimisation of the objectives in line with that presented in [100]. In addition to the efficacy revealed in this sub-chapter of expanded metal as daylight shading, the material is more likely to be mass-fabricated and supplied to the market due to manufacturing availability and capability. Due to the advantages of extensive manufacturing and environmentally favourable qualities, the components that construct

expanded metal tend to be more easily modified in relatively low-level customisation than other parametric window shadings. In line with [4], the preferable opening is in the range of 40%–60%. However, in this research, the shading opening ratio was made among the MOO targets. The aggregated outcomes were influenced by the trade-offs associated with each optimisation objective. Similar findings were reported in [156], albeit under different sky circumstances.

This research was significant because it resulted in the development of a complete computation and a discussion of daylight performance using parametric, complementing prior research on expanded metal [134,149] with the same principle as the research conducted in [99]. This research comprehensively investigated daylight performance specifically of expanded-metal shading, mainly using Japan's sky condition. This sub-chapter examined the link between objectives and independent design variables while optimising daylight and geometrical objectives.

The tools used in this research were close to acceptable level of accuracy [72,157]. However, this research focused less on the distribution of daylight generated by sunray reflection on the shading-angle surface, as demonstrated in [53,75]. As mentioned previously, increasing the number of generations in the optimisation process might yield outcomes with a better level of optimisation because the number of solutions sampled for research grows.

The limitations of the sub-chapter have been noticed. In this sub-chapter, the simulation of expanded-metal shading excludes thickness and consists of a single flat surface. The parameter for the thickness of expanded metal necessitates more sophisticated calculations, which necessitate longer simulation times and additional hardware specifications. Thus, it is recommended that future studies increase the number of MOO generations and incorporate the shading thickness of expanded metal.

5.5. Expanded metal shading toward Daylight Glare Probability (DGP)

5.5.1. Introduction

The relationship between shade with expanded metal and daylight glare probability (DGP) will be described. This subchapter tests the application of parametric design method and MOO in creating expanded metal shading and optimizing daylight glare probability (DGP) as one of the daylight metrics for assessing visual comfort, using weather data from Shimonoseki, Japan. Based on the research objectives, the purpose of this sub-chapter is to address the following research questions:

- What is the relationship between the View (aperture) and the DGP based on the MOO results?
- What is the relationship between the expanded metal parameters and the objectives based on the MOO results?
- What is the most influencing parameter toward the DGP and the View (aperture)?
- How significant is the optimization of the DGP?

The hypothesis (H_a) of the research is parametric, and MOO can optimize DGP through the iteration (form-findings) of expanded metal shading. While the null hypothesis of this research is the deployment of parametric and MOO has no affect in optimizing DGP performed by expanded metal shading (H_0).

5.5.2. Methodology

5.5.2.1. Overview

This research was conducted through a series of sequential steps. Initially, the problem formulation and daylight metric were determined. Using Rhino and Grasshopper, the benchmark and enlarged metal models were created realistically. In this step, design factors were structured as dynamic parameters. Thirdly, Ladybug and Honeybee were used to organize the daylight parametric specification. In this stage, meteorological data and an analysis period are entered. Fourthly, Octopus was used to execute the MOO processes. After the Octopus generated design solutions through iterative and

optimization methods, the DGP, View (aperture), and tendencies between parameters and objectives were analyzed and compared.

5.5.2.2. Geometry modelling

In the modelling of the geometry, both the benchmark model and a simulated room with increased metal shading are included. The benchmark model is a room simulation without shading, but the primary model is the same room simulation with extended metal shading. The simulated room has been designed to resemble a basic, windowless modular workspace. Given the sky conditions of Shimonoseki, the simulated room is positioned along the north-south axis and faces south, with a set glazing ratio of 70%. The uncontrollable characteristics also include the room's height, width, and length, in addition to the glazing ratio. The benchmark model will be outfitted with enlarged metal geometry, which functions as an external solar shield and is also subjected to the entire daylight study, for the purpose of further comparing results. The enlarged metal geometry was configured to iterate based on the many parameter values provided via the number slider. The dynamic parameters of the shading and the attributes of the geometry are presented in Table 5.4.2 and Figure 5.6.

5.5.2.3. Daylight simulation

EnergyPlus weather data (EPW) set to be December 21 at 12:00 JST was used as a weather data to supply the data that represent the sky condition of the city through the historical weather data observation. The Global Horizontal Illuminance, Diffuse Horizontal Illuminance, and Direct Normal Illuminance, together with the sun position according to certain day in Shimonoseki, are presented in Figure 5.33.

The simulated room and the expanded metal geometry uses the office zone program and Radiance material as adopted in, and it is presented in Table 5.5.1. the number then applied in the construct material components in Honeybee to become an input for simulation components. The choice of material was meant to mimic the needs of general building purposes. Specific material use will need more justification and properties calculation that will impact simulation time.

Table 5.5.1. Interior surface reflection and transmission properties

Surface	ρ	ρR	ρG	ρB	Specularity	Roughness
Ceiling	0.800	0.800	0.800	0.800	0.000	0.000
Interior wall	0.750	0.750	0.750	0.750	0.000	0.000
Floor	0.210	0.210	0.200	0.200	0.000	0.000
Glazing [a]	0.750	0.750	0.750	0.750	0.000	0.000
Shading	0.800	0.800	0.800	0.800	0.000	0.200

[a] *for glazing, the value should be read as transmittance* τ

5.5.2.4. Optimization setting

To collect the assumed best individuals according to the targeted objective value, the MOO uses the expanded metal attributes (Table 5.4.2) as an input parameter and the DGP value as well as the view (aperture) percentage as an optimization objective or genome.

The optimization engine used was called Octopus given the setting of 0.5 Elitism, 0.2 mutation probability, 0.9 mutation rate, 0.8 crossover rate, 100 individuals per generation, and 200 maximum generation, the optimization engine used the HyPe Reduction ranking method. The target objective is to achieve a minimum DGP subtraction of 0.375, the median perceptible glare value range between 0.35 and 0.4, and a maximum optical opening of the diamond shaped expanded metal profile.

The setting represents the default calculation engine from the Octopus. It requires a knowledge of informatics in defining the combination in the setting. The more generation number is set, the more probability the optimization come up with higher level of optimization. However, it will directly implicate to the time taken for optimization process as well as requiring more hardware capability. The setting adopted in this sub-chapter does not a generalization rather it can be adjusted according to simulation needs.

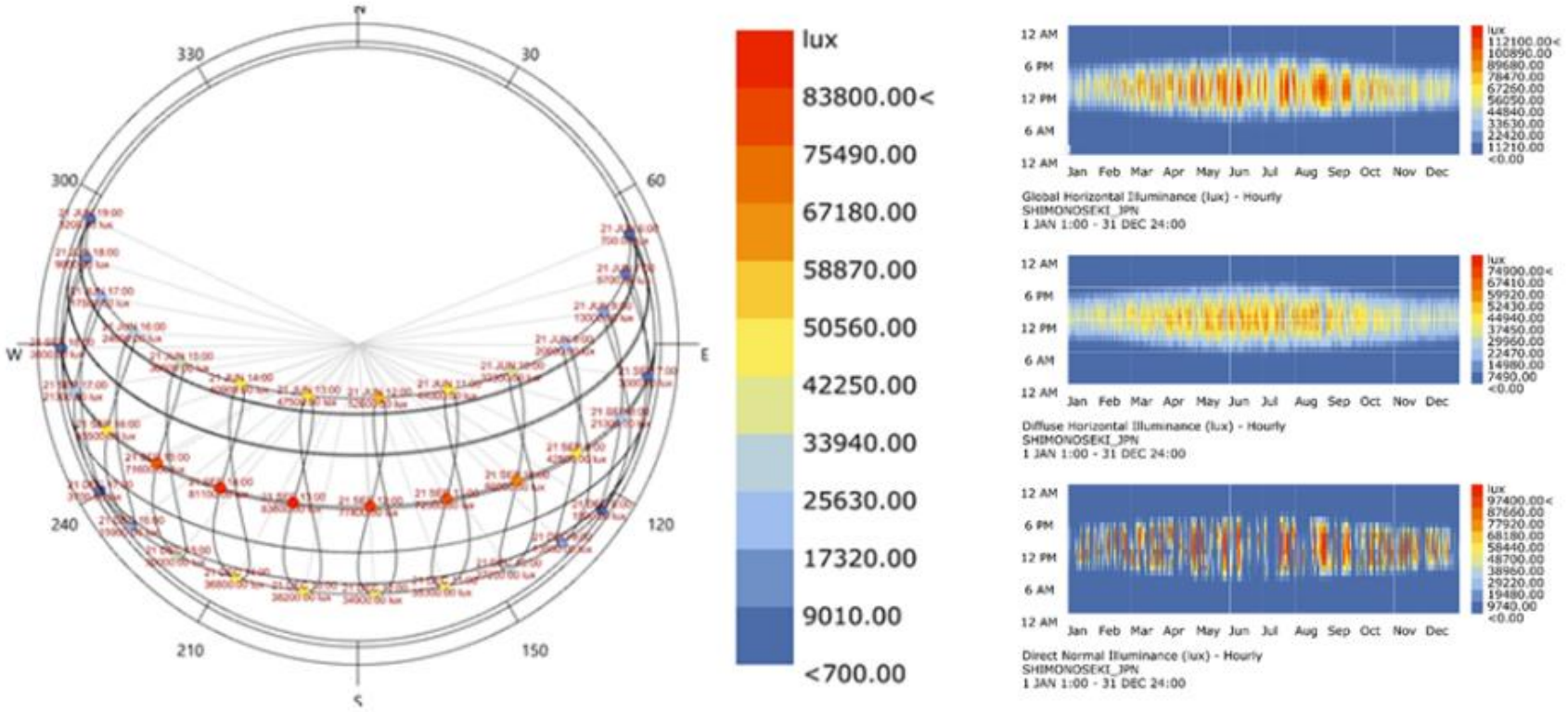

Figure 5.33. Daylight profile and sky condition of Shimonoseki

5.5.3. Results

5.5.3.1. Optimization results

Having a perceptible glare as optimization target, the genome was set through minimizing the subtraction factor upon 0.375 DGP value. Due to the time constrain, optimization process was intentionally stopped at generation 47. Up to this point, 2322 solutions and 88 Pareto frontiers solutions has been generated. The distribution of individuals as a design solution categorized by all generations, Pareto frontiers, benchmark model and the chosen individuals are displayed in Figure 5.34. Analizing the results, it is clear the optimization process was tended to find the solution that has a value distributed along with the axis View (aperture) maximum and DGP minimum. However, related to the targeted value of DGP, only limited Pareto front solution included as DGP perceptible glare. In line with this, the majority of Pareto frontier solutions was distributed over the DGP intolerable glare.

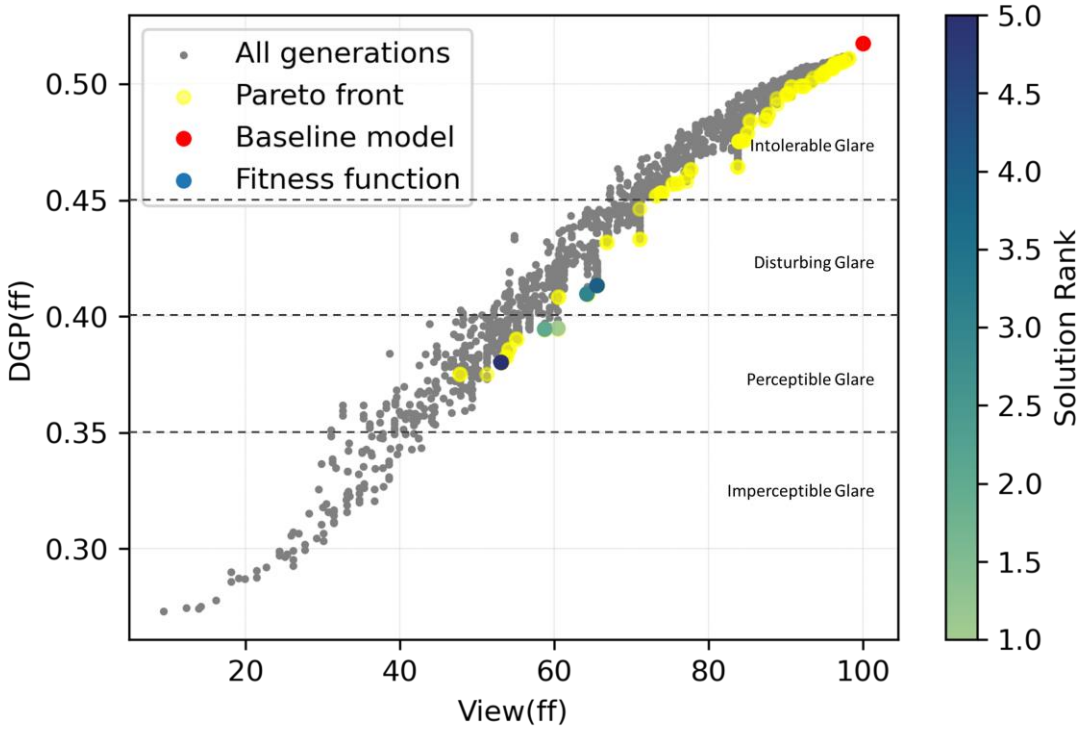

Figure 5.34. The scatter plot of the optimization results

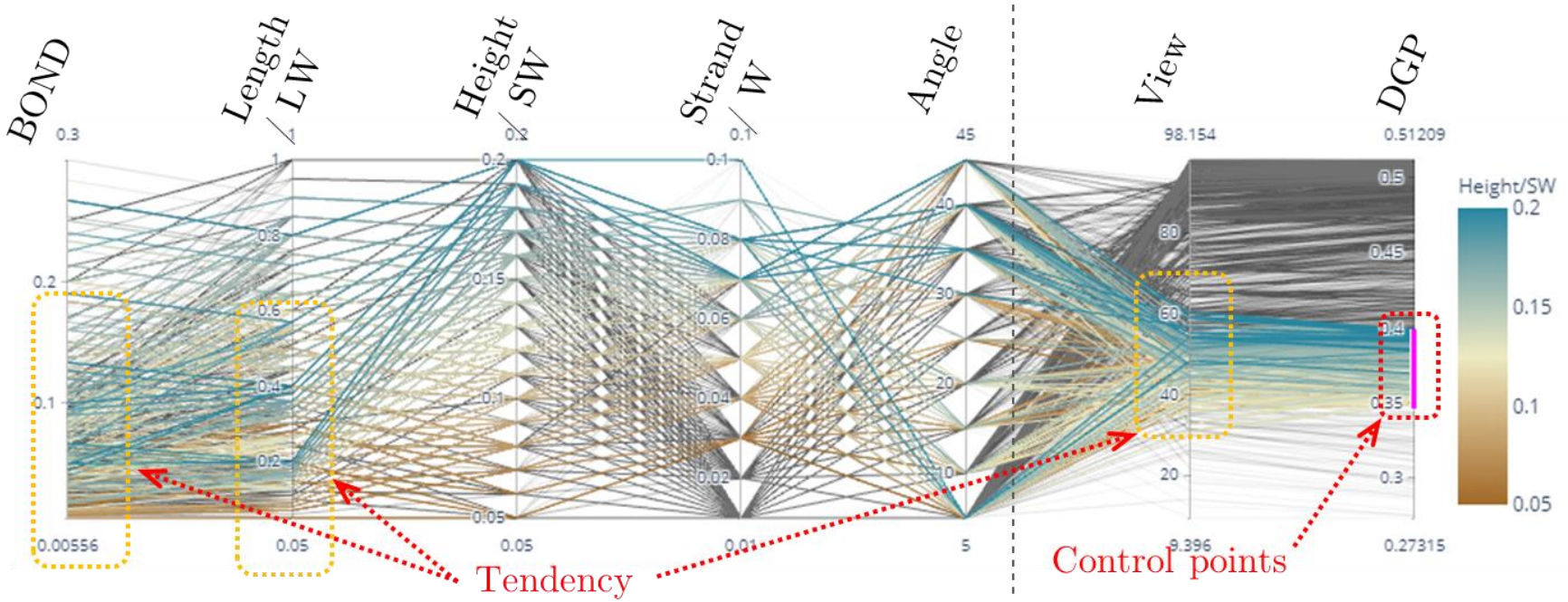

Figure 5.35. Parallel plot showing connection between parameters and objectives

The design objectives were evenly distributed across four DGP categories. Perceptible glare was dispersed along the view (aperture) axis between 40% and 60%, while undetectable glare was present below 40%, and distressing glare occurred when the aperture size exceeded 60%. The benchmark model's coordinates and the selected individual's coordinates indicate the DGP optimization. The other subchapter will cover the contrast of the benchmark model and the explanation of the chosen individual.

The parallel coordinate plot showing the relationship between parameters and objectives in terms of value connection has been displayed in Figure 5.35. The purple highlighted values along the axis of DGP indicate the individuals for whom DGP performs perceptible glare. Confirming the aformentioned relationship between DGP and View (aperture), here the connection of the highlighted wires shows the swarm in View (aperture) ranged from about 40% to about 60%. The connection to the parameter shows rather unclear precedent, thus it needs more close analysis. The DGP perceptible glare is yielded by the combination of Strand/W 0.03, parameter bond below 0.3, and length/LW below 0.9. In terms of height and SW, it displays an even distribution.

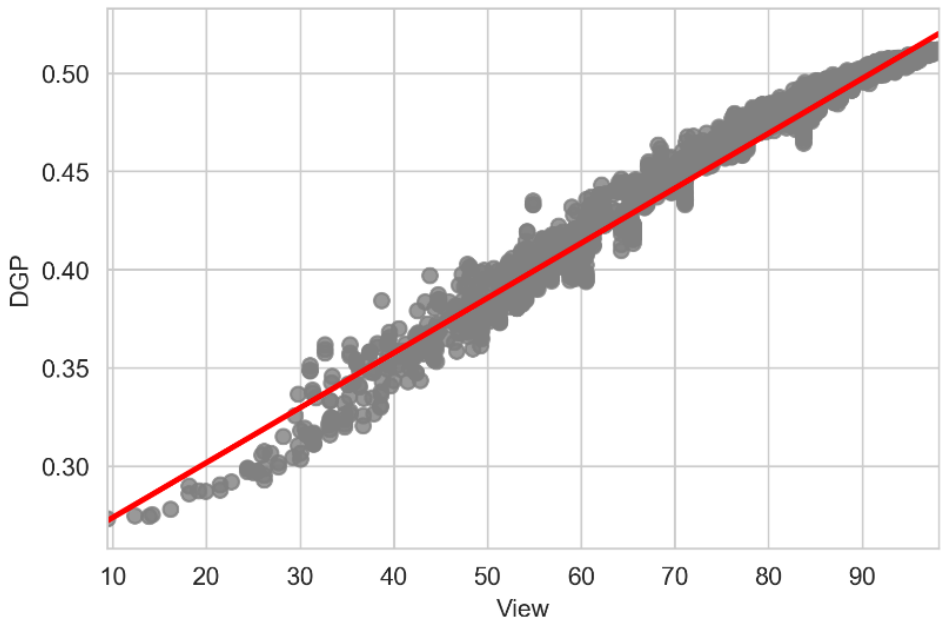

Figure 5.36. Correlation between View (aperture) and DGP

Figure 5.36 illustrates the correlation and fit line between the objectives (aperture) and DGP. Analyzing the scatter plot, the DGP demonstrates a significant positive correlation in relation to the optical opening. Through this correlation value, further analysis using the same sky condition and radiance material can be accurately predicted.

By applying fitness function calculation to the Pareto frontier, five best solutions have been chosen based on fitness function rank. The solution attributes are displayed in Table 5.5.2 and presented visually both for DGP and the expanded metal pattern in Figure 5.37. Among the finest solutions in the table, the variation of parameters was still deemed insufficient. Height/SW and Length/LW have the same ratio and multiplication factor, with a multiplication factor of 2 for solution rankings 1 to 4 and 1 for solution rank 5. Similarly, the parameter angle has a multiplication factor of just 8 and 7, and a height/SW greater than 0.15, particularly 0.16, 0.17, and 0.2.

Table 5.5.2. Selected solutions based on fitness function values

Rank	Model	Bond	Length/LW	Height/SW	Strand/W	Angle	View	Sub FF	Fitness Function	DGP
1	1668	0.133333	0.4	0.2	0.07	40	60.48	0.01964	105.54	0.39
2	2237	0.113333	0.34	0.17	0.06	35	58.77	0.01952	102.23	0.39
3	2008	0.133333	0.4	0.2	0.06	40	64.25	0.03466	101.95	0.41
4	2129	0.133333	0.4	0.2	0.06	35	65.56	0.038297	101.87	0.41
5	2139	0.053333	0.16	0.16	0.07	40	53.13	0.005198	101.60	0.38

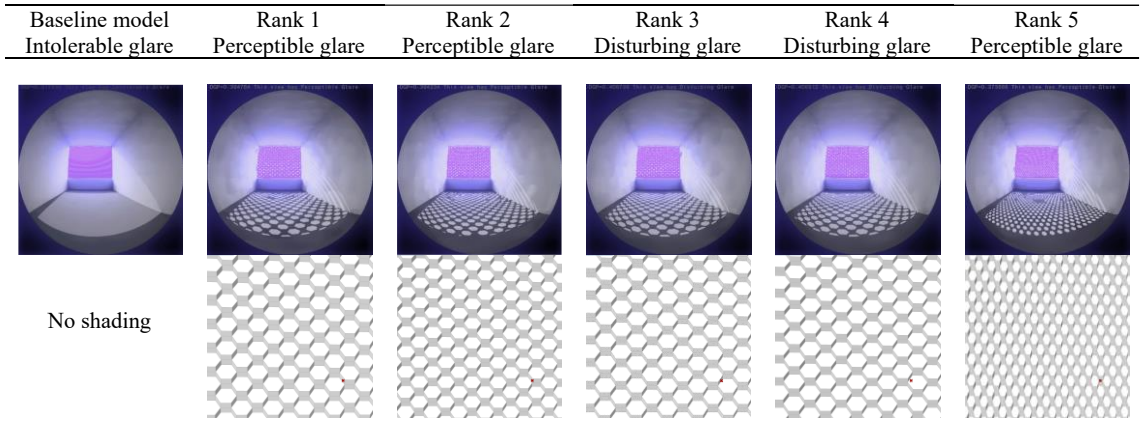

Figure 5.37. Chosen solutions and visualization

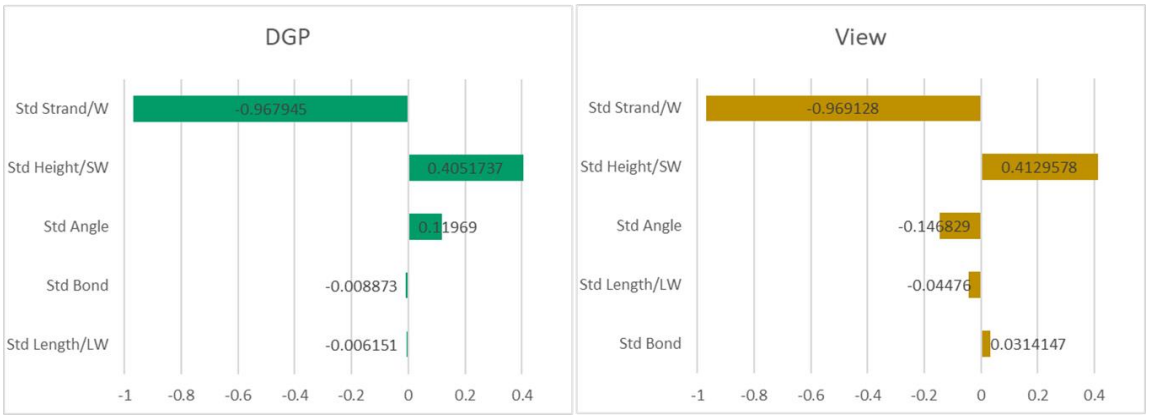

Figure 5.38. Sensitivity analysis: (a) DGP, (b) View

Standardized Regression Coefficient (SRC) was used to measure the t-test in order to conduct sensitivity analysis and determine which parameter has the most significant impact on the movement of the objective's value. The SRC was executed with the analytic software JMP using the fit model command to search for the parameter estimate with each standardized objective set as a role variable and each standardized parameter as the model effect construction. The sensitivity ranking of the design variables showing the important of each parameter towards the related objective are presented in Figure 5.38.

The positive sign (direct effect) indicates positive relationship and implication between the parameter to the objective and vice versa (Inverse effect). From the chart, for both objectives, parameter Strand/W, followed by Height and Angle are the most affected parameters driving the value of DGP and View (aperture). However, reverse implication in each objective happens for parameters Angle, Bond and Length/LW.

The boxplot (Figure 5.39) portrays the role of parameter Strand/W in driving both the objective view (aperture) and the DGP. Each graph illustrates a similar link between simulation parameters and objectives. Analyzing the chart, variance samples of Strand/W occurred between 56% and 72% in DGP irritating glare and view (aperture). The detectable DGP has been altered by Strand/W samples with concentrations ranging between 0.06 and 0.07. This distribution was also responsible for the view (aperture) objective values ranging between 9.39% and 56%, which is greater than fifty percent. Nonetheless, a substantial number of outliers may compromise the validity of this section.

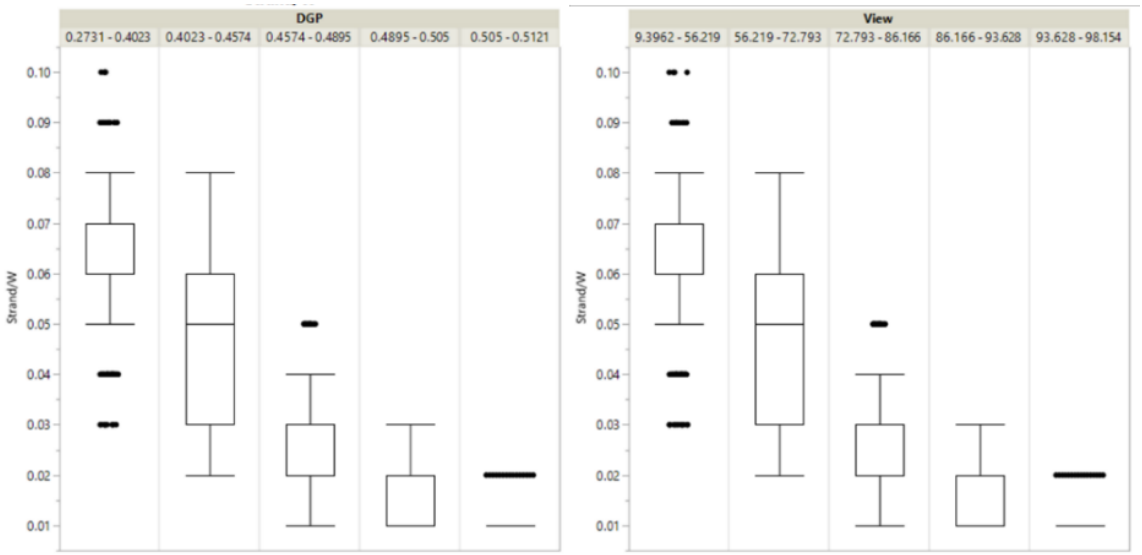

Figure 5.39. Box plot showing Strand's role towards objectives: (a) DGP, (b) View (aperture)

5.5.3.2. The validation results

To study the occurrence and significance of the optimization with respect to the two objectives, view (aperture) and DGP, the validation analysis must be performed by applying the performance of the benchmark model and the chosen solutions. The comparison between benchmark model performance and the best five solutions based on fitness function calculations is displayed in Figure 5.40.

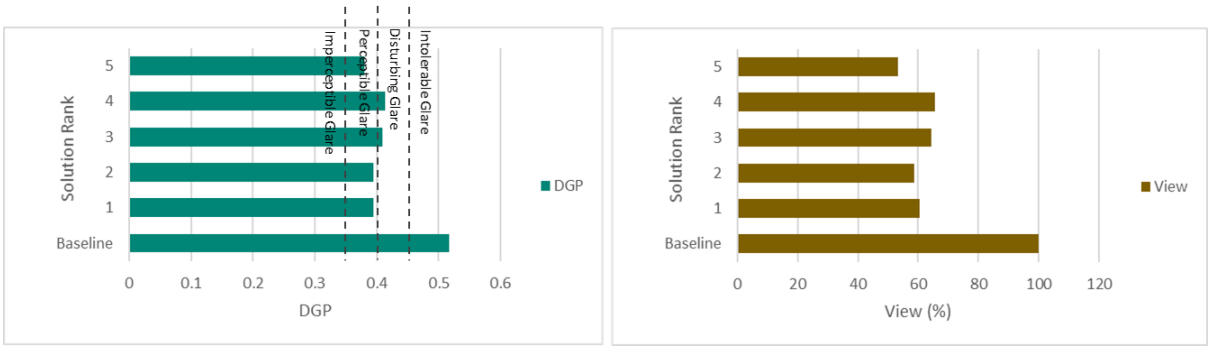

Figure 5.40. Validation: (a) DGP, (b) View (aperture)

In terms of DGP, the parametric optimization processes successfully reduced the DGP value by about 0.1 point. However, according to the DGP criteria, none of the best solutions performs DGP imperceptible glare. This is probably due to the specific optimization setting where the target value of the median perceptible glare median has been used. Solution Rank 3 and 4 exceed the perceptible glare threshold, showing the trade-offs happening during the iteration process. In terms of view (aperture), since the benchmark model was not equipped with shading, it is considered to be performing a 100% view (aperture) to the outside. In this condition, no optimization has been made. The trade-offs between objectives yielded a solution with a maximum view (aperture) of about 62%, which means that the percentage was reduced by about 38%.

Considering the research question (Sub-chapter 5.5.1), the proposed parametric and optimization platform has been successfully finding the best solution that indicates optimization related to DGP when expanded metal shading is used. Besides, by applying the proposed method, the most significant parameters driving the objectives' constant changes have been identified. It is answering the hypothesis (H_a) positively, and by seeing the results, H_0 is not applicable. The significance of this research is that the relatively popular building material has been investigated deeply. The scope of the investigation was specific and included parameter performance and roles. This study supporting previous research in investigating the role of expanded metal shading [22] toward daylight performance and confirming the expanded metal as an environmentally conscious building material [131]. However, the lack of simulation is considered the limitation of the results. Thus, given the same simulation model and setting, further research is encouraged to run longer simulations.

5.6. Chapter conclusion

This chapter presented the application of parametric design and MOO as a design approach that investigated the use of expanded-metal shading associated with daylight performance given the sky condition of Japan. This chapter aimed to confirm the capability of expanded-metal shading as an environmentally friendly building material in

terms of daylighting by developing an integrated parametric-design platform and optimisation processes iterating expanded-metal logic to optimise daylight objectives. The proposed system proved that expanded metal is a building material that can support environmentally friendly architectural design and is one of the shading devices that can be relied upon in incorporating passive-design strategy related to daylight. In some daylight objectives, the proposed methodology showed improvisation that met the merit of daylight standard LEED v4.1. The design method and analysis demonstrated that expanded-metal shading design still provides a considerable range of possibility for improvement.

Focusing on the Japanese standard JIS G3351 expanded metal grating type, the XG24 is the found type from fitness function calculation together with the best type targeting DGP. the XG13 and XG14 are the best type for UDI, while XG91 is the grating type with maximum view to the outside. The limited samples make the observation of the tendency become unclear. What is more, the regression shows that the aperture is highly correlated with the UDI, while it is negatively corelated with DGP.

From a comprehensive daylight investigation, based on the given context and among the 3,176 design solutions produced during the MOO, the best design solution identified from the sensitivity analysis towards the 155 Pareto-front individuals was model number 1,728. This model was equipped with parameter configurations of 4 cm Bond, 12 cm Length/LW, 12-cm Height/SW, 4-cm Strand/W and 5° in Angle. The best design solution performed 0% $ASE_{1000,250}$, 96.09% $sDA_{300/50\%}$, 89.93% $UDI_{100\text{-}2000lx}$ and 66.75% View. Compared to the benchmark model, the best design solution showed a reduction in $ASE_{1000,250}$ by 100%, $sDA_{300/50\%}$ by about 4%, View by about 34% and an improvement in $UDI_{100\text{-}2000lx}$ by about 50%. Furthermore, the DGP test showed that the best design solution (rank one) performed a 0.081 lower DGP value, improving the category from an intolerable glare to a disturbing glare. However, solution rank two improved the DGP into a perceptible glare.

Focusing on the DGP study, The DGP and View values per-test points has been successfully generatively iterated, distributed and investigated. View and DGP correlated positively. The View ranged 40% to 60% correspond Perceptible DGP ranged from 0.35

to 0.4. Seeing at the tendency, despite the unclear correlation between parameter and objectives, the Perceptible DGP yielded by the combination of Strand/W 0.03, Bond below 0.3, and Length/LW below 0.9. 6 cm to 7 cm strand responsible for smallest DGP value but still in the range of Perceptible glare criteria. On the other hand, smaller strand corresponds to the highest View to the outside. Solution number 1668 was found as the best solution. The solution configured of Bond: 0.1333, Length/LW: 0.4, Height/SW: 0.2, Strand/W: 0.07, Angle: 40, performed 60.48% View and 0.39 DGP. The most influencing parameter was the strand. By comparing the results and the benchmark model, the optimization achieved a reduction in DGP by 38%. However, the View objective was not considered to set any optimization.

The optimization of DGP was accomplished by the use of parametric and MOO processes in conjunction with expanded metal shading that simulated Shimonoseki's sky condition. The use of the parametric is to be able to iterate design solution rather than to evaluate phase by phase after the design solution is done (classical design processes). The major findings of the research are the occurrence of the best design solutions with their parameter configuration optimizing DGP and the Strand that has been identified as the most influential parameter driving the optimization objective. What is more, it is found that smaller apertures lead to preferable DGP phenomena. Through this experiment, the decision-making related to the design process can be supported in a relatively less time-consuming manner. Thus, the proposed parametric and MOO processes might well be applied to broader research on environmentally friendly architecture design and the built environment.

The significant findings of this particular chapter include the apparent achievement in daylight performance optimisation and improvement through the use of parametric and MOO, the identification of optimal design solutions and their variable configurations, the identification of the correlations between four optimisation objectives' Pareto fronts, the observation of the design variable's tendency to shape the objective values and the discovery of Strand as the most influential parameter defining the value of daylight objectives.

Chapter 6. Design exploration and optimization of twisted *Releaux* triangle geometry toward outdoor thermal comfort and energy consumption

6.1. Introduction

This research aims to investigate the outdoor microclimate in the early phase of designing a two-level wooden house in the Orio District, Kitakyushu, Japan through parametric and generative algorithms platforms. This research is an early design stage of the intended project and aims to utilize computational design, which is parametric and multi-objective optimization using a generative algorithm to make environmentally friendly design considerations towards its microclimate [127].

The designated geometry will undergo the simulation and optimization of surface and site radiation and outdoor microclimate analysis using input weather data from the extreme hot week of summer in Shimonoseki, Yamaguchi, Japan [119], which is the closest available data around the city of Kitakyushu, where the project is planned to be constructed. The research employed hypothetical investigation on the energy consumption efficiency using the computational definition arrangement processes. Subsequently, the result was compared to the benchmark model with no computational treatment.

To achieve the objectives, a parametric design workflow was demonstrated to iterate the geometries in form-finding processes. Then, its response to the microclimate, where the radiation and the Universal Urban Thermal Climate Index (UTCI) that becomes a target analysis, was observed. Moreover, the trade-offs between design parameters and its indication toward the performance simulation was identified and compared to what the benchmark model is performing.

6.2. Methodology

6.2.1. Overview

In order to get the radiation and UTCI results and to see the impact of geometry on the urban microclimate of the intended design, the design parameters such as base radius, twisting factor, roof slope, scale factor, and orientation are based. Figure 6.1. shows the parametric workflow [158–160] conducted in this research. The initial phase is the modelling of the site as the context. The next phase is the consideration of the house's parameters, sliders and it's followed by the arrangement of its parametric definitions to

construct the design virtual model. Furthermore, the environmental analysis platform using ladybug and the honeybee is arranged. This definition is used to generate radiation and UTCI results based on input weather data. After the modelling of the site, context, building and the definition of environmental analysis are ready, the results and the iteration are being iterated and optimized in a generative algorithm-based optimization plug in called Octopus [95,161]. The benchmark model will be analyzed separately to produce a single result as a comparison. The data obtained from the iteration and the comparison will be multiplied by per-hour electricity fare to have an image of how much money is spent to pay kWh/m^2 of the radiation result. The desired design solution will undergo a single analysis and being compared to the benchmark result to see the interval that indicates the efficiency.

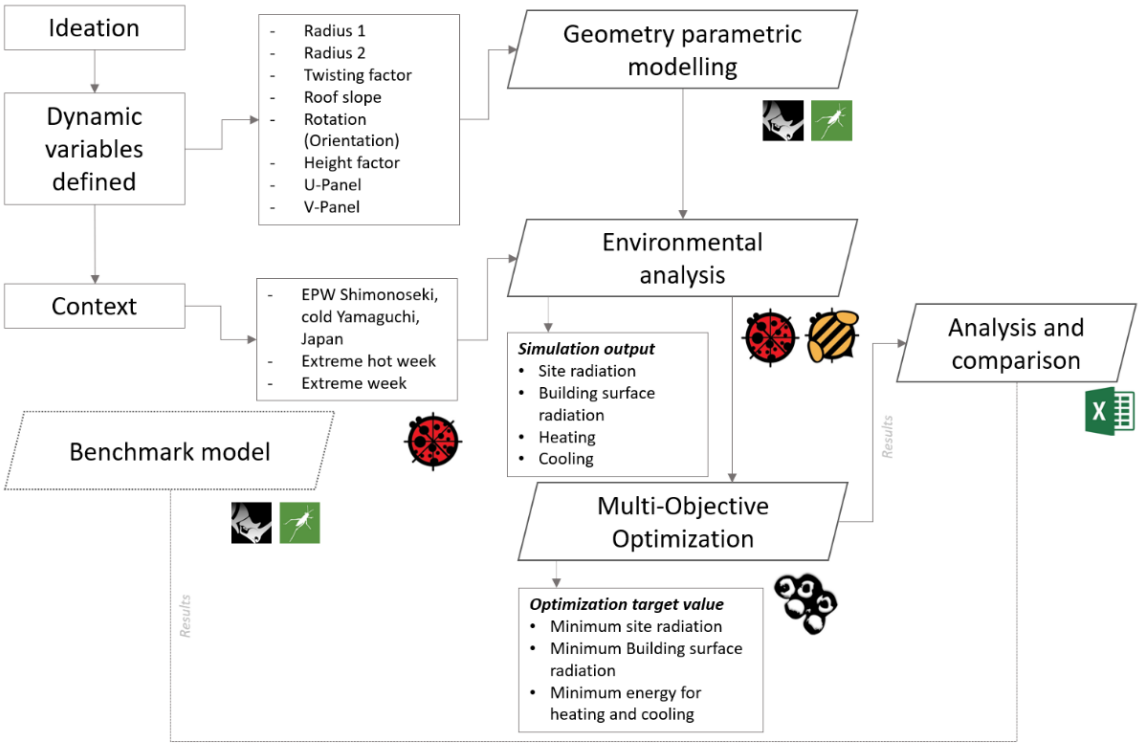

Figure 6.1. Research workflow

6.2.2. Site and analysis period

The intended project is situated in Orio district, 5 Chome 2 Orio, Yahata-Nishi Ku, Kitakyushu city, Japan. The site is in the coordinate 33°51'48. 9"N 130°42'29. 4"E. The topography of the site is formed by multistep terrain, which has a different level of about 13 m. The site is surrounded by detached houses with a distance of approximately 8 m to 10 m between each, apartments, and a small area of greenery. In general, the site has covered an area of 350 m^2 with dimensions of 33.7 m in length and 9.72 m in width. The surface area is covered by sand, gravel, and grass, and the surrounding area is covered mostly by paving and asphalt. The site and the surface have different radiation analyses.

For the analysis period, the simulation uses an EPW file of Shimonoseki as the nearest historical recorded weather data available surrounding Kitakyushu city. The period of the year that is incorporated for simulating the radiation and UTCI analysis is the extreme hot week in the summer from 5 to 11 August JST, generated by the Ladybug component "Import stat". The selected period has been chosen on purpose to give the hottest temperature to the building surface throughout the year. Thus, it could give an idea of how the conditions during the hottest period are related to the surface and site radiation. The simulation prefers the hottest period in August for the radiation and UTCI simulations and the single day of August 8 for a single simulation for evaluation and comparison.

6.2.3. Geometry and benchmark modelling

The geometry of the house is designed to adopt the shape of a twisted cylinder. The *Reuleaux* triangle [162] is designed to be the base profile if the cylinder. The geometry was built into the Grasshopper environment with several dynamic and fixed parameters as a design variable for the iteration processes. The dynamic parameters are meant to be constantly moving during the search for the best design solution. It is applied by deploying a number slider that is divided into several movement divisions. The dynamic parameters hold an important role in determining the alternative geometry in collaboration with the generative algorithm iterator and the result of the environmental

analysis. The dynamic parameters designed in this research are building orientation, circle radius that forms the *Reuleaux* triangle, scaling factor to form the gradually greater profile in the upper part of the building, twisting factor to perform the twisted cylinder, and roof slope. For the construction materials, the geometry's material has not been specifically defined to see the general tendency and only rely on the honeybee component named "Honeybee_masses2zones". However, to have an insight into the maximum implications of the geometry on the UTCI, concrete was set to be the site's material.

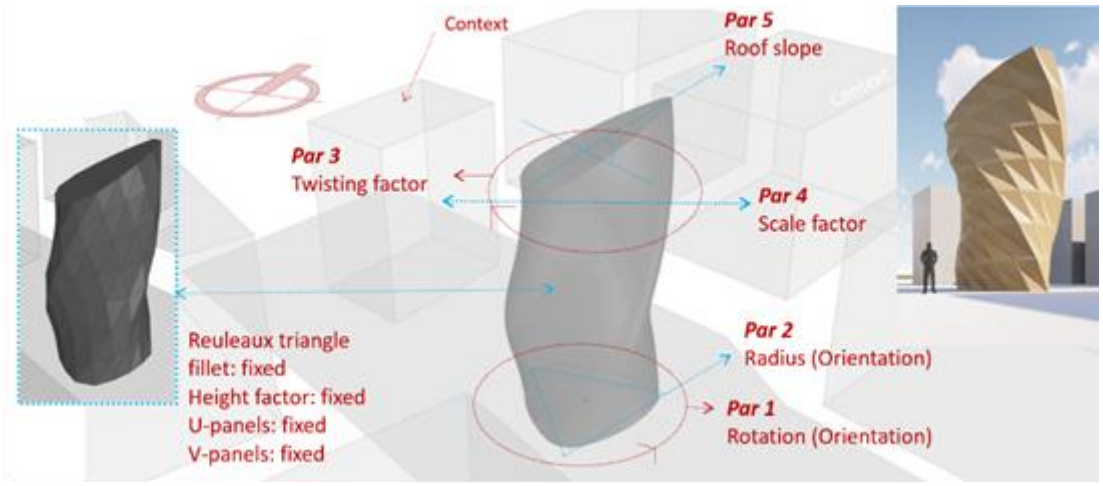

Figure 6.2. Design parameters

Table 6.2.1. Design variables

Design variables (Parameters)	Unit	Range	Unit per step	Steps
Orientation (rotation)	°	5 - 180	5	36
Base radius	m	2 - 3	0.1	10
Twisting factor	-	-125 - 125	5	50
Scale factor	-	-25 - 25	5	10
Roof slope	°	0 - 30	5	12

Figure 6.2 illustrates the position and movement of the parameters and Table 6.2.1 describes steps of each design attributes. The first designated dynamic parameter is the orientation translated in the rotation of the base profile toward the center points of its

area. The rotation angle is set to have 36 parameter's movements with 5° for each movement ranged from the minimum 5° to 150°. The second variable is the radius of the base profile of the geometry formed by the *Reuleaux* triangle which is the subtraction of three identical circles with dynamic diameter ranged from minimum 2 m to 3 m with 10 movements, 0.1 m for each step. The third variable is the twisting factor which has 50 variable movements with 5units for each step, the factor ranged from the minimum value of -125 units to 125 units. The fourth variable is the scale factor with 10 movements with 5 units for each step. The variable ranged from -25 units to 25 units. The last design variable is the roof slope. This variable has 12 variable's movements with the 5° unit for each step. The parameters ranged from a minimum angle of 0° to 30°. Besides the dynamic parameters, the fixed parameters are set. The fixed parameters are the triangle's fillet, height factor, U and V axis for planar panelling. From, the number of several design movements contributed by each design parameter, the system could possibly iterate 2.160.000 design solutions. However, not all the design variables will undergo the simulation due to the limitation of the engine hardware and optimization process.

6.2.4. UTCI radiation

The radiation simulation and analysis are conducted entirely on the parametric platform of the Grasshopper. The model of the geometry driven by the design parameters, the site, and context as an input parameter will further be simulated using the plugins Ladybug and Honeybee. The non-uniform rational basis spline (NURBS) geometry that is generated in Grasshopper is first penalized using a plugin called the Lunchbox. The closed brep geometry merged with the brep of the site, and the context became a test point to spread the results points. In terms of climatology data, the component of the ladybug radiation analysis is used. It is supplied by the data of the selected sky matrix, obtained from the component "Ladybug export stat". For the site radiation, the process is similar to that for the surface radiation. Both use the same analysis period for the extremely hot week of the year.

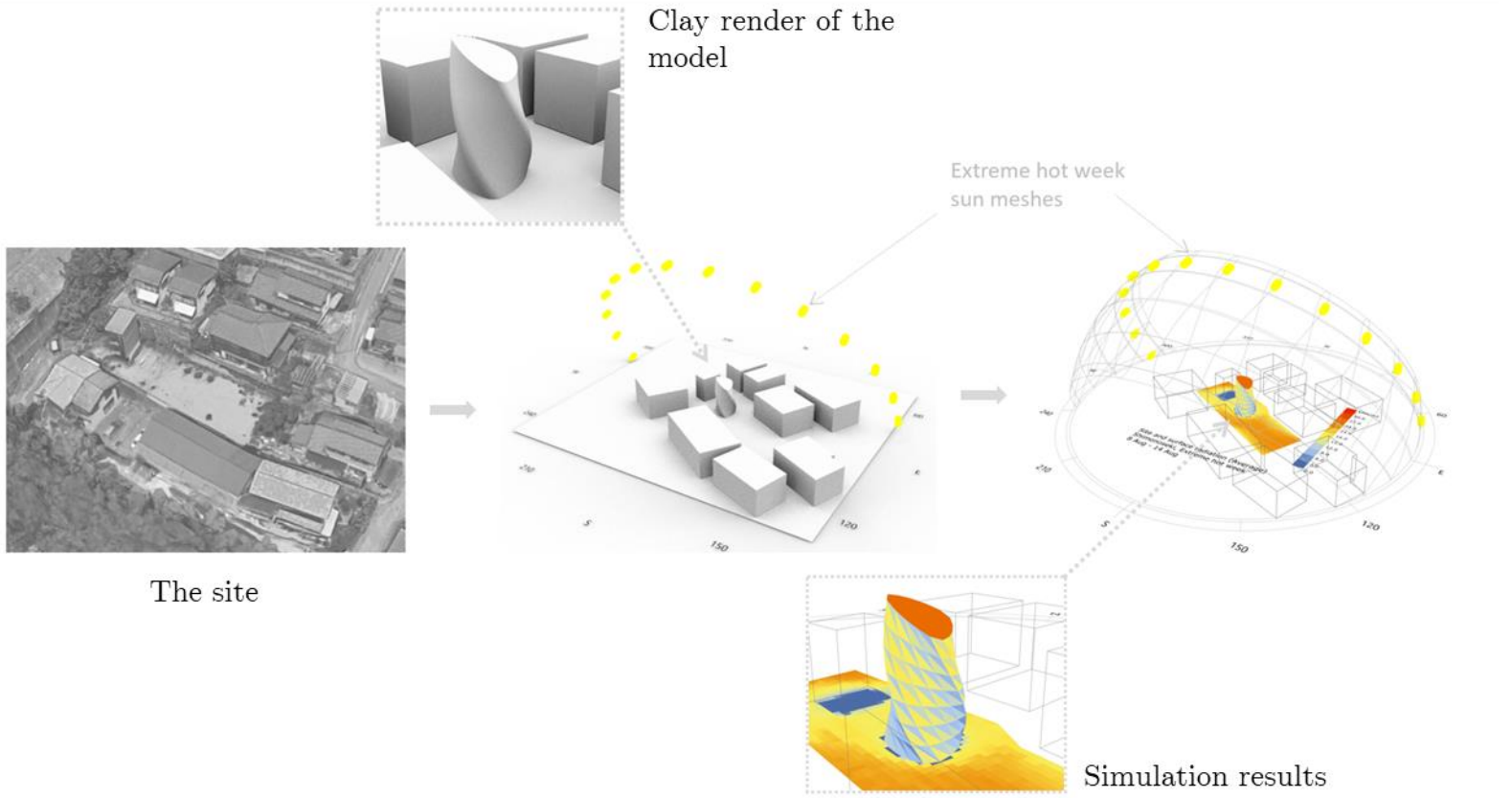

Figure 6.3. The site and context, modelling, and analysis

Besides the arrangement of radiation analysis, the UTCI parametric definition and analysis uses the component of the outdoor solar temperature adjustor that calculates data input of sky matrix, radiation diffuse, base temperature, horizontal infrared radiation, and analysis period. After the data calculated in the "Outdoor solar temperature adjustor", UTCI is computed in the component of the "Outdoor Comfort Calculator" with the wind speed, mean radiant temperature, and relative humidity as additional input data. Figure 6.3 illustrates the building model and simulation workflow in which situated in the middle of the site and being iterated and simulated simultaneously to obtain the site and surface radiation results and the value of UTCI during the hottest week of the year.

6.2.5. Optimization and benchmark model comparison

The optimization phases are conducted utilizing the plugin called Octopus. This plugin works with the parametric platform Grasshopper. It allows the solution to find a process with multiple objectives at one-time optimization running. The optimization process is based on SPEA-2 [163] and Hype algorithm [117] and by the Galapagos single objective optimization engine. The feature uses the default setting, which is elitism 0.00, Mutation probability 0.1, Mutation rate 0.1, cross-rate 0.8, population size 100, and maximal generation 100. After the alternative solutions being spread on the octopus population field, the desired solution will be selected with a reinstate solution. Furthermore, the solution will be simulated according to the fare for electricity and be compared to the performance of the benchmark model. The benchmark model is the virtual typical two-story house box with the dimension of 5 m long, 4 m wide, and 8 m height. The model facing north, south axis and it is fixed and has no dynamic parameters.

6.3. Results

The results are organized according to the sequences that were previously explained. First, the general findings of the optimization process from the Octopus will be described. Second, the findings and analysis of the benchmark model and the two preferred solutions

will be explained. Third, performance-related energy consumption is described, and last, the results of each model's performance will be generally compared.

6.3.1. Genetic algorithm optimization process

The optimization processes were conducted in Octopus, incorporating the dynamic design variable as a genome and the results of the site and surface radiation, UTCI, volume's gap, and area's gap, as the Octopus's phenotype. The simulation was run with a maximum of 100 populations, with no maximum generation. The simulation tends to minimize all the phenotypes entered into the engine, which will be spread in a 3D population field. In Figure *6.4* the elite of the spread individual indicates the distribution of the explored design solutions, in which each design solution contains the information of the calculated analysis results (phenotype). The population field has five axes, which are the average surface radiation (X-axis), average site radiation (Y-axis), average UTCI (Z-axis), volume's gap (color axis), and the surface area gap (scale axis). The scale of each axis is provided according to the minimum and maximum results of each phenotype. The three X, Y, and Z-axis are measured according to the value that goes along the axis. For the color axis, the gradual color change from red to green represents the value of the volume gap. The red color represents a more significant gap, and the green represents the opposite, while the brown represents the gap in between. For the scale axis, the small area gap is presented in a bigger mesh size and the smaller surface area gap is presented in a small mesh size.

The targeted solution is in the minimum X, T, Z-axis, with small mesh scale and in green color. The two desired solution is highlighted in the yellow circle (Figure *6.4*). The solutions selected are categorized in the minimum UTCI model and minimum surface radiation model. The minimum UTCI model is located in the minimum axis of Z and X, and the minimum surface radiation model is located in the minimum axis of Y. Accordingly, based on the distribution in the population field, the targeted model for the minimum site radiation is the same as the minimum UTCI model. Hence, there are only two desired solutions will be reinstated and compared with the benchmark model's

performance. Each value will further be investigated through reinstating solution process from a single simulation.

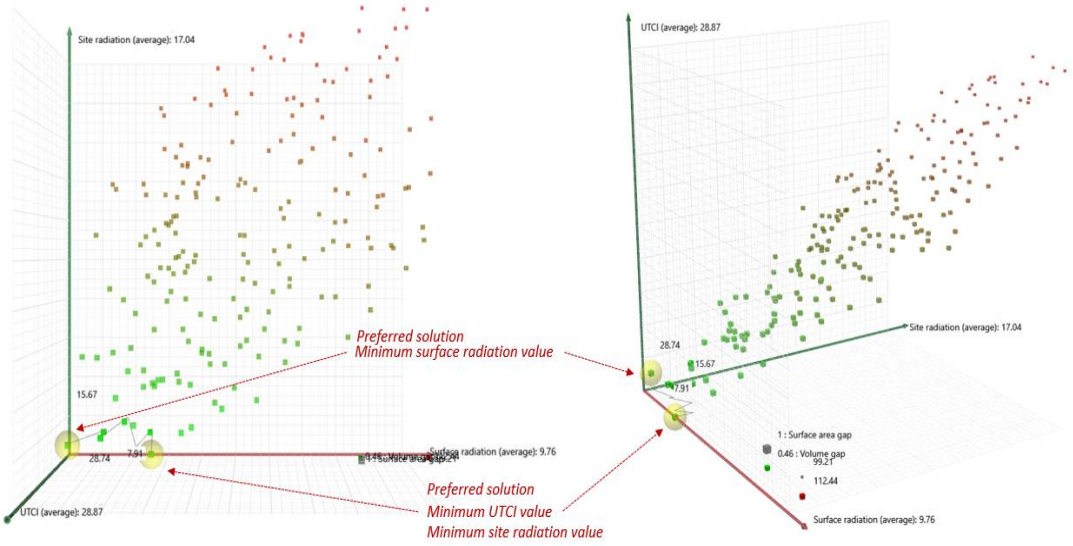

Figure 6.4. 3D population field of the optimization result, top and perspective view

6.3.2. Benchmark model

The single simulation for the benchmark model has been carried out using the extreme hot week analysis period from the EPW file data of Shimonoseki. It is simulated without incorporating genetic algorithm processes and incorporating fixed parameters. The results show that the 8 m experiment box performs several outcomes for the site's UTCI, site radiation, and surface radiation. The outcomes of average UTCI stated 28.74 °C on average. In the other analysis, the benchmark model resulted in a value for the average site radiation of 15.706 kWh/m^2 and a surface radiation of 9.008 kWh/m^2.

Figure 6.5 shows the visualization of the results for each target result for the benchmark model. From the results legend on the site, both UTCI and site radiation analysis recorded almost equal data dominated by a high range of temperature and radiation. In UTCI result, the site is almost covered with the average temperature of about 29.2 °C to 29.6 °C. Small parts of the site recorded the colder temperature, affecting by the context,

of 28.2 °C to 28.9 °C. For site radiation, the site is dominated by spots valuing 18 kWh/m^2 to 24 kWh/m^2. In the surface temperature analysis, the building stated a quite prevalent distribution of 12 kWh/m^2 to 18 kWh/m^2.

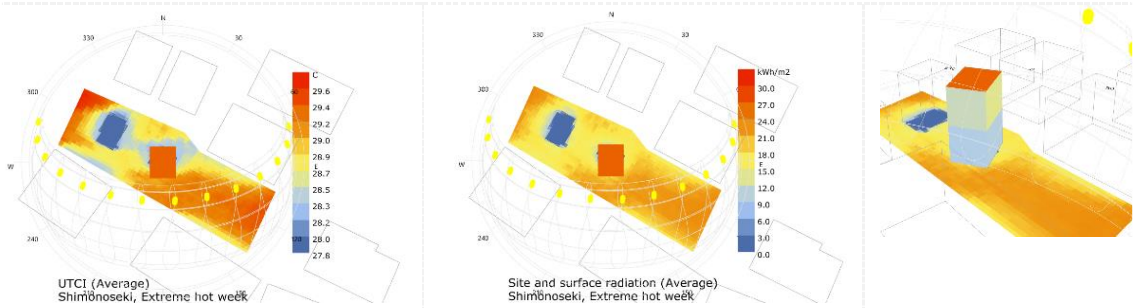

UTCI (average): ***28.74° C***	*Site radiation (average):* ***15.706 kWh/m^2***	*Building surface radiation (average)* ***9.008 kWh/m^2***

Figure 6.5. Analysis results for benchmark model

6.3.3. Minimum UTCI model

Different from the simulation of the benchmark model, the minimum UTCI and Radiation model are the manifestations of MOO processes. The geometry produced from the form-finding process is consist of the design variables as follows: 115° rotation, 3 meters of the base's radius, 85° twisting factor, 15 units scaling factor and 0° of the roof slopes. For the performance, the minimum UTCI model results show that the outcomes of average UTCI of 28.74 ℃ on average. In the other analysis, the benchmark model resulted in a value of the average site radiation of 15.67 kWh/m^2 and the surface radiation of 8.36 kWh/m^2.

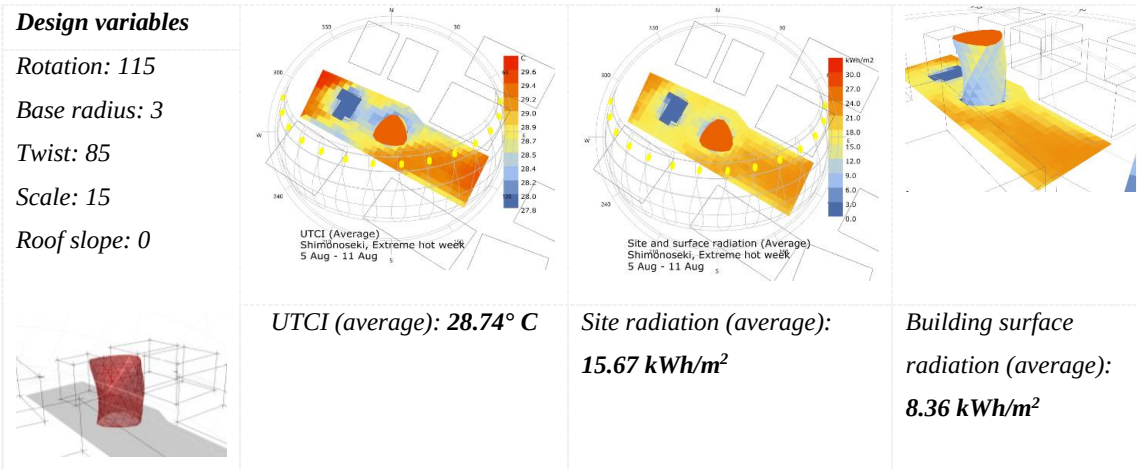

Figure 6.6. Analysis results from minimum UTCI model

Figure 6.6 shows the results visualization of each analysis result from the minimum UTCI model. From the result's legend in the site, both UTCI and site radiation analysis recorded almost equal data dominated by a high range of temperature and radiation. In UTCI result, the site is almost covered with the average temperature of about 29.2 ℃ to 29.6 ℃. Small parts of the site recorded the colder temperature, affecting by the geometry, of 28.4 ℃ to 28.5 ℃. For the site radiation, the site is dominated by the spots with radiation of 18 kWh/m^2 to 24 kWh/m^2. For the surface temperature analysis, the surface building distributed value of 9 kWh/m^2 to 18 kWh/m^2 and a small area under 9 kWh/m^2.

6.3.4. Minimum surface radiation model

For the minimum surface radiation model, the geometry produced from the form-finding process consists of the design variables as follows: 70° rotation, 2.9 meters of the base's radius, 5° twisting factor, 25 units scaling factor and 25° of the roof slopes. For the performance, the minimum UTCI model results show that the outcomes of average UTCI of 28.74 ℃ on average. In the other analysis, the benchmark model results in the average site radiation of 15.71 kWh/m^2 and the surface radiation of 7.91 kWh/m^2.

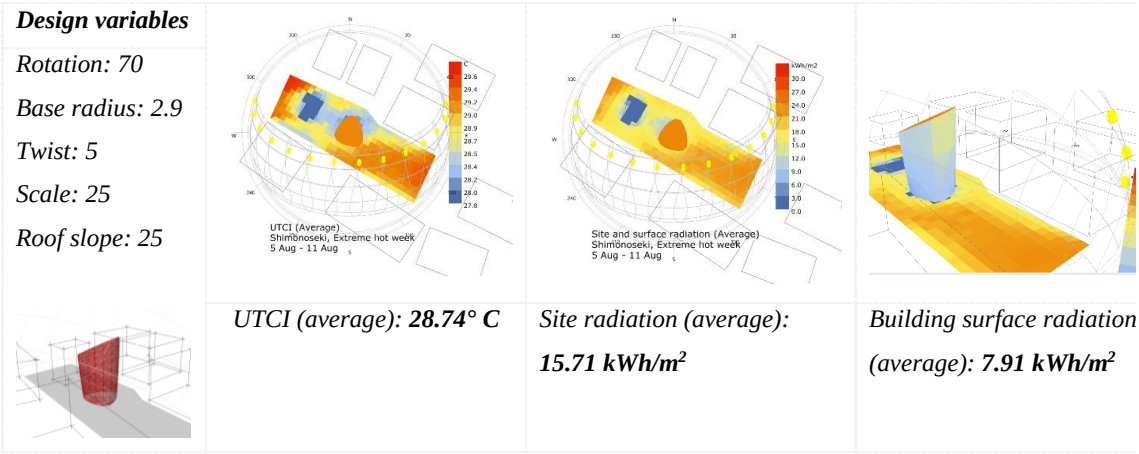

Figure 6.7. Analysis results for minimum radiation model

Figure 6.7 shows the results visualization of each analysis result from the minimum UTCI model. From the result's legend in the site, both UTCI and site radiation analysis recorded almost equal data dominated by a high range of temperature and radiation. In UTCI result, the site is majorly covered with the average temperature ranged 29.2 ℃ to 29.6 ℃. Small areas of the site resulted in colder temperature, affecting by the geometry, of 28.2 ℃ to 28.5 ℃. For the site radiation, the site is dominated by the spots with the value of 18 kWh/m^2 to 24 kWh/m^2 and a small area under 18 kWh/m^2. For the surface temperature analysis, the surface building distributed majorly value of 9 kWh/m^2 to 18 kWh/m^2.

6.3.5. Energy consumption

The simple calculation has been conducted parametrically on Grasshopper platform using the components *Honeybee export to OpenStudio* regarding energy simulation. The simulation resulted in the outdoor and indoor surface temperature that furthermore will be multiplied by the fare per-kWh of the electricity. The simulation calculates the per-month bill for the input geometry that's being converted into Honeybee zones. The period is taken for this calculation in a whole year from the EPW file of Shimonoseki.

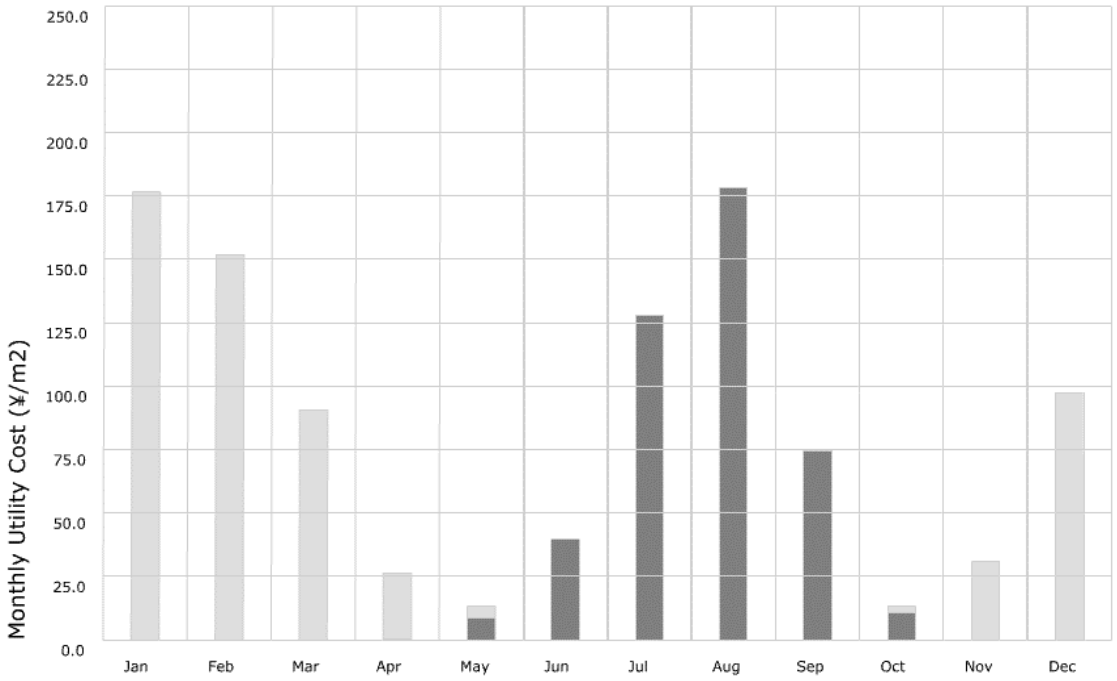

Figure 6.8. Monthly utility costs for minimum benchmark model

The first simulation was conducted to the benchmark model. The results produced are the six months of normalized cooling and heating electric energy for the building. The graphic both for cooling and heating are fluctuating along the year. Figure 6.8 illustrates the monthly utility cost, which is the bill of the cooling and heating spent on the electricity of the benchmark model. Light grey is floor normalize heating electric energy for building (monthly) while dark grey is floor normalize cooling electric energy for building (monthly). In May, the bill for cooling is 8.47 Japanese yen, and it is going up to 39.54 Japanese yen in the next month. The peak is in August with the expense for electricity reach 178.16 Japanese yen. The bill drops more than half in September and set the lowest amount after the peak of 10.89 Japanese yen in October. For the heating needs, January is the peak that set for 176.50 Japanese yen, and it slightly goes down in February to about 151.94 Japanese yen. The following two months the bill is set for 90.60 Japanese yen and 26.23 Japanese yen. In May and October, the bill is a sphere between heating and cooling needs.

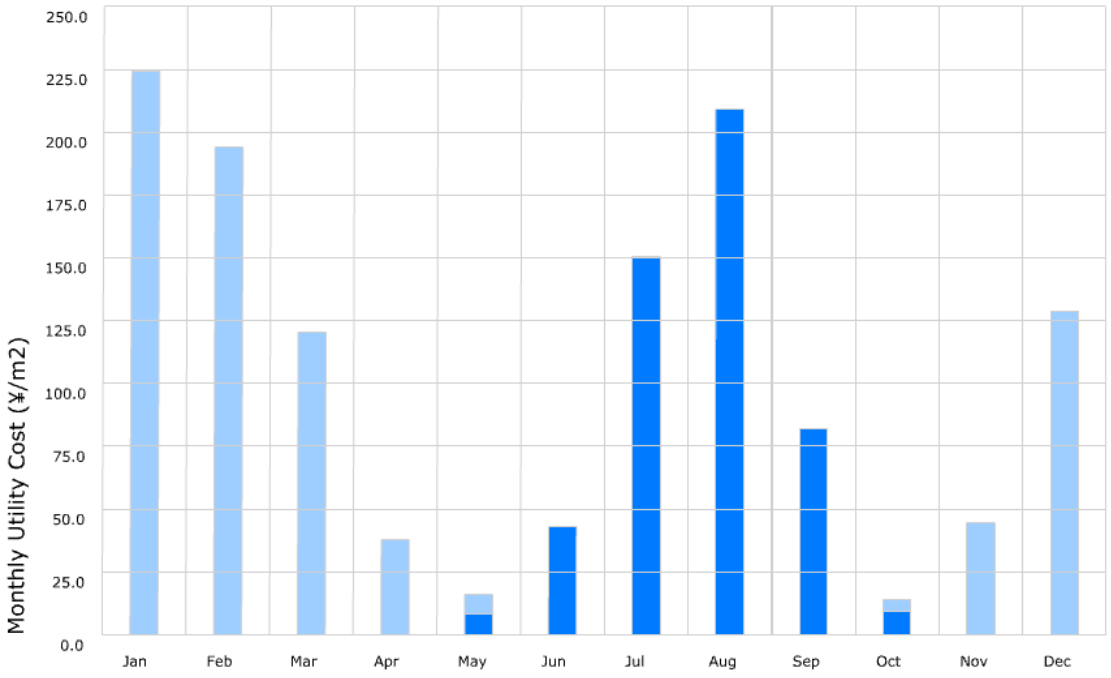

Figure 6.9. Monthly utility costs for minimum surface radiation model

Figure 6.9 illustrates the monthly utility cost for the minimum surface radiation model. Light blue is floor normalize heating electric energy for building (monthly) while darker blue is floor normalize cooling electric energy for building (monthly). The cooling electricity bill appears in April with the cost of 0.21 Japanese yen. In May, the cost increases to about 8.4 Japanese yen, and there is a significant increase for 110 Japanese yen to reach 150.49 Japanese yen. In August, the cost is reaching a peak with a value of 209.16 Japanese yen. After reaching the peak, for the following month (September), the cost is drastically decreasing to the value of 81.9 Japanese yen. Moreover, the last month to cover the electricity bill for cooling is in October with 9.4 Japanese yen. For the heating electricity bill. January, February, and December stated the three highest costs for cooling within one year. The cost of three respective months is 224.33, 193.8 and 128.82 Japanese yen. The lowest electricity bill for cooling is recorded in two months of July (0.095 Japanese yen) and October (4.50 Japanese yen).

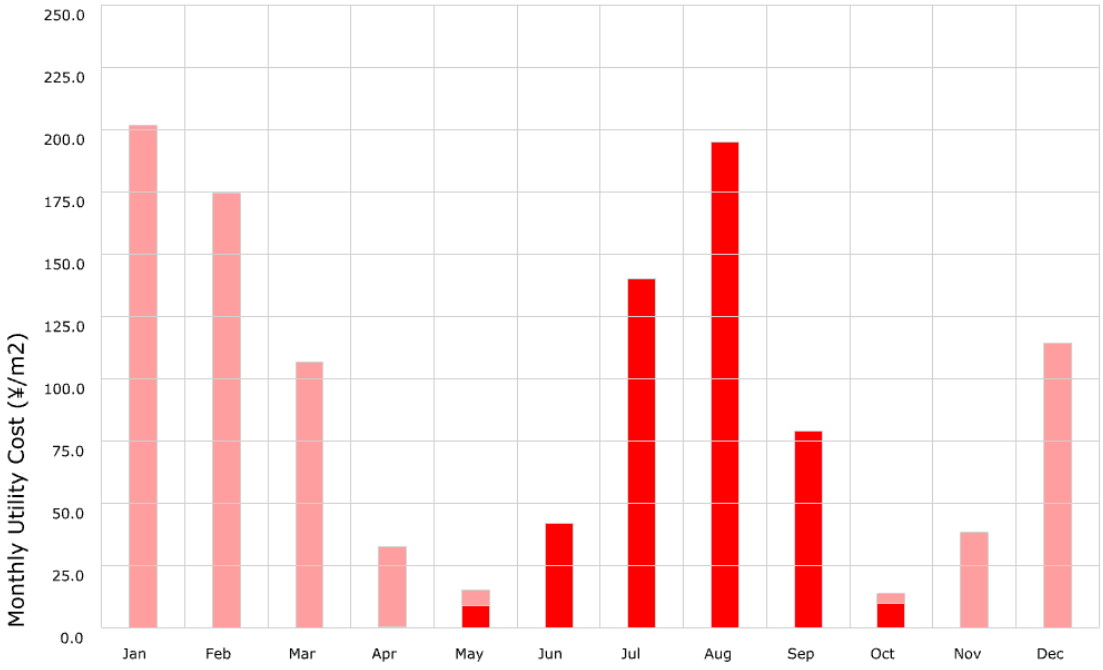

Figure 6.10. Monthly utility costs for minimum UTCI model

For the next electricity expense calculation, model the open studio calculation is based on the selected model that considered to have minimum average UTCI among the distributed solution. The cost for the electricity of cooling and heating needs are fluctuating along the year. Figure 6.10 shows the cost of the utility bill of the minimum UTCI model. Lighter red is floor normalize heating electric energy for building (monthly) while darker red is floor normalize cooling electric energy for building (monthly). The cooling cost in started to appear in April sharing the portion with heating load cost 0.23 Japanese yen. In the following months, the cost is increased by 8.82 Japanese yen in May, 41.94 Japanese yen in June, 139.98 Japanese yen in July and it is reaching the peak in August with the cost of 194.96 Japanese yen. The cost is gradually decreasing for September and October with 79 Japanese yen and 9.89 Japanese yen respectively. For the heating cost, January, February, and December stated the highest cost within one year (201.73, 174.23 and 114.34 Japanese yen). From March to June, the cost is gradually decreasing from 106.53 Japanese yen to 0.07 Japanese yen.

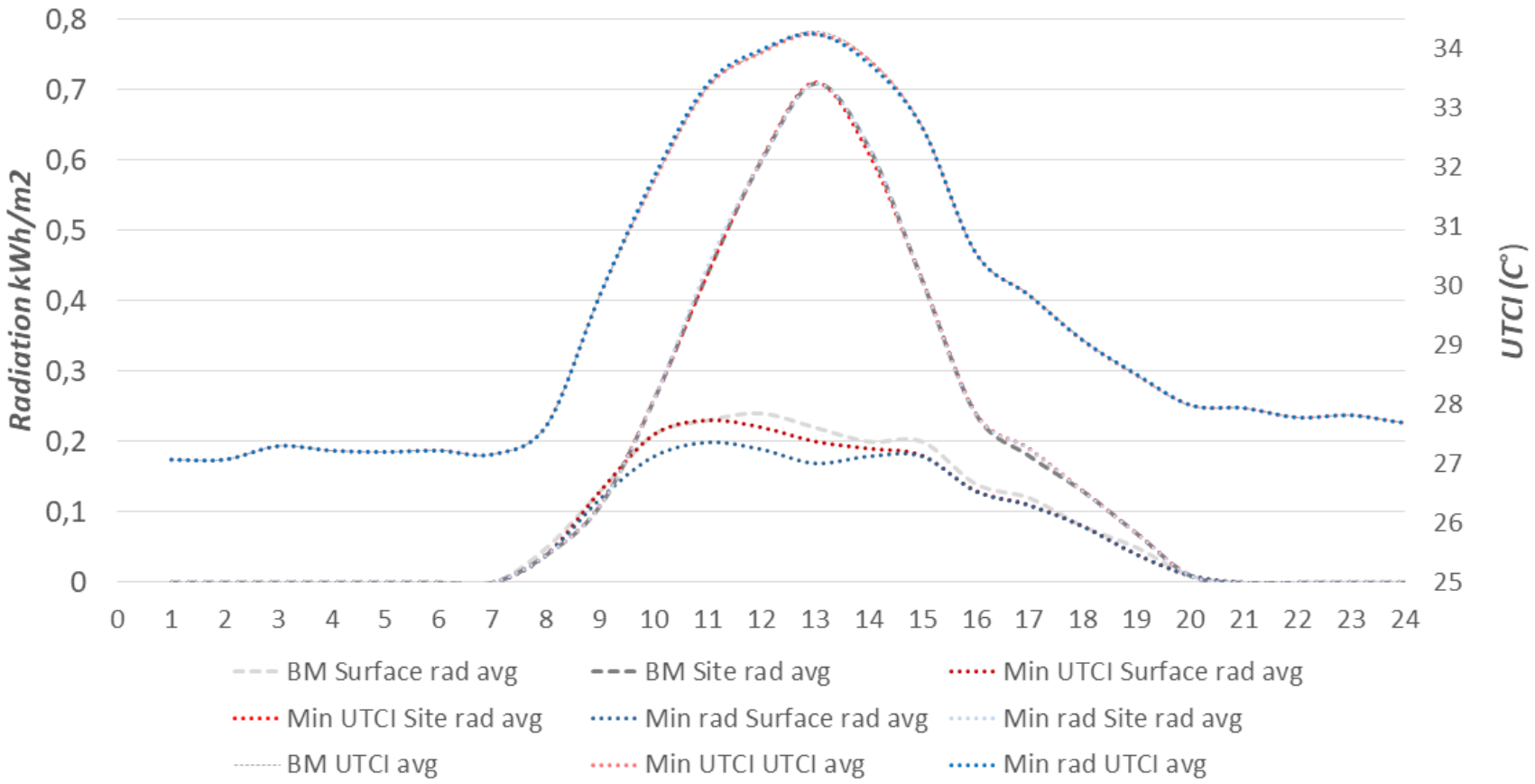

Figure 6.11. Monthly utility costs for minimum UTCI model, Aug 8

From a series of parametric and optimization processes, the results show several tendencies and exciting findings. The two selected solutions produced by the genetic algorithm optimization tend to perform better in relation to the designated objectives with an insignificant difference. This can be interpreted that because of lack of enough iteration processes and observation. However, from the comparison of each model that is simulated with a single simulation on the hottest day on August 8 at 14.00 JST, the findings confirm the hypothesis of the improvisation through parametric and generative optimization in several aspects, such as minimum surface, site radiation, and the UTCI. Besides, there is an interesting finding that indicates that better performance in radiation and UTCI analysis is not equally a better expense related to the electricity cost for heating and cooling. Each phenomenon will be described in the following explanation.

Figure 6.11 illustrates the performance of each model's designated target performance simulated, which are the UTCI, site and surface radiation of the benchmark model, the minimum UTCI model and the minimum surface radiation model on the hottest day of August 8, at 14:00 JST. From the calculation of UTCI, the targeted performance does not set the desired gap in temperature. In all the models, the average value of 28.74 ℃ (in the extreme hot week) is stated.

In a single simulation, the performance almost shares a fluctuating calculation. The better UTCI of the two models only performs better after 13:00 with insignificant different from 33.84 to 33.77 °C. In the site radiation, similar to the UTCI, better radiation appears after 13:00 and continues between 16:00 to 18:00 again with an insignificant difference from 0.62 kWh/m^2 to 0.61 kWh/m^2. In terms of building surface radiation, better calculations stated better performance from 11:00 to 20:00 with a slightly significant amount compared to the other two objectives, with an improvement of 0.2 kWh/m^2 to 0.18 kWh/m^2.

In terms of energy consumption, the improvement in radiation and UTCI is not followed by a decrease in utility bills within one year. The two selected models from the optimization process have a more expensive cost compared to the benchmark model. The estimation gap between the benchmark model electricity cost in August (the peak) is 31

Japanese yen with the minimum radiation model and about 16 Japanese yen with the minimum UTCI model.

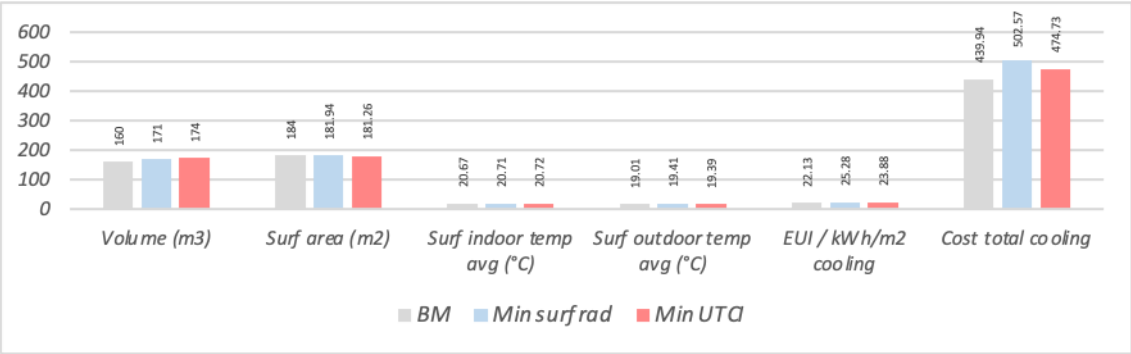

Figure 6.12. Trend in energy consumption of cooling for each model

It is indicated that the minimum surface radiation and the area did not guarantee a lower electricity bill for the cooling needs. In general, the tendencies and trade-offs of the dynamic design parameters with the targeted design performance are not visible. First, because of the lack of generation number in the iteration process, and second, because it is a multi-objective optimization deploying multiple parameters (genotype) and objectives (phenotype).

Figure 6.12 illustrates the calculation in the OpenStudio simulation. From the data presented in the chart, interestingly, the cost depends on the EUI, yet it has no relation to the volume and the surface area. The finding contradicts the assumption that the area of the building surface and the volume of the building would affect energy consumption and its cost.

6.4. Chapter conclusion

This chapter describes the parametric and multi-objective approaches to investigating the building form toward outdoor thermal comfort in the Orio district, Kitakyushu City, Japan. Comprehensive parametric calculations of the dynamic parameters-driven geometry design, environmental analysis for UTCI, and radiation have been conducted

parametrically. The arrangement of parametric operations produces two selected design solutions that match the preferences.

The results show minor improvement in the three designated design objectives, which confirms the hypothesis. It is stated 0.02 kWh/m^2 improvement in surface radiation, 0.01 kWh/m^2 improvement in site radiation, and 0.07 °C improvement in UTCI. However, the opposite results appear in the annual utility bill for cooling and heating needs within one year. The two found solutions perform cost 31 Japanese yen with the minimum radiation model and about 16 Japanese yen with the minimum UTCI model. It is shown that the minimum surface radiation and area did not ensure a lower electricity cost for cooling requirements. Raise a question of re-considering other factors beyond the geometry. In general, the research guides the design considerations related to the variables needed to build the geometry of the house according to the targeted goals using the site's weather data.

The iteration in genetic algorithm optimization is still considered lacking due to the hardware and optimization setting's limitations. Thus, it needs more investigation to validate the information provided above. Despite the limitations mentioned above, the simulation has successfully come up with a design solution that performs better than the benchmark model. It offers the possibility of sharpening the improvement by addressing the shortcomings. Further work is encouraged to set more generations in the optimization process to get better validation and observation.

Chapter 7. Design exploration and optimization of a *Hyperboloid* wooden structure concerning cost, structural, and daylight objective

7.1. Introduction

7.1.1. Wood in environment and construction

Recent years have witnessed the emergence of climate change as a significant issue requiring response from individuals from a variety of fields. Global warming can only be caused by massive CO_2 emissions, and technological advancements have led to an increase in CO_2 output. The majority of human activities that involve automobiles or the combustion of fossil fuels can directly contribute CO_2 to the atmosphere. This process is known as the greenhouse effect, or in a broader sense, global warming. Approximately 3,3 billion tons of carbon dioxide are discharged into the environment every year. This process causes the temperature at the earth's surface to rise gradually and damages the ozone layer.

Wood has always been a valuable resource as an easily sculptable yet long-lasting material [28]. In addition, wood is a common material for architecture. Wood's role in the history of the built environment began since humans knew what to build. Wood is recorded as one of the oldest materials in architecture. Besides this material usually being used for its aesthetical and strength factors, it is also be used to affect human psychology [40], give a relaxing sensation and can help to maintain an optimum living environment [41].

Japan has a long tradition of wood construction. In Japan, wood is more than just a building resource; it is also a cultural element. In this country, the usage of wood signifies respect for life and nature. The fact that wood grows organically sets it apart from nearly all other building materials. Wood possesses both physical and aesthetic properties. It is both an antique and modern material. Wood is a fragile and very sensitive material that necessitates a high degree of care in its handling and imparts a warm and significant ambiance when used as construction components. The usage of wood also offers numerous benefits. It is simple to distribute and effective for assembly [42]. In addition, wood is a material that is available in both in global and local markets [43]. Compared to other building materials, wood has a special character in terms of design uniqueness, as it is naturally grown, fully recyclable and an extremely energy efficient

building material [44,45]. According to the characteristics mentioned above, the design of wood will continue to challenge the creation of wooden designs in architecture in the future.

The use of wood in construction can reduce CO_2 in nature [46]. It can also be the trigger to raise the spirit of environmentally friendly vision in design and construction. According to the relationship with nature, wood is the only significant building material that is grown [43]. The wood installed on the construction component will never have the same appearance or qualities as the other wood. Recently, the benefit of utilizing wood has also been linked to its possible earthquake resistance. In tandem with the development of Japanese wooden construction, Japan has endeavored to expand the use of wood in architectural practice. Japan possesses numerous varieties of wood that are primarily employed in building. The application of various types of wood is always determined by the function of the component. Both structural and non-structural components have a function.

This chapter focused on the usage of Japanese cedar wood, also known as Cryptomeria Japonica, among the different varieties of wood available in Japan. In its natural habitat, Cryptomeria Japonica is a fast-growing tree that can reach 55 m in height and 3.7 m in diameter. The trees are native to Japan, the highlands of southern China, and certain regions with considerable annual precipitation. Due to its rapid growth, Japanese cedar can attain a height of 7.6 m in ten years. Along with the development of industries and wooden construction, Japan has pushed the use of wood as a key building material. The benefit of selecting Japanese cedar is that it grows rapidly, thus the price is reasonable. It is readily available because its habitat, lumber companies, workshops, and retailers, are common in the majority of Japan's regions. In addition, this wood is lighter for use in building structures than other types of wood, such as Japanese cypress.

In terms of wood modulation, the simulation employs 105 mm x 105 mm x 4000 mm Japanese cedar as the primary framework of the desired house's shape. In Japan, notably in Kitakyushu, the module is frequently employed as the primary framework for residential construction. In addition to enabling design research utilizing the market's accessible wood materials, the module of the cedar is suited to support the concept of

Hyperboloid construction with the human ergonomic element, which was the motivation for adopting this particular wood. The straight-line axis of the *Hyperboloid* could be arranged according to the timber module. It is expected that by presenting an irregular design method and analysis to the exploitation of common material modulation, the findings will advance the state of the art of timber design in Japan and contribute to environmental sustainability.

7.1.2. Hyperboloid structure

The revolution in *Hyperboloid* structure has been tremendously affected by the advancement in computational tools [52]. It is a doubly ruled surface and mainly known for its structural stability and is more economical in construction because of the less material required to construct the structure compared to other conventional structures, having a similar capacity to withstand load, and having greater strength. Following the logic in Figure 7.1, The *Hyperboloid* surface can be created by rotating a hyperbola along its semi-minor axis, or, more precisely, by twisting two surfaces in opposite directions and lofting them. The relationship between two points can also be used to define the features of a *Hyperboloid*. The point that spreads across two surfaces' edges is known as the Hyperboloid's foci. The line would remain straight if the foci were connected by a straight line and the second foci shifted along the edge of the surfaces. The *Hyperboloid* structure can be formed by groups of foci that are related to one another.

The early use of the *Hyperboloid* principal can be seen in Antoni Gaudi's building, Sagrada Familia, in Barcelona. Gaudi used this kind of curved surface to design the surface of the windows of his buildings. Vladimir Shukov expanded on this principle's application in structural form. Vladimir Shukov was a Russian engineer born in 1853. His specialty was to design and build *Hyperboloid* towers. In his career, he built more than 200 different *Hyperboloid* towers with a height of up to 70 M. His most renowned *Hyperboloid* tower is the Shokov Tower, also known as the Shabolovka Radio Tower. Built in the period 1920–1922, during the Russian Civil War that reached 350 m, which was 50 m taller than the Eiffel Tower.

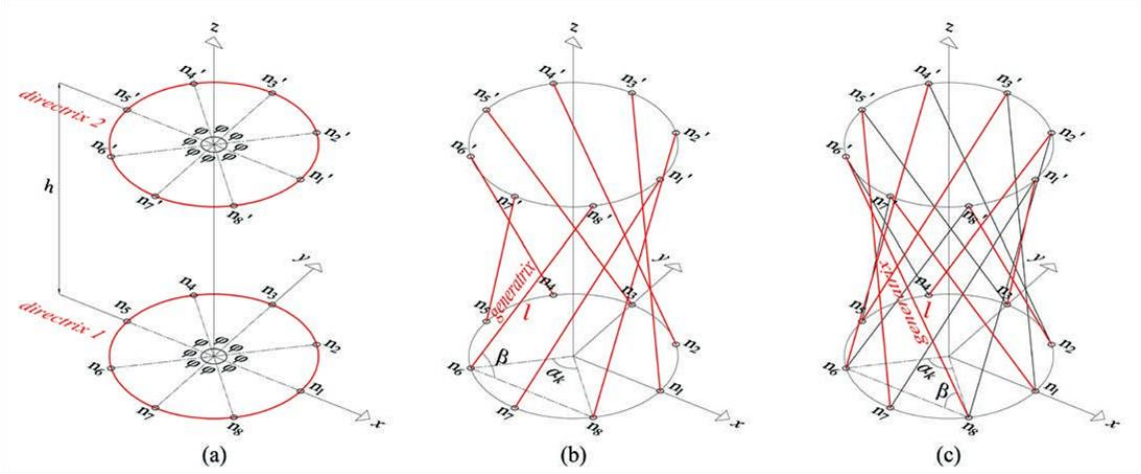

Figure 7.1. Generation process of doubly ruled Hyperboloid [164]. Reproduced with permission from Feray Maden, Geometric and Kinetic Analysis of Deployable Doubly Ruled Hyperboloids; published by MEGARON/Yıldız Technical University Faculty of Architecture E-Journal

Recently, the common application of this structure ought to utilize the minimum thickness of the concrete shell to construct a power station cooling tower. The well-known projects using this structure are the Canton Tower in Guangzhou, China, the Port Tower in Kobe, Japan, and the Aspire Tower in Dubai. For the smaller scale wooden projects, Juberg Tower Hemer, designed by Birk Heilmeyer and Frenzel Architekten, Carlos Jarpa's Vigilante Maule is a Timber Frame Tower, *Hyperboloid* Boruvka wooden tower in the Czech Republic, and Tsuzumi-Mon (Wooden Gate) Kanazawa Station, Japan, were adopt the *Hyperboloid* structure.

There are several advantages to the use of the *Hyperboloid* structure. It is associated with aesthetics, structural integrity, and efficiency that influence modern architecture [164]. Due to the straight member, it is extremely resistant to buckling. Due to the fact that Hyperboloid structures are double curved, i.e., concurrently curved in opposite directions, they are extremely resistant to buckling. This allows them to employ less material than would otherwise be required, making them incredibly cost-effective. Even though it is bent in two directions, it is still composed of straight lines due to its aesthetics. As a result, the use of *Hyperboloid* generates the paradox that the designer can obtain

the best local buckling resistance because all the members are straight. Due to the twofold curvature of the surface, the overall form would also demonstrate the highest resistance to buckling.

7.1.3. Aims and objectives

Even though some study has utilized parametric design and MOO to conduct form discovery to determine the optimal solution for design objectives, the approach that is applied to *Hyperboloid* wooden structures that combine structural and daylight performance objectives has been documented infrequently. Thus, the purpose of this chapter is to investigate the feasibility of implementing parametric design processes in the early design phase of a two-story *Hyperboloid* wooden house made of Japanese cedar in order to aid the designer in decision-making and design while taking structural and daylight optimization into account. [165]. In addition, the intention behind the exploration is to design a structure for a two-story *Hyperboloid* wooden house made of Japanese timber, 105 mm × 105 mm × 4000 mm, which has a structural and aesthetic function, through parametric design in the early steps of the design process, answering the following questions:

- Does the proposed approach lead to the optimization of the structural and daylight performance of the intended house?
- What is the parameter combination that produces the best design solutions in terms of structural and daylight objectives?
- What is the relationship between the geometry parameters and the structural objectives?
- What is the relationship between the opening parameters and the daylight objectives?
- What parameter is the most influential in each of the structural and daylight objectives?

To realize the research aims, the specific objectives are:

- To conduct theoretical studies about the implementation of parametric design and MOO.
- To build a parametric system based on design objectives.

- To build the parametric system of the optimization process, both structural and daylight analysis.
- To conduct an empirical analysis based on the data obtained.

The hypothesis of this chapter is that the offered methodologies of parametric design and MOO can result in the optimization of design objectives and the identification of the most relevant parameters influencing design objectives. The purpose of this chapter is to contribute to the field of wood design, particularly Japanese wood, and to aid the designer in the decision-making process from the earliest stages of the design process.

7.2. Methodology

7.2.1. Overview and project description

This chapter presents a design strategy for a two-story *Hyperboloid* timber house that takes into account structural and daylight design objectives in addition to the geometry and aesthetic purpose. The design scope is comprised of the creative design idea, the whole early-stage virtual parametric model, and data processing and analysis.

Figure 7.2 shows the schemes used for the entire parametric system developed in this research, which is related to structural considerations similar to the approach in [111,114,166–169] and in daylight consideration [25,87,170–172]. As shown in the Figure 7.2, Ideation, motivation, a literature study, and the determination of research and design objectives comprised the initial phase of creating a two-story wooden house. The processes continue following the conclusion of the ideation phase with the formulation of parametric definitions for geometry modelling, structural analysis, daylight analysis, data collection, and optimization. The logic of the *Hyperboloid* structure was applied during the making process of the main geometry, the structure following the vector produced during the modelling process of the wooden bars, and the joint following the cross section between two bars with different twist directions in a *Hyperboloid* constrain and the daylight follows the logic of the geometry panel Sub-chapter 7.2.4.

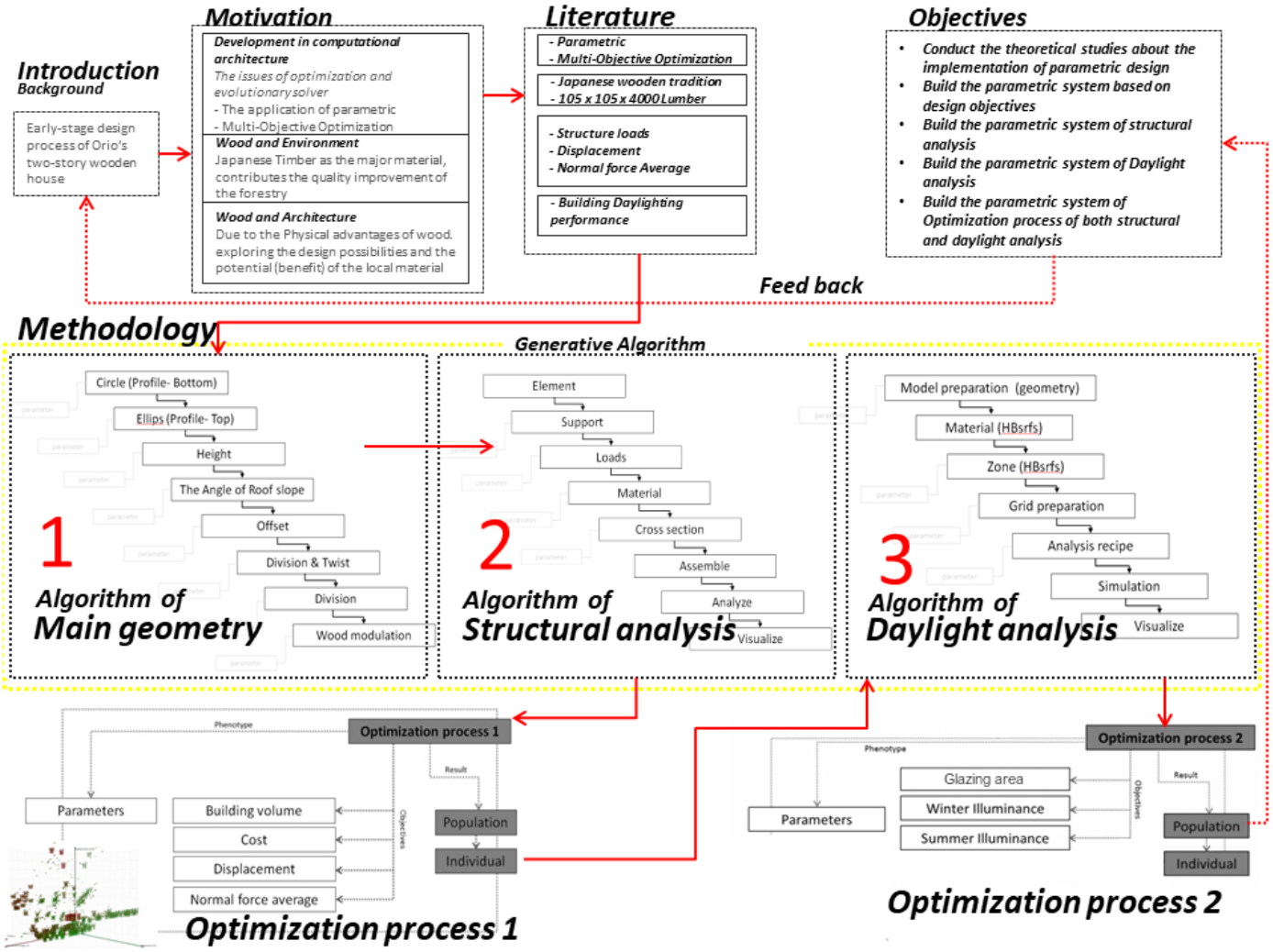

Figure 7.2. Research framework.

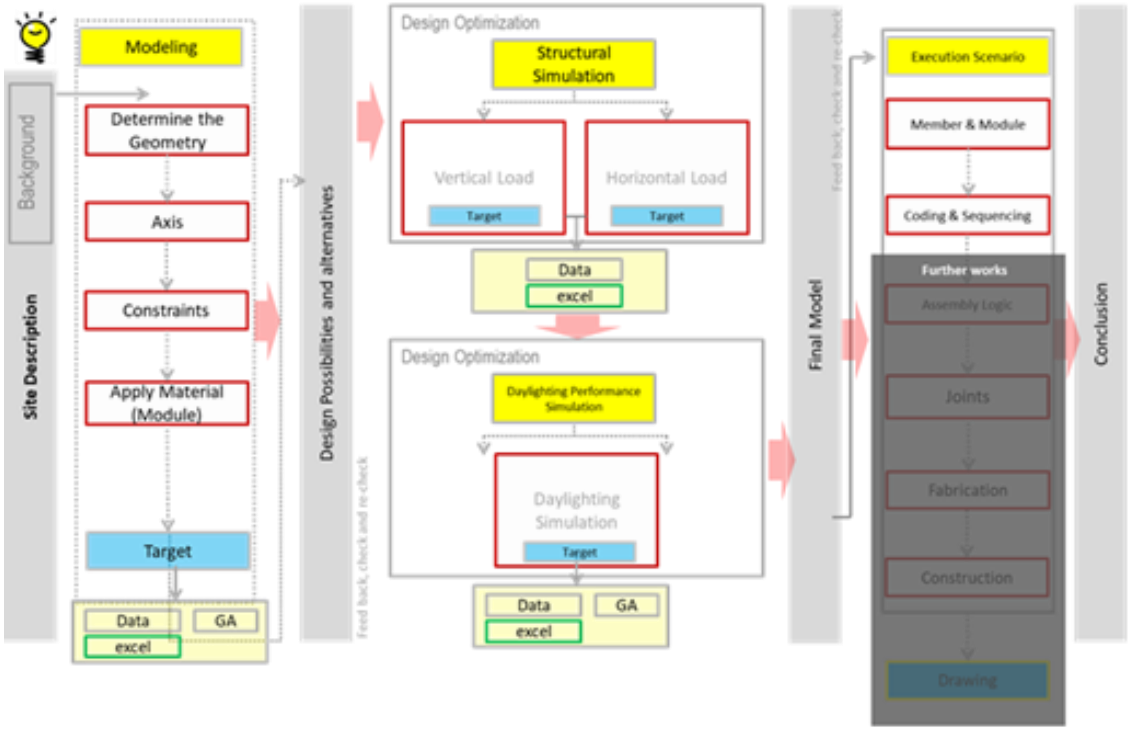

Figure 7.3. The scheme of the geometry and analysis

A set of tools was used to prepare the parametric and optimization platform. Figure 7.3 (a) illustrates the main process of the modelling and Figure 7.3 (b) depicts the tools used in this research. The main platform for building the parametric definition is a plugin called Grasshopper [121] working in the non-uniform rational basis spline (NURBS) based 3D modeler called Rhinoceros [120]. For the structural analysis, the plugin called Karamba has been utilized. Simulations are conducted by using the plug-in Karamba. Karamba plugin fully works in the environment of Grasshopper. Karamba is a special plugin that is used in parametric structure analysis. Just like the Grasshopper component, the Karamba component works by using algorithms. Karamba is the plugin software for structural analysis that makes it easy to use for non-structural experts. This makes easy to combine parametrized geometric models, finite element calculations, and optimization algorithms like Octopus or Galapagos. Karamba provides accurate analysis of spatial trusses, frames, and shells. It is easy to use for non-experts and is tailored to the needs of architects, specifically, in the early design phase [36].

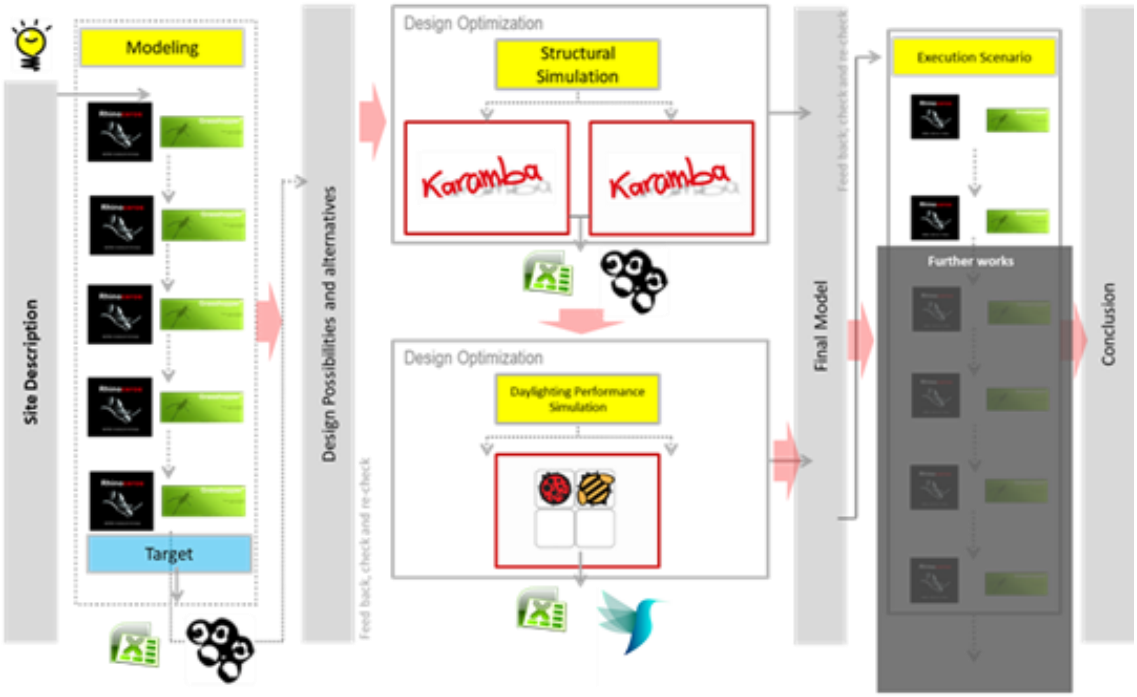

Figure 7.4. Software used in Chapter 7

An environmental analysis plugin called Ladybug and Honeybee [122] has been used to conduct the daylight analysis. Ladybug is a plugin software used to analyze microclimates based on the parametric platform of Grasshopper. It links the early phase design process with environmental study, allowing an effective way to evaluate the design process related to environmental consideration in a relatively less time-consuming manner. The plugin allows importing EnergyPlus Weather (EPW) data into the data analysis and visualization according to the designer's needs. In addition, Honeybee's tools are complementary to Ladybug in formulating calculations related to energy analysis. Ladybug and Honeybee integrated well-known simulation engines such as DAYSIM in Radiance, THERM, EnergyPlus, and OpenStudio to generate energy-related analysis and visualization. The MOO process was conducted using a plugin called Octopus [146]. In addition, in the daylight simulation optimization, the iteration was conducted using Colibri from Thornton Tomasetti (TT) Toolbox as it was also utilized in [76]. The data was analyzed and visualized using Microsoft Excel, the statistical analysis software JMP, and the Jupiter Notebook,

a phyton-based platform run in the Anaconda launcher, after the data on the dynamic parameters and target value were collected.

The original location for the wooden home was the Orio district of Kitakyushu, Fukuoka, Japan. Figure 7.5 shows the situation of the site where the wooden house is intended to be constructed. Figure 7.6 depicts the cluster and sequencing phase in parametric definition digital making. In the phase of main geometry, the closed brep representing Japanese wooden bars was made following the logic of *Hyperboloid* structure. In this phase, the parameters that shape the intended *Hyperboloid* geometry were applied (Figure 7.7). In addition to the goal of the geometry modelling, the volume of the wood used, and the volume of the building affected by the geometry constructed in this phase were computed for the cost analysis. The next stage, after completing the geometry of the Hyperboloid, was to organize the definition for structural analysis in Karamba. During this phase, cross sections, loads, and supports were specified in order to collect data on average normal force and displacement. After the answer from the first (structural) optimization process was found and decided, the modelling step of environmental analysis was done. In this step, the EnergyPlus EPW file was utilized. The research utilized the EPW file of Shimonoseki in Yamaguchi, Japan, as the closest available file on the map to the city of Kitakyushu [119].

Figure 7.5. Site location and situation: (a) The site plan; (b) The photo of the situation in the site. Photograph by the author.

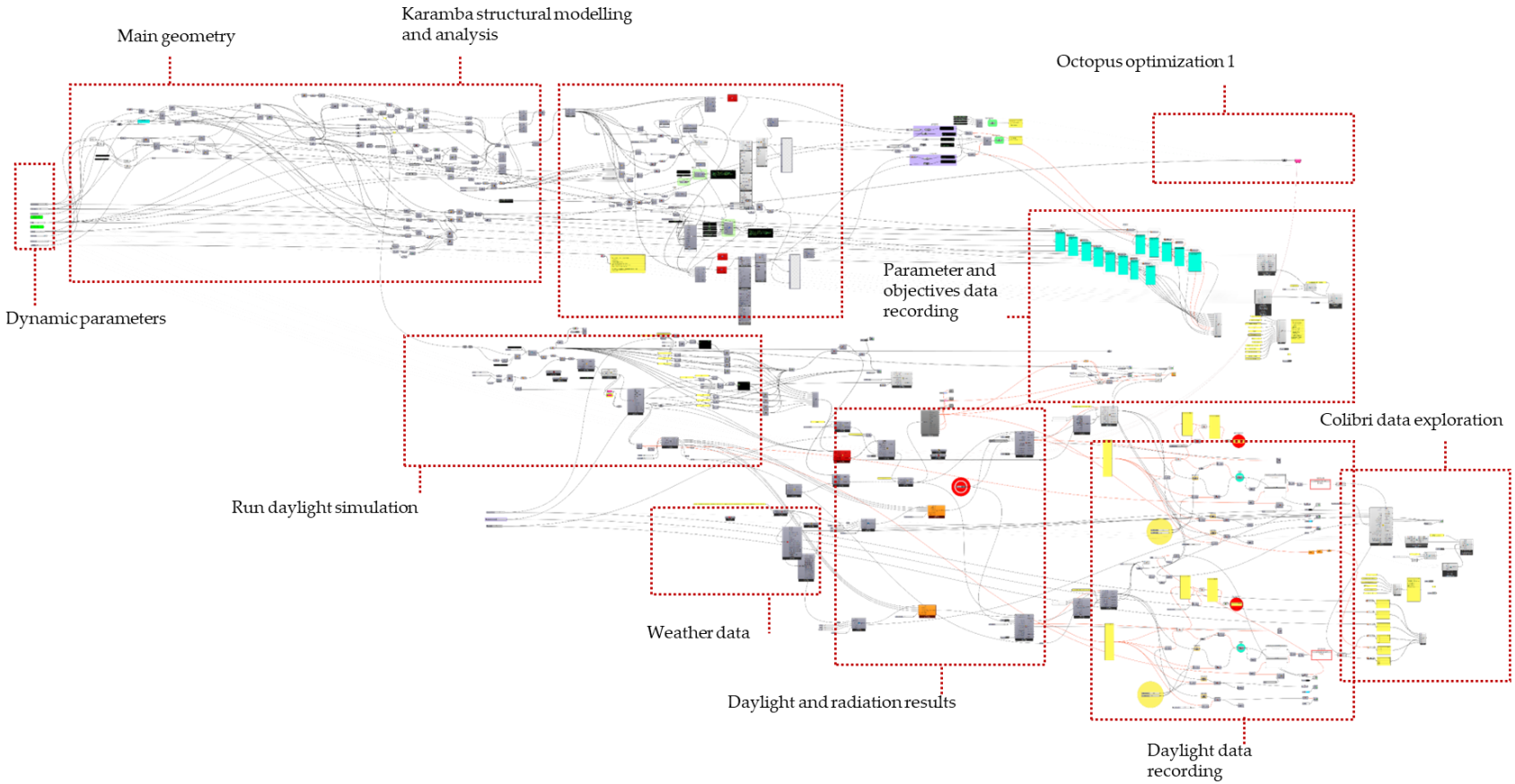

Figure 7.6. Parametric definition clustering of the entire system.

7.2.2. Geometry modelling

The geometry was built following the logic of a Hyperboloid structure, incorporating the Japanese timber bars. Figure 7.7 illustrates the geometry modelling logic for the structural analysis needs. The geometry has eight dynamic parameters named radius-bottom, offset distance, timber members, twist, height, radius-top 1, radius-top 2, and the roof slope. Each parameter determines the overall shape according to each parameter's movement and value (Figure 7.7 a). The vector of the wooden bars was set to follow the connection between the division point in the bottom profile and the division point on the top profile (Figure 7.7 b, c). Figure 7.7 (d) illustrates the appearance of a wooden structure designed with different twisting levels and the wooden bars used.

Table 7.2.1 shows the parameters for units, division, and the number of movements. To avoid miscalculation and unexpected errors during the iteration processes, the geometry modelling includes multiplication and division factors that influence the movement of one parameter to another parameter. For instance, the number of timbers used was a multiplication between timber members and twist level. Radius top 1, as the value control for the ellipse profile of the roof, was influenced by the value of radius bottom, and radius top 2, was influenced by radius top 1.

Table 7.2.1. Geometry parameters.

Parameters	Lower Limit	Upper Limit	Interval	Units	Driven Factor	Movement
Radius-bottom	1.5	2.5	0.1	m		11
Offset distance	−0.2	0	0.01	m		21
Timber members	3	5	1	unit	Twist	3
Twist	2	5	1	unit		4
Height	4	7	1	m		4
Radius-top 1	0.1	0.4	0.01	m	Radius bottom	31
Radius-top 2	0.1	0.3	0.01	m	Radius bottom and top	21
Roof slope	5	15	1	Degree (°)		11

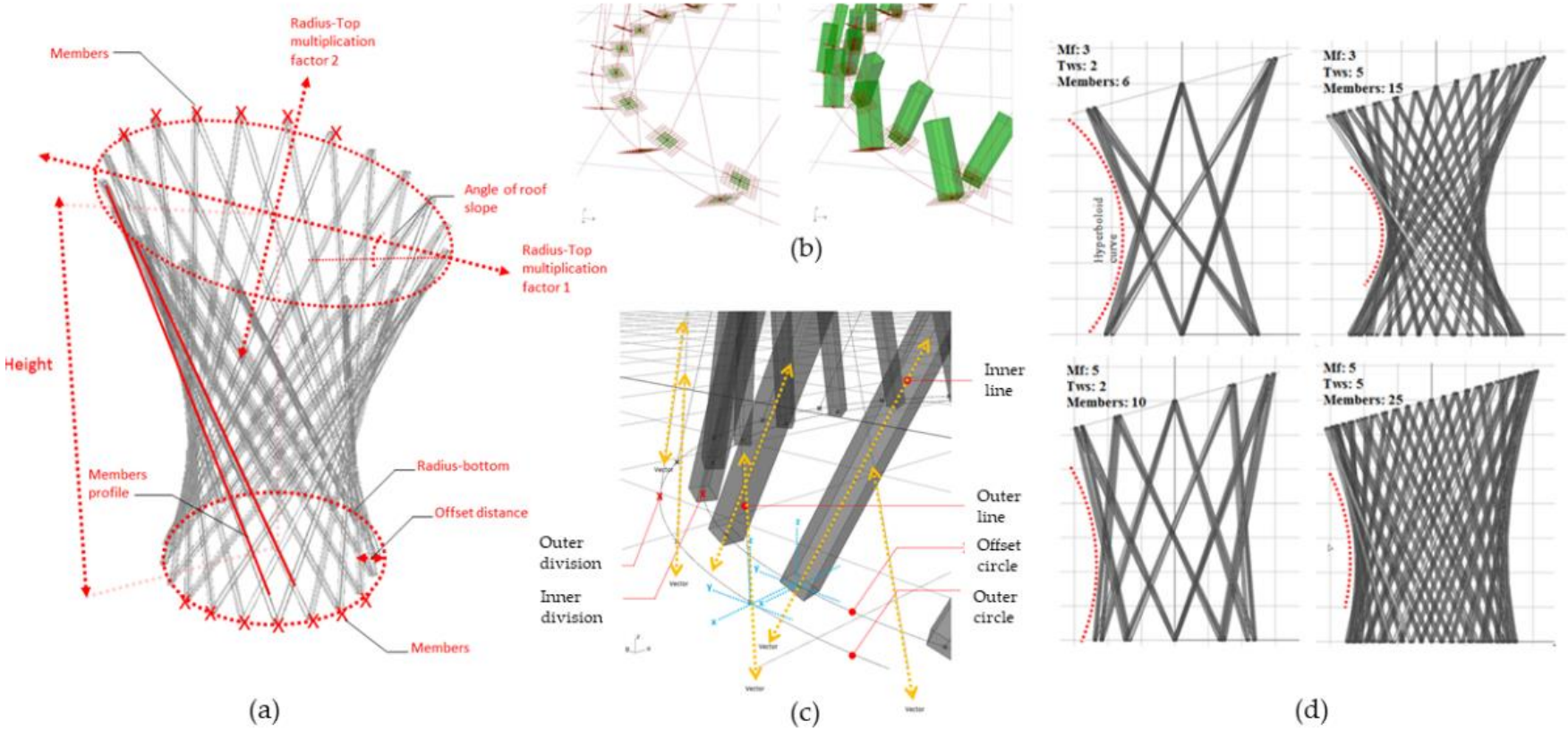

Figure 7.7. Modelling logic of the Hyperboloid wooden structure: (a) the set of dynamic parameters; (b) plan vector profiling; (c) illustration of random angle; (d) random examples of the structure with certain parameter combination.

7.2.3. Structural simulation setting and analysis

Figure 7.8 demonstrates the modelling method for the step of structural analysis. The definition of supports, loads, cross sections, materials, assembly, analysis, and visualization comprise structural analysis. As supports, the beginning points of each wooden beam's center line were utilized. The cross section was determined to be a profile of a Japanese hardwood bar with an upper and lower width of 105 mm x 105 mm. Karamba's loads were gravity-based weight loads and wind loads directed from the side of the timber structure. In this chapter, the Karamba components representing material attributes were manually set rather than using the default material list.

The analysis requires material properties of the used components to be able to calculate the force. In this research, the setting of wooden material properties in a component called MatProps in Karamba is presented in Table 7.2.2.

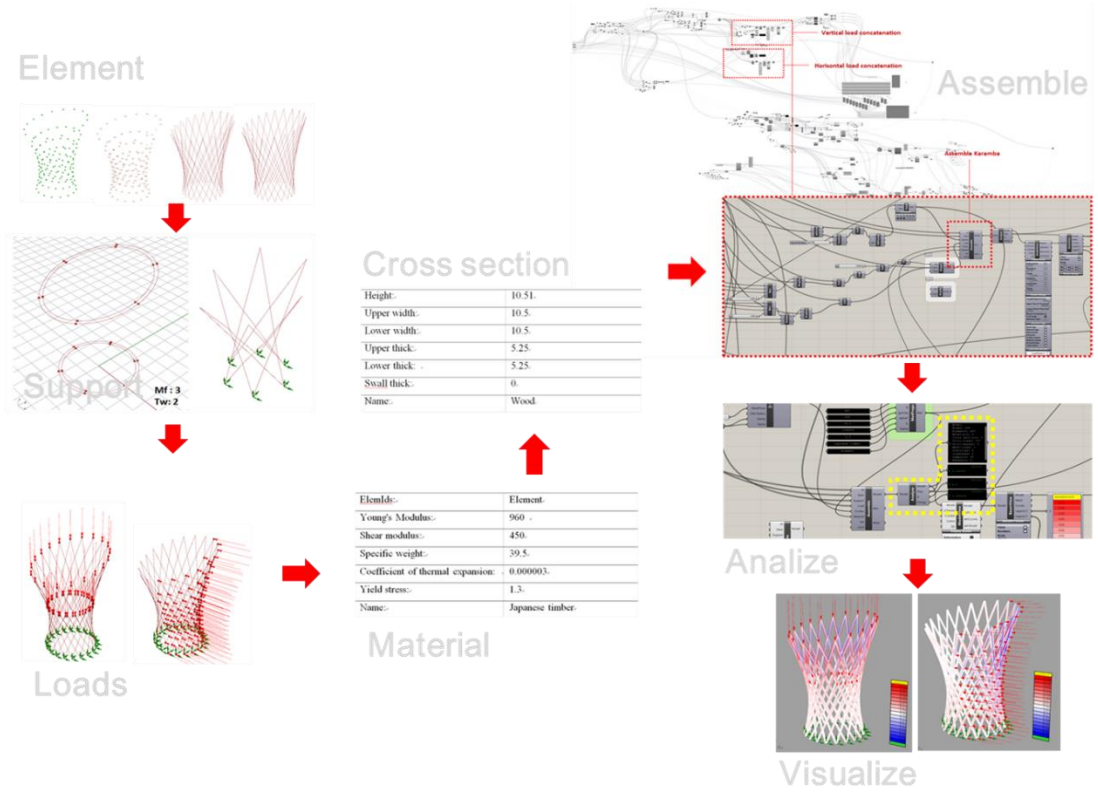

Figure 7.8. Structural modelling workflow

Table 7.2.2. Wooden bar properties

ElemId	Element	Units
Young's modulus (E)	960	kN/cm^2
Shear's modulus (G)	450	kN/cm^2
Specific weight (Gamma)	39.5	kN/cm^2
Coefficient of thermal expansion (AlphaT)	0.000003	1/°C
Yield stress (FY)	1.3	kN/cm^2
Name	Japanese Timber	

7.2.4. Daylight simulation setting

The daylight simulation setting, and analysis were entirely arranged in Grasshopper targeting the UDI 300 lux to 500 lux data collection. The relationship between windows and daylight utilizes the panelized division surface from the *Hyperboloid* cylinder yielded from the optimization process 1. The glazing modelling logic is presented in Figure 7.9. As it can be seen in the figure, after the zone has been divided, the glazing ratio was applied following the design (Figure 7.9 b). The consideration behind the glazing design was both aesthetic and the basic triangulation surface, as a consequence of making the curve of the cylinder become a planar surface. Figure 7.9 shows the scenario of the panel division to locate the glazing as windows and the material type for the analysis. Figure 7.9 (d) illustrates the visualization of daylight conditions inside the building and in relation to the site regarding the building orientation.

The dynamic parameters used in this phase were the glazing units representing the location of the glazing towards the building orientation. The parameters are the movement for glazing in zone 1, or first floor, and zone 2, or second floor, and the glazing ratio. The parameter upper and lower limits of each movement and glazing ratio together with their units are presented in Table 7.2.3, and the visualization of different combinations of the parameters is illustrated in Figure 7.10.

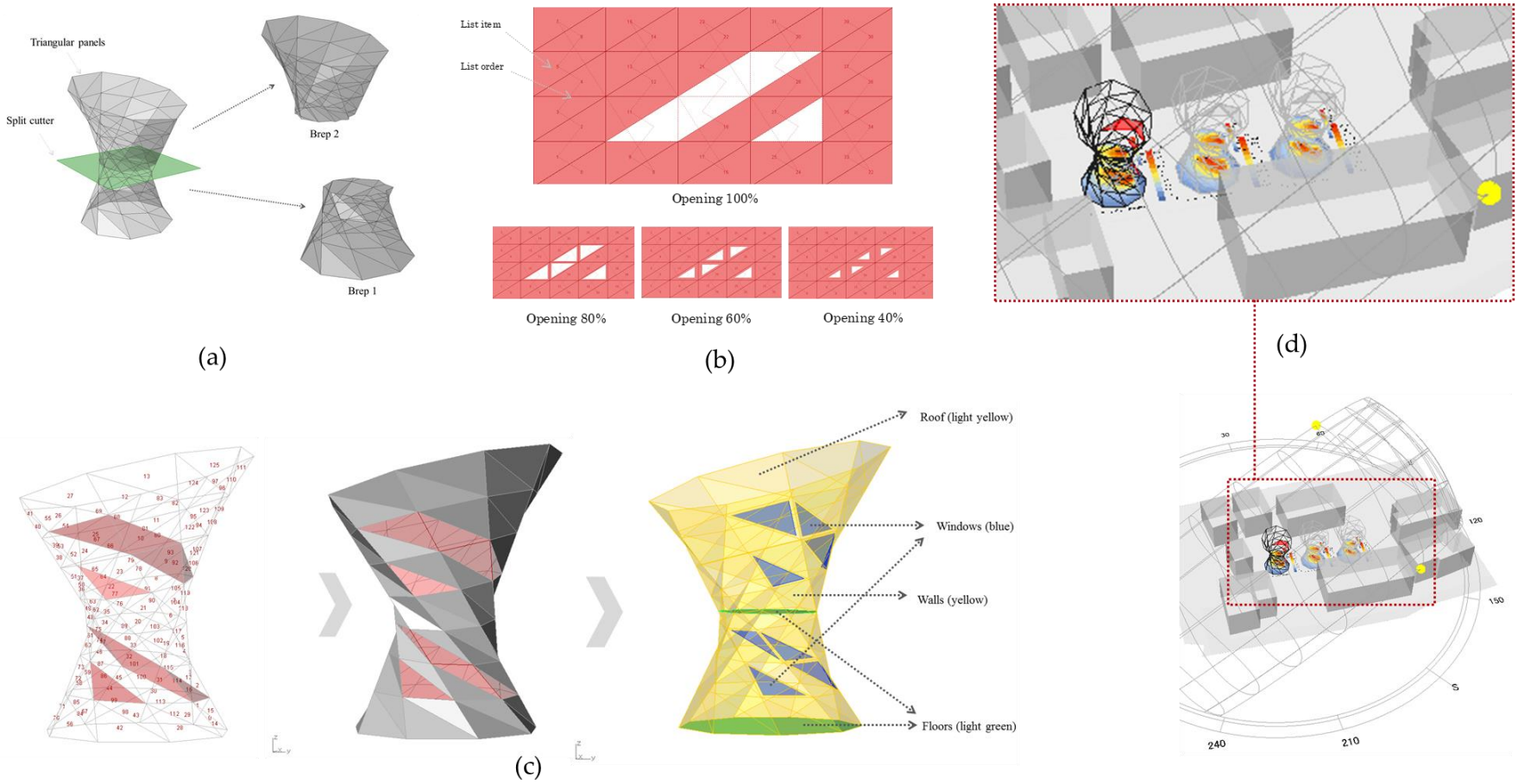

Figure 7.9. Modelling preparation for daylight analysis: (a) split brep to divide zones; (b) windows ratio setting; (c) windows application in Hyperboloid structure; (d) daylight analysis and visualization

Table 7.2.3. Dynamic parameters for daylight consideration

Parameters	Lower Limit	Upper Limit	Interval	Unit	Driven Factor	Movement
Movement list top	0	8	1	unit		9
Movement list bottom	0	8	1	unit		9
Glazing ratio	5	9	1	%	0.1	5

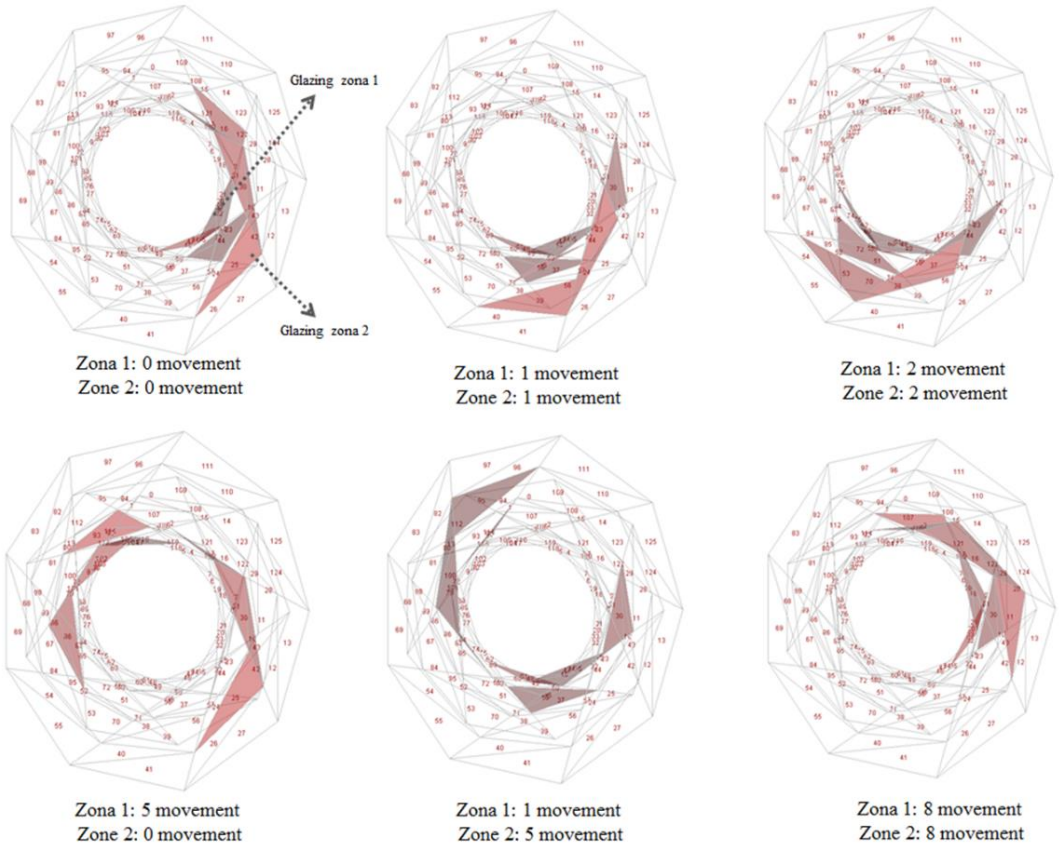

Figure 7.10. Samples of the glazing movement in Zone 1 and Zone 2

August 21 represent illuminance in the summer and 21 January represent illuminance in the winter were used as the analysis periods. The selection behind the selected date is based on the cooling design day and heating design day from the EPW stat file [173]. The weather data provided by EnergyPlus, called the EPW file, was used as a weather data input. With regard to the weather data availability, the analysis used the Shimonoseki EPW file as the closest data available surrounding Kitakyushu [119].

The metric used to measure the daylight was called useful daylight illuminance (UDI). UDI is defined as the annual occurrence of daylight illuminances across the work plane where the illuminances are within the range of 100 lux to 2000 lux and are within a range considered "useful" by occupants [125,126]. However, this research only calculated the area with UDI ranged from 300 lux to 500 lux as it was developed and adopted in [23,53].

7.2.5. Multi-objective optimization

The optimization was based on genetic algorithms (GA) conducted using a plugin called Octopus as the MOO solver, as it was also adopted in [128,174,175]. This phase's main goal is to optimize the design objective in terms of both structural and daylight. In structural analysis, the optimization was intended to find the targeted solution such as a minimum or as close to zero of normal force average (NFA), displacement (D), cost (C), and maximum building volume (BV). In daylight analysis, the iteration did not utilize the GA while it iterated the whole possibilities of the parameter combination. The iteration engine used was Colibri, developed by Thornton Tomasetti's CORE Studio, TTtoolbox [123].

7.2.6. Sensitivity analysis and fitness function calculation

The sensitivity analysis and fitness function calculation were performed outside of the Rhino and Grasshopper platforms following the generation of data from the first and second optimizations. The objective of the sensitivity analysis was to identify the most influential design parameter, whereas the fitness function calculation was to determine the optimal design parameters [80,87] The Pareto front solution from the first optimization and the iteration in the second optimization were analyzed to determine the optimal solution in terms of the targeted value of each goal in MOO. Utilizing traditional least square for personality and emphasizing impact leverage, the analysis was conducted.

7.3. Results

7.3.1. General results

There were two simulations conducted. The first iteration was for structural optimization, while the second iteration was for gathering daylight-related data. Each optimization and iteration comprised of a single simulation parameter that served as a genetic optimization genome to mold the optimization targets. The structural and geometrical optimization processes lasted nearly 24 hours and produced 10,098 persons or design solutions, whilst the daylight design exploration lasted 14 hours and produced 406 individuals or design solutions.

The general outcome of the optimization is the generational datasets. The lists were populated with information regarding a person's parameters and the objective value. In Octopus, the structural and daylight objectives were dispersed to the 3D population field based on its axis value. Sometimes, the fourth and fifth axes must be shown with color and scale.

The genetic iteration's raw data will undergo additional statistical analysis for sensitivity analysis and general comparison. Using the fitness function calculation, the Pareto front from the structural optimization was filtered to collect the nine best design choices for future design consideration. Due to the absence of Pareto optimality, the fitness function was applied to the overall result for the daylight iteration, which was not a genetic algorithm. front solutions. The details of each finding will be described in the following sub-section.

7.3.2. Structure optimization results

As previously mentioned, the structural optimization process comes up with a population field with four axes used, which are normal force average (NFA), displacement (D), cost (C), and building volume (BV). Figure 7.11 populates the population field with the specified individuals. The left population field indicates that the persons or intended solutions tend to congregate in a certain location. During the training time, the MOO tends to pull an individual out based on the matching of criteria and objectives to the desired area

of minimal normal force average, cost, displacement, and maximum building volume. The more generations that are established, the more design solutions will be generated, and the greater the optimization result will be.

Figure 7.11 (b) demonstrates how the Pareto front affected the last generations (Generation 99 to 100). The Pareto front solutions are the assemblages of selected individuals who satisfy the MOO requirements. A total of 177 Pareto front solutions were generated from the complete iteration in order to determine the optimal solution for balancing the four design objectives. The color gradient represents the price of the persons. Red symbolizes a high cost, brown a moderate cost, and green a low cost for the timber utilized. The individual determines the maximum and lowest performance of each design target through observation in this field. To create the desired individuals, a feature known as the "reinstatement solution" was employed. Prior to this phase, the design objective may be chosen based on assumptions; however, empirical calculation and analysis are required to assure balance. Therefore, the calculation of the fitness function was performed.

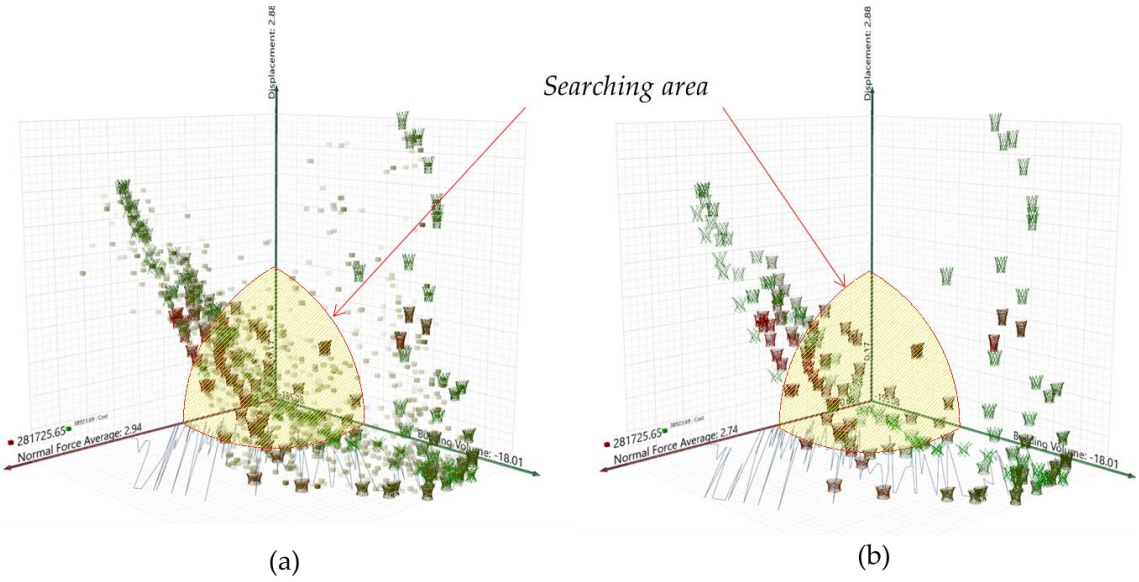

Figure 7.11. 3D population field as an original design distribution yielded during MOO processes: (a) History; (b) pareto front

7.3.3. Fitness function

In this stage, the original Pareto front solution is shortened by applying a fitness function (FF) computation. The calculated values and attributes were prioritized according to the fitness function value. The nine best design solutions and their attributes, including parameters and objectives, are presented in Table 7.3.1.

In terms of parameters, the FF radius bottom results ranged between 1.5 m and 2.5 m, which represent the minimum and maximum radius bottom parameter settings. Except for solutions number five and eight, the offset distance appeared to vary at random but generally fell between 0.18 m and 0.2 m, with the exception of solutions number five and eight. Most timber members are optimized with 5 bars multiplication, which is the most allowed by the configuration (Table 7.2.1). As a member's multiplication factor, the twist occurred predominantly at 2, with the exception of those ranked 4, 8, and 9. The majority of the optimal solutions fell between 4 and 4.8 meters, with the exception of solution rank 8, which was 5.7 meters.

Table 7.3.1. Nine best design solutions, attributes, and objectives

Radius-Bottom	Offset Distance	Timber Members	Twist	Height	Radius-Top 1	Radius-Top 2	Roof Slope	NFA	D	C	BV	Timber Volume	Ranking	Solution Number
1.5	−0.18	5	2	4	2.09	2.628	7	0.840007	0.477199	62,567.32626	36.781507	1.013919	1	9052
1.5	−0.2	5	2	4	2.09	2.628	7	0.771499	0.644391	62,510.88343	36.781508	1.012752	2	7974
2.5	−0.2	5	2	4	2.871	3.264	8	1.490737	0.433516	67,534.92485	74.876282	1.12736	3	7470
1.5	−0.19	5	3	4.2	2.079	2.616	6	0.755567	0.367732	104,091.2108	38.433623	1.576698	4	7939
2.5	−0.09	5	2	4.1	2.915	3.528	7	1.559383	0.529867	69,522.70367	81.22864	1.168452	5	10,056
2.5	−0.19	4	2	4	2.86	3.24	5	1.544786	0.420685	57,526.35573	64.761463	0.974208	6	6612
2.5	−0.19	5	2	4.3	2.915	3.54	5	1.586519	0.591833	70,858.80102	85.557888	1.196072	7	9415
2.5	−0.08	5	4	5.7	2.992	3.624	5	1.069103	0.634972	189,466.6977	116.958725	2.933119	8	9518
2.5	−0.19	5	3	4.8	2.871	3.264	8	1.414321	0.459468	119,503.7762	89.888523	1.906061	9	8798

According to the established parameters, the structural and cost objectives tend to move the design solution towards the setting's lower limit. For the top radius one, which forms the ellipse profile of the home, the values ranged from 2.09 to 2.992, but for the top radius two, the values ranged from 2.628 to 3.624. The optimal solutions have roof slopes between 5 and 8. The number of roof slopes indicated, based on the parameter settings, that the lower limit height parameter happened between the lower and middle limits. Table 7.3.1 reveals that the best answers were generated after solution number 7000.

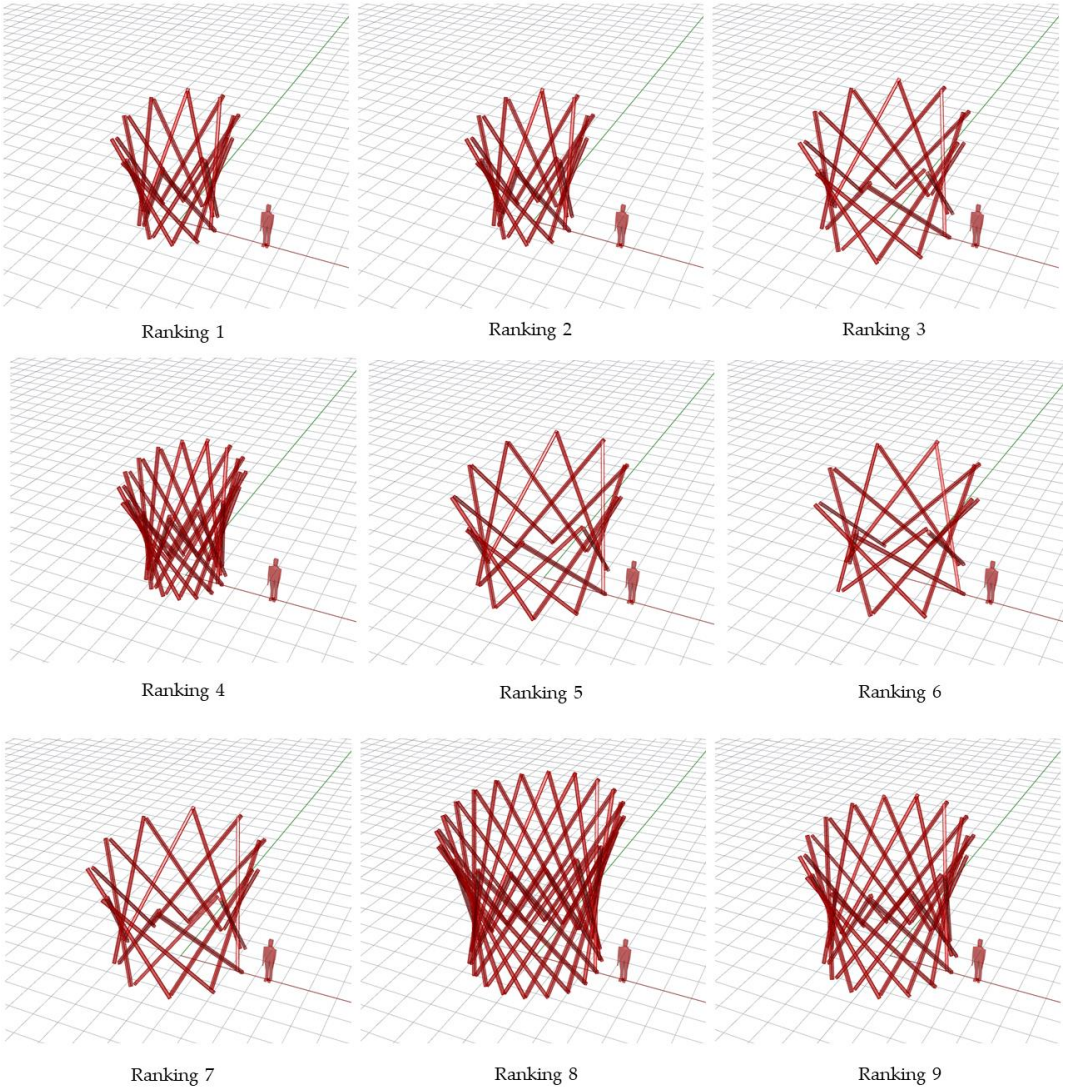

Figure 7.12. Nine best design solution based on fitness function calculation

Figure 7.12 shows the geometry of the nine best solutions based on the FF calculation. Even though the original population field in Octopus featured instant geometry feedback, up to this point, the menu has filtered into several choices, highlighting the consideration of performance-based design. As shown in Figure 7.12, the appearance of solution rank 1 and solution rank 2 are similar. In addition, solution ranks 3, 5, 6, and 7 also share a similar visual look. The options ranked 4, 8, and 9 have more wood than the other solutions. This was a result of the greater combination of twist level and amount of utilized timbers. Choosing the individual presumed to be the best involves mainly subjectivity. In this case, as seen in the figure, almost all solutions have a height of less than 5 m (Table 7.3.1).

The search for the least amount of timber used to achieve the least amount of cost may have influenced the trend of less height among individuals, which is later confirmed in Figure 7.17 where height, along with twist and timber members, is one of the parameters with the most implications for cost. Taking into account sufficient height for a two-story home, the author selected option number 8 with a height of 5.70 m for additional optimization processes connected to daylight. The height finding reveals unexpected outcomes when the height was examined as a whole rather than as a result of the relationship between the heights of the first and second levels. Nonetheless, this discovery and consideration serves as feedback for future experiments to set the lower limit in the height parameter setting to a reasonable value for a two-story house and to determine the interconnection between levels.

Figure 7.13 shows a scatterplot illustrating the correlation between two objectives that originated in the population field in Figure 7.11. In this graph, the position and distribution of Pareto front solutions and fitness function solutions across all individual generations are depicted. According to the preceding diagram, it is impossible to determine the association between each objective. All correlations had a rather small RSquare value (below 0.4). It appears that the Pareto distribution is evenly distributed. A suitable logic of iteration should have drawn the individuals into the searching area, given the weight of MOO activities (Figure 7.11).

However, as it can be seen from the dedicated scatterplot, a proper swarm individual can only be found in Figure 7.13 b and f, which indicates that multi-objective optimization employs a weighting complexity to balance the search. The absence of generation number may result in conflicting trade-offs among objectives; increasing the generation number during MOO to a maximum or closely matching the mass multiplication of the parameters' movement value is advised for future and comparable work routes.

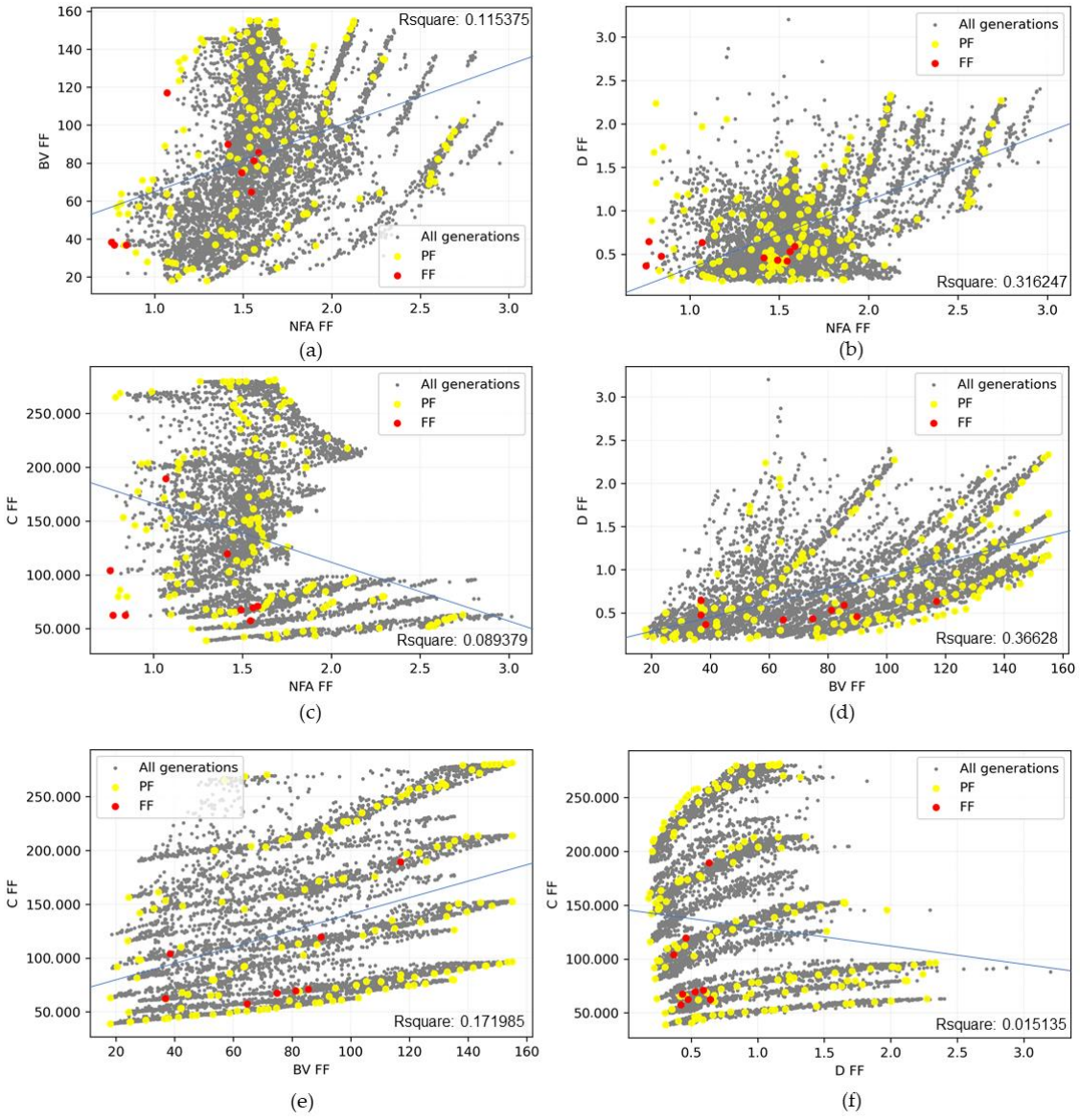

Figure 7.13. Scatterplot between two objectives and the Pareto front position: (a) NFA and BV; (b) NFA and D; (c) NFA and C; (d) BV and D; (e) BV and C; (f) D and C

7.3.4. Daylight optimization results

After one individual has chosen from the first optimization processes, a similar workflow has been applied to the second optimization related to daylight objectives. The different type of iteration between the two optimizations is that in this phase, instead of utilizing the mating of parameters through a generative algorithm, daylight objective search was utilized for design exploration from the plugin called Colibri, provided by TT Toolbox [2,124,160,176,177]. The exploration was iterated to all possible solutions from the parameter combinations that were set in the Grasshopper definition. The step is possible to be conducted when the expected number of solutions, together with the consideration of simulation time, is considered possible.

Daylight optimization parameters only have a few possible design solutions (Table 7.2.3) and yielded 406 individuals representing the design solution and its attributes. Figure 7.14 shows the 3D scatter plot that plots the design solution from the daylight objective iteration in optimization two. The objectives were to measure the useful daylight illumination (UDI) ranged between 300 lux and 500 lux [23,53] during designated days in summer and winter. In addition, the geometry objective, which was a glazing area to ensure the view quality to the outside, was also incorporated. According to Figure 7.14 (a), the results of the glazing ratio setting in parameters show several levels in UDI summer and winter. The glazing area objective has a strong correlation with the glazing ratio according to the color gradation.

Aside from being related to the ratio (Figure 7.9 (b)), the glazing area is also affected by the size of the panel produced by the exploded geometry from the optimization one when it was rotated. Figure 7.14 b highlights the ten best individuals based on the FF calculation. The objectives were successfully located at the maximum values of UDI and glazing area, indicating that the FF calculation was performed and applied properly. To check the position of the individuals, the relationship between the two objectives in daylight optimization will be presented in a 2D scatterplot (Figure 7.15).

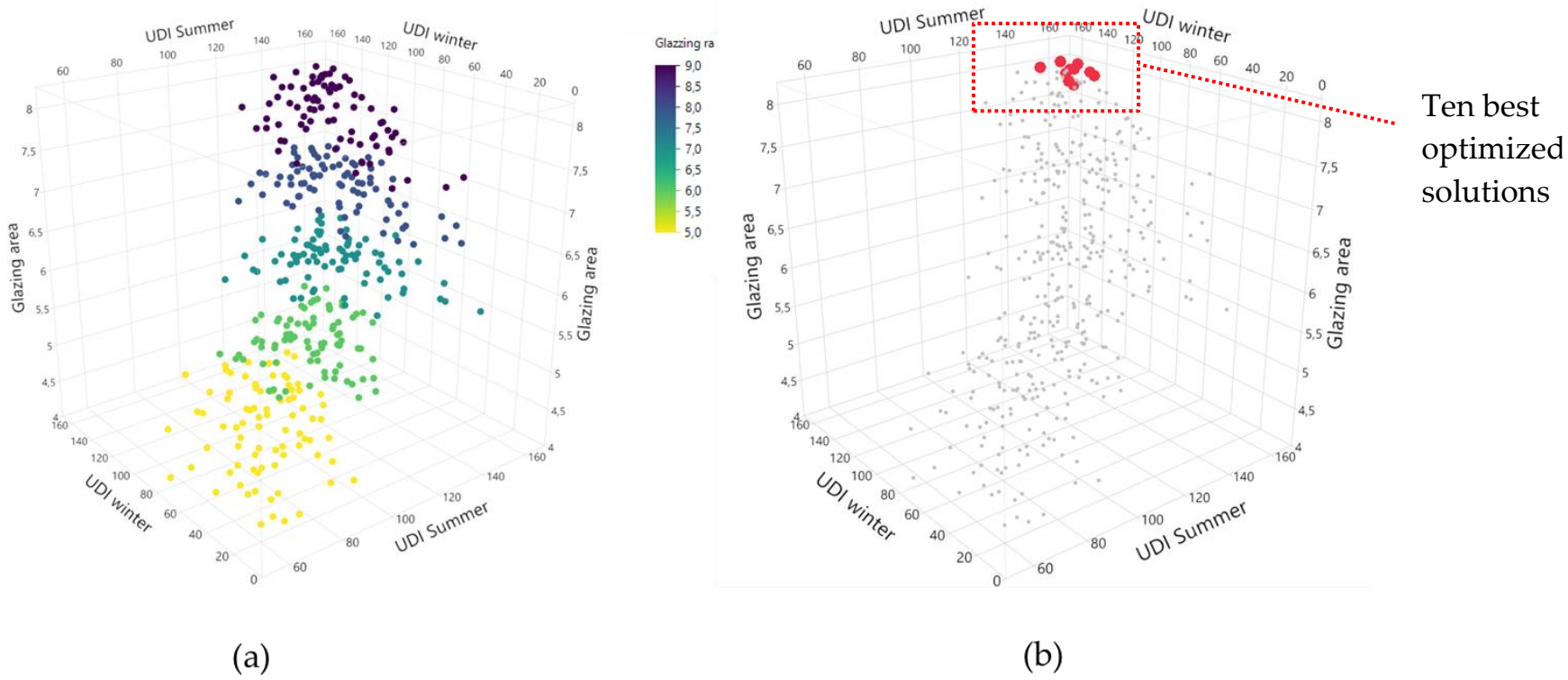

Figure 7.14. Scatterplot for daylight objectives iteration results: (a) overall generations; (b) optimized solution from FF calculation (red)

Table 7.3.2 lists the ten best solutions' attributes, parameters, and objective values. In terms of parameters, the glazing movement for the top zone (second floor) ranges from 5 to 8, while for the bottom zone (first floor), it ranges from 4 to 8. The range from movement items 5 to 8 directs the windows from the Northwest to the Northeast sides of the house (Figure 7.9).

The range of movement items from 4 to 8 for the bottom zone (first floor) has the same orientation as the top zone. As is often believed, the glazing ratio for FF pushed the individual's parameter setting to its maximum value. The summer's highest UDI was achieved by solution rank 1. The winter solution with the highest UDI and the largest glazing area was solution rank 7. After individual number 360, the optimal solution was found. Interestingly, the eighth option was the final result of the iteration process.

Table 7.3.2. The 10 best design solutions, attributes, and objectives

Rank	Movement Item Top FF	Movement Item Bottom FF	Glazing Ratio FF	UDI Summer FF (m^2)	UDI Winter FF (m^2)	Glazing Area FF (m^2)	Solution Number
1	8	7	9	159.866523	136.44026	7.9648	397
2	8	5	9	154.025604	138.908534	8.021715	379
3	8	4	9	153.782105	135.71133	8.10186	370
4	7	7	9	150.854576	136.910236	8.04021	396
5	7	4	9	145.344506	134.664192	8.177271	369
6	8	6	9	155.822131	126.311041	7.986382	389
7	7	5	9	140.49215	142.017143	8.097126	378
8	8	8	9	151.082026	134.135437	7.856945	406
9	5	7	9	147.017711	130.940005	7.942779	394
10	7	6	9	144.570966	128.956859	8.061792	387

To ease the observation of the individual distribution within the population fields (3D scatterplots), 2D scatterplots have been incorporated. Figure 7.15 shows scatterplots comparing two daylight objectives as part of the daylight optimization process. Initially, the FF has successfully identified the 10 optimal solutions in the search areas for each

plot, which are maximum UDI and maximum glazing area. Second, there was no strong correlation between the objectives. In terms of UDI in summer and winter, the swarm of solutions or distribution was approximately 100 m^2 in the summer and greater than 60 m^2 in the winter. Regarding the connection between glazing area and UDI, however, Summer saw the emergence of an ambiguous trend that resulted in a positive correlation between the solutions of the iteration, while in Figure 7.15 (c), The trend had a uniform distribution. Due to the low correlation, in the daylight objective analysis, the value of each objective cannot be determined by the value of the other objective.

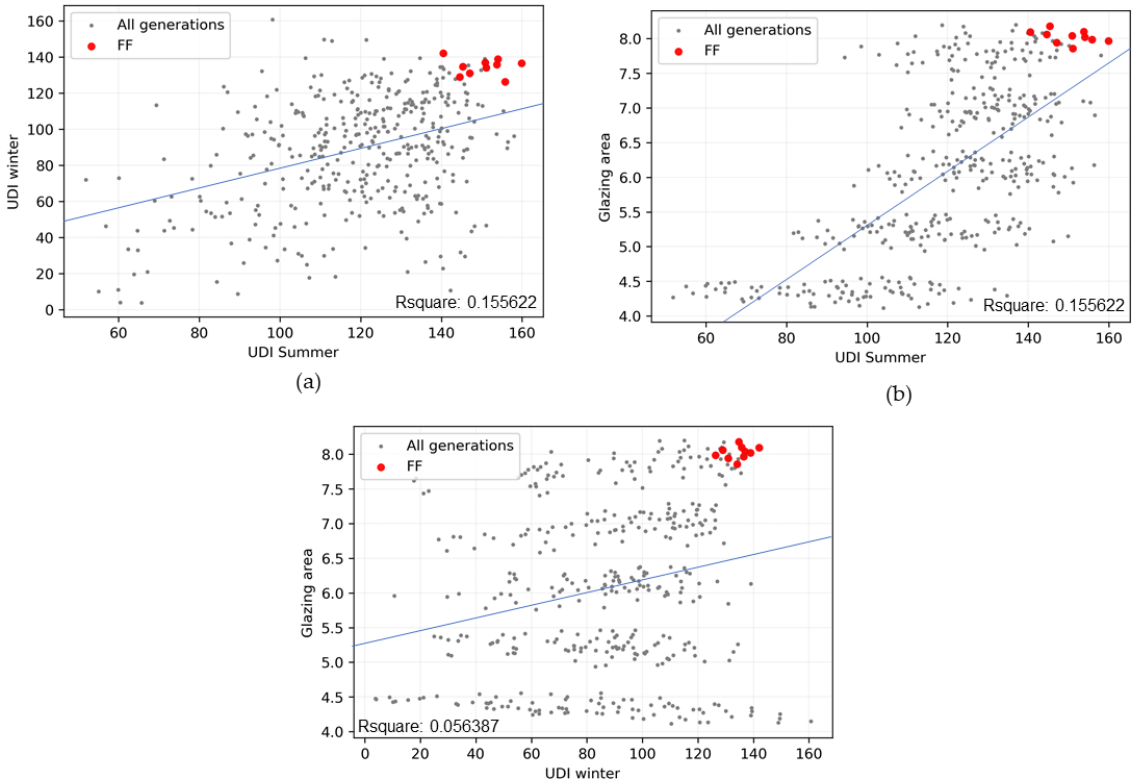

Figure 7.15. Scatterplot between two objectives and the Pareto front position; (a) UDI summer and UDI winter; (b) UDI summer and glazing area; (c) UDI winter and glazing area

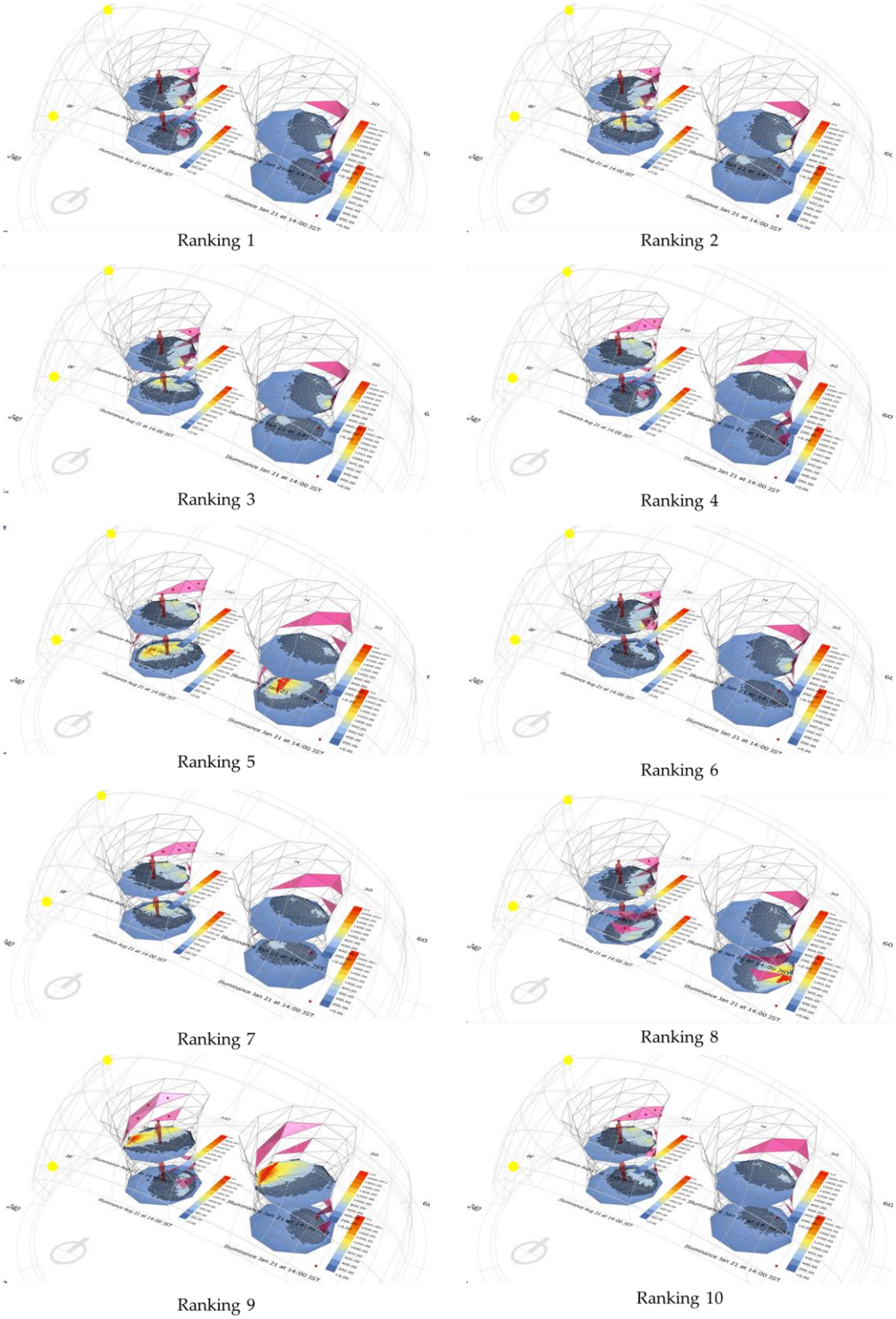

Figure 7.16. Best design solution related to daylight based on fitness function calculation

In addition to UDI performance, the various glazing positions and their effects on the UDI distribution have been visualized in Figure 7.16. Two different sky positions are represented by the two visuals of each solution rank. The illustration on the left displays the UDI for a summer scenario, while the illustration on the right depicts the UDI for a winter scenario. The majority of the glazing space in zone two (second story) is oriented to the northeast, with the exception of ranks 9 and 5 in zone one (first floor). As a result of the building's orientation to the north-west, an area with a UDI more than 2000 lux emerged and presented in Figure 7.16 (rank 5 in zone one, and rank 9). During the winter, Rank 8 in Zone 1 has an area with overly lit UDI. This was due to the sun vector striking the glazing region directly.

Regarding the desired UDI of 300 lux to 500 lux (blacked border), solution rank 1 indicates the greatest region with the UDI during the summer, while solution rank 7 depicts the largest area with the targeted UDI during the winter. In the summer, the UDI distribution primarily occupied the central region in both zone one and zone two, however in the winter, the 300 lux to 500 lux UDI distribution primarily occupied the area above the glass that extended to the center. It is indicated that the useful range according to [75] consists of areas extending from beneath the glazing to the test floor's center. The darkest section of the top 10 solutions based on the FF calculation was approximately 200 lux, while the brightest was over 2,000 lux.

In addition, nearly all solutions performed UDI between 800 lux and 1200 lux (shown by the color gradient from light green to yellow), with the exception of solutions four and six in zone one during winter. based on the site orientation (Figure 7.5), None of the daylight optimization options included front-facing or primary orientation glazing. The majority of building designs tend to position the glazing facing the front side of the site or toward the main entry to the site; nevertheless, the results of this study indicate the exact opposite. This research employs a performance-based design that allows for additional considerations on the view outside.

7.3.5. Sensitivity analysis results

A sensitivity analysis was performed to determine which characteristics have the greatest effect on particular design objectives. The formulation and action (Sub-chapter 7.2.6) based on the cumulative generations that have been iterated during MOO procedures. In this step, the findings of the sensitivity analysis will be separated into two parts: the sensitivity analysis of the structural analysis and optimization intention, and the analysis for the daylight optimization intention. The findings are shown as tornado plots, with the parameter with the greatest influence listed first.

The standard least squares for personality were used, with an emphasis on effect leverage. Figure 7.17 depicts the results of sensitivity analysis on four design objectives related to the optimization of structural and geometry goals. Figure 7.17 a present the influential parameter value to the normal force average (NFA). The results indicate that wood members, twist level, and house height by order have the most influence on the normal force average, whereas radius-bottom, roof pitch, and offset distance have the least impact. Figure 7.17 (b) depicts the results of sensitivity analysis between parameter to displacement (D). In terms of displacement, height, twist level, and radius bottom are the parameters that implicate the displacement the most, and the least are radius top, timber members, and the roof slope. Figure 7.17 (c) parameters to cost (C), twist level, timber members, and height are the parameters that implicate cost the most. This is due to the fact that these three parameters have a direct impact on the volume of wood used and the number of joints.

The parameters radius-top, bottom, and offset distance have no direct implications for the wooden volume. Figure 7.17 (d) demonstrates the effects of factors on building volume (BV). The results indicate that building height, number of members, and bottom radius have the most impact on building volume. In general, building height is one of the most influential factors on design objectives. The twist has an impact on NFA, C, and D, but not on BV. The parameter with the fewest implications in NFA, C, and BV, but not in D, is offset distance. Further analysis or research is urged to focus just on the best parameters in order to acquire stronger results and optimization when it is known which parameters have a significant impact on achieving particular design goals.

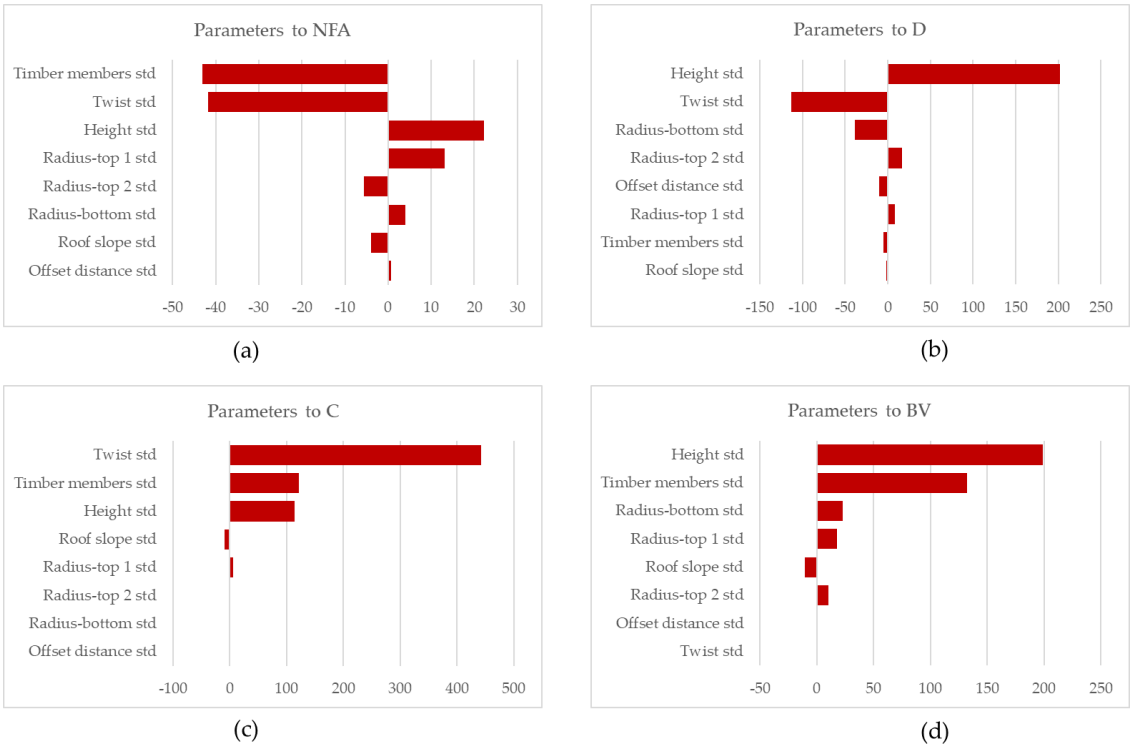

Figure 7.17. Sensitivity analysis showing the significant implication of each parameter toward the objective: (a) parameters to NFA; (b) parameters to D; (c) parameters to C; (d) parameters to (BV)

Figure 7.18 depicts the sensitivity analysis results for the daylight optimization. Figure 7.18 a show that movement item bottom in zone one and the glazing ratio are the parameters that most implicate the UDI in winter, while the glazing movement in zone two (second floor) is the least parameter driving the value of the UDI distribution in winter. The situation in summer (Figure 7.18 (b)) the glazing ratio and glazing movement on the second level are the most critical factors in determining the UDI value distribution. According to common sense and comprehension, the glazing ratio effects the glazing area directly in terms of the glazing area goal; hence, it becomes the most relevant parameter driving the view objective with a substantial value of almost 200. In the daylight and view objective analysis, because a genetic algorithm approach was not used and the number of parameters and their value range were not as extensive as in the structure analysis, the number of parameters as an optimization genome was only three, so the significant value among the parameters was not displayed except in Figure 7.18 (c).

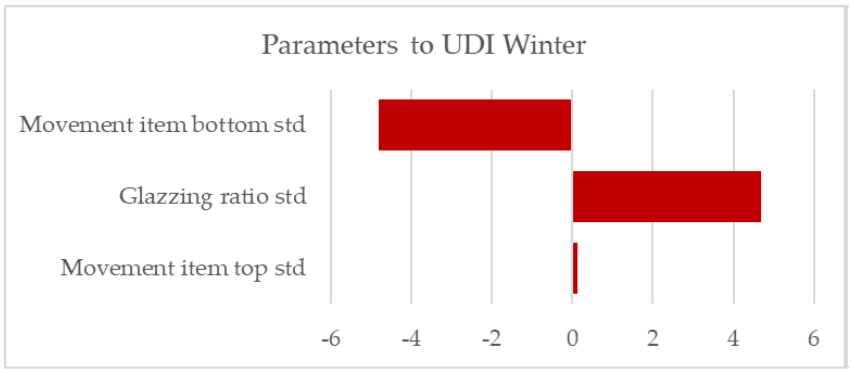

(a)

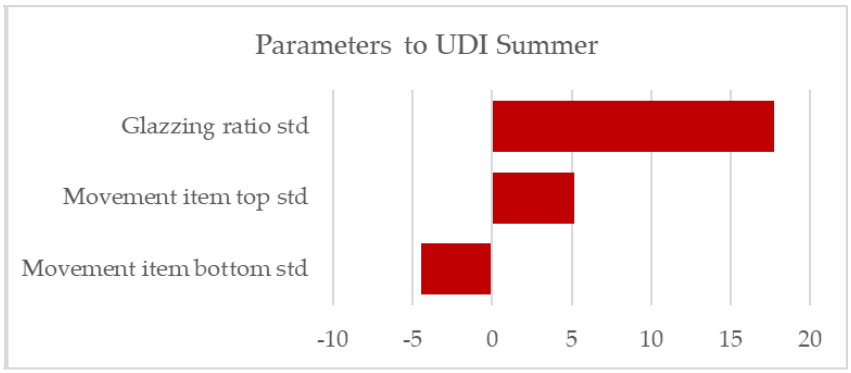

(b)

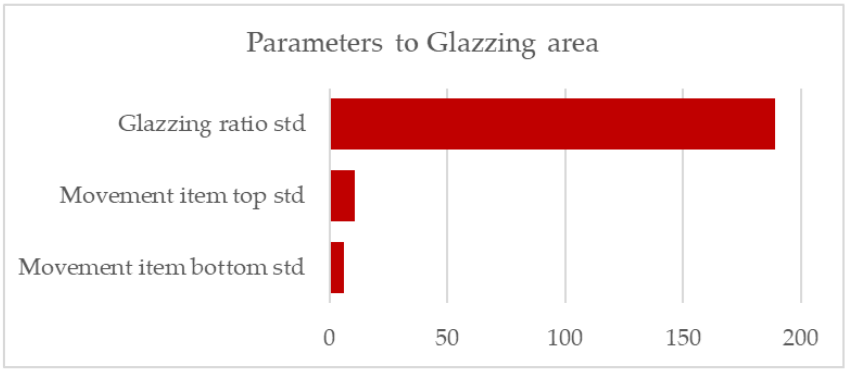

(c)

Figure 7.18. Sensitivity analysis showing the significant implication of each parameter toward the objective: (a) parameters to UDI winter; (b) parameters to UDI summer; (c) parameters to glazing area

7.3.6. Parameter to objective tendencies

The parallel coordinate plots (Figure 7.19, Figure 7.20, and Figure 7.21) offer another method for displaying the link between the design parameters and design objectives. The range of values along each axis represents the design variable and the objectives. According to design objectives, each of the four plots in Figure 7.19 and Figure 7.20 depicts a distinct trend. The gradient color was chosen to indicate the objective's value. Due to the utilization of numerous design objectives, the tendency would not result in a single definitive solution. The purple line in each figure was utilized to show only the goal range of objective values (minimum NFA, D, and C, and maximum BV) in addition to the unselected value (gray-colored).

The highlighted lines in Figure 7.19 (a) highlight the relationship between the low Normal Force Average (NFA) value and the parameters and other objectives. In terms of parameters, a minimum or preferable NFA is connected with largely minimum radius-bottom and minimum radius-top, as seen in the graph. The distribution of values for the remaining parameters, such as offset distance, timber members, twist, building height, and roof pitch, tends to be uniform with relation to the minimal NFA. Low NFA value is also correlated with minimum displacement (D) and building volume (BV), but not cost (C).

In Figure 7.19 (b), the minimum value of displacement is correlated with the middle to minimum value of NFA. In the same way that Figure 7.19 (a) did not exhibit a specific trend with C and BV, nor did the minimum D exhibit a specific trend with C and BV. However, the slope indicates that the value appears to range from the average to the minimum. In terms of parameters, nearly all value ranges contribute to the minimal D, with the exception of building height, where the swarm exhibits a value range trending from middle to minimum.

In terms of the lowest cost, the tendency Figure 7.20 (a) presents a correlation between a low twist level and a shorter building height. Except for twist and height, the other characteristics have an even distribution. Concerning the remaining objectives, least cost is related to the middle value of NFA, minimum D, and minimum BV.

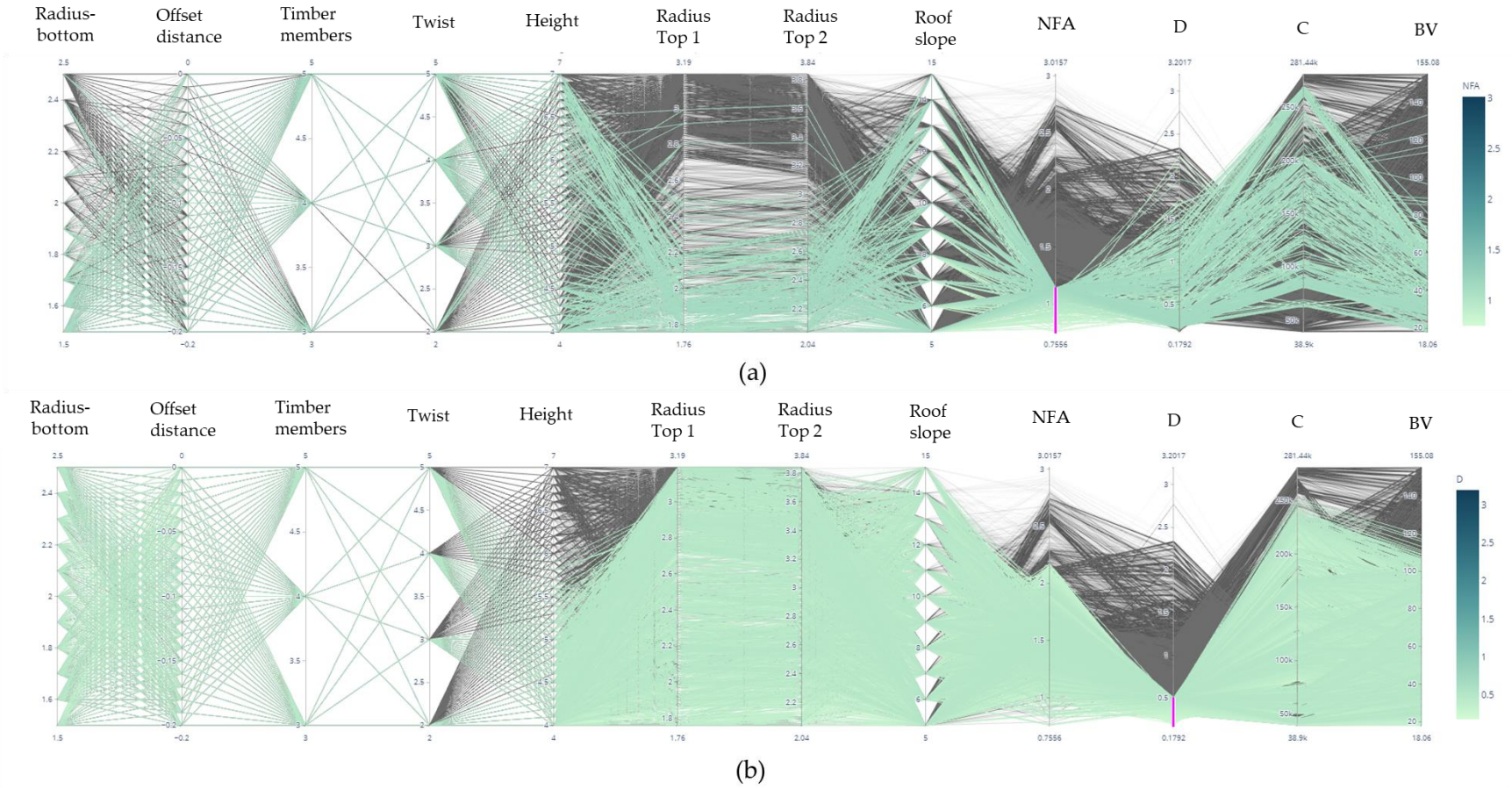

Figure 7.19. Parallel coordinate plots for structural optimization: (a) relation to lowest NFA; (b) relation to lowest D; (c) relation to lowest C; relation to highest BV

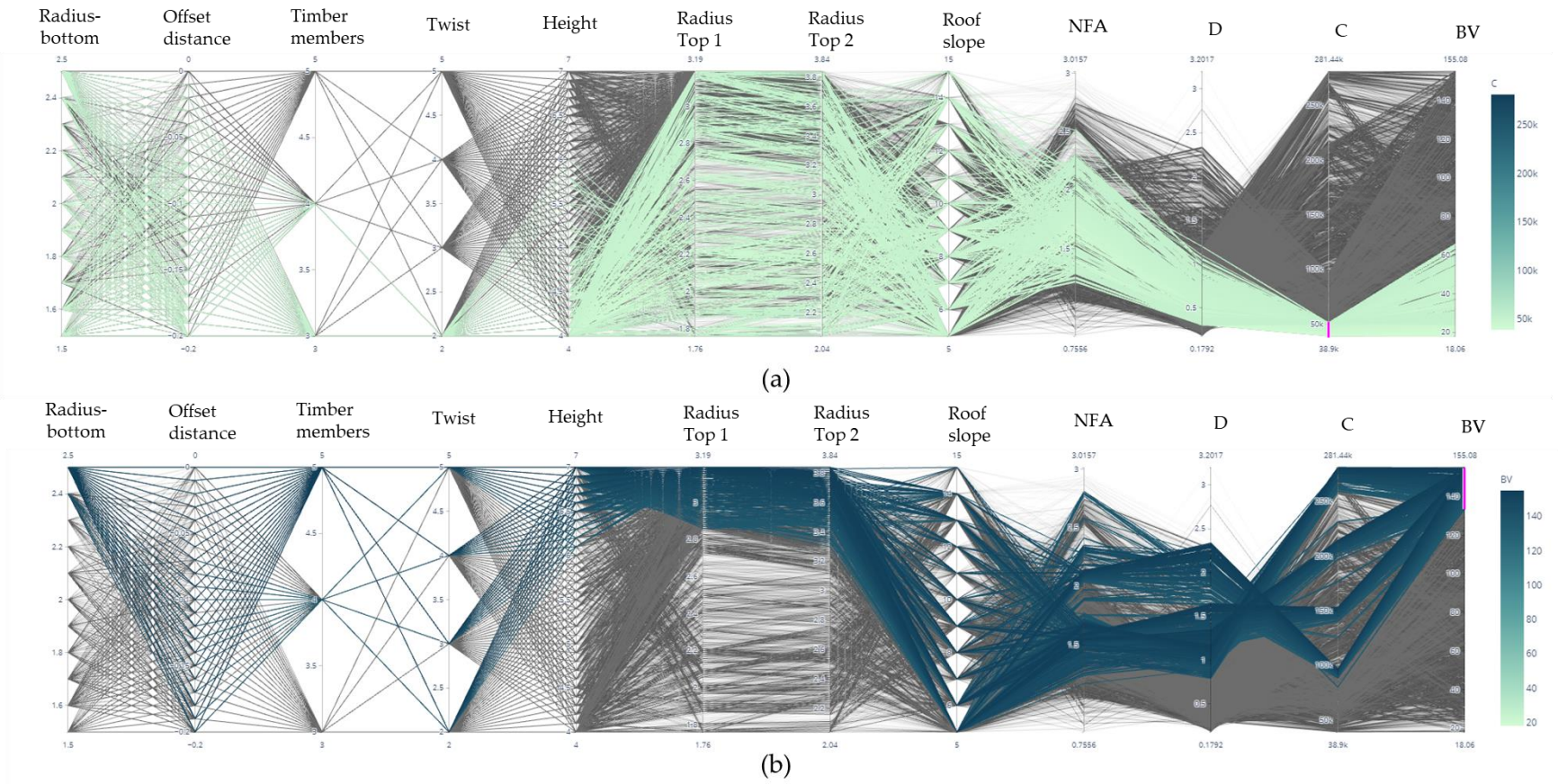

Figure 7.20. Parallel coordinate plots for structural optimization: (a) relation to lowest C; (b) relation to highest BV

The observation based on minimum cost correlates with minimum value of twisting factor as well as minimum building height, but not radius bottom, offset distance radius top, and the roof slope where there is an even value distribution emerge. It is also can be observed that minimum value of timber members contributes to minimum cost. The argument stating that minimum twisting factor, timber members, and building height implicates the minimum cost could be interpreted that the tendency observation is suggesting a common sense in terms of geometry and cost. This is confirmed that the proposed optimization platform in this thesis reliable to be adopted.

In Figure 7.20 (b), The trend indicates that maximum radius-bottom, height, radius-top 1, and radius-top 2 are connected with maximum BV where the coloured lines highlight the expected maximum value of BV. Maximum BV is merged with the middle range of NFA and D, as well as the range from middle to maximum value of C, in respect to the other objectives.

Related to the tendency between maximum building height with the parameters, the clear tendency can only be observed in maximum value of height, radius top 1 and 2, also timber members and radius bottom, but not in offset, roof slope, and twist distance where it is showing an even value distribution. The target opposes the finding in cost tendency with almost all mentioned factors perform reversing values. The phenomena also could be interpreted as supporting common sense where maximum building value is implicated by maximum value of the geometry parameter. Both finding in tendency observation confirm the research questions and hypothesis.

Based on this observation, justification among objective has not to be identified due to the fact that the study involves more than two objectives where trade-off during the optimization process tend to come up with no absolute single solutions. On the other side, the tendency study using observation into the parallel coordinate plot has been successfully identify almost clearly several parameters to have implications for forming targeted design solution. This benefit further study about structure optimization of *Hyperboloid* to only focus for this value range when setting the parameters.

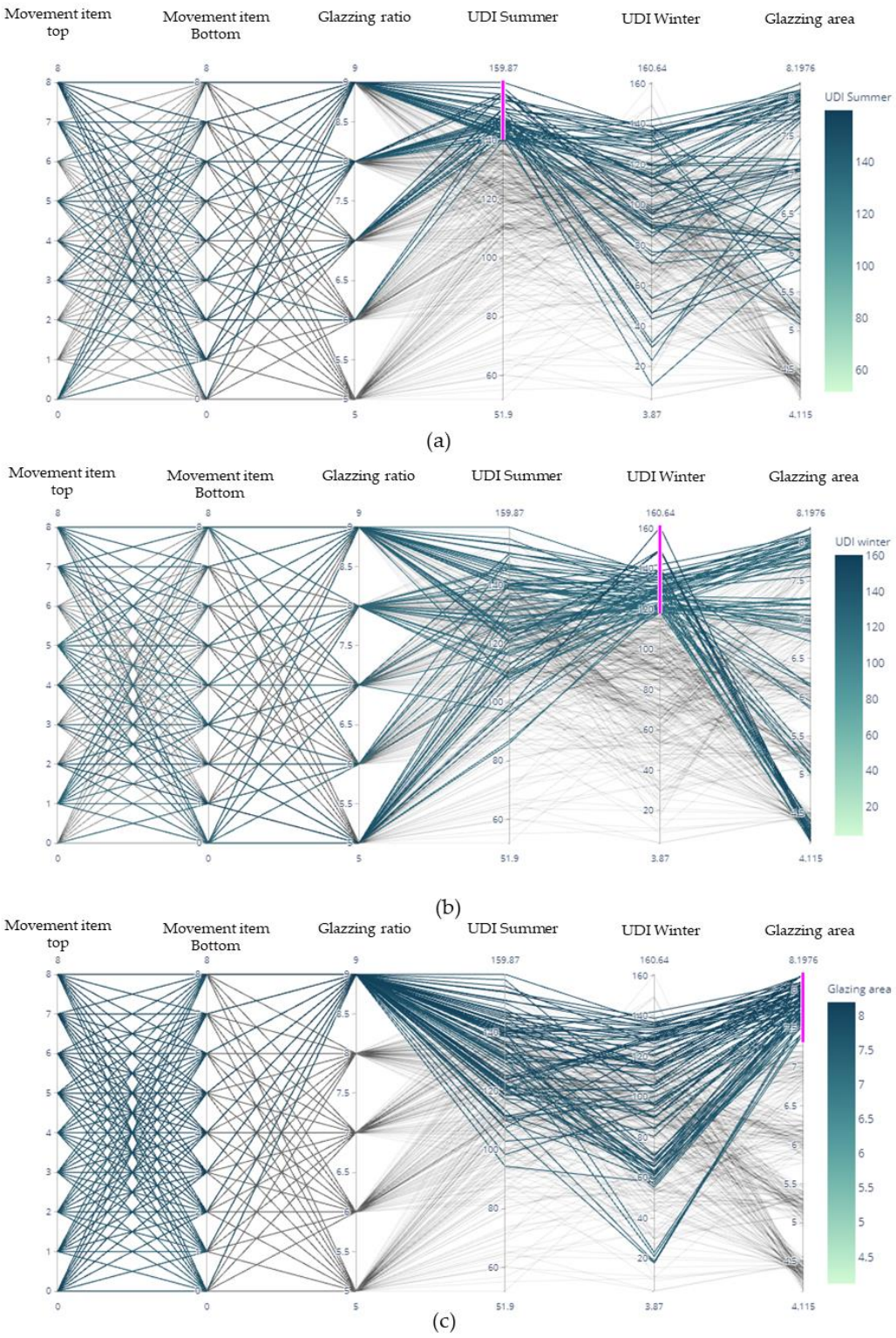

Figure 7.21. Parallel coordinate plots for daylight iteration: (a) relation to highest UDI summer; (b) relation to highest UDI winter; (c) relation to highest glazing area

Figure 7.21 displays scatterplots illustrating the link between parameters and objectives in the data from the iteration of the daylight objective. In these plots, similar to Figure 7.19, the color gradient and highlight were applied in accordance with the design objective value. Summertime UDIs of 300 to 500 lux are often linked with a middle-to-high glazing ratio. While there is no discernible pattern regarding the movement of objects at the bottom and top, nor the other objectives. In Figure 7.21 (b), the greatest UDI value in winter is related with a median to maximum UDI value in summer, but the trend is even in terms of parameters and glazing area. Maximum glazing ratio is correlated with maximum glazing area in Figure 7.21 (c), whereas the distribution of movement elements at the top and bottom is uniform. In addition, maximum glazing area is connected with the range from middle to maximum UDI area in the summer and the range from medium to high UDI area in the winter.

7.4. Chapter conclusion

In accordance with the hypothesis, the results indicate that the proposed methodology applied in the initial phase of designing a two-story wooden house can identify the optimal design solution in terms of structural and daylight performance goals and answer the question of whether the proposed method can lead to optimization and find the optimal solution from the exploration and optimization processes. The best solution in structural optimization with minimum force load, cost, and maximum building volume, balancing the trade-offs of the design objectives, was found to have a specific parameter combination, explained in Sub-chapter 7.3.3, that the designer should consider when determining the *Hyperboloid* design factors and parameters. Through this research, the designer can be enlightened and concentrate on the key aspects for minimizing displacement, normal force average, and cost, while increasing building volume. In addition, as described in Sub-chapter 7.3.4, the proposed method identifies the appropriate glazing location and ratio to achieve an optimal UDI of 300 to 500 lux for the dwelling. Confirmation that the performance-based design has been implemented successfully.

In discovering correlations, patterns, and links among the gathered data (objectives), the MOO generated linkages that were ambiguous and correlations that were weak. Due to the insufficiency of correlation, the value of one objective developed in MOO was unable to become a significant reasoning factor that influenced another objective's design. By observing the scatterplots, it became apparent that the MOO and fitness function calculation processes had successfully located the pareto front and the based design solution within the desired searching area (Figure 7.13 and Figure 7.15). Consequently, it facilitates the designer's ability to identify and examine design options with quick data and geometrical feedback during decision-making. The use of parallel coordinate plots in Sub-chapter 7.3.6 reveals many tendencies and trends in the parameter value in connection to the objectives and the parameters. Observing this pattern, future research can concentrate solely on the range of parameters in which the lines are densely populated and densely packed. Moreover, parallel coordinate plots provide adaptable and interactive methods for observing design solution implementations (purple line). Moreover, sensitivity analysis has been integrated (Sub-chapter 7.3.5), Successfully determined the most influential parameter that drives the design objectives. Knowing the parameter definitions and their range increases the likelihood of achieving better optimum design objectives.

The study of this chapter was intended to be utilized in the preliminary stages of architectural design. This is because its characteristics, geometry, and performance are unique. Typically, efficiency is determined by comparing the performance of the iterative model to the performance of the benchmark or benchmark model. Due to the complexity of the design situation presented in this chapter, no particular constraints on the benchmark model were defined. This chapter solely evaluated displacement and normal force average for structural considerations, and the useful daylight intensity (UDI) for daylight performance. The finite element measurement is another structural metric. [178] in daylight analysis, as well as Spatial Daylight Autonomy (SDA), Annual Sunlight Exposure (ASE), and Daylight Glare Probability (DGP) [144].

This chapter contributes a novel knowledge to the construction of *Hyperboloid* wooden structures. The objective of this study was to investigate and apply parametric

design approaches and multi-objective optimization (MOO) to the design of a *Hyperboloid* two-story timber house in the Orio neighbourhood of Kitakyushu, Japan, taking structural and daylight performance into account. The study centred on the use of Japanese timbers measuring 105 mm x 105 mm x 4000 mm as the building's primary framework.

On the basis of the data generated by the optimization and iteration processes, it can be concluded that the suggested method is capable of achieving optimization and locating the most desirable design solution that achieves the specified design objectives in terms of structure and daylight. In addition, the study identifies the most influential parameters on the design objectives, as well as the relationship between the design objectives and the parameters in relation to the design objectives. The best design option based on structural analysis was solution 9052, with the following parameter combination: radius bottom: 1.5; offset distance: 0.18; timber members: 5; twisting level: 2; building height: 4; radius-top 1: 2.09; radius-top 2: 2.628; roof slope: 7. Regarding the daylight aim, solution number 397 with the following parameter combination was the optimal solution: movement item top: 8, movement item bottom: 7, and glazing ratio: 9. The most influential criterion in determining displacement and building volume was building height, while the most influential element in determining cost was twisting level. This research demonstrates conclusively that the MOO and parametric design should be compatible and effective with the performance-based design approach in the early phases of architectural design processes, where the intention of performance-based design has emerged. Based on these findings, designers and stakeholders should explore employing parametric design and MOO, both of which require a set of parameters, to accomplish more desirable design objectives.

Chapter 8. Discussion

Considering the development in computational architecture and the pivotal role in involving the mindset of the generative process during the early architectural design phase in approaching the global rising temperature phenomena, this thesis introduces the method for investigating the relationship between design parameters and design performance goals through the use of generative and parametric approaches and multi-objective optimization via genetic algorithms. This research aims to explore possible design solutions produced during the optimization process and find the optimum design alternative according to the specific given context, together with the investigation of the relationship between design parameters and the design objective as well as the identification of the most influential parameter at the micro scale. To answer the question of whether a parametric and generative algorithm approach may help a designer or engineer make design decisions by discovering connections between parameters and objectives, as well as locating the most influential parameters and optimizing building performance during the early stages of design.

The thesis consists of nine chapters. Chapter 1 provides the context for this study, research aims and objectives, originality, and contributions, as well as the format of the thesis. Recent literature on the use of parametric and multi-objective optimization platforms in the architectural design process is compiled and explained in Chapter 2. The subject includes daylight, geometry, shading and energy-related issues, structure optimization, and material considerations, including expanded metal, louver shading, and the usage of wood. Chapter 3 describes a broader insight of the computational process which include the use of parametric and generative optimization followed by the mechanism of data collection and analysis.

The main body of the thesis consists of four chapters where each provide a specific result responding the specific experiment scenario. Chapter 4 describes a methodology for investigating the daylight performance relationship between louver or slat shading devices and room orientation. This chapter contains five topics or cases, each describing a distinct method for observing the role of louvres in daylight provision using parametric and MOO. In the first scenario, room slats or louver considered in addition to a method for determining the optimal solution for daylight objective. Using design exploration, the

results show 13.1% improvement of useful daylight illuminance (UDI) goals. In the second scenario, a design exploration platform and a two-story residence were developed to serve as a benchmark model for overhang and building orientation as dynamic design variables. The results show efficiency calculated for a whole year period stated by the winter's best performance model reached 2.58 kWh/m^2 in cooling and 3.36 kWh/m^2 in heating. Summer's best performance model stated an efficiency of 6.17 kWh/m^2 for cooling but slightly exceeded in terms of energy for heating compared to the base case. Only cooling had a stated efficiency of 6.15 kWh/m^2 for the tolerable model. The best sun hours in the summer model stated efficiency of 6.12 kWh/m^2 in terms of cooling but slightly exceeded the performance for heating. Both cooling and heating energy consumption stated a significant value of about 20 kWh/m^2 for cooling and about 14% kWh/m^2 for heating for the best sun hours in the winter model. In the third scenario, daylight performance and energy consumption in several cities with different locations over the equator have been analyzed. The results stated an improvement in UDI for Birmingham, Jakarta, and Sydney of 80%, 146.26%, and 79.48% and cooling energy consumption of 28%, 3.26%, and 2.99% respectively. The data suggest that the used of generative approach and the multiple data analysis proposed in this study can lead to the identification of the best louver design solution, right glazing size, and orientation, that can optimize the daylight situation also reduce the energy consumption. Chapter 4 offers novelty and significance by providing an optimization platform in iterating a well-known type of shading, louver, or slats, to optimize daylight performance in specific regional contexts such as Sydney, Australia; Jakarta, Birmingham; Bandung, Indonesia. The previous research is analyzing one regional context and without form-finding approach while this chapter simulate and optimized and compare different sky conditions of three regions. Thus, it is giving an insight in how shading condition should behave or treated differently, lead the stakeholders to a general justification in using louver shading device. The findings in this chapter complement the previous research in parametric louver shading investigation in the way its provided daylight penetrations and the environmental context [78,91,179–182]. In each context, the finding contributes to design consideration and assists in shading design strategy according to the given sky condition.

Providing right solution to a specific environmental context in providing equilibrated daylight provision can invest in future betterment related to human health and economics. Besides, by knowing the right glazing, louver configuration, and building or room orientation, the stakeholders such as designer, industries, and regulators can rely on or refer to this finding in addressing micro-scale environmental consideration related to shading-daylight optimization.

Chapter 5 characterizes an approach for improving the configuration of a material with a long-standing and well-known reputation, expanded metal, as a shading device, to demonstrate that the material can improve daylight provision and serve as an alternative material for shading devices. This chapter entails three study cases and a review of its application in a recent architectural project. In the first instance, the expanded metal in Japanese Industrial Standard JIS G3351 was simulated to determine which type of standard performed best in daylight. The results show that XG13 and XG14 are the most preferable for UDI objective, XG24 was the most preferable performance of daylight glare probability (DGP) objective, XS91 was the most preferable option for aperture objective, while fitness function calculation recommend XG24 as the best solution by rank. In the second instance, a comprehensive parametric and optimization analysis was conducted in Japan to prove that expanded metal can satisfy the daylight credit requirements. Adopting the proposed framework successfully met the LEED v4.1 daylight requirements by decreasing ASE by 100% and increasing UDI by approximately 50 % compared to the benchmark model, as demonstrated by the results. In addition, the process of iteration revealed a variety of aesthetic patterns, providing designers with an additional factor to consider during the design decision-making procedure. In the third instance, increased metal shading was the subject of a simulation on the probability of daylight glare (DGP). The MOO's analysis of 2,322 solutions and 88 Pareto frontiers resulted in the presentation of several findings. The shading View (aperture) has a statistically significant positive correlation with the DGP. The parameter Strand/W was determined to be the most influential in driving the objectives, and the validation process reveals a 38% improvement in DGP. The proposed system and research findings can contribute to the world of building shading devices, building

performance simulations and automation in design and construction. First, the contribution of this research introduces a design methodology for investigating daylight, which incorporates a generative approach to optimise daylight performance through the use of a unique expanded-metal shading material. Second, the methodology revealed that the expanded-metal shading improved daylight performance, which confirms the recognition of expanded-metal mesh by USGBC LEED. Third, the expanded-metal parameter configuration that is implicated in the optimum daylight performance has been successfully revealed. The finding considers design configuration adjustment according to the given geometrical and climate context before manufacturing and installation. Fourth, the proposed methodology has successfully identified the significant factors that shape the daylight results, including the most critical design variable that constructs expanded metal and its value range. Through this identification, a thorough analysis of a similar study on expanded-metal-inspired shading or design can be conducted by focusing only on these identified details. Last, the research investigates the application of daylight shading using the context of Japan's sky conditions, enhancing the architectural exploration and building-material market in Japan. The data in this chapter indicate that the used of generative approach and the multiple data analysis proposed in this study toward the expanded metal shading design logic can lead to the identification of the best expanded metal sheet design solution that optimizes the daylight situation, confirming the metal sheet as environmentally friendly material for architectural design components. Besides, the tendency among design components as well as the role of each parameter has been revealed, answering research questions of this thesis, and confirming the hypothesis. Chapter 5 provides significance and a novel way of investigating a well-known and long-standing reputable material, expanded metal sheet, as a solar shade device. Complementing the previous expanded metal inspired shading related to daylight provision conducted by [99] and supporting daylight investigation conducted by Hariyadi [139] and Rico-Martinez [134]. Given the context of Japan's sky conditions, the best expanded metal configuration and daylight performance was successfully identified and proven to merit the daylight requirements of LEED v4.1 Daylight credits [183]. The findings contribute to the field by providing stakeholders such as designers,

manufacturers, and regulators with the proper expanded metal as a complementary aesthetic component in meeting with proper daylight performance. In addition, stakeholders like designers, industries, and regulators can rely on or reference this finding in addressing micro-scale environmental consideration related to shading-daylight optimization, as well as advance the field of metal design options using local and reliable metal material, by knowing the proper type of expanded metal to be implemented.

Chapter 6 describes and develops a parametric and optimization model to observe the building geometry-affected potential for optimizing energy consumption. The purpose of this chapter was to examine how the geometry of a two-story wooden house with a *Reuleaux* triangle base profile affects the outdoor thermal comfort situated in Orio District, Kitakyushu, Japan. The results show minor improvement in the three designated design objectives, which confirms the hypothesis. Some improvement has been achieved as follow, 0.02 kWh/m^2 improvement in surface radiation, 0.01 kWh/m^2 improvement in site radiation, and 0.07 °C improvement in UTCI. However, the annual utility bill for cooling and heating needs demonstrates the opposite trend. The two found solutions perform cost 31 Japanese yen with the minimum radiation model and about 16 Japanese yen with the minimum UTCI model. It is demonstrated that the minimum surface radiation and area did not result in a cheaper cost of power for cooling needs. Raise the possibility of reconsidering elements outside geometry. The data in this chapter supports that the proposed approach could lead to the investigation of the best twisted *Releaux* triangle geometry performing optimum UTCI and radiation, confirming the research hypothesis and answering the thesis questions. However, the findings indicate contradiction in which the optimization of the geometry has negative impact on energy consumption. This finding lead to the re-consideration of design variable to be set in the early parameter definition setting process. Further research is recommended to include the opening and glazing toward the geometry when relate the building geometry to energy consumption. Chapter 6 provides significance in finding the best twisted *Reuleaux* triangle cylinder to respond to the climate of Kitakyushu. The study combines the objectives of surface radiation and outdoor thermal comfort and comes up with an improvement in the universal thermal climate index (UTCI) and a slight improvement

in energy consumption. The results contribute to the geometry consideration especially in wooden building and the use of unique *Reuleaux* triangle profile, enhancing wooden architecture in consideration with unique geometry and environmental performance.

Chapter 7 investigates the relationship between parametric simulation in terms of structure optimization. A parametric and multi-objective optimization strategy for optimizing a two-story hyperbolic wooden structure with iterative window ratio and orientation is presented. The optimization and exploration yielded 10,098 structural analysis solutions and 406 daylight exploration solutions. Based on the data analysis, the proposed method has successfully produced the optimal design solution by identifying the optimal balance between objective trade-offs. Moreover, the most influential parameter that influences the value of design objectives has been identified. Supporting the hypothesis, the analysis identifies that the use of the proposed methodology as a proper approach in finding best *Hyperboloid* wooden structure [184] design performing desired structural and daylight objectives. Chapter 7 provides a novelty in the structural investigation and cost efficiency of a unique *Hyperboloid* wooden structure made of 105 mm x 105 mm x 4000 mm Japanese cedar, together with the identification of the best glazing size and position that performed the best daylight situation. Related to the position of this research in the literature of parametric design and MOO discussion, The study provides a new insight into the performance-based design in the early phase of designing wooden structure especially in *Hyperboloid* design [52,112,185], But with using more specific materials which was a Japanese lumber 105 mm x 105 mm x 4000 mm. The use of optimization method and platform in structural optimization could find the best design solution confirming research in [186–188]. Related to the daylight objective, the proposed study using a metric that developed and adopted in [53,75] and optimized like in [87]. The optimization of daylight has successfully produced the best window position by iterating the glazing location and glazing ratio [87]. The combination of two disciplines of structural and daylight was in line with the ideation in [189] yet more to the application in building geometry rather than shell structure. The study contributes to the field where it suggests achievements of reducing structural force together with minimizing the

construction cost related to wooden volume. The stakeholders can be benefit in terms of cost and construction strategy.

The methods proposed in this thesis have shown the importance of the utilization of computational architecture in exploring and finding design solutions based on the given data set of parameters. However, several limitations have been noticed. In terms of design approach, the limitation of this research is including the requirement of basic informatics knowledge to follow the logic of computational process. In terms of material and weather data used, the details in determining material properties and actual weather data since the EPW file is a historical database provided by outside authorization and also easy to be retrieved, might be complemented by for instance data from actual measurement in the field. Besides, related to the virtual hypothetical model or geometry, the thickness has been neglected due to the capability of the hardware used. Recommendation based on the findings following the research limitation are include the involvement of virtual model thickness or the detail definitions of the model surface. What is more, enhance the simulation using actual weather data, as well as increase the number of design generation to obtain more optimized design solution.

The methods described in this thesis have demonstrated the benefit of employing computational architecture by contributing to the establishment of the foundation for such tactics, so that future research can continue to expand on them and bring further advancement. The expected beneficiaries of this study's findings include architects or designers, regulators, manufacturers, and other practitioners in the built environment. The methodology proposed can be applied to a range of purposes, deploying different materials and climate models. It provides insight into the potential of design goal optimization during the early design stages using less time-consuming and less expensive tools than onsite measurement using actual material. Furthermore, it holds promise in mitigating and reducing the negative impact of the building. This thesis contributes to establishing the framework for such strategies. Therefore, future research can continue to build on it and provide greater advancements. The result of this study is expected to benefit stakeholders such as architects or designers, regulators, manufacturers, and other practitioners in the field of the built environment.

Chapter 9. Conclusion

In the field of study, researchers and practitioners have done a lot of work on the use of parametric and multi-objective optimization approaches to environmentally friendly design. However, a comprehensive optimization approach from scratch to the design solution ranking process has still been limitedly reported. In response to the issues of global raising phenomena that are could be potentially scaled down through the design perspective, the thesis proposed a computational design platform to be implemented during the early phase design process using parametric and generative algorithm optimization approach aims to investigates the relationship between design parameters and design objective and the potential of design objective optimization concerning environmental performance indicators. The thesis challenges design thinking by trying to answer how the proposed computational approach can contribute to the design objective optimization as well as discover the role of parameters in driving the design goals. It highlights the hypothesis where the computational and generative approaches can lead to optimization together with the identification of parameter roles in affecting design goals. The proposed method is particularly pivotal in dealing with multiple design targets and multiple dynamic parameters in response to additional data input such as climate data or material properties. By defining design logic of the intended design object, the computational design mechanism is applied to four different scopes of investigation: louver and glazing-daylight investigation; expanded metal-daylight investigation; a twisted *Releaux* triangle geometry-energy consumption investigation; and the *Hyperboloid*-structure and daylight investigation.

The thesis consists of four main chapters. In Chapter 4, the intended parametric and generative simulation scenarios are applied to investigate the daylight of the louver shading device, glazing ratio, and room orientation. The investigation is implemented in three different experiments. The first experiments iterate the parameters of louver shading design parameters for Jakarta, Indonesia context. The exploration and investigation process led to the identification of the best louver design performing a 13.1% UDI improvement. The second experiment iterates a proposed benchmark model equipped with design parameters such as glazing ratio, overhangs, and building orientation model responding to the Kitakyushu, Japan context for daylight and energy

consumption comparison purposes and successfully concludes with multiple design solution categories. The third experiment simulates the louver logic plus additional parameters of room orientation set to undergo three different sky conditions: Birmingham, U.K.; Jakarta, Indonesia, and Sydney, Australia. The third experiment concludes the identification of the best design solutions performing desired UDI and unique perspectives of louver conditions, where the Birmingham situation recommends a smaller louver configuration compared to the other two case studies. The chapter concluded that the proposed approach is fit to identify design factors to target optimum environmental factors when involving louver shading devices. By the use of proposed geometry designer can only focus on the found value range and refer to the design tendency when designing louver shading. Besides, the information in this chapter, benefits stakeholders such as designer, industry, or regulator in design decision making process to properly act and apply louver design according to specific regional context to achieve daylight and energy consumption optimization.

In Chapter 5, the logic of the well-known metal material named expanded metal has been an object for parametric and generative daylight simulation and optimization. The first experiment in this chapter examines the 27 types of the commercial Japanese Industrial Standard (JIS) G3351 expanded metal grating type. The findings have successfully classified the commercial type according to its desired daylight performance. Furthermore, in the second experiment, a comprehensive daylight investigation is conducted to see the relationship and the possibility of expanded metal design configuration toward daylight optimization. In this experiment, besides that the best design solution with its expanded metal configuration targeted by the multi-objective optimization process has been identified, the findings confirm the expanded metal's environmental friendliness where it is used as shading devices. In addition, the optimization results revealed that the best design solution fulfils the daylight requirements stated in the LEED v4.1 standard. The third experiment focuses on the relation of expanded metal shading to the phenomena of glare probability. Along with the findings, the best expanded metal configuration has been successfully found to perform 38% glare probability reduction to come up with a perceptible glare category.

When developing expanded metal shading using the given geometry, the designer can merely focus on the found value range and refer to the design tendency. In addition, the information in this chapter is useful for stakeholders such as the designer, industry, or regulator in the design decision-making process in order to appropriately act and use expanded metal design in accordance with the regional context in order to optimize daylight.

In Chapter 6, we utilize multi-objective optimization process to see the possibility of optimization of outdoor thermal comfort and energy consumption affected by building geometry in the early phase of designing a twisted *Releaux* triangle to be located in Kitakyushu, Japan. The logic of the intended geometry such as triangle radius, roof slope, twisting level, rotation, and scale factor was iterated to undergo environmental simulation. The results suggest that the form-finding process leads to insignificance improvement in outdoor thermal comfort. However, unexpected phenomena occurred where the preferable solution for outdoor thermal comfort consume more energy and have more expensive utility cost. The findings suggest possibility to a re-consideration of design parameter definition besides the geometry to be implemented during the define parameter process. The study combines surface radiation with outdoor thermal comfort to improve UTCI and energy usage. The results contribute to geometry consideration in wooden building and the utilization of a distinctive *Reuleaux* triangle profile, increasing wooden architecture with unique geometry and environmental performance.

In Chapter 7, a *Hyperboloid* structure become an object to the structure and daylight simulation and optimization. In the optimization process, the logic of *Hyperboloid* structure such as height, member profile, offset distance, radius bottom and top, roof slope angle, twisting level, was implemented to the commercialize 105 mm x 105 mm x 4000 mm Japanese wooden bar. The results suggest that the proposed methodology has successfully ranked the best design solution that have lower structural force and cost and maximum building volume. In the second exploration and regarding daylight consideration, the exploration process that have conducted and have successfully locate glazing position with the right size to come up with maximum UDI in winter and summer period. The chapter contributes to the design and optimization field especially

in the effort in promoting wood applied in a *Hyperboloid* structure together with showing a success in reducing structural force and minimizing building costs associated with wooden volume. The stakeholders can profit in terms of cost and time spent conducting experiments.

In general, this set of experiments conducted in this research proposed novelty and contributions into the field of study that explained in two scopes of significance. Firstly, is shaped wide contribution covering the big idea behind this research, secondly, the novelty and contribution presented in more detail according to the study case. The research contributes to the field of computational architectural design by giving an insight into how form finding leads to design goal optimization and providing a way to investigate the relationship between design parameters and design objectives at different scales of the design process. In the context of early-phase architectural design, by knowing the relationship and the tendency between parameters and design objectives, the design goals can be quantitatively justified and the more optimized solution, in this instance, human comfort and structural consideration, can be achieved. For example, related to each experiment explained above, the information of a certain louver and expanded metal configuration, also known as the geometry information, benefits designers, manufacturers, users, and regulators in recommending the proper configuration based on the regional context to achieve the efficiency and optimize daylight and energy consumption that can have a positive impact on human health, economics, stability, and the environment in the long run.

Implicating by the results and the findings of this research, the field of architecture is enhanced by the alternative approach not only by its subjectivity, but it can also be justified and confirmed quantitatively to the micro level of specific parameter value range, especially in the early phase of designing. In the architectural design field, by the time this approach is applied during the early design stages, an unimaginable number of design alternatives and consequences will emerge. Thus, the way that design decision making is conducted can be more justified. "Good" will no longer be subjective but can be assessed and generalized. As confirmed by the findings in each example scale, the findings would approach design theory by introducing an alternative way of assessing the design process

during the early stages in order to save time dealing with uncertainty factors. The thinking will probably tend to pull the design performance consideration to the earlier steps, instead of being considered during the evaluation steps.

References

[1] E.D. Giouri, M. Tenpierik, M. Turrin, Zero energy potential of a high-rise office building in a Mediterranean climate: Using multi-objective optimization to understand the impact of design decisions towards zero-energy high-rise buildings, Energy Build. 209 (2020). https://doi.org/10.1016/j.enbuild.2019.109666.

[2] J. Natanian, O. Aleksandrowicz, T. Auer, A parametric approach to optimizing urban form, energy balance and environmental quality: The case of Mediterranean districts, Appl. Energy. 254 (2019) 113637. https://doi.org/10.1016/j.apenergy.2019.113637.

[3] D. Mohammad, A. Hamdan, F.L. De Oliveira, D.M.A. Hamdan, F.L. de Oliveira, The impact of urban design elements on microclimate in hot arid climatic conditions: Al Ain City, UAE, Energy Build. 200 (2019) 86–103. https://doi.org/10.1016/j.enbuild.2019.07.028.

[4] F. Olivieri, R.C. Grifoni, D. Redondas, J.A. Sánchez-Reséndiz, S. Tascini, An experimental method to quantitatively analyse the effect of thermal insulation thickness on the summer performance of a vertical green wall, Energy Build. 150 (2017) 132–148. https://doi.org/10.1016/j.enbuild.2017.05.068.

[5] P. IEA, Global energy use and energy-related CO2 emissions by sector, 2020, IEA, Tracking Buildings 2021, (2021). https://www.iea.org/reports/tracking-buildings-2021 (accessed April 18, 2022).

[6] P. IEA, Final residential energy use covered by mandatory minimum energy performance standards (MEPS), 2000-2021, IEA, Final residential energy use covered by mandatory minimum energy performance standards (MEPS), 2000-2021, (2021). https://www.iea.org/data-and-statistics/charts/final-residential-energy-use-covered-by-mandatory-minimum-energy-performance-standards-meps-2000-2021 (accessed April 15, 2022).

[7] P. IEA, Global CO2 emissions from building operations in the Net Zero Scenario, 2010-2030, IEA, Global CO2 emissions from building operations in the Net Zero Scenario, 2010-2030, (2021). https://www.iea.org/data-and-

statistics/charts/global-co2-emissions-from-building-operations-in-the-net-zero-scenario-2010-2030%0A%0A (accessed April 15, 2022).

[8] P. IEA, Global energy use and energy-related CO2 emissions by sector, 2020, IEA, Global energy use and energy-related CO2 emissions by sector, 2020, (2021). https://www.iea.org/data-and-statistics/charts/global-energy-use-and-energy-related-co2-emissions-by-sector-2020 (accessed April 15, 2022).

[9] P. Terri, H. Anna, How our homes impact our health: using a COVID-19 informed approach to examine urban apartment housing, Archnet-IJAR Int. J. Archit. Res. ahead-of-p (2020). https://doi.org/10.1108/ARCH-08-2020-0159.

[10] L. Dietz, H. Patrick F., D. Coil, M. Fretz, J. Eisen, K. Van Den Wymelenberg, 2019 Novel Coronavirus (COVID-19) Outbreak: A Review of the Current Literature and Built Environment Considerations to Reduce Transmission, (2018) 1–29. https://doi.org/10.20944/preprints202003.0197.v2.

[11] Y. Fang, S. Cho, Design optimization of building geometry and fenestration for daylighting and energy performance, Sol. Energy. 191 (2019) 7–18. https://doi.org/10.1016/j.solener.2019.08.039.

[12] A. Cincinelli, T. Martellini, Indoor air quality and health, Int. J. Environ. Res. Public Health. 14 (2017). https://doi.org/10.3390/ijerph14111286.

[13] P. Höppe, Different aspects of assessing indoor and outdoor thermal comfort, Energy Build. 34 (2002) 661–665. https://doi.org/10.1016/S0378-7788(02)00017-8.

[14] M.B.C. Aries, M.P.J. Aarts, J. Van Hoof, Daylight and health: A review of the evidence and consequences for the built environment, Light. Res. Technol. 47 (2015) 6–27. https://doi.org/10.1177/1477153513509258.

[15] M. Münch, A. Wirz-Justice, S.A. Brown, T. Kantermann, K. Martiny, O. Stefani, C. Vetter, K.P. Wright, K. Wulff, D.J. Skene, The Role of Daylight for Humans: Gaps in Current Knowledge, Clocks & Sleep. 2 (2020) 61–85. https://doi.org/10.3390/clockssleep2010008.

[16] M.H. Issa, J.H. Rankin, M. Attalla, A.J. Christian, Absenteeism, performance and occupant satisfaction with the indoor environment of green Toronto schools,

Indoor Built Environ. 20 (2011) 511–523.
https://doi.org/10.1177/1420326X11409114.

[17] A. Wirz-Justice, D.J. Skene, M. Münch, The relevance of daylight for humans, Biochem. Pharmacol. (2020) 114304. https://doi.org/10.1016/j.bcp.2020.114304.

[18] A. Kaminska, A. Ozadowicz, Lighting control including daylight and energy efficiency improvements analysis, Energies. 11 (2018).
https://doi.org/10.3390/en11082166.

[19] E. Taveres-cachat, G. Lobaccaro, F. Goia, G. Chaudhary, A methodology to improve the performance of PV integrated shading devices using multi-objective optimization, Appl. Energy. 247 (2019) 731–744.
https://doi.org/10.1016/j.apenergy.2019.04.033.

[20] R.A. Mangkuto, D.K. Dewi, A.A. Herwandani, M.D. Koerniawan, Faridah, Design optimisation of internal shading device in multiple scenarios: Case study in Bandung, Indonesia, J. Build. Eng. 24 (2019) 100745.
https://doi.org/10.1016/j.jobe.2019.100745.

[21] D. D'alessandro, M. Gola, L. Appolloni, M. Dettori, G.M. Fara, A. Rebecchi, G. Settimo, S. Capolongo, COVID-19 and living space challenge. Well-being and public health recommendations for a healthy, safe, and sustainable housing, Acta Biomed. 91 (2020) 61–75. https://doi.org/10.23750/abm.v91i9-S.10115.

[22] A. Hariyadi, H. Fukuda, Q. Ma, The effectiveness of the parametric design 'Sudare' blind as external shading for energy efficiency and visibility quality in Jakarta, Archit. Eng. Des. Manag. 13 (2017) 384–403.
https://doi.org/10.1080/17452007.2017.1296811.

[23] A. Eltaweel, Y. Su, Controlling venetian blinds based on parametric design; via implementing Grasshopper's plugins: A case study of an office building in Cairo, Energy Build. 139 (2017) 31–43. https://doi.org/10.1016/j.enbuild.2016.12.075.

[24] P. Janssen, J. Frazer, Generative Evolutionary Design : a Framework for Generating and Evolving Three-Dimensional Building Models, (n.d.).

[25] J. Zhang, N. Liu, S. Wang, A parametric approach for performance optimization of residential building design in Beijing, Build. Simul. 13 (2020) 223–235.

https://doi.org/10.1007/s12273-019-0571-z.

[26] R. Talami, J.A. Jakubiec, Early-design sensitivity of radiant cooled office buildings in the tropics for building performance, Energy Build. 223 (2020) 110177. https://doi.org/10.1016/j.enbuild.2020.110177.

[27] R. Oxman, Thinking difference: Theories and models of parametric design thinking, Des. Stud. 52 (2017) 4–39. https://doi.org/10.1016/j.destud.2017.06.001.

[28] A. Menges, T. Schwinn, O.D. Krieg, Advancing wood architecture: A computational approach, 2016. https://doi.org/10.4324/9781315678825.

[29] J. Nembrini, S. Samberger, G. Labelle, Parametric scripting for early design performance simulation, Energy Build. 68 (2014) 786–798. https://doi.org/10.1016/j.enbuild.2013.09.044.

[30] S. Wang, Y.K. Yi, N. Liu, Multi-objective optimization (MOO) for high-rise residential buildings' layout centered on daylight, visual, and outdoor thermal metrics in China, Build. Environ. 205 (2021) 108263. https://doi.org/10.1016/j.buildenv.2021.108263.

[31] D. Yang, D. Di Stefano, M. Turrin, S. Sariyildiz, Y. Sun, Dynamic and interactive re-formulation of multi-objective optimization problems for conceptual architectural design exploration, Autom. Constr. 118 (2020) 103251. https://doi.org/https://doi.org/10.1016/j.autcon.2020.103251.

[32] S. Attia, J.L.M. Hensen, L. Beltrán, A. De Herde, Selection criteria for building performance simulation tools: Contrasting architects' and engineers' needs, J. Build. Perform. Simul. 5 (2012) 155–169. https://doi.org/10.1080/19401493.2010.549573.

[33] R. Evins, P. Pointer, R. Vaidyanathan, B. Happold, N. Street, MULTI-OBJECTIVE OPTIMISATION OF THE CONFIGURATION AND CONTROL OF A DOUBLE-SKIN FACADE University of Bristol , Tyndall Avenue , Bristol , BS8 1TH , UK ., Simulation. (2011) 14–16. http://www.ibpsa.org/proceedings/BS2011/P_1463.pdf.

[34] N.R.M. Sakiyama, J.C. Carlo, L. Mazzaferro, H. Garrecht, Building optimization

through a parametric design platform: Using sensitivity analysis to improve a radial-based algorithm performance, Sustain. 13 (2021). https://doi.org/10.3390/su13105739.

[35] M. Turrin, D. Yang, A. D'Aquilio, R. Sileryte, Y. Sun, Computational Design for Sport Buildings, Procedia Eng. 147 (2016) 878–883. https://doi.org/https://doi.org/10.1016/j.proeng.2016.06.285.

[36] C. Preisinger, M. Heimrath, Karamba - A toolkit for parametric structural design, Struct. Eng. Int. J. Int. Assoc. Bridg. Struct. Eng. 24 (2014) 217–221. https://doi.org/10.2749/101686614X13830790993483.

[37] C. Preisinger, Linking structure and parametric geometry, Archit. Des. 83 (2013) 110–113. https://doi.org/10.1002/ad.1564.

[38] J. Wienold, Dynamic daylight glare evaluation, IBPSA 2009 - Int. Build. Perform. Simul. Assoc. 2009. (2009) 944–951.

[39] A. Tani, Interdisciplinary discussion on sustainable use of wood structure and free risk. situation in Japan and Austria, (n.d.) 202–207.

[40] Y. Tsunetsugu, Y. Miyazaki, H. Sato, Visual effects of interior design in actual-size living rooms on physiological responses, Build. Environ. 40 (2005) 1341–1346. https://doi.org/10.1016/j.buildenv.2004.11.026.

[41] E. Matsubara, S. Kawai, VOCs emitted from Japanese cedar (Cryptomeria japonica) interior walls induce physiological relaxation, Build. Environ. 72 (2014) 125–130. https://doi.org/10.1016/j.buildenv.2013.10.023.

[42] Think Wood, Benefits of Using Wood in Construction, (2020) 16964. https://www.thinkwood.com/benefits-of-using-wood.

[43] M.H. Ramage, H. Burridge, M. Busse-Wicher, G. Fereday, T. Reynolds, D.U. Shah, G. Wu, L. Yu, P. Fleming, D. Densley-Tingley, J. Allwood, P. Dupree, P.F. Linden, O. Scherman, The wood from the trees: The use of timber in construction, Renew. Sustain. Energy Rev. 68 (2017) 333–359. https://doi.org/10.1016/j.rser.2016.09.107.

[44] R. Heath, Material Information, Encycl. Public Relations. (2014) 151–157. https://doi.org/10.4135/9781452276236.n295.

[45] A. Menges, Performative wood: Integral computational design for timber constructions, ACADIA 09 ReForm() Build. a Better Tomorrow - Proc. 29th Annu. Conf. Assoc. Comput. Aided Des. Archit. (2009) 66–74.

[46] S. Gold, F. Rubik, Consumer attitudes towards timber as a construction material and towards timber frame houses - selected findings of a representative survey among the German population, J. Clean. Prod. 17 (2009) 303–309. https://doi.org/10.1016/j.jclepro.2008.07.001.

[47] C. Graciano, G. Martínez, Structural applications of expanded metal meshes, (2017).

[48] H. Kim, M.J. Clayton, A multi-objective optimization approach for climate-adaptive building envelope design using parametric behavior maps, Build. Environ. 185 (2020) 107292. https://doi.org/10.1016/j.buildenv.2020.107292.

[49] K. Konis, A. Gamas, K. Kensek, ScienceDirect Passive performance and building form : An optimization framework for early-stage design support, Sol. Energy. 125 (2016) 161–179. https://doi.org/10.1016/j.solener.2015.12.020.

[50] S. Motamedi, P. Liedl, Integrative algorithm to optimize skylights considering fully impacts of daylight on energy, Energy Build. 138 (2017) 655–665. https://doi.org/10.1016/j.enbuild.2016.12.045.

[51] M. Marzouk, M. ElSharkawy, A. Eissa, Optimizing thermal and visual efficiency using parametric configuration of skylights in heritage buildings, J. Build. Eng. 31 (2020) 101385. https://doi.org/10.1016/j.jobe.2020.101385.

[52] J. Dzwierzynska, Multi-objective optimizing curvilinear steel bar structures of hyperbolic paraboloid canopy roofs, Buildings. 10 (2020). https://doi.org/10.3390/buildings10030039.

[53] A. Eltaweel, Y. Su, Q. Lv, H. Lv, Advanced parametric louver systems with bi-axis and two-layer designs for an extensive daylighting coverage in a deep-plan office room, Sol. Energy. 206 (2020) 596–613. https://doi.org/10.1016/j.solener.2020.06.035.

[54] H. Kim, M.J. Clayton, Parametric behavior maps: A method for evaluating the energy performance of climate-adaptive building envelopes, Energy Build. 219

(2020) 110020. https://doi.org/10.1016/j.enbuild.2020.110020.

[55] Patrik Schumacher, Smart Work – Patrik Schumacher on the growing importance of parametrics, RIBA J. (2008). https://www.patrikschumacher.com/Texts/Design Research at Zaha Hadid Architects.htm (accessed May 28, 2022).

[56] I. Caetano, L. Santos, A. Leitão, Computational design in architecture: Defining parametric, generative, and algorithmic design, Front. Archit. Res. 9 (2020) 287–300. https://doi.org/10.1016/j.foar.2019.12.008.

[57] R. Oxman, Thinking difference: Theories and models of parametric design thinking, Des. Stud. 52 (2017) 4–39. https://doi.org/10.1016/j.destud.2017.06.001.

[58] A. Stals, S. Jancart, C. Elsen, Parametric modeling tools in small architectural offices: Towards an adapted design process model, Des. Stud. 72 (2021) 100978. https://doi.org/10.1016/j.destud.2020.100978.

[59] T. Wortmann, B. Tunçer, Differentiating parametric design: Digital workflows in contemporary architecture and construction, Des. Stud. 52 (2017) 173–197. https://doi.org/10.1016/j.destud.2017.05.004.

[60] E. Suzuki, What Is Parametric Design in Architecture, and How Is It Shaping the Industry?, (2020).

[61] J. Wassim, Parametric design for architecture, Laurence King Publishing, 2013.

[62] R. Woodbury, S. Williamson, P. Beesley, Prarmetric Modelling As a Design Representation in Architecture: a Process Account, Proc. Can. Eng. Educ. Assoc. (2011). https://doi.org/10.24908/pceea.v0i0.3827.

[63] R. Aish, R. Woodbury, Multi-level interaction in parametric design, Lect. Notes Comput. Sci. 3638 (2005) 151–162. https://doi.org/10.1007/11536482_13.

[64] S. Brell-Çokcan, M. Reis, H. Schmiedhofer, J. Braumann, Digital Design to Digital Production: Flank Milling with a 7-Axis CNC-Milling Robot and Parametric Design, 27th ECAADe Conf. Proc. (2009) 323–330.

[65] J. Braumann, S. Brell-Cokcan, Digital and Physical computing for industrial robots in architecture: Interfacing Arduino with industrial robots, Beyond Codes

Pixels - Proc. 17th Int. Conf. Comput. Archit. Des. Res. Asia, CAADRIA 2012. (2012) 317–326.

[66] A. Zani, M. Andaloro, L. Deblasio, P. Ruttico, A.G. Mainini, Computational Design and Parametric Optimization Approach with Genetic Algorithms of an Innovative Concrete Shading Device System, Procedia Eng. 180 (2017) 1473–1483. https://doi.org/10.1016/j.proeng.2017.04.310.

[67] P.J. Bentley, D.W. Corne, An introduction to Creative Evolutionary Systems, 2002. https://doi.org/10.1016/b978-155860673-9/50035-5.

[68] D.J. Gerber, S.H. Lin, B. Pan, A.S. Solmaz, Design optioneering: Multi-disciplinary design optimization through parameterization, domain integration and automation of a genetic algorithm, Simul. Ser. 44 (2012) 33–40.

[69] W. Pan, M. Turrin, C. Louter, S. Sariyildiz, Y. Sun, Integrating multi-functional space and long-span structure in the early design stage of indoor sports arenas by using parametric modelling and multi-objective optimization, J. Build. Eng. 22 (2019) 464–485. https://doi.org/10.1016/j.jobe.2019.01.006.

[70] M. Li, S. Yang, X. Liu, Shift-based density estimation for pareto-based algorithms in many-objective optimization, IEEE Trans. Evol. Comput. 18 (2014) 348–365. https://doi.org/10.1109/TEVC.2013.2262178.

[71] P. Bakmohammadi, E. Noorzai, Optimization of the design of the primary school classrooms in terms of energy and daylight performance considering occupants ' thermal and visual comfort, Energy Reports. 6 (2020) 1590–1607. https://doi.org/10.1016/j.egyr.2020.06.008.

[72] E. Taveres-Cachat, F. Goia, Co-simulation and validation of the performance of a highly flexible parametric model of an external shading system, Build. Environ. 182 (2020) 107111. https://doi.org/10.1016/j.buildenv.2020.107111.

[73] E. Taveres-Cachat, K. Bøe, G. Lobaccaro, F. Goia, S. Grynning, Balancing competing parameters in search of optimal configurations for a fix louvre blade system with integrated PV, Energy Procedia. 122 (2017) 607–612. https://doi.org/10.1016/j.egypro.2017.07.357.

[74] E. Elbeltagi, H. Wefki, S. Abdrabou, M. Dawood, A. Ramzy, Visualized strategy

for predicting buildings energy consumption during early design stage using parametric analysis, J. Build. Eng. 13 (2017) 127–136. https://doi.org/10.1016/j.jobe.2017.07.012.

[75] A. Eltaweel, S. Yuehong, Y. Su, Using integrated parametric control to achieve better daylighting uniformity in an office room: A multi-Step comparison study, Energy Build. 152 (2017) 137–148. https://doi.org/10.1016/j.enbuild.2017.07.033.

[76] Y. Fang, S. Cho, Design optimization of building geometry and fenestration for daylighting and energy performance, Sol. Energy. 191 (2019) 7–18. https://doi.org/10.1016/j.solener.2019.08.039.

[77] D.J. Gerber, E. Pantazis, A. Wang, A multi-agent approach for performance based architecture: Design exploring geometry, user, and environmental agencies in façades, Autom. Constr. 76 (2017) 45–58. https://doi.org/10.1016/j.autcon.2017.01.001.

[78] Y.J. Grobman, G. Austern, Y. Hatiel, I.G. Capeluto, Evaluating the Influence of Varied External Shading Elements on Internal Daylight Illuminances, Buildings. 10 (2020) 22. https://doi.org/10.3390/buildings10020022.

[79] M. Ayoub, Integrating illuminance and energy evaluations of cellular automata controlled dynamic shading system using new hourly-based metrics, Sol. Energy. 170 (2018) 336–351. https://doi.org/10.1016/j.solener.2018.05.041.

[80] K. Konis, A. Gamas, K. Kensek, Passive performance and building form: An optimization framework for early-stage design support, Sol. Energy. 125 (2016) 161–179. https://doi.org/10.1016/j.solener.2015.12.020.

[81] M. Qingsong, H. Fukuda, Parametric Office Building for Daylight and Energy Analysis in the Early Design Stages, Procedia - Soc. Behav. Sci. 216 (2016) 818–828. https://doi.org/10.1016/j.sbspro.2015.12.079.

[82] A.H.A. Mahmoud, Y. Elghazi, Parametric-based designs for kinetic facades to optimize daylight performance: Comparing rotation and translation kinetic motion for hexagonal facade patterns, Sol. Energy. 126 (2016) 111–127. https://doi.org/10.1016/j.solener.2015.12.039.

[83] M. Mahdavinejad, N.S. Nazar, Daylightophil High-Performance Architecture:

Multi-Objective Optimization of Energy Efficiency and Daylight Availability in BSk Climate, Energy Procedia. 115 (2017) 92–101. https://doi.org/10.1016/j.egypro.2017.05.010.

[84] A. Ebrahimi-Moghadam, P. Ildarabadi, K. Aliakbari, F. Fadaee, Sensitivity analysis and multi-objective optimization of energy consumption and thermal comfort by using interior light shelves in residential buildings, Renew. Energy. 159 (2020) 736–755. https://doi.org/10.1016/j.renene.2020.05.127.

[85] E. Naderi, B. Sajadi, M.A. Behabadi, E. Naderi, Multi-objective simulation-based optimization of controlled blind specifications to reduce energy consumption, and thermal and visual discomfort: Case studies in Iran, Build. Environ. 169 (2020) 106570. https://doi.org/10.1016/j.buildenv.2019.106570.

[86] S. Naji, L. Aye, M. Noguchi, Multi-objective optimisations of envelope components for a prefabricated house in six climate zones, Appl. Energy. 282 (2021) 116012. https://doi.org/10.1016/j.apenergy.2020.116012.

[87] P. Pilechiha, M. Mahdavinejad, F. Pour Rahimian, P. Carnemolla, S. Seyedzadeh, F. Pour, Multi-objective optimisation framework for designing office windows: quality of view, daylight and energy efficiency, Appl. Energy. 261 (2020) 114356. https://doi.org/10.1016/j.apenergy.2019.114356.

[88] M. Rabani, H. Bayera, N. Nord, Achieving zero-energy building performance with thermal and visual comfort enhancement through optimization of fenestration , envelope , shading device , and energy supply system, Sustain. Energy Technol. Assessments. 44 (2021) 101020. https://doi.org/10.1016/j.seta.2021.101020.

[89] R.A. Rizi, A. Eltaweel, A user detective adaptive facade towards improving visual and thermal comfort, J. Build. Eng. 33 (2021) 101554. https://doi.org/10.1016/j.jobe.2020.101554.

[90] A.P. de Almeida Rocha, G. Reynoso-Meza, R.C.L.F. Oliveira, N. Mendes, A pixel counting based method for designing shading devices in buildings considering energy efficiency, daylight use and fading protection, Appl. Energy. 262 (2020) 114497. https://doi.org/10.1016/j.apenergy.2020.114497.

[91] S. Samadi, E. Noorzai, L.O. Beltra, S. Abbasi, L.O. Beltrán, S. Abbasi, A computational approach for achieving optimum daylight inside buildings through automated kinetic shading systems, Front. Archit. Res. 9 (2020) 335–349. https://doi.org/https://doi.org/10.1016/j.foar.2019.10.004.

[92] H. Samuelson, S. Claussnitzer, A. Goyal, Y. Chen, A. Romo-castillo, Parametric energy simulation in early design : High-rise residential buildings in urban contexts, Build. Environ. 101 (2016) 19–31. https://doi.org/10.1016/j.buildenv.2016.02.018.

[93] A. Tabadkani, M. Valinejad Shoubi, F. Soflaei, S. Banihashemi, Integrated parametric design of adaptive facades for user's visual comfort, Autom. Constr. 106 (2019) 102857. https://doi.org/10.1016/j.autcon.2019.102857.

[94] L. Le-Thanh, T. Le-Duc, H. Ngo-Minh, Q.H. Nguyen, H. Nguyen-Xuan, Optimal design of an Origami-inspired kinetic façade by balancing composite motion optimization for improving daylight performance and energy efficiency, Energy. 219 (2021) 119557. https://doi.org/10.1016/j.energy.2020.119557.

[95] A. Toutou, M. Fikry, W. Mohamed, The parametric based optimization framework daylighting and energy performance in residential buildings in hot arid zone, Alexandria Eng. J. 57 (2018) 3595–3608. https://doi.org/10.1016/j.aej.2018.04.006.

[96] S. Vera, D. Uribe, W. Bustamante, Optimization of a fi xed exterior complex fenestration system considering visual comfort and energy performance criteria n Molina d, 113 (2017). https://doi.org/10.1016/j.buildenv.2016.07.027.

[97] A. Wagdy, F. Fathy, A parametric approach for achieving optimum daylighting performance through solar screens in desert climates, J. Build. Eng. 3 (2015) 155–170. https://doi.org/10.1016/j.jobe.2015.07.007.

[98] A. Wagdy, A. Sherif, H. Sabry, R. Arafa, I. Mashaly, Daylighting simulation for the configuration of external sun-breakers on south oriented windows of hospital patient rooms under a clear desert sky, Sol. Energy. 149 (2017) 164–175. https://doi.org/10.1016/j.solener.2017.04.009.

[99] Y.K. Yi, J. Yin, Y. Tang, Developing an advanced daylight model for building

energy tool to simulate dynamic shading device, Sol. Energy. 163 (2018) 140–149. https://doi.org/10.1016/j.solener.2018.01.082.

[100] A. Zhang, R. Bokel, A. Van Den Dobbelsteen, Y. Sun, Q. Huang, Q. Zhang, Optimization of thermal and daylight performance of school buildings based on a multi-objective genetic algorithm in the cold climate of China, Energy Build. 139 (2017) 371–384. https://doi.org/10.1016/j.enbuild.2017.01.048.

[101] J. Zhao, Y. Du, Multi-objective optimization design for windows and shading configuration considering energy consumption and thermal comfort : A case study for office building in different climatic regions of China, Sol. Energy. 206 (2020) 997–1017. https://doi.org/10.1016/j.solener.2020.05.090.

[102] L. Zhu, B. Wang, Y. Sun, Multi-objective optimization for energy consumption , daylighting and thermal comfort performance of rural tourism buildings in north China, Build. Environ. 176 (2020) 106841. https://doi.org/10.1016/j.buildenv.2020.106841.

[103] Y.K. Yi, A. Tariq, J. Park, D. Barakat, Multi-objective optimization (MOO) of a skylight roof system for structure integrity, daylight, and material cost, J. Build. Eng. 34 (2021) 102056. https://doi.org/10.1016/j.jobe.2020.102056.

[104] N.C. Brown, C.T. Mueller, Design for structural and energy performance of long span buildings using geometric multi-objective optimization, Energy Build. 127 (2016) 748–761. https://doi.org/10.1016/j.enbuild.2016.05.090.

[105] D. Yang, D. Di Stefano, M. Turrin, S. Sariyildiz, Y. Sun, Dynamic and interactive re-formulation of multi-objective optimization problems for conceptual architectural design exploration, Autom. Constr. 118 (2020) 103251. https://doi.org/10.1016/j.autcon.2020.103251.

[106] J. Dzwierzynska, Rationalized algorithmic-aided shaping a responsive curvilinear steel bar structure, Buildings. 9 (2019). https://doi.org/10.3390/buildings9030061.

[107] J. Dzwierzynska, A. Prokopska, Pre-rationalized parametric designing of roof shells formed by repetitive modules of Catalan surfaces, Symmetry (Basel). 10 (2018). https://doi.org/10.3390/sym10040105.

[108] L. Bande, A. Alshamsi, A. Alhefeiti, S. Alderei, S. Shaban, M. Albattah, M.D. Scoppa, Parametric design structures in low rise buildings in relation to the urban context in UAE, Sustain. 13 (2021). https://doi.org/10.3390/su13158595.

[109] D.A. Chi, D. Moreno, J. Navarro, Correlating daylight availability metric with lighting, heating and cooling energy consumptions, Build. Environ. 132 (2018) 170–180. https://doi.org/10.1016/j.buildenv.2018.01.048.

[110] N. Emami, H. Giles, P. von Buelow, Structural, daylighting, and energy performance of perforated concrete shell structures, Autom. Constr. 117 (2020) 103249. https://doi.org/10.1016/j.autcon.2020.103249.

[111] R. Danhaive, C.T. Mueller, Design subspace learning: Structural design space exploration using performance-conditioned generative modeling, Autom. Constr. 127 (2021) 103664. https://doi.org/10.1016/j.autcon.2021.103664.

[112] M.T. R. Afghani, P. Kazemi, Adaptation of Hyperboloid Structure for High-Rise Buildings With Exoskeleton, 5 Th Int. Conf. Archit. Built Environ. with Award. B. Abstr. (2017) 62.

[113] L. He, Q. Li, M. Gilbert, P. Shepherd, C. Rankine, T. Pritchard, V. Reale, Optimization-driven conceptual design of truss structures in a parametric modelling environment, Structures. 37 (2022) 469–482. https://doi.org/10.1016/j.istruc.2021.12.048.

[114] F. Cascone, D. Faiella, V. Tomei, E. Mele, Stress lines inspired structural patterns for tall buildings, Eng. Struct. 229 (2021) 111546. https://doi.org/10.1016/j.engstruct.2020.111546.

[115] C.P. Quaglia, N. Yu, A.P. Thrall, S. Paolucci, Balancing energy efficiency and structural performance through multi-objective shape optimization: Case study of a rapidly deployable origami-inspired shelter, Energy Build. 82 (2014) 733–745. https://doi.org/10.1016/j.enbuild.2014.07.063.

[116] A. Toutou, A Parametric Approach for Achieving Optimum Residential Building A Parametric Approach for Achieving Optimum Residential Building Performance in Hot Arid Zone A Thesis submitted in partial fulfilment of the requirements for the degree of Master of Science, (2018).

[117] F. Demarco, F. Bertacchini, C. Scuro, E. Bilotta, P. Pantano, The development and application of an optimization tool in industrial design, Int. J. Interact. Des. Manuf. 14 (2020) 955–970. https://doi.org/10.1007/s12008-020-00679-4.

[118] A.H. Primanti, R.A. Mangkuto, M.D. Koerniawan, R.C.G.M. Loonen, S.B. de Vries, Sensitivity Analysis on Daylighting, Visual Comfort, and Energy Consumption of Automated Venetian Blinds for Open-Plan Offices in Tropical Climate, 192 (2020) 48–52. https://doi.org/10.2991/aer.k.200214.007.

[119] Ladybug EPW Map, (n.d.). https://www.ladybug.tools/epwmap/ (accessed October 6, 2020).

[120] Robert McNeel, Rhino 3D, (n.d.). https://www.rhino3d.com/ (accessed October 8, 2020).

[121] Grasshopper 3D, (n.d.). https://www.grasshopper3d.com/ (accessed October 8, 2020).

[122] M.S. Roudsari, M. Pak, Ladybug: A parametric environmental plugin for grasshopper to help designers create an environmentally-conscious design, Proc. BS 2013 13th Conf. Int. Build. Perform. Simul. Assoc. (2013) 3128–3135.

[123] Thornton Tomasetti CORE studio, Design Explorer, (n.d.). http://core.thorntontomasetti.com/design-explorer/.

[124] A. Bernett, T. Dogan, Early Design Decision-Making Framework Based on Multi-Objective Building Performance Simulation Incorporating Energy, Carbon Footprint and Cost, Proc. Build. Simul. 2019 16th Conf. IBPSA. 16 (2020) 1617–1624. https://doi.org/10.26868/25222708.2019.210856.

[125] A. Nabil, J. Mardaljevic, Useful daylight illuminances: A replacement for daylight factors, Energy Build. 38 (2006) 905–913. https://doi.org/10.1016/j.enbuild.2006.03.013.

[126] A. Nabil, J. Mardaljevic, Useful daylight illuminance: A new paradigm for assessing daylight in buildings, Light. Res. Technol. 37 (2005) 41–59. https://doi.org/10.1191/1365782805li128oa.

[127] B. Paramita, H. Fukuda, R.P. Khidmat, A. Matzarakis, Building configuration of low-cost apartments in Bandung-its contribution to the microclimate and

outdoor thermal comfort, Buildings. 8 (2018). https://doi.org/10.3390/buildings8090123.

[128] K. Lakhdari, L. Sriti, B. Painter, Parametric optimization of daylight, thermal and energy performance of middle school classrooms, case of hot and dry regions, Build. Environ. 204 (2021) 108173. https://doi.org/10.1016/j.buildenv.2021.108173.

[129] J. Bader, E. Zitzler, HypE : An algorithm for fast optimization, Evol. Comput. 19 (2011) 45–76.

[130] D. Smith, C. Graciano, G. Martinez, Recent Patents on Expanded Metal, Recent Patents Mater. Sci. 2 (2010) 209–225. https://doi.org/10.2174/1874465610902030209.

[131] P.J. Arsenault, Expanded Metal Mesh in Architecture, (2014).

[132] Y.S. Tsay, C.Y. Yeh, A machine learning based prediction model for the sound absorption coefficient of micro-expanded metal mesh (Memm), Appl. Sci. 10 (2020) 1–22. https://doi.org/10.3390/app10217612.

[133] M. Merklein, D. Junker, A. Schaub, A. Kretschmer, M. Lechner, Development of a new method for producing plane expanded metal by laser cutting and forming of metal plates under uniaxial tension, Key Eng. Mater. 639 (2015) 131–136. https://doi.org/10.4028/www.scientific.net/KEM.639.131.

[134] J.M. Rico-Martinez, M. Brzezicki, C.G. Ruiz-Mugica, J. Lech, Daylight transmittance through expanded metal shadings, J. Facade Des. Eng. 8 (2020) 85–114. https://doi.org/10.7480/jfde.2020.1.4698.

[135] J.M. Martínez Rico, A. Leceta Murguzur, S. Santamaría Fernández, Design of assessment tools for solar control performance of expanded metal, VI Int. Congr. Archit. Envel. San Sebastian, Spain. (2012).

[136] New Art Museum / SANAA, (n.d.). https://www.archdaily.com/70822/new-art-museum-sanaa (accessed March 4, 2021).

[137] New York's New Museum, (n.d.). https://www.expandedmetalcompany.co.uk/case-studies/museum-of-art (accessed February 3, 2021).

[138] Messe Basel New Hall / Herzog & de Meuron, (n.d.). https://www.archdaily.com/332188/messe-basel-new-hall-herzog-de-meuron?ad_source=search&ad_medium=search_result_all (accessed March 4, 2021).

[139] A. Hariyadi, Study on Side Shading Optimization with Expanded Metal in Kitakyushu, (2017) 21–24.

[140] E. Brembilla, J. Mardaljevic, Climate-Based Daylight Modelling for compliance verification: Benchmarking multiple state-of-the-art methods, Build. Environ. 158 (2019) 151–164. https://doi.org/10.1016/j.buildenv.2019.04.051.

[141] R.A. Mangkuto, F. Feradi, R. Eka, R.T. Atmodipoero, F. Favero, Optimisation of daylight admission based on modi fi cations of light shelf design parameters, J. Build. Eng. 18 (2018) 195–209. https://doi.org/10.1016/j.jobe.2018.03.007.

[142] S. Carlucci, F. Causone, F. De Rosa, L. Pagliano, A review of indices for assessing visual comfort with a view to their use in optimization processes to support building integrated design, Renew. Sustain. Energy Rev. 47 (2015) 1016–1033. https://doi.org/10.1016/j.rser.2015.03.062.

[143] J. Wienold, J. Christoffersen, Evaluation methods and development of a new glare prediction model for daylight environments with the use of CCD cameras, Energy Build. 38 (2006) 743–757. https://doi.org/10.1016/j.enbuild.2006.03.017.

[144] USGBC, LEED v4 CREDITS for Building Design and Construction, LEED Publ. (2019) 147. https://www.usgbc.org/resources/leed-v4-building-design-and-construction-current-version.

[145] A. Tabadkani, M.V. Shoubi, F. Soflaei, S. Banihashemi, Automation in Construction Integrated parametric design of adaptive facades for user ' s visual comfort, Autom. Constr. 106 (2019) 102857. https://doi.org/10.1016/j.autcon.2019.102857.

[146] R. Vierlinger, D IPLOMARBEIT Master Thesis Multi Objective Design Interface, (2015). https://doi.org/10.13140/RG.2.1.3401.0324.

[147] A. Eltaweel, Y. Su, M.A. Mandour, O.O. Elrawy, A novel automated louver with parametrically-angled reflective slats; design evaluation for better practicality

and daylighting uniformity, J. Build. Eng. 42 (2021) 102438. https://doi.org/10.1016/j.jobe.2021.102438.

[148] R.A. Rizi, A. Eltaweel, A user detective adaptive facade towards improving visual and thermal comfort, J. Build. Eng. 33 (2021) 101554. https://doi.org/10.1016/j.jobe.2020.101554.

[149] A. Hariyadi, Study on Side Shading Optimization with Expanded Metal in Kitakyushu, (2017) 21–24. https://dorxlab.ft.ugm.ac.id/wp-content/uploads/sites/348/2018/06/AIJ-2017-Agus.pdf.

[150] Jaloxa Colour Picker, (n.d.). https://www.jaloxa.eu/resources/radiance/colour_picker.shtml (accessed March 12, 2021).

[151] M.C. Peel, B.L. Finlayson, T.A. McMahon, Updated world map of the Köppen-Geiger climate classification, Hydrol. Earth Syst. Sci. 11 (2007) 1633–1644. https://doi.org/10.5194/hess-11-1633-2007.

[152] K. Negendahl, T.R. Nielsen, Building energy optimization in the early design stages: A simplified method, Energy Build. 105 (2015) 88–99. https://doi.org/10.1016/j.enbuild.2015.06.087.

[153] C.J. Hopfe, Uncertainty and sensitivity analysis in building performance simulation for decision support and design optimization, 2009. https://doi.org/10.6100/IR643321.

[154] N. Delgarm, B. Sajadi, K. Azarbad, S. Delgarm, Sensitivity analysis of building energy performance: A simulation-based approach using OFAT and variance-based sensitivity analysis methods, J. Build. Eng. 15 (2018) 181–193. https://doi.org/10.1016/j.jobe.2017.11.020.

[155] K. Asadi, H. Ramshankar, H. Pullagurla, A. Bhandare, S. Shanbhag, P. Mehta, S. Kundu, K. Han, E. Lobaton, T. Wu, Vision-based integrated mobile robotic system for real-time applications in construction, Autom. Constr. 96 (2018) 470–482. https://doi.org/10.1016/j.autcon.2018.10.009.

[156] D.A. Chi, D. Moreno, J. Navarro, Design optimisation of perforated solar façades in order to balance daylighting with thermal performance, Build. Environ. 125

(2017) 383–400. https://doi.org/10.1016/j.buildenv.2017.09.007.

[157] F. Kharvari, An empirical validation of daylighting tools: Assessing radiance parameters and simulation settings in Ladybug and Honeybee against field measurements, Sol. Energy. 207 (2020) 1021–1036. https://doi.org/10.1016/j.solener.2020.07.054.

[158] D. Mohammad, A. Hamdan, F.L. De Oliveira, Energy & Buildings The impact of urban design elements on microclimate in hot arid climatic conditions : Al Ain City , UAE, Energy Build. 200 (2019) 86–103. https://doi.org/10.1016/j.enbuild.2019.07.028.

[159] J. Natanian, O. Aleksandrowicz, T. Auer, A parametric approach to optimizing urban form, energy balance and environmental quality: The case of Mediterranean districts, Appl. Energy. 254 (2019) 113637. https://doi.org/10.1016/j.apenergy.2019.113637.

[160] J. Natanian, T. Auer, Balancing urban density, energy performance and environmental quality in the Mediterranean: A typological evaluation based on photovoltaic potential, Energy Procedia. 152 (2018) 1103–1108. https://doi.org/10.1016/j.egypro.2018.09.133.

[161] E. Touloupaki, T. Theodosiou, Optimization of Building form to Minimize Energy Consumption through Parametric Modelling, Procedia Environ. Sci. 38 (2017) 509–514. https://doi.org/https://doi.org/10.1016/j.proenv.2017.03.114.

[162] G. Conti, R. Paoletti, Reuleaux Triangle in Architecture and Applications, Lect. Notes Networks Syst. 88 (2020) 79–89. https://doi.org/10.1007/978-3-030-29796-1_7.

[163] S. Sansri, S.W. Kielarova, Multi-objective shape optimization in generative design: Art deco double clip brooch jewelry design, Lect. Notes Electr. Eng. 449 (2017) 248–255. https://doi.org/10.1007/978-981-10-6451-7_30.

[164] F. Maden, Geometric and Kinematic Analysis of Deployable Doubly Ruled Hyperboloids, MEGARON / Yıldız Tech. Univ. Fac. Archit. E-Journal. 12 (2017) 343–354. https://doi.org/10.5505/megaron.2017.75010.

[165] N. Emami, H. Giles, P. von Buelow, Structural, daylighting, and energy

performance of perforated concrete shell structures, Autom. Constr. 117 (2020) 103249. https://doi.org/10.1016/j.autcon.2020.103249.

[166] R. Aguiar, C. Cardoso, A. Leitão, Algorithmic design and analysis fusing disciplines, Discip. Disrupt. - Proc. Cat. 37th Annu. Conf. Assoc. Comput. Aided Des. Archit. ACADIA 2017. (2017) 28–37.

[167] S. Tseranidis, N.C. Brown, C.T. Mueller, Data-driven approximation algorithms for rapid performance evaluation and optimization of civil structures, Autom. Constr. 72 (2016) 279–293. https://doi.org/10.1016/j.autcon.2016.02.002.

[168] F. Weldegiorgis, A.R.A.J. Dhungana, Parametric design and optimization of steel and Development of a workflow for design and, 2020.

[169] S. Fernando, S. Weir, D. Reinhardt, A. Hannouch, Towards a multi-criteria framework for stereotomy – Workflows for subtractive fabrication in complex geometries, J. Comput. Des. Eng. 6 (2019) 468–478. https://doi.org/10.1016/j.jcde.2018.07.005.

[170] Y. Kyu, H. Kim, Universal Visible Sky Factor : A method for calculating the three-dimensional visible sky ratio, Build. Environ. 123 (2017) 390–403. https://doi.org/10.1016/j.buildenv.2017.06.044.

[171] N. Delgarm, B. Sajadi, F. Kowsary, S. Delgarm, Multi-objective optimization of the building energy performance: A simulation-based approach by means of particle swarm optimization (PSO), Appl. Energy. 170 (2016) 293–303. https://doi.org/10.1016/j.apenergy.2016.02.141.

[172] A. Eltaweel, Y. SU, Parametric design and daylighting: A literature review, Renew. Sustain. Energy Rev. 73 (2017) 1086–1103. https://doi.org/10.1016/j.rser.2017.02.011.

[173] Open STAT File, (n.d.). http://grasshopperdocs.com/components/ladybug/openSTATFile.html (accessed January 15, 2022).

[174] H.J. Kim, C.S. Yang, H.J. Moon, A Study on Multi-Objective Parametric Design Tool for Surround-Type Movable Shading Device, Sustain. 11 (2019). https://doi.org/10.3390/su11247096.

[175] X. Shen, Environmental parametric multi-objective optimization for high performance facade design, CAADRIA 2018 - 23rd Int. Conf. Comput. Archit. Des. Res. Asia Learn. Prototyp. Adapt. 2 (2018) 103–112.

[176] Y. Zou, Q. Zhan, K. Xiang, A comprehensive method for optimizing the design of a regular architectural space to improve building performance, Energy Reports. 7 (2021) 981–996. https://doi.org/10.1016/j.egyr.2021.01.097.

[177] M. Talaei, M. Mahdavinejad, R. Azari, A. Prieto, H. Sangin, Multi-objective optimization of building-integrated microalgae photobioreactors for energy and daylighting performance, J. Build. Eng. 42 (2021) 102832. https://doi.org/10.1016/j.jobe.2021.102832.

[178] R. Zhang, C. Waibel, T. Wortmann, Optimization for Integrating and validating parametric design , (fast) fluid dynamics , 1 (2019) 37–45.

[179] A. Zayed, M. Elkhateib, M. Mahdy, I. Elwy, Exploring dynamic slat system for enhancing daylighting distribution at deep office spaces in hot arid regions, Energy Procedia. 153 (2018) 290–294. https://doi.org/10.1016/j.egypro.2018.10.003.

[180] B. Ercan, S.T. Elias-Ozkan, Performance-based parametric design explorations: A method for generating appropriate building components, Des. Stud. 38 (2015) 33–53. https://doi.org/10.1016/j.destud.2015.01.001.

[181] A. Eltaweel, Y. Su, Q. Lv, H. Lv, Advanced parametric louver systems with bi-axis and two-layer designs for an extensive daylighting coverage in a deep-plan office room, Sol. Energy. 206 (2020) 596–613. https://doi.org/10.1016/j.solener.2020.06.035.

[182] K.S. Lee, K.J. Han, J.W. Lee, The impact of shading type and azimuth orientation on the daylighting in a classroom-focusing on effectiveness of façade shading, comparing the results of da and udi, Energies. 10 (2017). https://doi.org/10.3390/en10050635.

[183] USGBC, LEED v4 CREDITS for Building Design and Construction, LEED Publ. (2019) 147.

[184] F. Maden, Geometric and Kinematic Analysis of Deployable Doubly Ruled

Hyperboloids, MEGARON / Yıldız Tech. Univ. Fac. Archit. E-Journal. (2017). https://doi.org/10.5505/megaron.2017.75010.

[185] T. Chahade, K.U. Schober, L. Morillas, Interactive structural design of hyperbolic grid shells, Proc. Inst. Civ. Eng. Struct. Build. (2021) 1–12. https://doi.org/10.1680/jstbu.19.00061.

[186] S. Mirniazmandan, M. Alaghmandan, F. Barazande, E. Rahimianzarif, Mutual effect of geometric modifications and diagrid structure on structural optimization of tall buildings, Archit. Sci. Rev. 61 (2018) 371–383. https://doi.org/10.1080/00038628.2018.1477043.

[187] R. Bialozor, M. Olszowski, Parametric modelling as a shift of decision-making process in structural engineering Parametric modelling as a shift of decision-making process in structural, (2017).

[188] M. Dragoljevic, S. Viscuso, A. Zanelli, Data-driven design of deployable structures: Literature review and multi-criteria optimization approach, Curved Layer. Struct. 8 (2021) 241–258. https://doi.org/10.1515/cls-2021-0022.

[189] N. Emami, Disregarded solution spaces: A proposed approach to draw connections between computationally generated solution spaces and actual built case studies, Int. J. Archit. Comput. 19 (2021) 273–290. https://doi.org/10.1177/1478077120969928.